1-1-2014

Pathogenic Mechanisms underlying the Early Epileptic Encephalopathy CDKL5 Disorder

I-Ting Judy Wang
University of Pennsylvania, wang7@mail.med.upenn.edu

Pathogenic Mechanisms underlying the Early Epileptic Encephalopathy CDKL5 Disorder

Abstract
Cyclin-dependent kinase-like 5 (CDKL5) is an X-linked gene associated with early infantile epileptic encephalopathy, atypical Rett Syndrome, and autism spectrum disorders. Patients with CDKL5 mutations display a heterogeneous array of clinical symptoms, the most prominent of which include early-onset epileptic seizures, intellectual disability, marked hypotonia, and autistic features. Despite the strong genetic linkage between CDKL5 mutations and neurodevelopmental disorders, the biological function of CDKL5 and its pathogenic mechanisms remain largely uncharacterized. Consequently, treatments for CDKL5 disorder have been largely ineffective and limited to symptom management. This study aims to dissect the molecular and cellular basis of CDKL5 disorder using novel mouse models and to identify signaling pathways that can be targeted for therapeutic development.

To determine the genetic causality of CDKL5 disorder, we generated the first Cdkl5 knockout (KO) mouse and found that mice lacking CDKL5 mimic key symptoms of CDKL5 disorder, including impaired motor control, poor learning and memory, and autistic-like behaviors. KO mice also show deficits in neural circuit communication and alterations in many signal transduction pathways, but do not develop spontaneous seizures. Previous studies using in vitro cell cultures and shRNA-mediated knockdown have implicated CDKL5 in dendritic morphogenesis and the phosphorylation of MeCP2, mutations of which cause Rett Syndrome, but the results of these studies are contentious. Therefore, to understand the in vivo function of CDKL5 and to investigate how loss of CDKL5 contributes to epileptic and autistic features, we have generated Cdkl5 conditional KO mice. Notably, our studies show that selective deletion of Cdkl5 from forebrain GABAergic neurons (Dlx-cKO) recapitulates autistic-like phenotypes, whereas selective removal of Cdkl5 from forebrain glutamatergic neurons (Nex-cKO) results in the development of spontaneous seizures. The separation of distinct aspects of CDKL5 disorder-related phenotypes in the two complementary conditional KO lines suggests that the epileptic and autistic phenotypes of CDKL5 disorder are mediated by distinct neural circuits and that loss of CDKL5 in specific cell types may differentially disrupt signaling pathways and impair neuronal function.

Degree Type
Dissertation

Degree Name
Doctor of Philosophy (PhD)

Graduate Group
Neuroscience

First Advisor
Zhaolan Zhou

Keywords
autism, behavior, CDKL5, epilepsy, MeCP2, Rett Syndrome

Subject Categories
Behavior and Ethology | Neuroscience and Neurobiology

PATHOGENIC MECHANISMS UNDERLYING THE EARLY EPILEPTIC ENCEPHALOPATHY CDKL5 DISORDER

Judy I-Ting Wang

A DISSERTATION

in

Neuroscience

Presented to the Faculties of the University of Pennsylvania

in

Partial Fulfillment of the Requirements for the

Degree of Doctor of Philosophy

2014

Supervisor of Dissertation

_____

Zhaolan (Joe) Zhou, Ph.D., Assistant Professor of Genetics

Graduate Group Chairperson

_____

Joshua I. Gold, Ph.D., Professor of Neuroscience

Dissertation Committee

Julie A. Blendy, Ph.D., Professor of Pharmacology

Thomas A. Jongens, Ph.D., Associate Professor of Genetics

Stewart A. Anderson, M.D., Associate Professor of Psychiatry

Eric D. Marsh, M.D., Ph.D., Assistant Professor of Neurology and Pediatrics

PATHOGENIC MECHANISMS UNDERLYING THE EARLY EPILEPTIC ENCEPHALOPATHY

CDKL5 DISORDER

ACKNOWLEDGMENT

To my family: Thank you mom, dad, and Michael for your unyielding love and support. Thank you for being my role models and for making home my favorite place to be. Also, thank you for tolerating years of overly vague descriptions of when I will graduate and what I will do with my degree.

To my mentor: Thank you Joe, for believing in me. Thank you for challenging me and instilling in me the confidence to think creatively and boldly. Thank you for your patience and kindness, your generosity in both time and resources, and for supporting me as a scientist and as a person. You have taught me a tremendous amount, and it is an honor to be your first graduate student. I couldn't have imagined a better fit.

To the labmates and neighbors: Thank you for the camaraderie and community. Thank you Darren, for teaching me that all science is made up, for sharing your love for Whitney Houston with me, and for being the Jack Donaghy to my Liz Lemon. Thank you Staci, for co-directing the (very effective) Party Planning Committee with me, for bringing Skipper into my life, and for being an overall amazing friend. Thank you to the CRB 4th floor (mainly Tanya and Hetty) for stealing my money in two World Cup tournaments and years of March Madness madness. I just wanted one win, guys. Just one.

To my thesis committee: Thank you Julie, Tom, Stewart, and Eric, for the discussions, advice, and thoughtful recommendations. Thank you for being a supportive and rational group and for fostering steady progress throughout my training.

To my life committee: Thank you Mikey, for being my sage, advocate, and cheerleader and for humanizing grad school for me. Thank you for always offering me a box of Kleenex, even though I'm almost positive I have never cried in front of you.

To the "Committee": Thank you Alexis, Colleen, and Lauren, for lunches on the steps, 5pm committee meetings at Mad Mex, and getting crunk at NGG events. Thank you for sharing past, present, and future life milestones with me. I expected to make just one friend in grad school, so I'm thankful for the 300% yield.

To the iTunes playlist: Thank you for sustaining me through hours of mouse behaviors, microscope imaging, and data analysis. Thank you NPR, for educational, thought-provoking, and sometimes hilarious podcasts that made me laugh out loud and look like a fool. Thank you Taylor Swift, for releasing 3 albums during my grad school years. I hope the joy that your music has brought me did not skew my data.

To the food: Thank you for the tiny victories of finding leftover sandwiches, snacks, and Diet Coke in the hallways. Thank you Shake Shack, for moving closer to me and for always being worth it. Please bring back crinkle fries.

ABSTRACT

PATHOGENIC MECHANISMS UNDERLYING THE EARLY EPILEPTIC ENCEPHALOPATHY CDKL5 DISORDER

Judy I-Ting Wang

Zhaolan (Joe) Zhou

Cyclin-dependent kinase-like 5 (*CDKL5*) is an X-linked gene associated with early infantile epileptic encephalopathy, atypical Rett Syndrome, and autism spectrum disorders. Patients with *CDKL5* mutations display a heterogeneous array of clinical symptoms, the most prominent of which include early-onset epileptic seizures, intellectual disability, marked hypotonia, and autistic features. Despite the strong genetic linkage between *CDKL5* mutations and neurodevelopmental disorders, the biological function of CDKL5 and its pathogenic mechanisms remain largely uncharacterized. Consequently, treatments for CDKL5 disorder have been largely ineffective and limited to symptom management. This study aims to dissect the molecular and cellular basis of CDKL5 disorder using novel mouse models and to identify signaling pathways that can be targeted for therapeutic development.

To determine the genetic causality of CDKL5 disorder, we generated the first *Cdkl5* knockout (KO) mouse and found that mice lacking CDKL5 mimic key symptoms of CDKL5 disorder, including impaired motor control, poor learning and memory, and autistic-like behaviors. KO mice also show deficits in neural circuit communication and alterations in many signal transduction pathways, but do not develop spontaneous seizures. Previous studies using *in vitro* cell cultures and shRNA-mediated knockdown have implicated CDKL5 in dendritic morphogenesis and the phosphorylation of MeCP2, mutations of which cause Rett Syndrome, but the results of these studies are contentious. Therefore, to understand the *in vivo* function of CDKL5 and to investigate how loss of CDKL5 contributes to epileptic and autistic features, we have generated *Cdkl5* conditional KO mice. Notably, our studies show that selective deletion of *Cdkl5*

from forebrain GABAergic neurons (Dlx-cKO) recapitulates autistic-like phenotypes, whereas selective removal of *Cdkl5* from forebrain glutamatergic neurons (Nex-cKO) results in the development of spontaneous seizures. The separation of distinct aspects of CDKL5 disorder-related phenotypes in the two complementary conditional KO lines suggests that the epileptic and autistic phenotypes of CDKL5 disorder are mediated by distinct neural circuits and that loss of CDKL5 in specific cell types may differentially disrupt signaling pathways and impair neuronal function.

TABLE OF CONTENTS

LIST OF ILLUSTRATIONS

Chapter 2

Chapter 3

Chapter 4

Chapter 5

Chapter 1:

THE PAST, PRESENT, AND FUTURE STATE OF CDKL5 RESEARCH

Mutations in the X-linked gene encoding cyclin-dependent kinase-like 5 (CDKL5) cause CDKL5 disorder, an infantile epileptic encephalopathy with features of intractable seizures, intellectual disability, and autism (Nabbout and Dulac, 2011; Prince and Ring, 2011; Sakai et al., 2011). Historically, CDKL5 disorder has been classified as a variant form of Rett Syndrome (RTT) and consequently, early mechanistic studies were limited to establishing a common pathway linking CDKL5 to MeCP2, the methyl-CpG binding protein underlying RTT (Amir et al., 1999; Bertani et al., 2006; Mari et al., 2005; Rusconi et al., 2008; Tao et al., 2004; Weaving et al., 2004). Emergent clarity in the CDKL5 clinical profile and evidence from recent studies in mouse models, however, have suggested that CDKL5 disorder is a early-onset epileptic encephalopathy that is distinct from Rett Syndrome (Bahi-Buisson et al., 2008b; Fehr et al., 2012) and that its disease mechanism is independent of MeCP2 (Amendola et al., 2014; Chen et al., 2010; Fuchs et al., 2014; Lin et al., 2005; Ricciardi et al., 2012; Wang et al., 2012; Zhu et al., 2013). This chapter aims to introduce the history of CDKL5 disorder and describe the current understanding of CDKL5 disorder, including CDKL5 clinical disease profile, animal models, and cellular functions. It will conclude with a discussion of how these findings have shaped the future challenges for the field.

CDKL5 History

The first report of CDKL5 disorder is credited to Dr. Folker Hanefeld in 1985, who described a patient presenting initially with infantile spasms and later developing symptoms consistent with Rett Syndrome (Hanefeld, 1985), although a *CDKL5* mutation in this patient was never confirmed. When *CDKL5* was initially cloned, it was named *STK9* (serine-threonine kinase 9), and its proximity to genes related to X-linked retinoschisis and Nance Horan Syndrome suggested that it may be a disease-related locus (Montini et al., 1998). It was not until 2003, however, that a link between *CDKL5* mutation and disease was described, in a report of infantile spasms and mental retardation in two patients with balanced autosomal translocations commonly disrupting *CDKL5* (Kalscheuer et al., 2003). In the following year, two independent studies reported that mutations in *CDKL5* are common to the early-onset seizure variant of RTT (Tao et al., 2004; Weaving et al., 2004). Subsequently, cohorts of atypical RTT patients were screened for *CDKL5* mutations (Evans et al., 2005; Mari et al., 2005; Scala et al., 2005). Although RTT and CDKL5 share several clinical features, it is likely that this early link between CDKL5 disorder and RTT has biased CDKL5 diagnosis and biochemical research (discussed below). In the recent years, a broader understanding of the features of CDKL5 patients has revealed that the clinical profile of CDKL5 disorder is distinct from that of Rett Syndrome (Bahi-Buisson et al., 2008b; Guerrini and Parrini, 2012) and therefore, CDKL5 disorder should be classified as a distinct early-onset epileptic encephalopathy (Fehr et al., 2012).

CDKL5 clinical profile

Concomitant with the emergence of clarity in CDKL5 disorder as an epileptic encephalopathy is a steady increase in rate of CDKL5 diagnoses each year, likely due to increased awareness of the disorder. Indeed, the frequency of *CDKL5* mutations in epileptic or autistic cohorts is notably high (Archer et al., 2006; Bahi-Buisson et al., 2008a; Nemos et al., 2009; White et al., 2010), suggesting that the disorder may be more prominent than currently understood, and confirms that CDKL5 disorder is not limited to RTT or atypical RTT populations. To date, less than 200 individuals with *CDKL5* mutations have been described, hampering the formation of a strong genotype-phenotype correlation. Publications from larger cohorts of CDKL5 patients, however, have described common phenotypes and a generalized clinical course for CDKL5 patients.

Distinction from Rett Syndrome

The diagnosis of the early-onset seizure, or Hanefeld, variant of Rett Syndrome requires the fulfillment of a subset of the following main RTT criteria: partial or complete loss of acquired purposeful hand skills and spoken language, gait abnormalities, and stereotypic hand movements, as well as a subset of the following supportive RTT criteria: breathing disturbances, bruxism, impaired sleep pattern, abnormal muscle tone, peripheral vasomotor disturbances, scoliosis, growth retardation, small cold hands and feet, inappropriate laughing/screaming spells, diminished response to pain, and intense eye gaze (Artuso et al., 2010; Neul et al., 2010). In addition, patients must demonstrate a period of regression followed by recovery or stabilization. The majority of CDKL5 patients, however, lack the clear period of regression and intense eye gaze, suggesting a departure from the Rett Syndrome clinical course (Bahi-Buisson et al., 2008b; Guerrini and Parrini, 2012). Indeed, a recent study of 86 CDKL5 patients found that less than 25% of the cohort fulfilled the diagnostic criteria for the early seizure variant of Rett Syndrome (Fehr et al., 2012).

Both the CDKL5 seizure phenotype and the percentage of CDKL5 patients with drug-resistant seizures are dramatically different from that of RTT (Pintaudi et al., 2008). In

RTT, seizures manifest in adolescence, usually decrease in severity after teenage years, and are amenable to therapies, whereas CDKL5 patients develop seizures that are largely intractable within the first few months after birth (Pintaudi et al., 2008). In addition, breathing disturbances and autonomic dysfunction, while reported in CDKL5 disorder, are much less prevalent than in classical RTT (Fehr et al., 2012; Hagebeuk et al., 2013; Pini et al., 2013), and the percentage of males with CDKL5 disorder is much higher than that of RTT (discussed below) (Mei et al., 2014; Mirzaa et al., 2013). Together, these data support CDKL5 disorder as an independent early-onset seizure disorder that is distinct from Rett Syndrome (Fehr et al., 2012).

Features of CDKL5 disorder

The key clinical features that identify CDKL5 patients are early onset seizures that develop into intractable epilepsy and result in severe intellectual disability (Archer et al., 2006; Artuso et al., 2010; Bahi-Buisson et al., 2008a; 2008b; 2010; 2012; Bartnik et al., 2011; Bertani et al., 2006; Boutry-Kryza et al., 2014; Castrén et al., 2011; Córdova-Fletes et al., 2010; Das et al., 2013; Elia et al., 2008; Erez et al., 2009; Ermel et al., 2013; Evans et al., 2005; Grosso et al., 2007; Guerrini and Parrini, 2012; Hadzsiev et al., 2011; Hagebeuk et al., 2013; Intusoma et al., 2011; Jähn et al., 2013; Kalscheuer et al., 2003; Klein et al., 2011; Liang et al., 2011; Maortua et al., 2012; Masliah-Plachon et al., 2010; Mei et al., 2014; 2010; Melani et al., 2011; Mirzaa et al., 2013; Nectoux et al., 2006; Nemos et al., 2009; Pini et al., 2013; Psoni et al., 2010; Rademacher et al., 2011; Raymond et al., 2013; Rosas-Vargas et al., 2008; Russo et al., 2009; Saitsu et al., 2012; Sartori et al., 2009; Scala et al., 2005; Sprovieri et al., 2009; Stalpers et al., 2011; Tao et al., 2004; Van Esch et al., 2007; Veeramah et al., 2013; Weaving et al., 2004; White et al., 2010; Willemsen et al., 2012; Wong and Kwong, 2014; Zhao et al., 2014). The majority of CDKL5 patients also show poor acquisition of language, hypotonia, and limited hand skills (Bahi-Buisson and Bienvenu, 2012; Bahi-Buisson et al., 2008b). Hand stereotypies, aberrant gait, sleep disturbances, and autistic phenotypes, including avoidance of eye gaze and reduced social interaction, are common (Bahi-Buisson et al., 2008b; Fehr et al., 2012) and some breathing abnormalities and autonomic dysfunction have been reported. Although the physical features of CDKL5 patients are fairly heterogeneous, subtle dysmorphisms including deep sunken eyes with straight and well-

defined eyebrows, a prominent or broad forehead, high hairline, and full lips have been described (Archer et al., 2006; Fehr et al., 2012).

Approximately 20% of reported cases of CDKL5 disorder are in boys (Elia et al., 2008; Liang et al., 2011; Masliah-Plachon et al., 2010; Mei et al., 2014; Mirzaa et al., 2013; Wong and Kwong, 2014). This small percentage may reflect the reduced probability of X-chromosome mutations in males relative to females, or it may be the consequence of an RTT-biased low ascertainment. Strikingly, however, this percentage is higher than that of boys diagnosed with RTT, suggesting that *CDKL5* mutations may be better tolerated in males than *MECP2* mutations. Boys with *MECP2* mutations rarely show RTT-like phenotypes, as they usually develop severe early postnatal encephalopathy and die shortly after birth (Kankirawatana et al., 2006). In contrast, boys with *CDKL5* mutations show a similar (Bahi-Buisson et al., 2008b; Elia et al., 2008; Liang et al., 2011; Mei et al., 2010; Nemos et al., 2009), or in some cases, more severe phenotype (Fehr et al., 2012; Mirzaa et al., 2013) relative to that of girls. Whether the CDKL5 clinical course is actually more severe in males has yet to be determined, owing the small number of CDKL5 patients overall. Regardless, it is clear that the CDKL5 clinical profile in boys is markedly different from that of RTT.

Descriptions of the adult CDKL5 phenotype are similarly limited by the small patient population. A 2011 review comprised of 10 female CDKL5 patients ages 18-47 showed intractable seizures and motor impairment in all 10 patients and concluded that adult CDKL5 patients show poor developmental and seizure outcome (Willemsen et al., 2012). As the prevalence of regression, autonomic disturbances, breathing abnormalities, and scoliosis appears to increase with age (Fehr et al., 2012), it is likely that the adult CDKL5 clinical profile includes multiple persistent handicaps.

Epilepsy

Epilepsy in CDKL5 patients spans a broad phenotypic range, depending on the severity of CDKL5 disorder. Milder forms involve seizures that are amenable to control with the possibility of autonomous walking, whereas severe forms involve intractable seizures lasting into adulthood, severe microcephaly, and absence of autonomous motor function

(Guerrini and Parrini, 2012; Jähn et al., 2013). On average, the onset of seizures occurs within 2 months after birth, and the majority of patients experience seizures daily (Fehr et al., 2012). Some patients experience seizures weekly or monthly, and a small number of patients report having seizures on a frequency of once a year or less.

Seizure types vary across individuals, and include infantile spasms (Weaving et al., 2004), brief subtle seizures evolving into choking or breath-holding (Archer et al., 2006), and partial and multifocal seizures, with tonic, myoclonic, atonic, and generalized tonic-clonic features (Mirzaa et al., 2013). The majority of MRIs are normal in CDKL5 patients, with scattered reports of white matter hyperintensities in temporal poles and dentate nuclei, as well as cerebellar atrophy (Bahi-Buisson et al., 2008b), and some reports of frontal lobe cerebral atrophies (Liang et al., 2011).

A spectrum of EEG patterns has been described, with some reports of hysparrythmia (Jähn et al., 2013), multifocal paroxysmal activity (Grosso et al., 2007), multifocal bursts of polyspike activity (Mirzaa et al., 2013), slow background, and continuous bihemispheric epileptiform discharges (Moseley et al., 2012). Despite this broad heterogeneity, some distinctive CDKL5 EEG patterns have been described. One study has proposed that the first year of CDKL5-related epilepsy may be characterized by a "prolonged generalized tonic-clonic" electroclinical pattern. In this pattern, seizures progress from tonic-tonic/vibratory contraction to clonus to spasms and gradually to rhythmic distal myoclonic jerks (Melani et al., 2011). Although this motor sequence is not associated with a specific EEG pattern, its relevance toward clinical diagnosis of CDKL5 disorder in infants has been suggested (Arts, 2011).

A distinctive seizure type in adolescents involving a hypermotor-tonic-spasms sequence characterized by distinct motor and EEG patterns has also been identified (Klein et al., 2011). The hypermotor phase, lasting 10-60 seconds, consists of rocking, kicking, and/or vocalization with delta waves; the tonic phase, lasting 20-45 seconds, consists of extension of all limbs with fast EEG; and the spasms phase, lasting 1-15 minutes, consists of extensor spasms with high voltage sharp complexes.

Another distinctive seizure pattern that has been described is a “three-stage epilepsy” (Bahi-Buisson et al., 2008a). The first stage, classified as “early epilepsy,” manifests as generalized convulsive seizures in a neurologically delayed baby with poor eye contact and axial hypotonia. The second stage, classified as “epileptic encephalopathy,” includes a “honeymoon” seizure-free period, developmental arrest, epileptic encephalopathy with infantile spasms, and hypsarrhythmia. The last stage, classified as “late multifocal and myoclonic epilepsy,” differs according to patient outcome, manifesting as fewer seizures and occurrence of physiological EEG features in patients with a favorable outcome, and refractory epilepsy with tonic seizure and myoclonia in patients with an unfavorable outcome. How accurately these seizure patterns describe the general CDKL5 population, however, will require more case reports, as they were identified in cohorts of 5 (Klein et al., 2011) and 12 patients (Bahi-Buisson et al., 2008a), respectively.

Neuropathology

Neuropathological data has been limited to a single study to date, a female with an exon 16 splice site mutation who was diagnosed with infantile spasms and atypical Rett Syndrome (Paine et al., 2012). Post-mortem histological examination showed significant abnormalities only in the central nervous system, particularly flatted occipital lobes and enlarged lateral and 3rd ventricles. The majority of pathological findings were in the cerebellum, where heterotopias in vermis white matter and gliosis in the Purkinje cell layer were identified. Degeneration was evident in the cerebellum and vermis, but whether this was a consequence of disease progression or seizure treatment was unknown. More neuropathological data is required to determine how generalizable these findings will be to the CDKL5 patient population. Of particular interest would be descriptions of neuronal migration and outgrowth in CDKL5 patients, as both are altered in CDKL5 mouse studies (Amendola et al., 2014; Chen et al., 2010; Ricciardi et al., 2012). The authors of this neuropathological study did not report any such findings (Paine et al., 2012), but it is unclear whether these phenotypes were investigated in detail.

Treatments

CDKL5 seizures are largely intractable and current treatments target symptom management, rather than disease mechanism (Bahi-Buisson and Bienvenu, 2012). The majority of prescribed therapeutics aim to reduce seizure frequency, but are largely ineffective (Bahi-Buisson and Bienvenu, 2012). Common anti-epileptic drugs include topiramate, valproate, and vigabatrin, and in some patients, a ketogenic diet and vagus nerve stimulators have demonstrated some efficacy (Evans et al., 2005; Moseley et al., 2012; Tao et al., 2004). The current limited understanding of the biological function of CDKL5 and of the mechanisms underlying disease pathogenesis has impeded the development of targeted therapeutics. Therefore, the identification of signaling pathways and proteins regulated by CDKL5 as well as the cell types and neural circuits in which CDKL5 functions is key to advancement in the treatment of CDKL5 disorder.

CDKL5 genetics

CDKL5 mutations

CDKL5 translocations, deletions, insertions, and missense mutations have been linked to disease (Bahi-Buisson and Bienvenu, 2012), and more than half of *CDKL5* patient mutations are located within the highly conserved kinase domain, suggesting that many *CDKL5* mutations disrupt kinase function. Due to the small number of CDKL5 patients to date and the mosaic expression of CDKL5 in females, a strong genotype-phenotype correlation has yet to be formed. Mutations in the N-terminal kinase domain, however, have been proposed to be more severe than mutations in the C-terminus (Bahi-Buisson et al., 2012). Furthermore, the pathogenicity of mutations in exons 22-23 has been questioned, as several *CDKL5* patient mutations in these regions have also been identified in healthy siblings or parents (Diebold et al., 2013). Because these exons are not conserved in lower organisms, including rodents, mutations in this region of the C-terminus have been proposed to be normal genetic variations or polymorphisms.

A small number of recurrent *CDKL5* mutations have been identified, but they do not appear to cluster within a specific region of the gene (Mastrangelo and Leuzzi, 2012). In addition, clinical phenotypes among patients with recurrent mutations are heterogeneous. For example, patients with the most common recurrent mutation, the A40V missense mutation, range from having severe epileptic encephalopathy to mild RTT-like phenotypes (Bahi-Buisson et al., 2012; Nemos et al., 2009).

Other mutation types, including somatic mosacism and gene duplications, have been reported in both boys and girls with CDKL5 disorder, suggesting that CDKL5 protein levels are also relevant to disease. Patients with somatic mosaic *CDKL5* mutations display early-onset seizures (Bartnik et al., 2011; Boutry-Kryza et al., 2014; Masliah-Plachon et al., 2010; Mei et al., 2014) whereas *CDKL5* duplications have been associated with autism and intellectual disability, but not epilepsy (Froyen et al., 2007; Szafranski et al., 2014; Thorson et al., 2010). CDKL5 dosage regulation has also been implicated in studies of balanced chromosomal abnormalities (BCAs) (Talkowski et al., 2012), where *CDKL5* has been identified as a BCA hotspot, and both deletion and duplication of *CDKL5* are associated with autism spectrum disorder.

Reports of skewed X-chromosome inactivation in CDKL5 patients are rare, but because X-chromosome inactivation is measured from peripheral blood samples, it is difficult to determine whether the same ratio is found in the brain. Skewed X-chromosome inactivation has been proposed to explain the cases of more severe CDKL5 patients or differing phenotypes in monozygotic twins or family members sharing the same mutation (Bahi-Buisson et al., 2008a; 2008b; Kalscheuer et al., 2003; Mirzaa et al., 2013; Weaving et al., 2004). Conversely, it is believed that skewed X-chromosome inactivation can be protective, particularly in the cases of *CDKL5* mutations that are present in both affected proband and unaffected family members (Szafranski et al., 2014; Wong and Kwong, 2014).

CDKL5 isoforms

The *CDKL5* gene (OMIM 300203), located in the Xp22.13 region, was originally cloned in a transcriptional mapping experiment in 1998. It was initially named serine-threonine kinase 9 (*STK9*), due to its homology to the catalytic domain of other serine-threonine kinases (Montini et al., 1998). It later became more commonly known as cyclin-dependent kinase-like 5 (*CDKL5*), due to the homology of its kinase domain to other cyclin-dependent kinases.

The *CDKL5* gene spans ~240kb and encodes 23 exons. The first three exons are noncoding (exon 1, 1a, and 1b), and the remaining 20 exons encode a 1030 amino acid protein product (Kalscheuer et al., 2003). The full-length CDKL5 protein is translated from two RNA isoforms, which differ in their 5' UTR but produce the same 115 kDa protein. *CDKL5* isoform I contains exon 1 and is expressed in a wide range of tissues and cell lines, whereas *CDKL5* isoform II contains exons 1a and 1b and is expressed only in the testis and fetal brain tissue (Kalscheuer et al., 2003).

In the recent years, other isoforms of CDKL5 and an additional coding exon have been identified. In 2011, a 123-bp interval between exons 16 and 17 with conserved sequence homology across multiple species was identified in two independent studies (Fichou et al., 2011; Rademacher et al., 2011). The novel exon, referred to as exon 16a or16b, is expected to encode a 41-aa product, thus producing a 1071-aa full-length

CDKL5 protein. Although the variant transcript was unable to be detected by *in situ* hybridization or Northern blot, quantitative RT-PCR showed low levels of transcript in the brains of adult mice, suggesting that this variant, if in existence, has a brain-specific function.

A truncated CDKL5 isoform terminating in intron 18 has also been identified and is predicted to encode a 107 kDa protein (Williamson et al., 2011). RT-PCR data indicates that the transcript encoding the 115 kDa protein is expressed primarily in the testis, whereas the novel transcript encoding the 107 kDa protein product is the predominant transcript in the brain. This expression pattern, however, has yet to be demonstrated at the protein level, and the *in vivo* relevance of the brain-specific truncated CDKL5 isoform remains unclear.

Animal models of CDKL5 disorder

Despite the strong clinical data supporting a link between mutations in *CDKL5* and neurodevelopmental disorder, the monogenic etiology underlying CDKL5 disorder was not established until the development and characterization of the first knockout mouse model in 2012 (Chapter 2) (Wang et al., 2012). In this study, we generated a mouse model recapitulating a CDKL5 patient mutation and identified clinically relevant behavioral phenotypes, impaired sensory information processing, and disruptions in multiple signaling pathways.

Specifically, we modeled our mice after a patient splice site mutation that leads to a premature stop codon in exon 8 (Archer et al., 2006). In order to mimic the effects of this mutation in mice, we deleted the homologous mouse *Cdkl5* exon 6, leading to an early truncation of CDKL5 in its N-terminal kinase domain, thereby disrupting kinase activity. Importantly, in CDKL5 knockout (KO) animals, truncated or full-length CDKL5 cannot be detected by Western blot using antibodies directed against CDKL5 N- or C-terminal domains, and *Cdkl5* transcript levels are dramatically reduced, likely due to nonsense-mediated mRNA decay (Wang et al., 2012).

Given the clinical relevance of CDKL5 disorders in males and the confounding effects of mosaic CDKL5 expression from X-chromosome inactivation in females, we necessarily constrained our study to male CDKL5 knockout mice (Wang et al., 2012). CDKL5 KO mice are viable and fertile, and we observed no gross anatomical or developmental abnormalities. Behavioral characterization, however, showed that CDKL5 KO mice mirror multiple symptoms associated with CDKL5 disorder, including impaired motor control on the rotarod, deficits in learning and memory on a fear conditioning assay, and hindlimb and forelimb clasping, a phenotype believed to mimic patient hand wringing. CDKL5 KO animals also demonstrate autistic-like deficits in sociability on a three-chambered social approach assay and in home-cage nesting behavior. Given the prominence of motor impairment, intellectual disability, and autism in CDKL5 disorder, these data support face validity in our CDKL5 KO mouse and established, for the first time, a causal relationship between *Cdkl5* mutation and disease phenotypes using a genetic mouse model.

Recently, a similar CDKL5 mouse model, a *Cdkl5* exon 4 deletion, was developed and characterized (Amendola et al., 2014). Importantly, these mice showed deficits in the Akt-S6 and Akt-GSK3b signaling pathways (Amendola et al., 2014; Fuchs et al., 2014), supporting a convergent deficit in downstream PTEN signaling (Wang et al., 2012). In addition, these mice demonstrate many phenotypes that are consistent with our mouse model, including hindlimb clasping, impaired working memory, and deficits in visual-evoked ERPs.

Deficits in neuronal outgrowth and postmitotic cell proliferation were identified in these KO mice. BrdU labeling of postmitotic dentate granule cells showed a transient increase in proliferation in CDKL5 KO mice relative to that of WT (Fuchs et al., 2014). These cells, however, were later preferentially targeted for apoptotic cell death and showed dendritic hypotrophy, resulting in a net reduction in the total number and growth of newborn dentate neurons in CDKL5 KO mice. No effect was found on gliogenesis, indicating that CDKL5 regulation is specific to neurons. In addition, neuronal tracing of GFP-labeled cells in adult CDKL5 KO mice showed reduction in dendritic length of both cortical layer 5 and hippocampal pyramidal neurons, accompanied by reduced cortical and hippocampal thickness (Amendola et al., 2014). Whether CDKL5 regulates neuronal outgrowth in a cell autonomous manner has yet to be determined. Moreover, the role of CDKL5 in adult neurogenesis, and its relation to the role of CDKL5 during neuronal development remains unknown.

Surprisingly, despite extensive video-EEG monitoring, neither CDKL5 KO mouse model developed spontaneous seizures or reduced seizure threshold in both C57BL/6 and DBA/2J genetic backgrounds (Amendola et al., 2014; Wang et al., 2012). Although CDKL5 KO mice showed altered EEG patterns following seizure induction (Amendola et al., 2014), the absence of this key phenotype has raised questions concerning the differences between human and mouse and challenged the usefulness of the constitutive KO mouse model. Therefore, the development of additional CDKL5 mouse models that recapitulate the seizure phenotype will be necessary to understand mechanisms underlying CDKL5 seizures.

What the two CDKL5 KO models do reveal, however, is that even in mice, CDKL5 disorder has a distinct disease profile from that of Rett Syndrome. Although disruptions in ERPs and Akt-mTOR signaling have been identified in both RTT and CDKL5 mouse models (Goffin et al., 2012; Ricciardi et al., 2011; Wang et al., 2012), these commonalities may reflect convergence in ASD genetics and molecular pathology (Bill and Geschwind, 2009; Geschwind, 2011; Voineagu et al., 2011) that are mediated by distinct cellular mechanisms, which will be discussed in the next section.

In addition to animal models, recent advances in the development of induced pluripotent stem cells (IPSCs) derived from human fibroblasts that can be differentiated into distinct cell types have introduced a new tool in which cellular function and gene regulation can be studied in a disease setting (Takahashi et al., 2007). IPSCs derived from CDKL5 patients show increased filipodial-type spines and reduced number of synaptic puncta, but fail to recapitulate the deficit in neuronal outgrowth identified in mouse models (Ricciardi et al., 2012). In a separate study, a small number of genes with altered expression have been identified in CDKL5 iPSCs, including the orphan glutamate receptor GRID1, but the functional relevance of these findings has yet to be determined (Livide et al., 2014). Overall, data from patient-derived IPSCs will be very beneficial for CDKL5 research, but the significance of these findings will require more integration in animal model studies.

CDKL5 protein

Expression pattern

Although several laboratories have characterized the time course of CDKL5 expression, these studies have often yielded inconsistent results, even when using similar experimental techniques. RNA *in situ* hybridization experiments were unable to detect embryonic *Cdkl5* expression in one study (Montini et al., 1998), but detected weak expression late embryonically in a separate study (Mari et al., 2005). Immunostaining of whole embryos showed broad CDKL5 expression in early embryogenesis in one study (Lin et al., 2005), whereas in a separate study, immunostaining of E16.5 slices showed minimal CDKL5 expression (Rusconi et al., 2008). Western blot data has been similarly conflicted, showing onset of CDKL5 expression late embryonically (Chen et al., 2010) or postnatally (Rusconi et al., 2008; Zhu et al., 2013) in different studies.

Similar to that of the CDKL5 time course, data supporting CDKL5 expression levels in organs including the heart, liver, spleen and lungs remains inconsistent (Chen et al., 2010; Lin et al., 2005). Multiple studies show consistently that CDKL5 is highly expressed in the brain. Within the brain, however, some *in situ* hybridization studies show *Cdkl5* enrichment throughout the brain (Chen et al., 2010; Mari et al., 2005; Weaving et al., 2004), while other *in situ* data show *Cdkl5* enrichment specifically in the forebrain (Thompson et al., 2014). The forebrain-specific enrichment is supported by Western blot data from our lab and others (Rusconi et al., 2008; Wang et al., 2012). Immunostaining of primary cultures indicates that CDKL5 is expressed in glutamatergic and GABAergic neurons, but not in glial cells (Rusconi et al., 2008; 2011), whereas a separate study has found a distinct CDKL5 isoform that is expressed in glia (Chen et al., 2010).

Early *in vitro* studies localized CDKL5 exclusively to the cell nucleus (Bertani et al., 2006; Lin et al., 2005). Later studies proposed that CDKL5 mislocalizes to the cytoplasm in disease (Bertani et al., 2006; Rosas-Vargas et al., 2008), is shuttled into the cytoplasm upon glutamate stimulation in excitatory cells (Rusconi et al., 2011), or is expressed in the cytoplasm in certain brain regions (Rusconi et al., 2008). Upon fractionation of nuclear and cytoplasmic proteins from the brains of WT mice followed by

Western blots, however, we and others have found that endogenous CDKL5 under basal conditions exists primarily in the cytoplasm, and not in the nucleus (Chen et al., 2010; Wang et al., 2012).

The inconsistencies related to the time course and distribution of CDKL5 may be partially attributed to differences in experimental methods and ineffective reagents. Indeed, immunostaining of both WT and CDKL5 KO brain tissue using commercially available and in-house generated CDKL5 antibodies yield a similar staining pattern, and Western blots of WT and CDKL5 brain lysate probed with these antibodies yields several non-specific bands (Wang et al., 2012). Due to the persistent bias in early CDKL5 research toward establishing a mechanistic link between CDKL5 and MeCP2, CDKL5 expression patterns were believed to mimic that of MeCP2, both within the cell and across brain development (Bertani et al., 2006; Lin et al., 2005; Mari et al., 2005). Recent compelling evidence from animal models across different laboratories, however, consistently show that the CDKL5 expression pattern is distinct from that of MeCP2, and that CDKL5 is expressed postnatally and mainly or exclusively in the cytoplasm (Chen et al., 2010; Ricciardi et al., 2012; Wang et al., 2012), an expression pattern that supports the current understanding of CDKL5 disorder as an independent epileptic encephalopathy with a distinct disease mechanism.

Function

Whereas data supporting CDKL5 time course and expression pattern is merely inconsistent, data supporting CDKL5 function is contentious. Several postulated mechanisms, some of which stem from the same experimental methods, are in direct opposition, including the role of CDKL5 in phosphorylation of MeCP2 (Lin et al., 2005; Mari et al., 2005), in regulation of neuronal outgrowth (Amendola et al., 2014; Chen et al., 2010; Fuchs et al., 2014; Ricciardi et al., 2012) and in dendritic spine development (Ricciardi et al., 2012; Zhu et al., 2013).

The first of these, the role of CDKL5 in the phosphorylation of MeCP2, is likely a consequence of the aforementioned Rett Syndrome bias in the early years of CDKL5 research. The phenotypic similarities between RTT and CDKL5 patients and the

discovery that MeCP2 is regulated by phosphorylation (Chen et al., 2003; Zhou et al., 2006), suggested that the two disorders may share a common pathway, wherein the putative kinase CDKL5 phosphorylates MeCP2. To this end, *in vitro* studies showed that overexpressed CDKL5 localizes to the nucleus (Lin et al., 2005) and that CDKL5 interacts with and phosphorylates MeCP2 (Mari et al., 2005). Subsequent studies, however, have challenged this hypothesis, and showed that CDKL5 phosphorylation of MeCP2 is indirect or nonspecific (Lin et al., 2005) and that CDKL5 does not localize with MeCP2-enriched heterochromatic foci (Ricciardi et al., 2009).

In addition to the contentious link to MeCP2 phosphorylation, the early belief that CDKL5 localizes exclusively to the nucleus led to other proposed nuclear functions identified *in vitro*, including phosphorylation of DNA methyl-transferase 1 (Dnmt1) (Kameshita et al., 2008) and regulation of RNA splicing factor-enriched nuclear speckles (Ricciardi et al., 2009). The *in vivo* relevance of these functions, however, has yet to be determined or confirmed.

As CDKL5 expression is now largely believed to be primarily cytoplasmic, research focus has shifted toward its particular function in excitatory neurons. This shift began in 2010, when shRNA-mediated knockdown of *Cdkl5* in primary neuronal cultures was shown to reduce neuronal outgrowth (Chen et al., 2010). *In utero* electroporation of the same shRNA construct not only reduced neuronal outgrowth *in vivo*, but also delayed neuronal migration. These authors showed evidence that cytoplasmic CDKL5 may regulate neuronal outgrowth and migration by complexing with Rac1, a known regulator of actin dynamics and neuronal morphology, thereby mediating Bdnf-dependent Rac1 signaling.

A separate study using the same method of *in utero* electroporation of an shRNA construct targeting *Cdkl5*, however, has challenged the role of CDKL5 in dendritic outgrowth. These authors were able to replicate delayed neuronal migration but not reduced dendritic outgrowth upon CDKL5 knockdown (Ricciardi et al., 2012). Instead of a dendritic phenotype, these authors found a spine development phenotype, where CDKL5 knockdown increases the density and length of dendritic spines. In primary hippocampal cultures, CDKL5 knockdown also increased density of spines but reduced

the number of excitatory synapses and both amplitude and frequency of mEPSCs, pointing to a role for CDKL5 in spine maturation. Furthermore, immunostaining data showed that CDKL5 is localized exclusively to excitatory synapses and not to inhibitory synapses, indicating that loss of CDKL5 impairs excitatory synapse development and results in the formation of more immature-type dendritic spines. These authors showed evidence supporting a mechanism by which CDKL5 directly phosphorylates NGL-1, a netrin-G1 receptor that regulates early synapse formation and maturation, and thus promotes an NGL-1—PSD95 interaction in order to stabilize dendritic spines (Ricciardi et al., 2012).

The mechanism by which CDKL5 localizes to dendritic spines, however, has also been challenged, as a recent study has shown that CDKL5 binds directly to palmitoylated PSD95, that this binding is independent of CDKL5 kinase function, and that it is the CDKL5-PSD95 direct interaction that recruits CDKL5 to excitatory spines (Zhu et al., 2013). Moreover, while the authors of this study used the same method of shRNA-mediated knockdown of *Cdkl5* and were able to replicate the decrease in excitatory synapse number and reduction in mEPSC amplitude and frequency identified by Ricciardi and colleagues (Ricciardi et al., 2012), they found a decrease, rather than an increase in spine density and width, and suggested a disease mechanism by which loss of CDKL5 inhibits both spine formation and growth (Zhu et al., 2013).

Overall, the shift in research focus from a nuclear role for CDKL5 that is relevant to MeCP2 and Rett Syndrome to a cytoplasmic role in regulation of neuronal development and migration represents great progress in understanding the biological function of CDKL5 and its disease mechanisms. Several uncertainties remain, including how CDKL5 is recruited to excitatory synapses and how neuronal outgrowth is affected upon *Cdkl5* loss-of-function. In addition, the mechanistic relevance or *in vivo* significance of other putative cytoplasmic functions, including phosphorylation of amphiphysin (Amph1) (Sekiguchi et al., 2013), which is proposed to regulate the Amph1-endophlin interaction and affect clatherin-mediated endocytosis, has yet to be determined.

CDKL5-related signaling pathways and neuronal circuits

Given the contentious data supporting CDKL5 kinase substrates, we took an unbiased approach to screen for signaling pathways disrupted in CDKL5 KO mice (Wang et al., 2012). Through a kinome profiling assay, we identified a large number of disruptions in signaling pathways, including the Akt-mTOR pathway, that were specific to the forebrain regions in which CDKL5 is enriched and minimal in the hindbrain regions of low CDKL5 expression. In addition, we observed that many of the identified pathways converge into downstream PTEN signaling, a pathway that has been implicated in both autism and epilepsy (Zhou and Parada, 2012), suggesting that PTEN downstream signaling pathways may be candidate therapeutic targets with *in vivo* relevance.

We also performed neurophysiological recordings in WT and CDKL5 KO mice and found that behavioral phenotypes demonstrated by CDKL5 KO mice may be mediated by deficits in neural circuit communication (Wang et al., 2012). Delayed and attenuated polarity peaks in auditory-evoked event-related potential (ERP) waveforms of CDKL5 KO mice revealed impairments in the strength and timing of cognitive processing in these mice (Roberts et al., 2010; Stauder et al., 2006). In addition, reduced oscillatory strength in event-related low-frequency neuronal oscillations in CDKL5 KO mice indicate ASD-like impairments in long-range circuit communication (Dawson et al., 1995; Stroganova et al., 2007). Together, these data support a disease mechanism by which *Cdkl5* loss-of-function disrupts multiple signaling pathways, leading to dysregulation of neuronal circuits and behavioral impairments. Figure studies will aim to dissect the particular signaling pathways and neural circuits in which CDKL5 plays a role.

Regulation of CDKL5

How CDKL5 itself is regulated is poorly understood and has been investigated across scattered studies. Reports include CDKL5 regulation by the oncogene MYCN (Valli et al., 2012), DNA methylation, or MeCP2 binding (Carouge et al., 2010). CDKL5 also may be regulated by cell death pathways, as both sustained glutamate activation of extrasynaptic NMDA receptors and hydrogen peroxide promote CDKL5 proteosomal degradation (Rusconi et al., 2011).

Future directions

Despite the advancements made in the CDKL5 field within the past 15 years, including cloning the *CDKL5* gene, establishing the link between *CDKL5* mutation and disease, generating CDKL5 animal models with face validity, and gaining insight into putative mechanisms underlying CDKL5 function and dysfunction, a number of questions still remain.

Classification of CDKL5 disorder has evolved from Infantile Spasms to Atypical Rett Syndrome, and finally to Epileptic Encephalopathy. To date, about 200 patients have been diagnosed with CDKL5 disorder, but whether this low prevalence is an accurate reflection of the global pervasiveness of CDKL5 disorder has yet to be determined. Certainly, the early Rett Syndrome bias has resulted in consideration of CDKL5 disorder mainly in RTT patient cohorts (Das et al., 2013; Evans et al., 2005; Hadzsiev et al., 2011; Huppke et al., 2005; Li et al., 2007; 2009; Maortua et al., 2012; Rademacher et al., 2011; Rajaei et al., 2011; Scala et al., 2005; Tao et al., 2004; Weaving et al., 2004; White et al., 2010). How significantly this bias has limited CDKL5 diagnosis will be determined in the upcoming years, as genetic testing for CDKL5 disorder becomes more efficient and expands to epileptic and autistic patient populations (Archer et al., 2006; Bahi-Buisson et al., 2010; Bartnik et al., 2011; Elia et al., 2008; Erez et al., 2009; Fehr et al., 2012; Intusoma et al., 2011; Liang et al., 2011; Mei et al., 2010; 2014; Mirzaa et al., 2013; Nectoux et al., 2011; Nemos et al., 2009; Psoni et al., 2010; Saitsu et al., 2012; Veeramah et al., 2013).

The severity of CDKL5 disorder in boys with *CDKL5* mutations remains unclear. It seems likely that the RTT bias has given rise to low male patient ascertainment, and perhaps selected for male CDKL5 patients with particular phenotypes. Therefore, how the CDKL5 disease profile differs between males and females and whether the disease is actually less prevalent in males than in females will require more detailed analysis of male CDKL5 patients in the future. Similarly, the establishment of a general CDKL5 genotype-phenotype correlation, as well as a characteristic EEG/seizure pattern, will require more patient data.

Neuropathological studies in post-mortem CDKL5 tissue will be useful in the future, not only to identify sites of disease pathogenesis and discover new diagnostic targets, but also to corroborate findings from animal studies. Currently, whether neuronal migration or morphology is impaired in CDKL5 patients has yet to be investigated. Given that developmental abnormalities have been reported by multiple groups (Amendola et al., 2014; Chen et al., 2010; Fuchs et al., 2014; Ricciardi et al., 2012; Zhu et al., 2013), establishing whether this phenotype is clinically relevant will prioritize future studies in this direction.

The development of CDKL5 animal models has not only revealed the role of CDKL5 in neuronal development, but also established a causal relationship between mutations in *Cdkl5* and disease etiology. Mice lacking CDKL5 mirror a number of clinical phenotypes, including impaired motor control, reduced learning and memory, and autistic-like behaviors (Amendola et al., 2014; Fuchs et al., 2014; Wang et al., 2012). Surprisingly, however, these mice do not develop spontaneous seizures, nor do they show a reduction in seizure threshold (Amendola et al., 2014; Wang et al., 2012). Given the severity and relevance of seizures in CDKL5 patients, the absence of the seizure phenotype challenges the usefulness of the constitutive CDKL5 KO mouse model and necessitates the development of a CDKL5 animal model that can faithfully recapitulate spontaneous seizures and subsequently be used to investigate seizure-related disease pathogenesis.

One CDKL5 mouse model with great potential to investigate disease pathogenesis is a conditional CDKL5 knockout mouse (see Chapter 3). Recent conditional knockout mouse studies have demonstrated that distinct neuronal subpopulations control different neural circuits, and that selective perturbation of these circuits can cause discrete behavioral phenotypes (Hong et al., 2014; Ozkan et al., 2014), some of which are not manifested in the constitutive knockout (Chao et al., 2010; Goffin et al., 2014). Therefore, the development of a conditional CDKL5 knockout mouse line may provide specific mechanistic insight that otherwise could not be obtained from the constitutive knockout mouse.

An imbalance in neuronal excitation and inhibition has been commonly proposed to underlie both ASDs and epilepsy, both of which are prominent in CDKL5 disorder. Therefore, it is possible that in CDKL5 patients, a shift in neuronal E/I balance results in seizures and autistic behaviors, and that in mice, selective ablation of CDKL5 from excitatory or inhibitory neurons would similarly shift E/I balance, producing exaggerated behavioral phenotypes that are somehow occluded in the constitutive knockout. Indeed, mice lacking CDKL5 from excitatory neurons show hindlimb clasping, whereas mice lacking CDKL5 from GABAergic neurons show homecage hypoactivity (Amendola et al., 2014), but a comprehensive behavioral assessment of these conditional knockouts has yet to be completed (see Chapter 3). The development and full characterization of excitatory or inhibitory CDKL5 conditional knockout mice would be a tremendous asset for the CDKL5 research field, not only in providing novel mouse models but also in isolating the neuronal circuits and cell types underlying disease pathogenesis.

Excitatory or inhibitory neuron conditional CDKL5 knockout mice will be useful in determining whether CDKL5 regulates neuronal development in a cell autonomous manner. Studies in constitutive CDKL5 KO animals suggest that loss of CDKL5 impairs excitatory neuron outgrowth (Amendola et al., 2014), but whether this deficit is mediated by loss of CDKL5 from the excitatory neurons themselves or the surrounding inhibitory neurons has yet to be determined. In addition, how loss of CDKL5 affects spine development *in vivo* remains unknown, as CDKL5 knockdown studies using the same experimental method have resulted in the development of more immature-type spines (Ricciardi et al., 2012) or fewer total spines (Zhu et al., 2013). As loss of Erbb4 from inhibitory neurons has been found to reduce spine density of excitatory neurons (Del Pino et al., 2013), it is important to determine the *in vivo* spine phenotype upon loss of CDKL5 and to discern the cell types regulating spine development. Moreover, additional studies will need to clarify the molecular mechanism by which CDKL5 localizes to dendritic spines, whether is it through direct interaction with PSD95 (Zhu et al., 2013) or indirectly through phosphorylation of NGL-1 (Ricciardi et al., 2012). Increased understanding of this mechanism will illuminate whether CDKL5 functions *in vivo* primarily as a kinase or in a kinase-independent role.

As a kinase, CDKL5 was believed to phosphorylate MeCP2 (Bertani et al., 2006; Mari et al., 2005), but conflicting data (Lin et al., 2005) and mounting evidence toward a cytoplasmic role for CDKL5 in neuronal development and synapse maturation (Chen et al., 2010; Ricciardi et al., 2012; Zhu et al., 2013) suggests that the CDKL5 biological function is independent from MeCP2, and that the phenotypic commonalities between the disorders may be due to convergent ASD molecular pathology (Bill and Geschwind, 2009; Geschwind, 2011; Voineagu et al., 2011). Indeed, impaired Akt signaling was found in 3 independent studies from CDKL5 KO mice, and our kinome profiling data revealed disruptions in multiple signaling pathways in CDKL5 KO mice (Amendola et al., 2014; Fuchs et al., 2014; Wang et al., 2012), although whether these pathway disruptions are primary or secondary effects of loss of CDKL5 has yet to be determined. Interestingly, the Akt-mTOR, Akt-S6, Akt-GSK3b, and AMPK, and MAPK pathways converge into signaling pathways downstream of PTEN, and disruptions in PTEN signaling have been described in both autism and epilepsy, (Clipperton-Allen and Page, 2014; Costa-Mattioli and Monteggia, 2013; Gkogkas et al., 2012; Santini et al., 2013; Zhou and Parada, 2012). These data suggest that CDKL5 may play a role in PTEN signaling pathways and that disruption of PTEN signaling may be relevant to CDKL5 disease pathogenesis. Future studies pharmacologically or genetically altering the PTEN pathway in mice lacking CDKL5, particularly in excitatory or inhibitory CDKL5 conditional knockouts, should pinpoint the relationship between CDKL5 and PTEN signaling and isolate cell type-specific signaling pathways relevant to disease.

Future studies should also aim to determine the relationship between CDKL5 regulation of adult neurogenesis and neuronal outgrowth (Fuchs et al., 2014), CDKL5 regulation of neuronal migration and outgrowth during brain development (Amendola et al., 2014; Chen et al., 2010), and whether the two processes share common mechanisms. Given that Bdnf1-Rac1 signaling has been implicated in the latter (Chen et al., 2010), while Akt-GSK3b has been implicated in the former (Fuchs et al., 2014), follow-up studies investigating these putative mechanisms in conditional CDKL5 knockouts should reveal their *in vivo* relevance to neuronal development. Moreover, although two independent studies have identified delayed neuronal migration upon CDKL5 knockdown, the consequences of this delay and its underlying mechanisms have not been investigated. It is possible that delayed excitatory neuron migration would result in aberrant neural

circuit connectivity, a phenotype that has been identified in both CDKL5 KO mouse models (Amendola et al., 2014; Wang et al., 2012). Assessing neural circuit function and synapse electrophysiology, particularly in conditional knockout mice, may illuminate the contribution of individual cell types toward neural circuit function and isolate cell type-specific mechanisms underlying disease manifestation, particularly how they affect neuronal E/I balance.

Ultimately, the development of mouse models that faithfully recapitulate CDKL5 clinical phenotypes and utilization of these animals to gain a clear understanding of CDKL5 biological function and disease mechanism may lead to the development of effective targeted therapeutics toward treatment or reversal of CDKL5 disorder. Therefore, future experiments should address the therapeutic relevance of these studies. Gene mutations occur in germ cells and persist throughout the organism's lifetime, but therapeutic intervention in the clinic is likely constrained to postnatal time points, either during development or in adulthood. Therefore, the reversibility of CDKL5 disorder must be established. In Rett Syndrome mouse models, restoration of MeCP2 in post-symptomatic adult mice is sufficient to rescue many, but not all, disease-related phenotypes (Guy et al., 2007), suggesting that Rett Syndrome is reversible and therefore, treatable. This finding also indicates that MeCP2 may play a maintenance role and that many circuits and pathways regulated by MeCP2 are plastic. Performing similar experiments on CDKL5 mouse models will be important steps in translating animal research into clinically relevant therapeutic strategies.

The paucity of effective animal models and reagents has led to inconsistent and often contradictory results, and it is likely that the early bias linking CDKL5 to Rett Syndrome and MeCP2 has impeded diagnosis and research progress. The development and characterization of the first CDKL5 KO mouse, described in Chapter 2, represents the first step toward establishing *in vivo* mechanisms underlying CDKL5 disease pathogenesis, where a causal role of mutations in *Cdkl5* was linked to disease etiology and disruptions in neural circuits and signaling pathways upon loss of CDKL5 were identified. Ongoing and future studies, described in Chapter 3, that integrate mouse behavior, circuit function, synapse physiology, and signaling pathways in conditional CDKL5 knockout mice will clarify the pathogenic mechanisms by which mutations in

CDKL5 lead to disease and thus expedite the development of mechanism-based therapeutics.

Chapter 2:

LOSS OF CDKL5 DISRUPTS KINOME PROFILE AND EVENT-RELATED POTENTIALS LEADING TO AUTISTIC-LIKE PHENOTYPES IN MICE

I-Ting Judy Wang[a], Megan Allen[a], Darren Goffin[a], Xinjian Zhu[b,c], Andrew H. Fairless[d], Edward S. Brodkin[d], Steve J. Siegel[d], Eric D. Marsh[b,c], Julie A. Blendy[e], and Zhaolan Zhou[a,1]

Departments of [a]Genetics, [b]Neurology, [d]Psychiatry, and [e]Pharmacology, Perelman School of Medicine at the University of Pennsylvania, Philadelphia, PA 19104; and [c]Division of Child Neurology, Department of Pediatrics and Neurology, Children's Hospital of Philadelphia, Philadelphia, PA 19104

Edited* by Gail Mandel, Howard Hughes Medical Institute and Oregon Health & Science University, Portland, OR, and approved November 15, 2012 (received for review October 1, 2012)

*This Direct Submission article had a prearranged editor.

This article contains supporting information online at

www.pnas.org/lookup/suppl/doi:10. 1073/pnas.1216988110/-/DCSupplemental.

21516–21521 | PNAS | December 26, 2012 | vol. 109 | no. 52

www.pnas.org/cgi/doi/10.1073/pnas.1216988110

This chapter consists of my 2012 first-author *Proceedings of the National Academy of Sciences of the United States of America* (*PNAS*) publication describing the development and characterization of the first CDKL5 knockout mouse model. This study established the genetic causality of mutations in *Cdkl5* in disease etiology and identified disruptions in neural circuits and signaling pathways as pathogenic mechanisms underlying CDKL5 disorder. In addition, it provided a framework and animal model for future mechanistic and therapeutic studies of CDKL5 disorder.

Abstract

Mutations in the X-linked cyclin-dependent kinase-like 5 (CDKL5) gene have been identified in neurodevelopmental disorders including atypical Rett syndrome (RTT), autism spectrum disorders (ASDs), and early infantile epileptic encephalopathy. The biological function of CDKL5 and its role in the etiology of these disorders, however, remain unclear. Here we report the development of a unique knockout mouse model of CDKL5-related disorders and demonstrate that mice lacking CDKL5 show autistic-like deficits in social interaction, as well as impairments in motor control and fear memory. Neurophysiological recordings reveal alterations in event-related potentials (ERPs) similar to those observed in RTT and ASDs. Moreover, kinome profiling uncovers disruption of multiple signal transduction pathways, including the AKT-mammalian target of rapamycin (mTOR) cascade, upon Cdkl5 loss-of-function. These data demonstrate that CDKL5 regulates signal transduction pathways and mediates autistic-like phenotypes and together establish a causal role for Cdkl5 loss-of-function in neurodevelopmental disorders.

Introduction

Cyclin-dependent kinase-like 5 (*CDKL5*) is an X-linked gene associated with early infantile epileptic encephalopathy 2 (EIEE2) (Nabbout and Dulac, 2011), atypical Rett syndrome (RTT) (Chahrour and Zoghbi, 2007), and autism spectrum disorders (ASDs) (Sakai et al., 2011; Talkowski et al., 2012). Patients with CDKL5 mutations display a heterogenous array of clinical phenotypes, the most prominent of which include early-onset seizures, intellectual disability, and autistic features (Bahi-Buisson et al., 2008b)

CDKL5 is a serine/threonine (S/T) kinase that is highly expressed in the brain (Kilstrup-Nielsen et al., 2012). *In vitro* studies have demonstrated that CDKL5 may mediate the phosphorylation of methyl-CpG binding protein 2 (MeCP2) (Mari et al., 2005), DNA methyltransferase 1 (DNMT1) (Kameshita et al., 2008), and netrin-G1 ligand (NGL-1) (Ricciardi et al., 2012). RNAi-mediated knockdown studies show that CDKL5 can regulate neuronal outgrowth and synapse stability (Chen et al., 2010; Ricciardi et al., 2012). Despite these proposed functions, the exact role of CDKL5 in the phosphorylation of MeCP2 (Lin et al., 2005; Mari et al., 2005) and in dendritic outgrowth (Chen et al., 2010; Ricciardi et al., 2012) remains unclear, and thus requires further investigation. The limited understanding of CDKL5 function and its associated signal transduction pathways has hindered the development of therapeutics for CDKL5-related disorders. Current treatments focus on managing symptoms and reducing seizure frequency, but have limited effectiveness (Bahi-Buisson and Bienvenu, 2012).

To investigate the function of CDKL5 in a disease model and identify potential avenues of therapeutic intervention, we developed a *Cdkl5* knockout mouse. We found that mice lacking CDKL5 show autistic-like behavioral abnormalities, deficits in neural circuit communication, and alterations in multiple signal transduction pathways. We establish a causal link between *Cdkl5* loss-of-function and disease-related phenotypes and identify the Akt-mammalian target of rapamycin (mTOR) pathway as a unique candidate for targeted therapeutic intervention of CDKL5-related disorders.

Results

Generation of *Cdkl5* Knockout Mice.

To investigate the pathophysiology underlying CDKL5-related disorders, we generated a *Cdkl5* knockout mouse that models a splice site mutation found in a CDKL5 patient. This mutation results in the skipping of human *CDKL5* exon 7, generating a premature termination codon and causing an early truncation of CDKL5 in its N-terminal kinase domain, thereby disrupting kinase activity (Archer et al., 2006). To mimic the effects of this splice site mutation, we deleted mouse *Cdkl5* exon 6 through homologous-mediated recombination in ES cells (**Fig. 1A**). Deletion of *Cdkl5* exon 6 leads to a similar shift in the reading frame and premature truncation within the N-terminal kinase domain (**Fig. 1 A and B**). The absence of *Cdkl5* exon 6 at the DNA and mRNA levels was verified by PCR of genomic DNA and sequencing of cDNA prepared from *Cdkl5* knockout mouse brains (**Fig. 1 C and D**). Loss of full-length CDKL5 protein was verified by Western blot (**Fig. 1E**). A truncated CDKL5 protein product in neurons isolated from *Cdkl5* knockout mice has not been detected by antibodies raised against CDKL5 N-or C-terminal domains, likely due to nonsense stop codon mediated mRNA decay (**Fig. S1A**). In addition, female heterozygotes show decreased CDKL5 protein expression relative to WT female mice, as expected from X-linked mosaicism (**Fig. S1B**). Thus, deletion of *Cdkl5* exon 6 likely represents a loss-of-function mutation. Experimental mice have been backcrossed onto the C57BL/6 background for at least six generations. Male mice lacking CDKL5 ($Cdkl5^{-/y}$) and female heterozygotes ($Cdkl5^{-/+}$) are viable, fertile, and display normal appearance, growth, and overall brain morphology (**Fig. S1 C and D**).

Hyperactivity, Motor Impairments, and Decreased Anxiety in $Cdkl5^{-/y}$ Mice.

Given the clinical relevance of CDKL5-related disorders in males (Liang et al., 2011; Moseley et al., 2012) and the confounding effects of mosaic CDKL5 expression in females from random X-chromosome inactivation, we characterized the behavioral profile of *Cdkl5* knockouts in male ($Cdkl5^{-/y}$) mice, compared with wild-type male littermates (WT, $Cdkl5^{+/y}$). We found that $Cdkl5^{-/y}$ mice exhibit motor and anxiety impairments similar to those observed in other ASD and RTT mouse models (Chahrour

and Zoghbi, 2007; Goffin et al., 2012; Schmeisser et al., 2012; Tsai et al., 2012; Won et al., 2012). In a locomotor assay within a home cage-like environment, *Cdkl5*$^{-/y}$ mice demonstrated significantly higher motor activity relative to WT littermate controls (**Fig. 2A**). Similar hyperactivity was also observed in the zero maze test and social approach test (**Fig. S2 A and B**).

On an accelerating rotarod assay, the latency to fall in *Cdkl5*$^{-/y}$ mice increased across trials similarly to that of WT mice, but was consistently lower than that of WT (**Fig. 2B**), indicating that *Cdkl5*$^{-/y}$ mice have comparable motor learning but impaired motor coordination relative to their WT littermates. *Cdkl5*$^{-/y}$ mice also showed decreased anxiety-related behavior in a zero maze test similar to that of *Mecp2* mouse models of RTT, spending more time in open areas and less time in the closed areas relative to WT littermates (**Fig. 2C**). In addition, we have observed hindlimb and forelimb clasping in *Cdkl5*$^{-/y}$ mice (**Fig. S2C**), a phenotype also exhibited in *Mecp2* mouse models (Chao et al., 2010; Goffin et al., 2012; Guy et al., 2001; Shahbazian et al., 2002b). These data demonstrate that *Cdkl5*$^{-/y}$ mice exhibit hyperactivity, impaired motor control, and decreased anxiety, phenotypes that have also been observed in ASD and RTT patients (Bahi-Buisson et al., 2008b; Chahrour et al., 2008; Geschwind, 2009).

Autistic-Like Social Behavior in *Cdkl5*$^{-/y}$ Mice.

Given that deficits in social interaction are a hallmark feature of ASDs and are prevalent in patients with *CDKL5* mutations (Abrahams and Geschwind, 2008; Bahi-Buisson et al., 2008b), we next examined sociability using a three-chambered social approach test and found that mice lacking CDKL5 demonstrate profound impairment in social interaction. During the initial habituation phase, both WT and *Cdkl5*$^{-/y}$ mice explored both chambers equally, demonstrating no initial chamber preference (**Fig. S2D**). However, upon introduction of a novel object into one chamber (nonsocial chamber, NS) and a novel gonadectomized male A/J stimulus mouse into the other chamber (social chamber, S), *Cdkl5*$^{-/y}$ mice showed reduced social preference relative to WT mice, spending less time in the social chamber and more time in the nonsocial chamber relative to WT mice (**Fig.**

2D). In addition, *Cdkl5*$^{-/y}$ mice spent more time sniffing the novel object and a trend toward less time sniffing the novel stimulus mouse relative to WT mice (**Fig. 2E**). Furthermore, when barriers were removed to allow freely mobile direct interaction, *Cdkl5*$^{-/y}$ mice spent significantly less time interacting (sniffing, allogrooming) with the stimulus mouse compared with WT littermates (**Fig. 2F**).

Cdkl5$^{-/y}$ mice also displayed impaired nesting, a phenotype related to home-cage social behavior that has been observed in ASD and RTT mouse models (Peñagarikano et al., 2011; Samaco et al., 2008; Won et al., 2012) (**Fig. 2G**). Importantly, we found no olfaction impairments in either genotype (**Fig. S2E**), suggesting that the social deficits in *Cdkl5*$^{-/y}$ mice are not the secondary consequence of an inability to discriminate between social and neutral odors. Together, these data demonstrate that *Cdkl5*$^{-/y}$ mice have ASD-like deficits in social behavior.

Impaired Learning and Memory in *Cdkl5*$^{-/y}$ Mice.

Because intellectual disability is a common clinical phenotype among CDKL5 patients (Bahi-Buisson and Bienvenu, 2012), we also assessed learning and memory in *Cdkl5* knockout mice using context-and cue-dependent fear conditioning. During the acquisition phase, both WT and *Cdkl5*$^{-/y}$ mice showed similar exploratory behavior before the foot shock and similar freezing behavior immediately following the foot shock (**Fig. 2H**). When re-exposed to the shock box or paired tone 24 h later, *Cdkl5*$^{-/y}$ mice froze significantly less than WT littermates, indicating impaired contextual and cued fear memory (**Fig. 2H**). Taken together, these behavioral studies demonstrate that mice lacking CDKL5 have deficits in motor function, social behavior, and learning and memory.

Normal EEG Patterns and Absence of Spontaneous Seizures in *Cdkl5*$^{-/y}$ Mice.

Given the prevalence of intractable seizures in patients with *CDKL5* mutations (Bahi-

Buisson and Bienvenu, 2012), we next examined the occurrence of spontaneous seizures in *Cdkl5* knockout mice through video-EEG recordings. We did not, however, observe any spontaneous seizures in *Cdkl5*$^{-/y}$ mice recorded for at least 72 h, with some mice recorded for as long as 240 h. Consistent with this finding, the basal EEG patterns and power distribution across different oscillation frequencies in *Cdkl5*$^{-/y}$ mice were similar to that of WT littermates (**Fig. S3 A and B**). Despite the large degree of homology between the murine and human CDKL5 protein, the absence of spontaneous seizures observed in our *Cdkl5*$^{-/y}$ mice may reflect a distinct function or modification of CDKL5 in humans that is absent in lower organisms. Moreover, the C57BL/ 6 genetic background is known to confer increased seizure resistance (McLin and Steward, 2006), thus potentially occluding spontaneous seizures in our *Cdkl5*$^{-/y}$ mice.

Event-Related Potential Deficits in *Cdkl5*$^{-/y}$ Mice.

The absence of spontaneous seizures in *Cdkl5*$^{-/y}$ mice, however, allowed us to examine neural circuit deficits that are mediated by *Cdkl5* loss-of-function rather than the secondary consequence of seizures. Sensory information processing measured as an event-related potential (ERP) has recently been proposed as a biomarker to monitor neural circuit function in ASD and RTT animal models (Gandal et al., 2010; Goffin et al., 2012; Liao et al., 2012). We therefore recorded auditory-evoked ERPs in adult WT and *Cdkl5*$^{-/y}$ mice, as these ERP assessments can be performed on nonanesthetized, freely mobile mice and are not confounded by the motor and cognitive deficits observed in *Cdkl5*$^{-/y}$ mice. Relative to the characteristic amplitude and latency of the P1 (positive), N1 (negative), and P2 polarity peaks in WT mice, *Cdkl5*$^{-/y}$ mice display an aberrant ERP waveform (**Fig. 3A**). We observed a significant decrease in the amplitude of the N1 and P2 peaks and a significant increase in latency of the P2 peak (**Fig. 3 A–C**). Importantly, auditory brainstem recordings detected no hearing impairments in either genotype. As the amplitude and latency of these polarity peaks are believed to reflect the strength and timing of cognitive processes, these data indicate that *Cdkl5* loss-of-function disrupts neural circuit communication. Notably, ASD and RTT patients have alterations in both ERP amplitude and latency (Roberts et al., 2010; Stauder et al., 2006).

Disruption of Low-Frequency Event-Related Neuronal Oscillations in *Cdkl5*$^{-/y}$ Mice.

Circuit communication is composed of neuronal oscillations over a range of frequencies. We therefore also performed time–frequency analysis of the ERPs to examine frequency-specific changes in instantaneous power and phase locking in response to the auditory stimuli. *Cdkl5*$^{-/y}$ mice demonstrated reduced oscillatory strength specifically at low frequencies, showing attenuated event-related depression in the low-frequency delta (δ,2–4 Hz), theta (θ,4–8 Hz), and alpha (α,8–12 Hz) oscillations, but no difference in the high-frequency beta (β,12–30 Hz), low gamma (γlow,30–50 Hz), and high gamma (γhigh,70–140 Hz) oscillations relative to WT controls (**Fig. 3 D and E and Fig. S4A**). Similarly, event-related phase locking, which reflects the reliability and sensitivity of circuit communication, and is measured by the phase-locking factor (PLF), were also significantly decreased in *Cdkl5*$^{-/y}$ mice exclusively in the low-frequency δ, θ, and α oscillations relative to WT littermates (**Fig. 3 F and G and Fig. S4B**). Given that oscillatory activity in low-frequency ranges is associated with long-range neuronal circuit communication and high-frequency oscillations with local circuit communication (Gandal et al., 2010; Winterer et al., 2000), our data suggest that ERP deficits in *Cdkl5*$^{-/y}$ mice may be mediated by impairments in long-range communication. Notably, EEG studies in ASD children have reported specific deficits in low-frequency δ, θ, and α oscillations (Dawson et al., 1995; Stroganova et al., 2007), indicating that similar neuronal network defects exist in *Cdkl5*$^{-/y}$ mice and ASD patients.

Disrupted Kinome Profile in *Cdkl5*$^{-/y}$ Mice.

Given the highly conserved S/T kinase domain in CDKL5 (**Fig. 1B**), we reasoned that *Cdkl5* loss-of-function may disrupt phosphorylation of CDKL5 kinase substrates and related signaling pathways, thereby mediating deficits in neuronal network communication and autistic-like behaviors in *Cdkl5*$^{-/y}$ mice. Previous studies have reported that CDKL5 may mediate the phosphorylation of MeCP2 (Mari et al., 2005), DNMT1 (Kameshita et al., 2008), and NGL-1 (Ricciardi et al., 2012) *in vitro*. The CDKL5 substrates *in vivo*, however, remain unknown. Therefore, to investigate the signaling networks affected by the absence of CDKL5 *in vivo* in an unbiased manner, we surveyed

the S/T kinome profile in *Cdkl5* knockout mice, assessing the consequence of *Cdkl5* loss-of-function on overall S/T phosphorylation events. Because CDKL5 expression is enriched in the forebrain regions of the striatum, cortex, and hippocampus (**Fig. S5**), we probed brain region–specific lysate from WT and *Cdkl5*$^{-/y}$ mice with multiple antibodies developed against a large set of well-characterized S/T phosphorylation motifs (Moritz et al., 2010; Zhang et al., 2002). We identified a range of phosphorylation profiles affected by the loss of CDKL5 (**Fig. 4A**). Of these, the phosphorylation of adenosine monophosphate-activated protein kinase (AMPK), protein kinase A (PKA), and AKT substrates were strongly decreased in *Cdkl5*$^{-/y}$ mice (**Fig. 4 B and C and Fig. S6**), whereas other phosphorylation profiles were moderately or mildly affected [e.g., mitogen-activated protein kinase (MAPK), ataxia-telangiectasia mutated/ataxia-telangiectasia and Rad3-related (ATM/ATR), and cyclin-dependent kinase (CDK) substrates] (**Fig. 4A and Figs. S7 and S8**). Importantly, changes in phosphorylation profiles were clearly evident in forebrain regions including the striatum, somatosensory cortex, and hippocampus where CDKL5 is enriched and less pronounced in hindbrain regions including the brainstem where CDKL5 expression is low (**Fig. 4 B and C and Figs. S5–S7**), supporting a role of CDKL5 in the regulation of these pathways.

Disruption of AKT–mTOR Signaling in *Cdkl5*$^{-/y}$ Mice.

The changes in the AMPK, AKT, PKC, and MAPK phosphorylation profiles suggested a convergence on the downstream signaling of phosphatase and tensin homolog (PTEN). Notably, mutations and dysfunction of components of this pathway, including PTEN, AKT, tuberous sclerosis complex (TSC), and mTOR, have been linked to ASDs, RTT, and epileptic encephalopathies (Ricciardi et al., 2011; Tsai et al., 2012; Zhou and Parada, 2012). To validate the disruption of AKT–mTOR signaling in *Cdkl5*$^{-/y}$ mice, we measured the phosphorylation of AKT S473 and mTOR S2448 and found decreased phosphorylation of both AKT and mTOR in *Cdkl5*$^{-/y}$ mice, with no concomitant alteration in total AKT or mTOR protein levels (**Fig. 4 D–H**). As phosphorylation of these residues promote AKT activation and mTOR complex 1 (mTORC1) assembly, respectively (Bhaskar and Hay, 2007; Rosner et al., 2010), this finding is consistent with the overall

decreased phosphorylation of AKT substrates in *Cdkl5*$^{-/y}$ mice **(Fig. 4C and Fig. S6 B and D**) and likely reflect decreased AKT and mTORC1 activity upon *Cdkl5* loss-of-function. Together, we conclude that multiple signal transduction pathways, including the AKT–mTOR cascade, are disrupted upon the absence of CDKL5.

Discussion

In this study, we show that loss of CDKL5 in mice results in autistic-like behavioral deficits, impairment in neuronal communication, and disruptions in serine/threonine phosphorylation profiles. We establish a unique causal relationship between Cdkl5 loss-of-function and disease-related phenotypes.

Core characteristics of CDKL5-related disorders include early-onset seizures, severe intellectual disability, and autistic-like features. In our behavioral analysis, we found that our *Cdkl5* knockout mice mirror the latter features, but not early-onset seizures. *Cdkl5*$^{-/y}$ mice display hyperactivity, motor defects, reduced anxiety, decreased sociability, and impaired learning and memory. These phenotypes have been described in other ASD and RTT mouse models (Chahrour and Zoghbi, 2007; Goffin et al., 2012; Guy et al., 2001; Peñagarikano et al., 2011; Schmeisser et al., 2012; Won et al., 2012) and may mimic the absence of hand skills, intellectual disability, hyperactivity, and poor response to social interactions that have been described in CDKL5 patients (Bahi-Buisson and Bienvenu, 2012; Willemsen et al., 2012).

While video-EEG monitoring revealed an absence of spontaneous seizures in *Cdkl5*$^{-/y}$ mice, ERP analysis showed attenuated and delayed ERP polarity peaks suggestive of impaired neuronal connectivity, which is consistent with findings in ASD and RTT patients (Roberts et al., 2010; Stauder et al., 2006) and animal models (Gandal et al., 2010; Goffin et al., 2012; Liao et al., 2012). Importantly, these behavioral and electrophysiological impairments are unlikely the secondary effects of an epileptic neuronal network, suggesting they are consequences of *Cdkl5* loss-of-function.

Time–frequency analysis of ERPs identified a specific deficit in event-related δ, θ, and α low-frequency neuronal oscillations in *Cdkl5*$^{-/y}$ mice. Interestingly, abnormalities in low-frequency neuronal oscillations have been reported in ASD children (Dawson et al., 1995; Stroganova et al., 2007). In addition, impairments in α and γ oscillations have also been described in ASDs, as α is believed to function in attention suppression of distracting stimuli and γ in feature binding (Foxe and Snyder, 2011; Uhlhaas et al.,

2011). Alpha oscillations have also been proposed to mediate long-distance coordination of γ oscillations (Palva and Palva, 2007). Thus, our data suggest that the oscillatory network of *Cdkl5*$^{-/y}$ mice may resemble that of ASD, where γ oscillations themselves are not affected, but rather, their α-mediated long-distance coordination. Moreover, as θ oscillations are proposed to support encoding and retrieval of memory (Buzsáki, 2005; Ward, 2003), the impairment in event-related power and PLF at the θ frequency are consistent with the learning and memory deficits in *Cdkl5*$^{-/y}$ mice and the prominent intellectual disability observed in patients with CDKL5-related disorders.

Lastly, our S/T kinome study revealed that many signal transduction pathways are disrupted in *Cdkl5* knockout mice. Of these, many pathway components, including the AKT–mTOR pathway, have been implicated in the etiology of ASDs (Jeste et al., 2008; Tsai et al., 2012). Given that mTOR is a known regulator of cell growth, proliferation, motility, and neural plasticity (Zoncu et al., 2011), one consequence of reduced AKT–mTOR activity in the absence of CDKL5 is the disruption of neuronal development. Accordingly, RNAi-mediated knockdown of CDKL5 results in impaired dendritic outgrowth, neuronal migration (Chen et al., 2010), and spine maturation (Ricciardi et al., 2012). Together, these data suggest a mechanism by which CDKL5 regulates AKT–mTOR-mediated cellular development, thus implicating the AKT–mTOR pathway as a potential therapeutic target for treatment of patients with CDKL5-related disorders.

In addition to the AKT–mTOR pathway, we found that the phosphorylation profiles of kinases involved in synaptic plasticity, including PKA, PKC, and protein kinase D (PKD), as well as kinases involved in cellular metabolism, including AMPK, ATM/ATR, and casein kinase (CK) (**Figs. S6 and S7**) were also decreased in *Cdkl5*$^{-/y}$ mice. Although many of these signaling changes may be indirect effects of *Cdkl5* loss-of-function, these data suggest that CDKL5 plays a critical role in coordinating multiple signaling cascades. Indeed, CDKL5 has been shown to regulate brain-derived neurotropic factor (BDNF)-induced activation of Rho family small GTPase Rac1 (Chen et al., 2010) and deficits in synaptic plasticity are commonly described in ASDs (Peça et al., 2011; Won et al., 2012). Consistent with these cellular functions, we found that CDKL5 is predominantly localized in the cytoplasm (**Fig. S9**). Notably, links between these signaling pathways

have been previously described, as CK regulates glutamatergic synaptic transmission (Chergui et al., 2005), ATM mediates AKT S473 phosphorylation (Viniegra et al., 2005), and mutations in ATM cause the neurodegenerative movement disorder ataxis telegiectasia (Barlow et al., 1996). It is possible, therefore, that CDKL5 may serve to mediate cross-talk between these signaling pathways.

Our data support an increasing awareness that CDKL5-related disorders are an independent clinical entity with an independent pathogenic mechanism, rather than a subclass of RTT. Strikingly, only less than one-quarter of individuals with *CDKL5* mutations meet the criteria for the early-onset seizure variant of RTT (Fehr et al., 2012; Neul et al., 2010). Its genetic link to neurodevelopmental disorders and recent identification as an ASD hotspot for balanced chromosomal rearrangements (Talkowski et al., 2012) highlight the need to characterize CDKL5 biological function, understand the mechanisms underlying CDKL5-related disorders, and identify effective therapies targeted toward slowing or reversing disease progression. Our study, therefore, provides a framework and an animal model for mechanistic and therapeutic studies of CDKL5-related disorders.

Figure 1

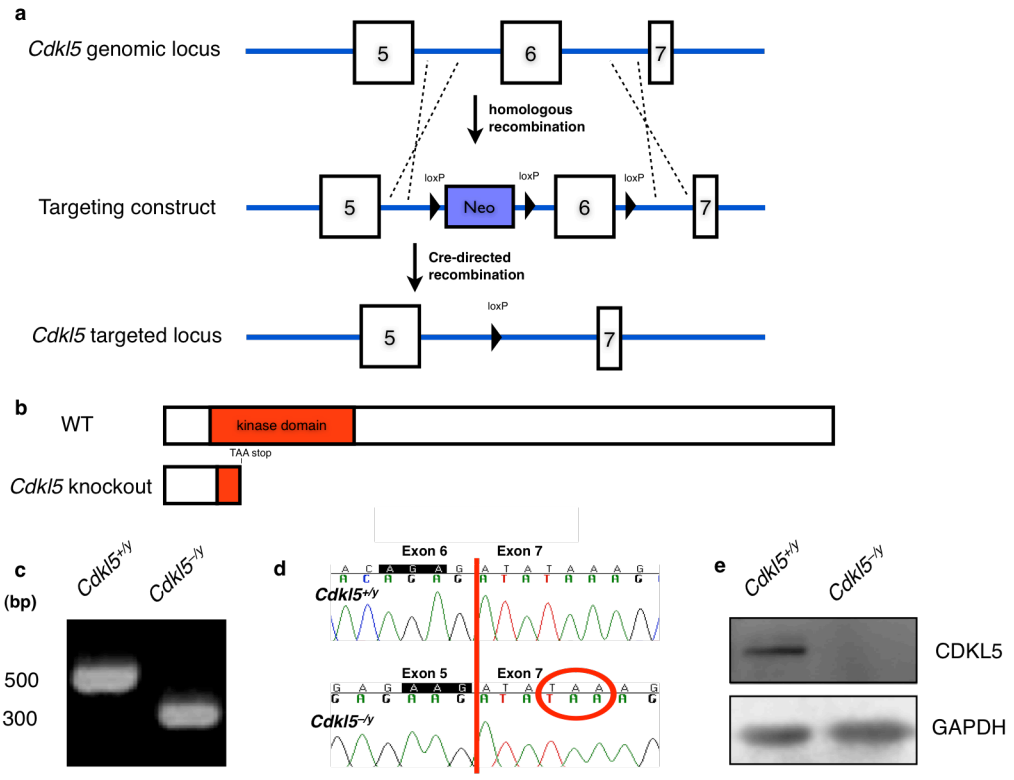

Figure 1. Generation and verification of *Cdkl5* knockout mice.

(a) Targeting strategy to generate *Cdkl5* knockout mice. Three loxP sites and a neomycin positive selection cassette (Neo) were inserted surrounding the genomic locus of *Cdkl5* exon 6 via homologous recombination. Upon Cre-directed recombination, both the Neo cassette and exon 6 were excised.

(b) Schematic of CDKL5 protein in WT and knockout. The excision of exon 6 causes a reading frame shift, resulting in a TAA stop codon in the 5' end of exon 7, leading to truncation of CDKL5 in its kinase domain (red).

(c) PCR of genomic DNA using primers flanking exon 6. A 300 bp PCR product in *Cdkl5*$^{-/y}$ mice indicates the absence of *Cdkl5* exon 6.

(d) Sequencing of cDNA generated from *Cdkl5* mRNA. Excision of exon 6 in *Cdkl5*$^{-/y}$ mice causes the reading frame, highlighted in black, to be shifted in *Cdkl5*$^{-/y}$ mice, resulting in a premature stop codon (TAA, circled in red) at the 5' end of exon 7.

(e) Western blot probed with an antibody directed against CDKL5. Full-length CDKL5 protein is absent in *Cdkl5*$^{-/y}$ mice.

Figure 2

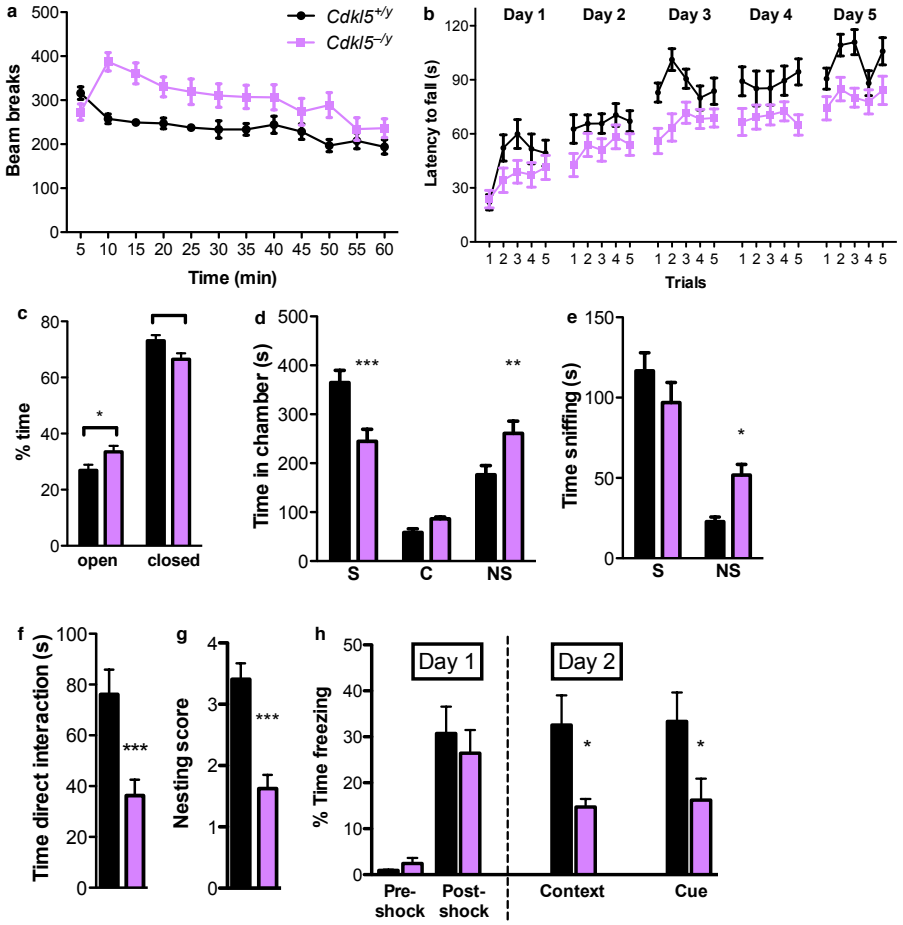

Figure 2. Behavioral phenotyping of *Cdkl5*$^{-/y}$ mice.

(a) 60-minute locomotor assay, measured by infrared beam breaks in a home cage-like environment. *Cdkl5*$^{-/y}$ mice (n=19) display increased activity relative to wildtype (WT, *Cdkl5*$^{+/y}$) littermates (n=15). Two-way repeated measures (RM) -ANOVA, $p<0.0001$ (interaction).

(b) Rotarod assay, measuring latency to fall from an accelerating rotating rod. Testing was performed 5 trials/day for 5 consecutive days. Latency to fall is decreased in *Cdkl5*$^{-/y}$ mice (n=18) relative to WT littermates (n=15), indicating impaired motor coordination in *Cdkl5*$^{-/y}$ mice. Two-way ANOVA, $p<0.01$ (main effect of genotype).

(c) *Cdkl5*$^{-/y}$ mice (n=14) spend more time in the open arms and less time in the closed arms of a zeromaze assay relative to WT littermates (n=12), showing decreased anxiety. *$p<0.05$, unpaired two-tailed Student's t-test.

(d) Three-chambered social approach assay. *Cdkl5*$^{-/y}$ mice (n=17) spend less time in a social chamber containing a stimulus mouse (S) and more time in a non-social chamber containing a novel object (NS) relative to WT mice (n=15). C: center. Two-way ANOVA with Bonferroni correction, $p<0.0001$ (interaction); **$p<0.01$, ***$p<0.001$.

(e) *Cdkl5*$^{-/y}$ mice (n=17) spend significantly more time sniffing a novel object (NS) and trend toward less time sniffing a stimulus mouse (S) relative to WT mice (n=15). Two-way ANOVA with Bonferroni correction, $p<0.01$ (interaction); *$p<0.05$.

(f) *Cdkl5*$^{-/y}$ mice (n=17) spend less time directly interacting with a freely moving stimulus mouse compared to WT littermates (n=15). ***$p<0.001$, unpaired two-tailed Student's t-test.

(g) *Cdkl5*$^{-/y}$ mice (n=12) show impaired nesting behavior relative to WT littermates (n=11) at 4-5 postnatal weeks. ***$p<0.001$, unpaired two-tailed Student's t-test.

(h) Fear conditioning paradigm, measuring time spent immobile. While *Cdkl5*$^{-/y}$ mice (n=14) freeze in response to a mild footshock similarly to WT littermates (post-shock), they show decreased freezing upon return to the testing chamber (context) and upon hearing the testing tone (cue) relative to WT littermates (n=14), demonstrating impaired learning and memory in *Cdkl5*$^{-/y}$ mice. Two-way ANOVA with Bonferroni correction, $p<0.01$ (interaction); *$p<0.05$. All data are presented as mean ± s.e.m.

Figure 3

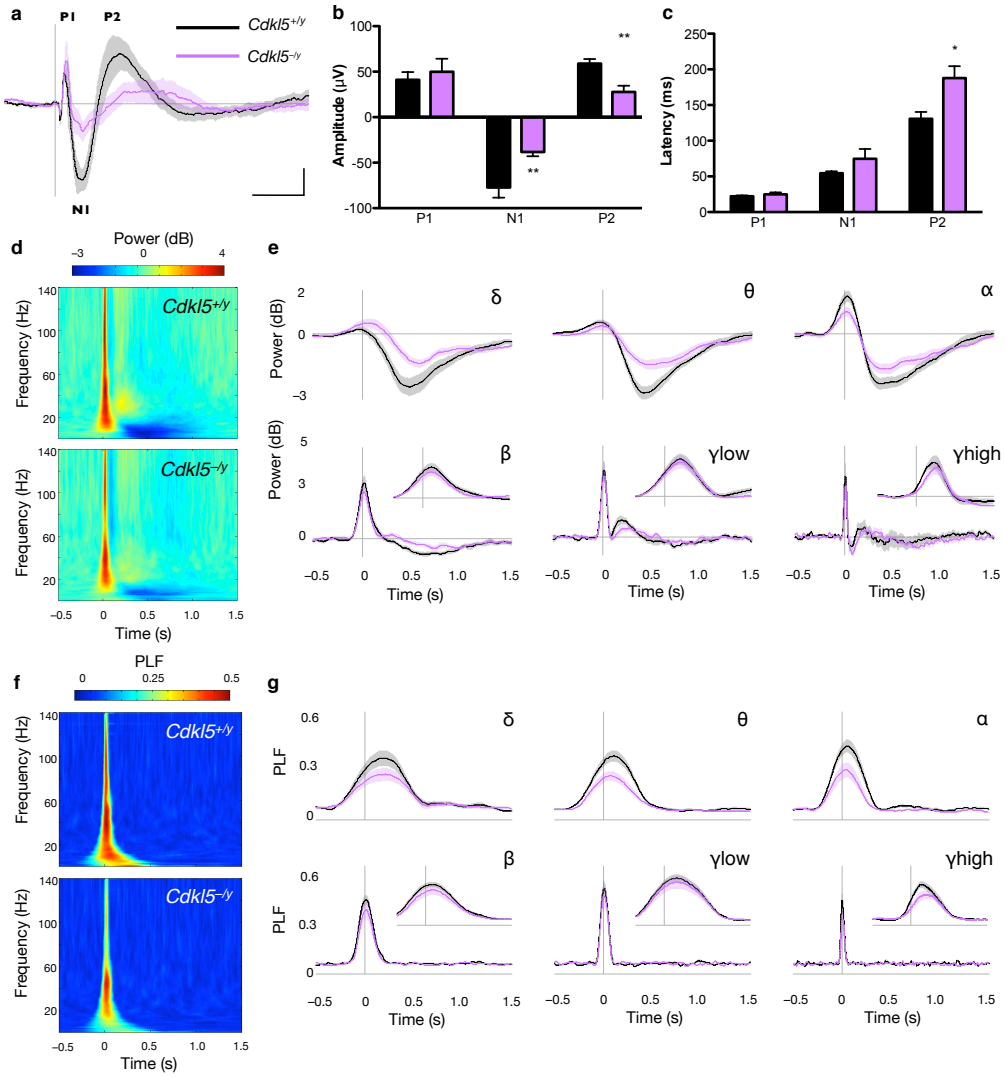

Figure 3. *Cdkl5*$^{-/y}$ mice display impaired ERP waveform and decreased event-related power and phase-locking.

(a) Grand-average ERP waveform following presentation of 250 85-dB white noise stimuli with 4 s interstimulus intervals in adult WT (*Cdkl5*$^{+/y}$) (n=9) and *Cdkl5*$^{-/y}$ mice (n=9). Traces represent mean amplitude ± s.e.m. Characteristic polarity peaks P1, N1, and P2 in WT are labeled. Scale bar corresponds to 100 ms (horizontal) and 20 mV (vertical).

(b, c) Amplitude (b) and latency (c) of ERP peaks. Bars represent mean ± s.e.m.; **p<0.01, *p<0.05, unpaired two-tailed Student's t-test with Bonferroni correction.

(d) Time-frequency plots showing changes in event-related power following an 85-dB auditory stimulus. Color represents mean power, where warmer colors correspond to increased power and cooler colors correspond to decreased power relative to pre-stimulus baseline.

(e) Changes in event-related mean power averaged across δ (2–4 Hz), θ (4–8 Hz), α (8–12 Hz), β (12–30 Hz), γ_{low} (30–50 Hz) and γ_{high} (70–140 Hz) oscillation frequencies. Scale bars represent the length of a single δ oscillation cycle. Insets show power traces on an expanded timescale, denoted by the length of a single oscillation cycle. Traces represent mean amplitude ± s.e.m.

(f) Time-frequency plots showing changes in event-related phase-locking factor (PLF) following an 85-dB auditory stimulus. Color represents PLF, where warmer colors correspond to a higher PLF or lower circular variance in EEG phase across trials.

(g) Changes in event-related PLF averaged across frequencies described above. Scale bars represent the length of a single oscillation cycle and insets show traces on an expanded timescale. Traces represent mean PLF ± s.e.m.

Figure 4

a

Phosphorylation motif	Fold change in *Cdkl5*$^{-/y}$ mice
AMPK substrate: LXRXX(s/t)	-0.88
PKA substrate: (K/R)(K/R)X(s/t)	-0.86
AKT substrate: RXX(s/t), RXRXX(s/t)	-0.81
CK substrate: t(D/E)X(D/E)	-0.74
PKD substrate: LXRXX(s/t)	-0.69
MAPK substrate: PXsP	-0.66
PKC substrate: (K/R)XsX(K/R)	-0.66
tXR	-0.60
ATM/ATR substrate: sQ, (s/t)QG	-0.54
PLK binding motif: StP	-0.32
PDK1 docking motif: (F/Y)(s/t)(F/Y)	-0.28
tP	-0.24
pY	-0.17
CDK substrate: (K/R)sPX(K/R)	-0.16
tPE	-0.04

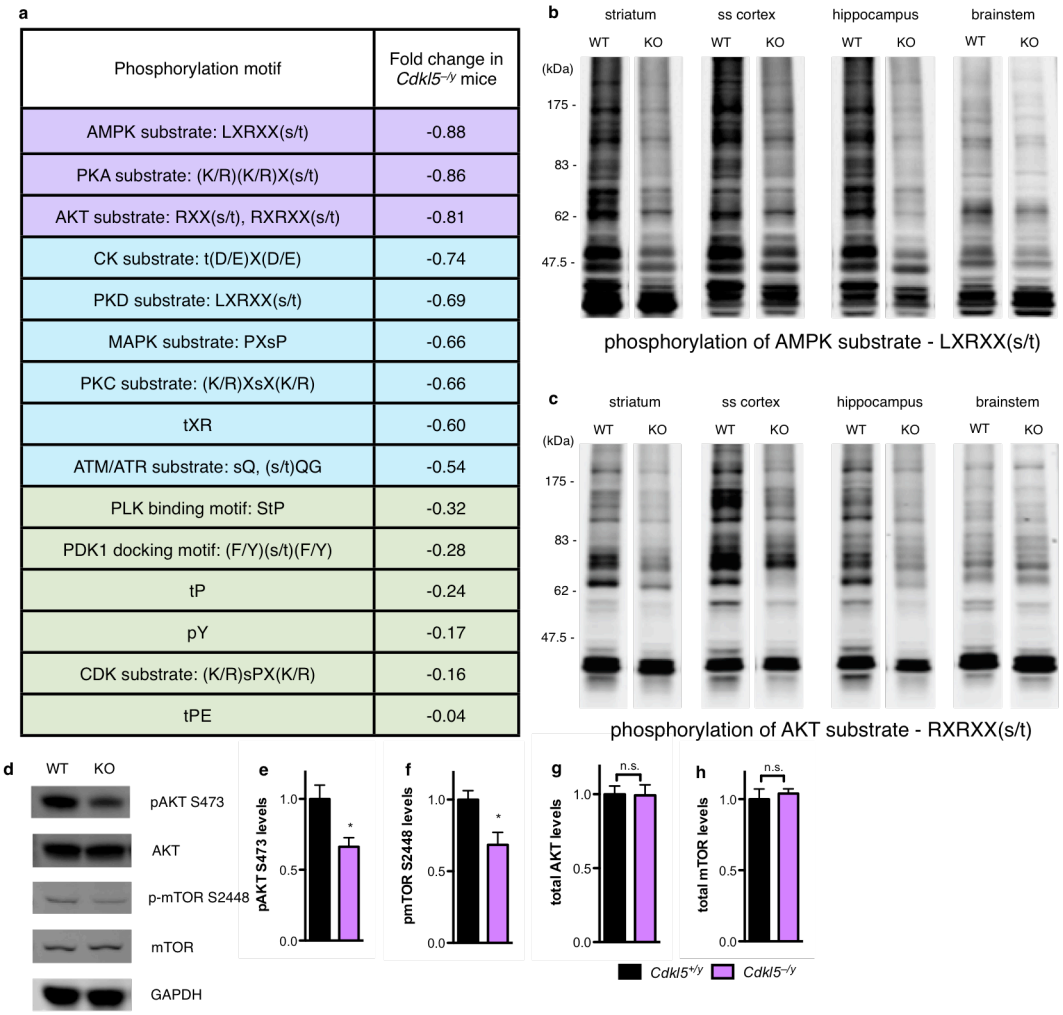

Figure 4. Altered kinome profile and disrupted AKT-mTOR signaling in *Cdkl5*$^{-/y}$ mice.

(a) Summary of changes in kinome profile in *Cdkl5*$^{-/y}$ mice relative to WT littermates. Whole cell lysates from the cerebellum, striatum, somatosensory cortex, olfactory bulb, hippocampus, and brainstem of WT (n=7) and *Cdkl5*$^{-/y}$ mice (n=8) were probed with antibodies raised against different phosphorylation motifs representing known S/T kinases. Western blots were quantified using the Odyssey Infrared Imaging system and fold change in phosphorylation level between *Cdkl5*$^{-/y}$ and WT mice across the six brain regions are expressed as $\log_2$(phosphorylation level in WT over phosphorylation level in *Cdkl5*$^{-/y}$). Color scheme indicates relative degree of phosphorylation reduction in *Cdkl5*$^{-/y}$ mice: purple - strong; blue - moderate; green - mild.

(b, c) Whole cell lysate probed with an antibody specific for an RXRXX(s/t) phosphorylation motif representing AKT kinase substrates (b) and an antibody specific for an LXRXX(s/t) phosphorylation motif representing AMPK kinase substrates (c) shows a marked decrease in phosphorylation profiles in *Cdkl5*$^{-/y}$ mice (KO) relative to WT littermates in the striatum, somatosensory cortex (ss cortex), and hippocampus, but moderate decrease in the brainstem, consistent with regions of high and low CDKL5 expression, respectively.

(d) AKT S473 and mTOR S2448 phosphorylation is reduced in whole brain lysate from *Cdkl5*$^{-/y}$ mice (KO) related to WT mice, while total levels of AKT and mTOR are unchanged.

(e-f) Quantification of reduced AKT S473 (e) and mTOR S2448 (f) phosphorylation in *Cdkl5*$^{-/y}$ mice. Phosphorylated protein levels are normalized to GAPDH loading control and expressed relative to WT levels. *p<0.05, unpaired two-tailed Student's t-test with Bonferroni correction.

(g-h) Quantification of total AKT (g) and mTOR (h) in WT and *Cdkl5*$^{-/y}$ mice. Protein levels are normalized to GAPDH loading control and expressed relative to WT levels. n.s.: not significant; unpaired two-tailed Student's t-test.

Figure S1

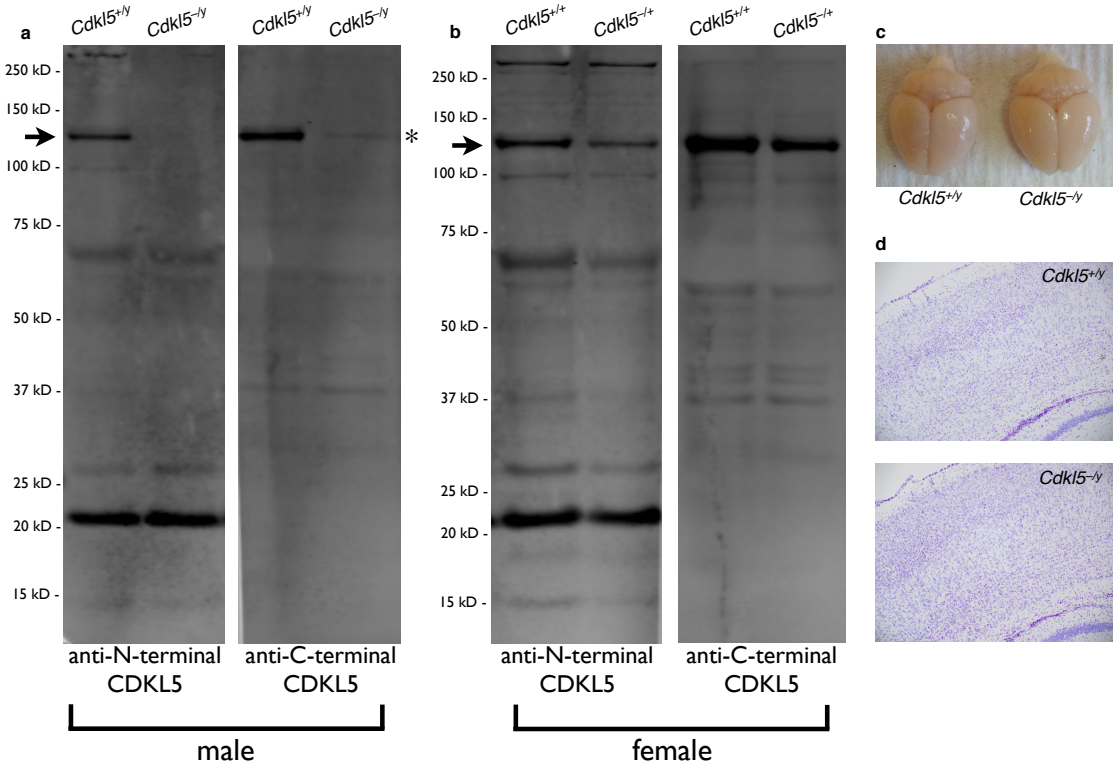

Figure S1. Western blot analysis of CDKL5 expression and examination of brain morphology in *Cdkl5* knockout mice.

(a) Western blot of cortical neurons (5DIV) isolated from WT (*Cdkl5*$^{+/y}$) and knockout *Cdkl5*$^{-/y}$ male embryos (E16.5) probed with antibodies raised up against the N or C-terminus of CDKL5. Full-length CDKL5, denoted by an arrow, is absent in *Cdkl5*$^{-/y}$ neurons. Non-specific bands detected by both antibodies are present in both WT and *Cdkl5*$^{-/y}$ lysate. A non-specific band running at the same size as full-length CDKL5, denoted by an asterisk, is detected by the C-terminal antibody. Additional truncated CDKL5 is not detected in *Cdkl5*$^{-/y}$ mice by either antibody.

(b) Western blot of cortical neurons (5DIV) isolated from WT female (*Cdkl5*$^{+/+}$) and heterozygous female *Cdkl5*$^{-/+}$embroyos (E16.5) probed with antibodies raised up against the N or C-terminus of CDKL5. Full-length CDKL5 is denoted by an arrow. CDKL5 protein levels are reduced in female heterozygous mice (*Cdkl5*$^{-/+}$) relative to female WT mice, indicative of typical X-linked mosaic expression.

(c) Brain size of *Cdkl5*$^{-/y}$ mice is comparable to that of WT littermates.

(d) Nissl staining of coronal brain sections reveals comparable cortical thickness in WT and *Cdkl5*$^{-/y}$ mice.

Figure S2

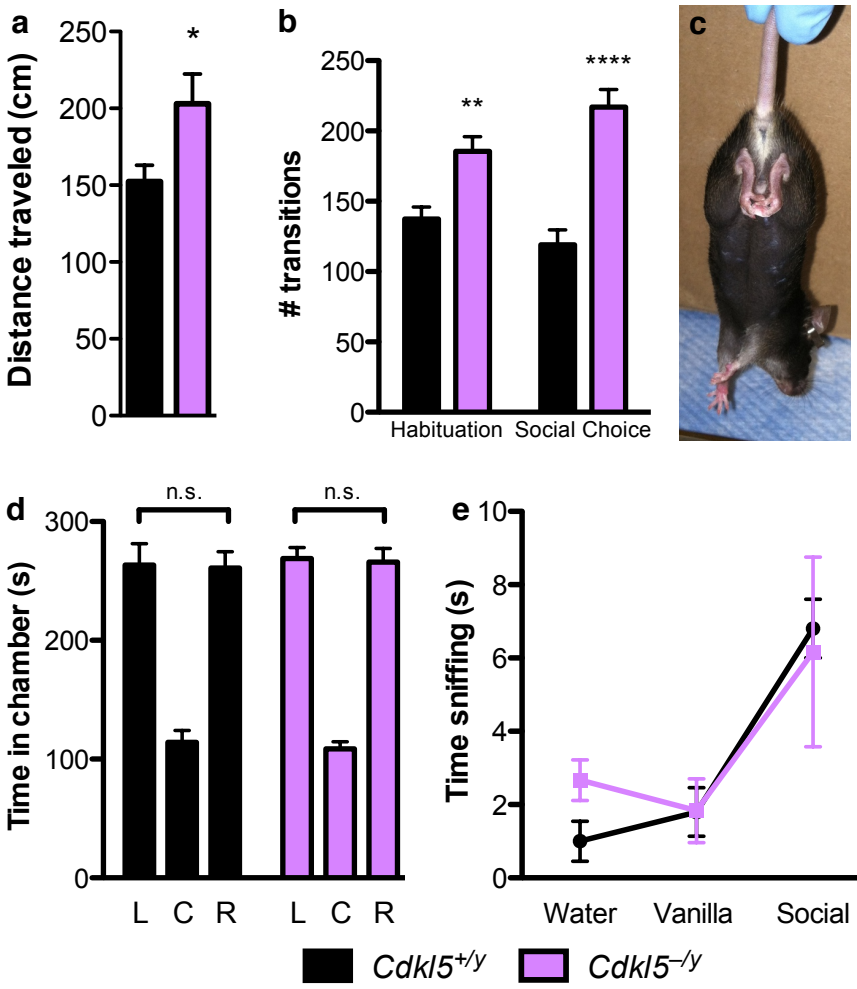

Figure S2. Behavioral characterization of *Cdkl5* knockout mice.

(a) *Cdkl5*$^{-/y}$ mice (n=14) travel a greater distance relative to WT (*Cdkl5*$^{+/y}$) littermates (n=12) in a zero maze assay. *p<0.05, unpaired two-tailed Student's t-test.

(b) Locomotor activity during three-chambered social approach test is increased in *Cdkl5*$^{-/y}$ mice (n=17) during both habituation and testing phase of social choice assay relative to WT littermates (n=15). Two-way ANOVA with Bonferroni correction, p<0.05 (interaction); **p<0.01, ****p<0.0001.

(c) Hindlimb clasping in *Cdkl5*$^{-/y}$ mice.

(d) Both WT (n=15) and *Cdkl5*$^{-/y}$ mice (n=17) explore both L (left) and R (right) chambers equally during the habituation phase of social approach assay, prior to introduction of novel object or stimulus mouse into either chamber. C: center. Two-way ANOVA with Bonferroni correction, p>0.05 (main effect of chamber); n.s., not significant.

(e) *Cdkl5*$^{-/y}$ mice (n=17) and WT littermates (n=15) show similar olfactory response in distinguishing neutral scents (water, vanilla), from social scents (swab from another cage). Two-way ANOVA, p>0.05 (interaction). All data are presented as mean ± s.e.m.

Figure S3

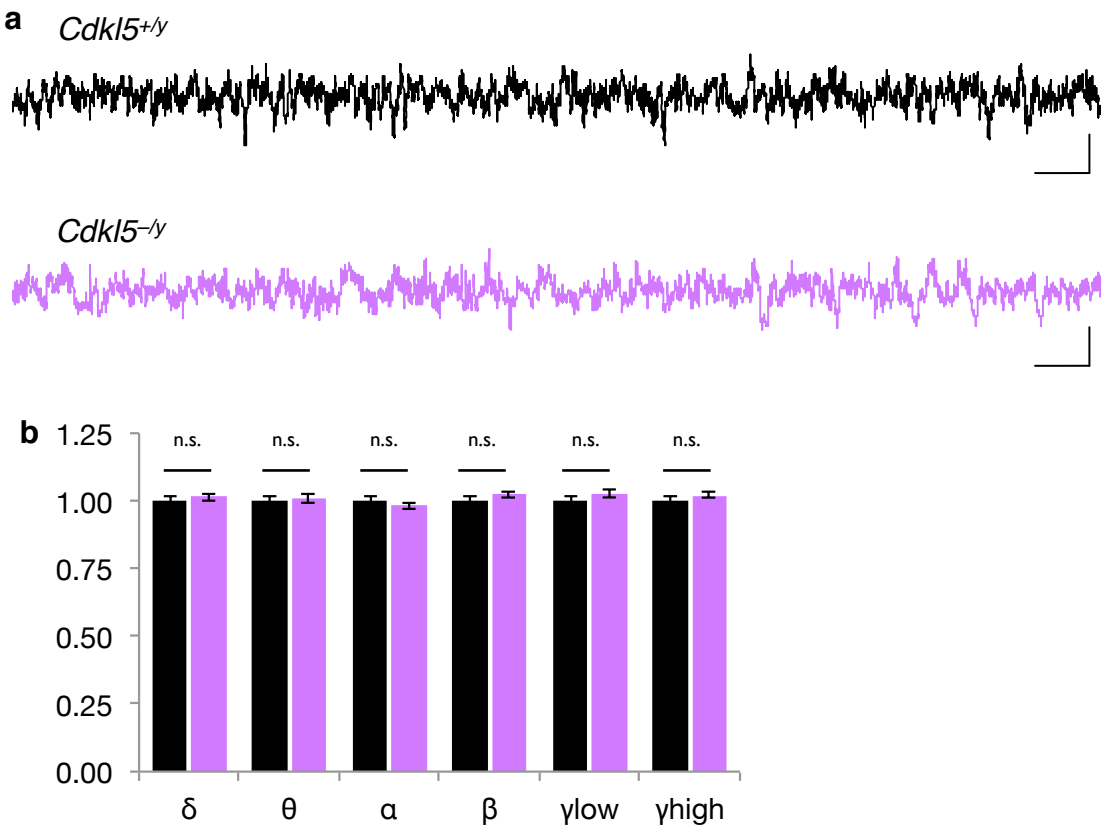

Figure S3. Basal EEG activity in *Cdkl5*$^{-/y}$ mice is similar to that of WT littermates.

(a) Representative EEG trace under basal conditions in awake, freely mobile mice. Scale bar corresponds to 1 s (horizontal) and 200 μA (vertical).

(b) Basal EEG power in WT (*Cdkl5*$^{+/y}$) (n=9) and *Cdkl5*$^{-/y}$ mice (n=9). Frequency bands are represented as follows: δ (2–4 Hz), θ (4–8 Hz), α (8–12 Hz), β (12–30 Hz), γ_{low} (30–50 Hz) and γ_{high} (70–140 Hz). Data are presented as mean ± s.e.m.; n.s., not significant, unpaired two-tailed Student's t-test with Bonferroni correction.

Figure S4

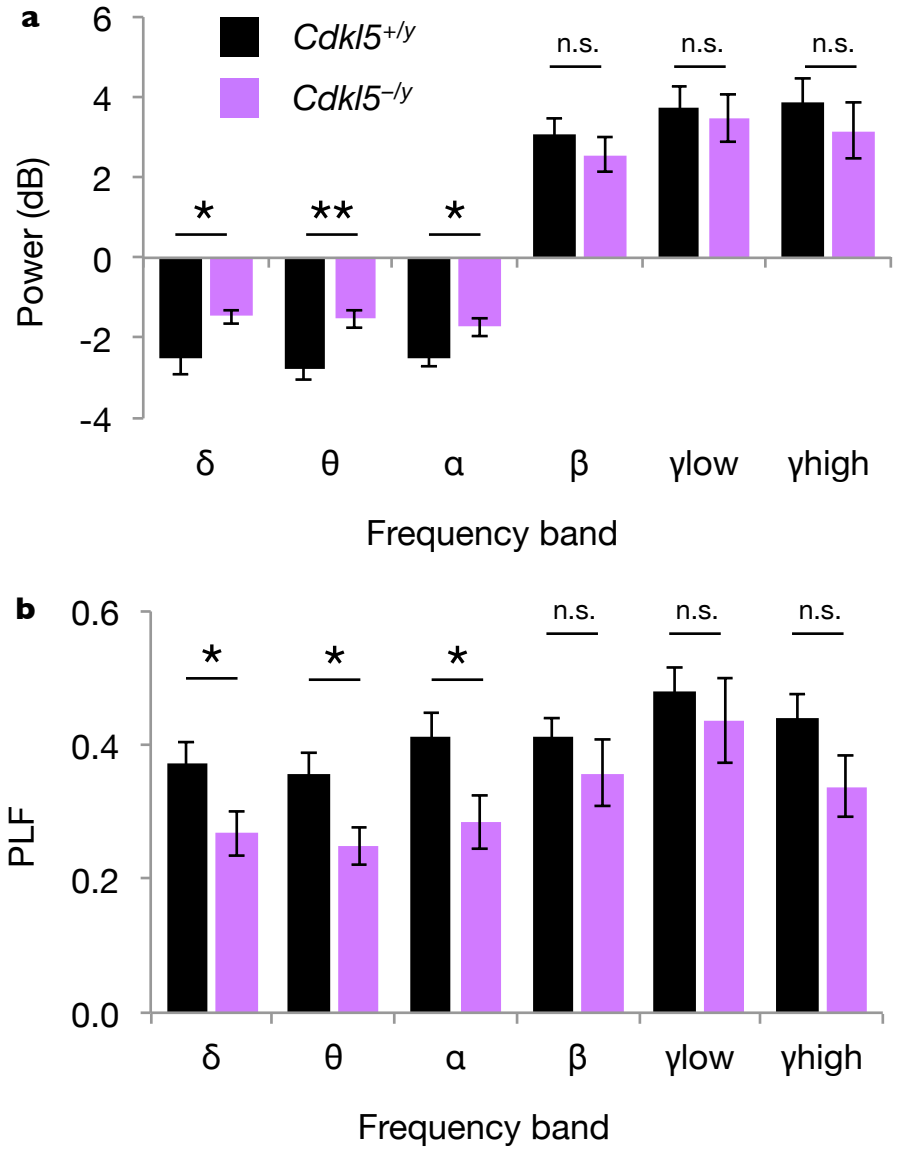

Figure S4. Decrease in event-related power and PLF in *Cdkl5*$^{-/y}$ mice are primarily found in low-frequency oscillations.

(a) Quantification of event-related power changes relative to pre-stimulus baseline in WT (*Cdkl5*$^{+/y}$) (n=9) and *Cdkl5*$^{-/y}$ mice (n=9). Frequency bands are represented as follows: δ (2–4 Hz), θ (4–8 Hz), α (8–12 Hz), β (12–30 Hz), γlow (30–50 Hz) and γhigh (70–140 Hz). *Cdkl5*$^{-/y}$ mice show decreased event-related power relative to WT in low-frequency δ, θ, and α oscillations. **p<0.01, *p<0.05, n.s., not significant, unpaired two-tailed Student's t-test with Bonferroni correction.

(b) Quantification of event-related PLF changes following 85-dB auditory stimulus. *Cdkl5*$^{-/y}$ mice have decreased event-related PLF power relative to controls in low-frequency δ, θ, and α oscillations. Data are presented as mean ± s.e.m.; *p<0.05, n.s., not significant, unpaired two-tailed Student's t-test with Bonferroni correction.

Figure S5

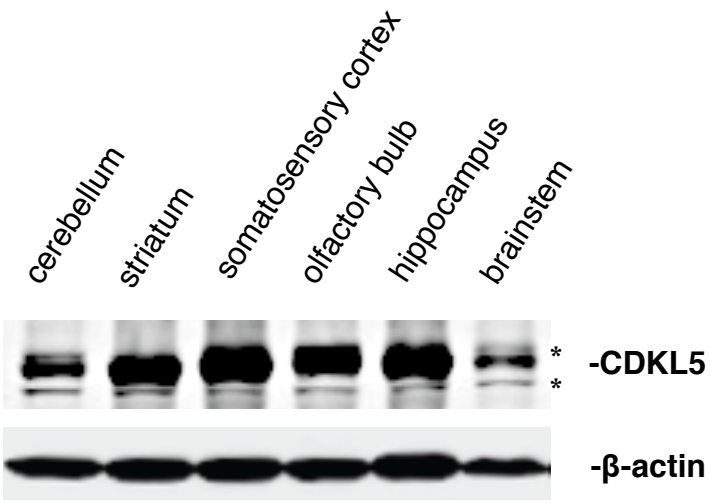

Figure S5. Enrichment of CDKL5 in forebrain regions.

Western blot of whole cell lysate prepared from indicated brain regions from WT mice probed with a polyclonal antibody raised against the N-terminus of CDKL5. CDKL5 (107 kDa) is enriched in the striatum, somatosensory cortex, olfactory bulb, and hippocampus relative to the cerebellum and brainstem. *cross-reacting bands

Figure S6

a

Lane	Genotype	Brain Region
1	WT	cerebellum
2	WT	striatum
3	WT	somatosensory cortex
4	WT	olfactory bulb
5	WT	hippocampus
6	WT	brainstem
7	WT	whole brain
8	KO	cerebellum
9	KO	striatum
10	KO	somatosensory cortex
11	KO	olfactory bulb
12	KO	hippocampus
13	KO	brainstem
14	KO	whole brain

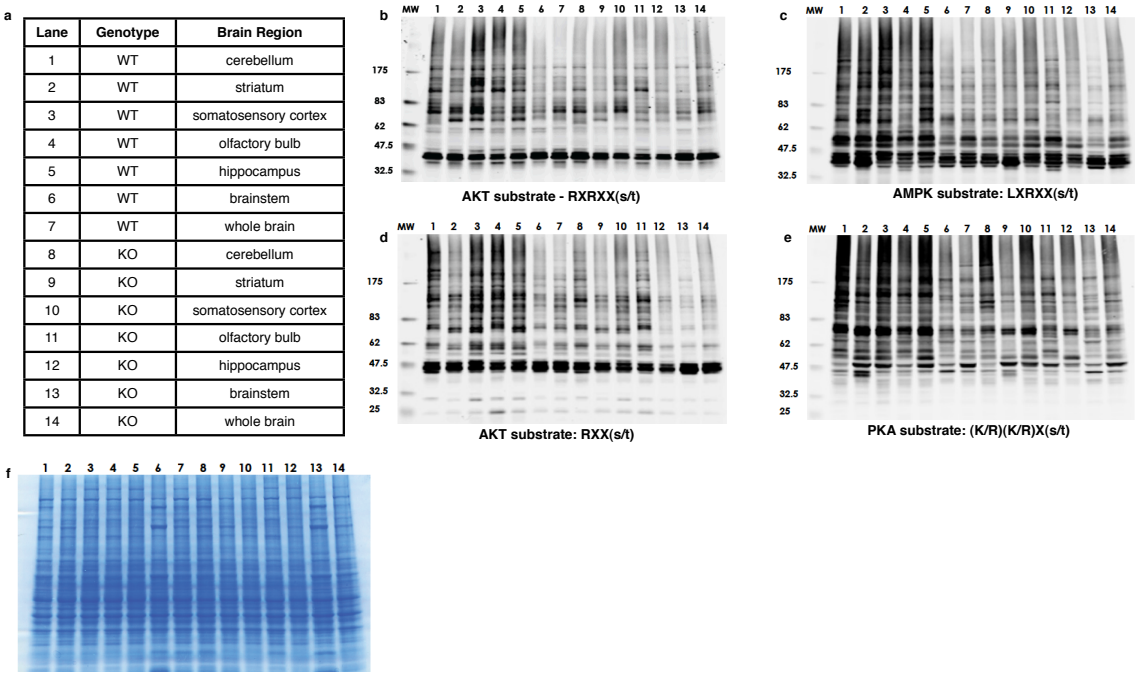

Figure S6. Strongly altered kinome profiles in *Cdkl5*$^{-/y}$ mice.

(a) Description of lane contents for (b)-(f). WT: *Cdkl5*$^{+/y}$; KO: *Cdkl5*$^{-/y}$

(b-e) Western blot of whole cell lysate isolated from indicated brain regions probed with an antibody specific for an RXRXX(s/t) phosphorylation motif representing AKT kinase substrates (b), an antibody specific for an LXRXX(s/t) phosphorylation motif representing AMPK kinase substrates (c), an antibody specific for an RXX(s/t), phosphorylation motif representing AKT kinase substrates (d), an antibody specific for a (K/R)(K/R)X(s/t) phosphorylation motif representing PKA kinase substrates (e).

(f) Commassie stain showing equal protein loading of all gels.

Figure S7

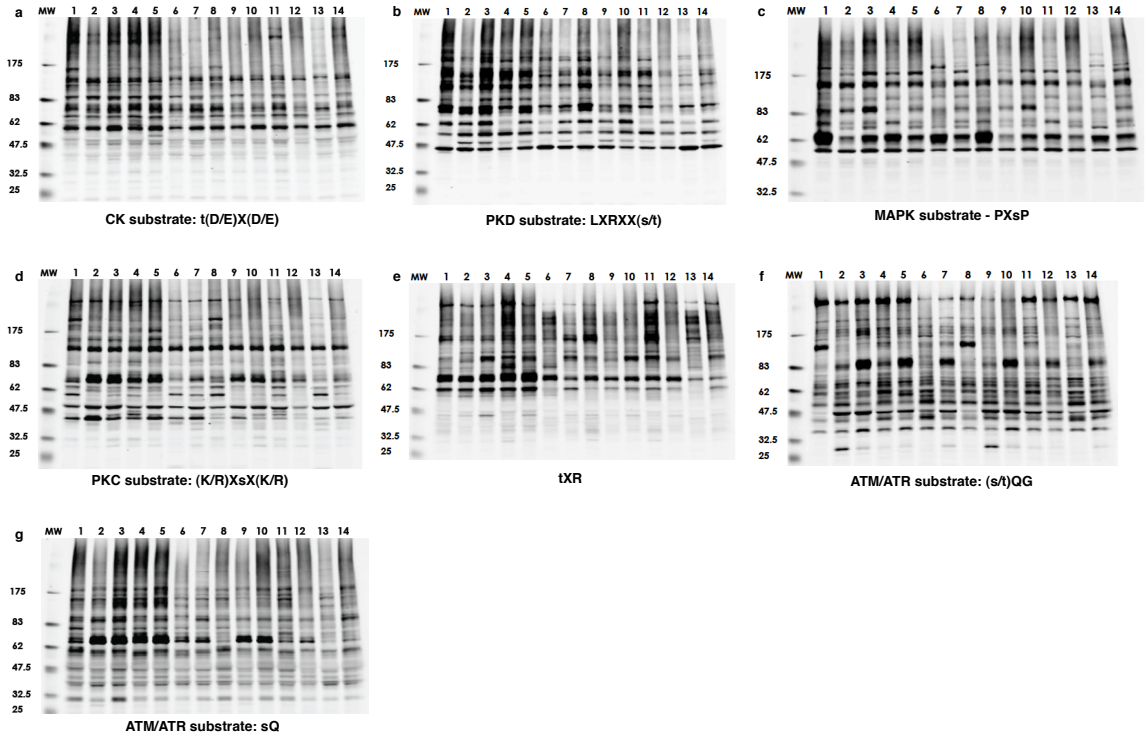

Figure S7. Moderately altered kinome profiles in *Cdkl5*$^{-/y}$ mice.

(a-g) Western blots of whole cell lysate isolated from different brain regions probed with antibodies specific for phosphorylation motifs as indicated. Brain regions 1-14 are described in Figure S6a.

Figure S8

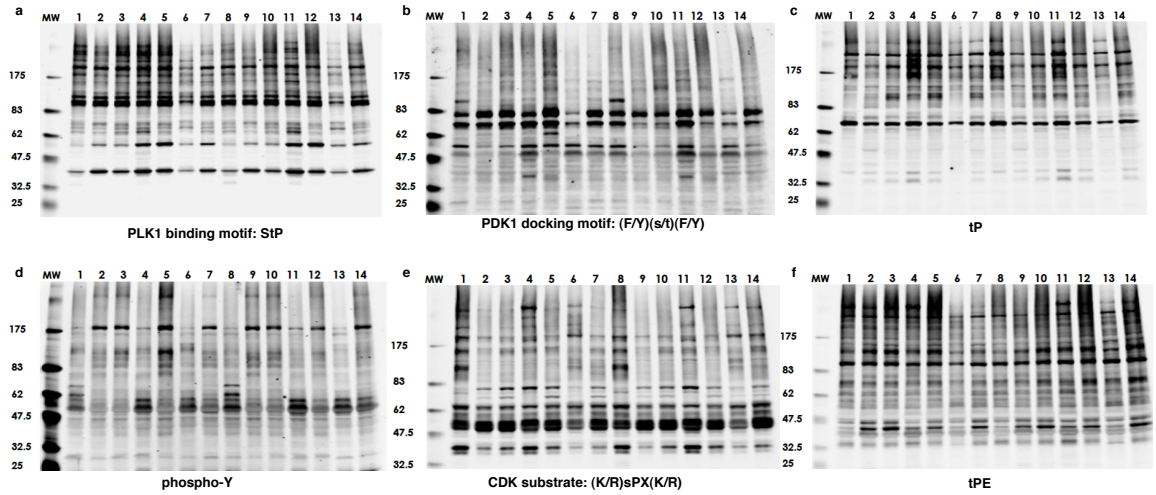

Figure S8. Mildly altered kinome profiles in *Cdkl5*$^{-/y}$ mice.

(a-f) Western blots of whole cell lysate isolated from different brain regions probed with antibodies specific for phosphorylation motifs as indicated. Brain regions 1-14 are described in Figure S6a.

Figure S9

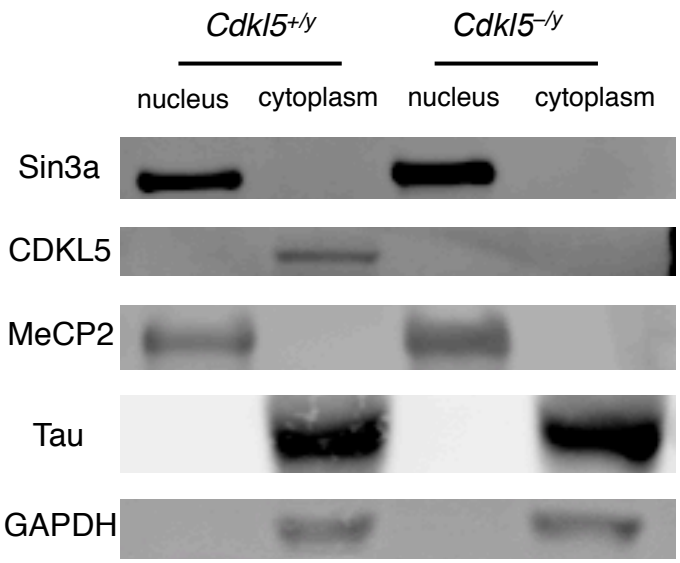

Figure S9. Enrichment of CDKL5 in the cytoplasm.
CDKL5 is predominantly found in the cytoplasm. As controls, Sin3a and MeCP2 are predominantly in the nucleus, while Tau and GAPDH are predominantly in the cytoplasm.

Chapter 3:

GENETIC DISSECTION OF CDKL5 DISORDER

I-Ting Judy Wang, Cuiyong Yue, Arith Reyes, Jun Lee, Darren Goffin, Edward Brodkin, Julie Blendy, Douglas Coulter, and Zhaolan Zhou

This chapter consists of unpublished and ongoing work investigating the mechanisms by which *Cdkl5* loss-of-function leads to disease. Using a conditional knockout mouse approach, this study has revealed that mice lacking CDKL5 in the brain recapitulate a number of behavioral phenotypes of the constitutive knockout. In addition, mice lacking CDKL5 from forebrain glutamatergic neurons and mice lacking CDKL5 from forebrain GABAergic neurons show distinct behavioral phenotypes suggestive of circuit- and cell type-specific mechanisms underlying CDKL5 disorder pathogenesis. Ongoing work aims to investigate the neuronal circuits, synapses, and signaling pathways mediating these behaviors, with the ultimate goal of identifying substrates or signaling pathways that can be targeted for therapeutics in order to restore circuit function and rescue behavioral abnormalities.

Introduction

Mutations in the X-linked gene encoding cyclin-dependent kinase-like 5 (CDKL5) cause CDKL5 disorder, an infantile epileptic encephalopathy with features of intellectual disability and intractable seizures (Nabbout and Dulac, 2011; Prince and Ring, 2011). CDKL5 patients show a heterogeneous array of other clinical phenotypes, the most prominent of which include autism, poor motor learning, stereotypical hand movements, and hypotonia (Bahi-Buisson et al., 2008b; Fehr et al., 2012). A subset of CDKL5 patients have also been diagnosed with Infantile Spasms (Kalscheuer et al., 2003), the early seizure, or Hanefeld, variant of Rett Syndrome (RTT) (Hanefeld, 1985; Neul et al., 2010; Tao et al., 2004; Weaving et al., 2004), and autism spectrum disorder (ASD) (Sakai et al., 2011). Despite the strong genetic linkage between *CDKL5* mutations and neurodevelopmental disorders (Archer et al., 2006; Nemos et al., 2009; White et al., 2010), the biological function of CDKL5 and the pathogenic mechanisms underlying disease remain largely uncharacterized. Consequently, treatments for CDKL5 disorder have been largely ineffective and limited to symptom management (Bahi-Buisson and Bienvenu, 2012; Kilstrup-Nielsen et al., 2012).

Although patients with CDKL5 disorder represent a small total population, the steady increase in rate of CDKL5 diagnoses each year and the notably high frequency of *CDKL5* mutations found in enriched populations of patients with epilepsy or autism (Archer et al., 2006; Bahi-Buisson et al., 2008b; Mei et al., 2014; Mirzaa et al., 2013; Nemos et al., 2009; White et al., 2010) suggests that the disorder may be more prominent than currently understood. Moreover, several clinical phenotypes of CDKL5 disorder are shared among epileptic encephalopathies, disorders of intellectual disability, and autism spectrum disorders. Therefore, a thorough understanding of the neural circuits and cellular mechanisms underlying this monogenic disorder may illuminate therapeutic targets that are relevant to autism and epilepsy disorders with more complex etiologies.

The presence of a highly conserved serine-threonine kinase domain in the CDKL5 N-terminus indicates that disrupted CDKL5 kinase function may underlie CDKL5 disease mechanism. The presence of Rett-like features in CDKL5 patients and that discovery

that MeCP2, the methyl-CpG binding protein genetically responsible for Rett Syndrome (Amir et al., 1999), is regulated by phosphorylation (Chen et al., 2003; Zhou et al., 2006), suggest that CDKL5 and MeCP2 may act in a common pathway. Indeed, CDKL5 has been shown to phosphorylate MeCP2 *in vitro* (Mari et al., 2005), but whether MeCP2 is a *bona fide* kinase substrate of CDKL5 is contentious (Lin et al., 2005). Other *in vitro* kinase substrates have been identified, including DNA methyltransferase 1 (Dnmt1) and Amphiphysin1 (Amph1), but their *in vivo* relevance has yet to be determined (Kameshita et al., 2008; Sekiguchi et al., 2013).

CDKL5 has also been found to bind and phosphorylate NGL-1, a netrin-G1 receptor that regulates early synapse formation and maturation, which then binds PSD95 and localizes to dendritic spines (Ricciardi et al., 2012). In this study, shRNA-mediated knockdown of *Cdkl5* increases spine density and length and reduces synapse number, indicating that CDKL5 plays a role in spine maturation and synapse morphogenesis by promoting the NGL-1—PSD95 interaction. This mechanism, however, is contested, as a separate group has shown that CDKL5 binds directly to palmitoylated PSD95 and is thus recruited to dendritic spines, and that shRNA-mediated knockdown of *Cdkl5* decreases spine density and width (Zhu et al., 2013). Moreover, while both groups have demonstrated that *in utero* electroporation of an shRNA construct targeting *Cdkl5* delays neuronal migration (Chen et al., 2010; Ricciardi et al., 2012), only one group identified impaired neuronal outgrowth using this technique (Chen et al., 2010). Therefore, despite the research progress made in establishing a developmental role for CDKL5 and localizing the protein to excitatory synapses, the field continues to be hindered by inconsistent findings and conflicting mechanisms.

The development and characterization of mouse models can serve as powerful tools to reconcile incongruous results and to establish the *in vivo* relevancy of proposed functions. To date, two CDKL5 knockout (KO) mouse lines have been generated, and reduced soma size (Wang, unpublished) and dendritic length have been identified in cortical layer 5 and hippocampal pyramidal neurons on CDKL5 KO mice (Amendola et al., 2014; Wang et al., 2012). In addition, postmitotic newborn dentate granule neurons from CDKL5 KO mice show decreased survival and dendritic outgrowth (Fuchs et al., 2014). Together, these data demonstrate an *in vivo* role for CDKL5 in neuronal

development, but the mechanisms underlying this regulation and how they contribute to behavioral impairments remain unknown.

Both CDKL5 KO mouse models mirror several CDKL5 clinical phenotypes, including poor motor coordination, impaired learning and memory, and autistic-like deficits in sociability (Fuchs et al., 2014; Wang et al., 2012). These behavioral phenotypes may be mediated by disruptions in neuronal circuit communication, as both visual and auditory sensory information processing are impaired in CDKL5 KO mice (Amendola et al., 2014; Wang et al., 2012). Additionally, disruptions in multiple signaling pathways, including the Akt/mTOR pathway have been identified in CDKL5 KO mice (Amendola et al., 2014; Fuchs et al., 2014; Wang et al., 2012), suggesting a disease mechanism by which loss of CDKL5 may disrupt signaling pathways relevant to neuronal development, leading to impaired neural circuit communication and behavioral abnormalities.

Interestingly, neither CDKL5 KO mouse model develop spontaneous seizures or demonstrate altered seizure threshold, despite extensive video-EEG monitoring (Amendola et al., 2014; Wang et al., 2012). Although EEG patterns in CDKL5 KO mice differ from that of WT mice upon seizure induction (Amendola et al., 2014), the absence of the spontaneous seizure phenotype, which is a diagnostic criterion for CDKL5 disorder (Neul et al., 2010), challenges the face validity of the constitutive knockout mice and prompts the need for a CDKL5 mouse model that can recapitulate this key phenotype.

Recent conditional knockout mouse studies have demonstrated that distinct neuronal subpopulations control different neural circuits, and that selective perturbation of these circuits can cause discrete behavioral phenotypes (Hong et al., 2014; Ozkan et al., 2014), some of which are not manifested in the constitutive knockout (Chao et al., 2010; Goffin et al., 2014). Moreover, these studies have illuminated the contribution of individual cell types toward neural circuit function and isolated cell type-specific mechanisms underlying disease manifestation. We hypothesized, therefore, that CDKL5 KO phenotypes may segregate upon cell type-specific CDKL5 ablation, and that a conditional knockout strategy may provide unique mouse models that recapitulate key features of CDKL5 disorder and pinpoint neuronal circuits and cell types through which

CDKL5 regulation is central, leading to novel mechanistic understanding of CDKL5 function.

A mechanism proposed to commonly underlie both ASDs and epilepsy is an imbalance in neuronal excitation and inhibition (E/I) (Brooks-Kayal, 2010; Rubenstein and Merzenich, 2003). Given the prominence of these features in CDKL5 disorder, we hypothesized that loss of CDKL5 creates a shift in E/I balance and that selective ablation of CDKL5 from excitatory or inhibitory neuronal populations would isolate the neuronal circuits and cell types underlying this shift. Interestingly, we found that selective deletion of CDKL5 from forebrain GABAergic neurons recapitulates autistic-like phenotypes, whereas selective deletion of CDKL5 from forebrain glutamatergic neurons results in spontaneous seizures, working memory deficits and context-dependent hyperactivity. The separation of distinct aspects of CDKL5 disorder-related phenotypes in the two complementary conditional KO lines suggests that epileptic and autistic phenotypes of CDKL5 disorder are mediated by distinct neural circuits and that loss of CDKL5 in specific cell types may differentially disrupt signaling pathways and impair neuronal function.

Results

Generation of CDKL5 floxed mice

We previously generated a CDKL5 KO mouse that mirrors many clinical CDKL5 features, including autistic-like phenotypes, impaired motor control, and deficits in learning and memory (Wang et al., 2012). These mice recapitulate a CDKL5 patient splice site mutation that leads the skipping of exon 7 and a reading frame shift that results in a premature stop codon in exon 8 (Archer et al., 2006). To mimic the effects of this splice site mutation in mice, we deleted the homologous mouse *Cdkl5* exon 6, leading to an early truncation of CDKL5 in its N-terminal kinase domain, thereby disrupting kinase activity. Importantly, the *Cdkl5* mRNA levels in these mice are dramatically reduced, which is likely a consequence of nonsense-mediated mRNA decay (**Figure 1b**). In addition, full-length or truncated CDKL5 cannot be detected by Western blot using antibodies directed against CDKL5 N- or C-terminal domains (**Figure 1c**) (Wang et al., 2012).

We used a similar genetic strategy to generate CDKL5 floxed mice, flanking exon 6 with loxP sites, such that a *Cdkl5* loss-of-function allele can be generated upon Cre-mediated recombination (**Figure 1a**). Male CDKL5 floxed mice ($Cdkl5^{2lox/y}$) mice express WT levels of *Cdkl5* mRNA transcript and CDKL5 protein (**Figures 1b, c**), are viable and fertile on a C57BL/6 background, and show no gross developmental or behavioral abnormalities, and will therefore be referred to as WT hereafter.

Loss of CDKL5 from the brain recapitulates many CDKL5-related phenotypes

Although the time course and expression patterns of CDKL5 vary across studies, we and others have consistently found that the CDKL5 protein is expressed in multiple tissues but enriched in the brain (Chen et al., 2010; Lin et al., 2005). To investigate the contribution of CDKL5 in the brain toward disease progression, we generated mice lacking CDKL5 specifically from the nervous system. Given that maternal transmission of the imprinted Nestin-Cre transgene has been demonstrated to result in reduced recombination frequency (Fan et al., 2001), we crossed male mice heterozygous for Nestin-Cre to female mice homozygous for the CDKL5 floxed allele (**Figure 2a**)

(Tronche et al., 1999). To avoid the confounding effects of mosaic CDKL5 expression from X-chromosome inactivation in females, we focused our study on male mice, and compared hemizygous male *Cdkl5*$^{2lox/y}$ mice carrying the Nestin-Cre allele (Nestin-cKO) to hemizygous male *Cdkl5*$^{2lox/y}$ mice (WT). We performed a battery of behavioral assays and found that mice lacking CDKL5 from the central nervous system recapitulate almost all behavioral phenotypes identified in the CDKL5 constitutive KO mice (Wang et al., 2012). In a locomotor assay within a homecage-like environment, Nestin-cKO mice demonstrate significantly higher motor activity than WT littermate controls (**Figure 2b**), and in a zeromaze assay, they show decreased anxiety, spending more time in the open arms and less time in the closed arms relative to controls (**Figure 2c**). We also observed ASD-like deficits in sociability, as Nestin-cKO mice spent less time directly interacting with a novel gonadectomized male A/J stimulus mouse relative to WT and displayed impaired nest building, a phenotype related to homecage social behavior (**Figures 2d,e**) (Deacon, 2006; Silverman et al., 2010). Overall, the behavioral similarities between Nestin-cKO and CDKL5 constitutive KO mice indicate that CDKL5 disorder is caused by *Cdkl5* loss-of-function within the brain.

Loss of CDKL5 from forebrain GABAergic neurons recapitulates ASD-like phenotypes

Within the brain, CDKL5 is likely to play a prominent role in neurons, as it is absent or expressed as a different isoform in glial cells (Chen et al., 2010; Rusconi et al., 2008), and loss of CDKL5 does not affect gliogenesis (Fuchs et al., 2014). In addition, CDKL5 is enriched in the forebrain (Thompson et al., 2014; Wang et al., 2012), and is expressed in both glutamatergic and GABAergic neurons (Chen et al., 2010; Rusconi et al., 2008). Therefore, we focused our studies on forebrain conditional neuronal knockouts. To test the hypothesis that loss of CDKL5 disrupts neuronal E/I balance, we generated mice lacking CDKL5 from forebrain glutamatergic neurons or forebrain GABAergic neurons by crossing female mice homozygous for the *Cdkl5* floxed allele to male mice heterozygous for Nex-Cre (Goebbels et al., 2006) or Dlx5/6-Cre (Monory et al., 2006), respectively (**Figure 4a**). Similarly to that of our Nestin-cKO studies, male hemizygous *Cdkl5*$^{2lox/y}$ mice carrying the Nex-Cre allele (Nex-cKO) or the Dlx5/6-Cre allele (Dlx-cKO) were compared to male hemizygous *Cdkl5*$^{2lox/y}$ littermates (WT).

Although these Cre-driver mouse lines are commonly used in conditional knockout studies (Chao et al., 2010; Goffin et al., 2014; Ka et al., 2014), we sought to assess the specificity of Cre-recombination in our complementary conditional knockout mouse lines. In our hands, commercially available and in-house purified CDKL5 antibodies show promiscuity, as Western blots using whole brain lysate from both WT and KO mice probed with CDKL5 antibodies detect full-length CDKL5 at the expected size (115 kDa) in addition to multiple non-specific immunoreactive bands (Wang et al., 2012). Indeed, brain tissue slices obtained from CDKL5 KO mice immunostained for CDKL5 are indistinguishable from that of WT mice (Wang, unpublished). To confirm the specificity and efficiency of Cre-mediated removal of CDKL5 expression in Dlx- and Nex-cKO mice, therefore, we performed Western blotting for CDKL5 on protein lysates prepared from dissected brain regions in which GABAergic or glutamatergic neurons are differentially enriched. We chose to isolate tissue from the striatum and cortex, given that about 98% of neurons in the striatum are GABAergic and express Dlx5/6, and about 80% of neurons in the cortex are glutamatergic and express Nex. As a negative control, we isolated the cerebellum, a brain region with low CDKL5 expression (Wang et al., 2012). Despite the presence of several nonspecific bands with consistent protein levels across samples, we found that CDKL5 expression (~115kDa) is significantly reduced in striatal lysate from Dlx-cKO but not Nex-cKO or WT mice, and that conversely, CDKL5 expression is significantly reduced in cortical lysate from Nex-cKO but not Dlx-cKO or WT mice (**Figure 3**). As expected, CDKL5 expression is consistently low in the cerebellum of all 3 genotypes (**Figure 3**). Together, these data validate the efficiency and specificity of forebrain glutamatergic or GABAergic CDKL5 ablation in our Nex- and Dlx-cKO mice.

To determine the phenotypic profile of our CDKL5 conditional knockouts, we performed a battery of behavioral assays and found that Dlx-cKO, but not Nex-cKO mice, display several autistic-like features. In a three-chambered social approach assay, all three genotypes demonstrate no initial preference for empty cylinders in opposite chambers (**Figure 4b**). Upon introduction of a novel object into one cylinder (non-social cylinder) and a novel gonadectomized A/J stimulus mouse into the other cylinder (social cylinder), both WT and Nex-cKO mice demonstrate increased preference for the social cylinder, reflecting the innate social nature of mice (**Figure 4c**) (Sankoorikal et al., 2006). In

contrast, Dlx-cKO mice do not show this increased preference, indicating an autistic-like deficit in sociability. Moreover, when the cylinders are removed to allow freely mobile direct interaction, Dlx-cKO, but not Nex-cKO mice, spend significantly less time interacting with the stimulus mice relative to WT mice (**Figure 4d**). A similar autistic-like phenotype is observed in homecage sociability nesting behavior, where Dlx-cKO mice demonstrate a selective deficit in nest building ability, while Nex-cKO mice build nests comparable to that of WT mice (**Figure 4e**). Importantly, no deficits in olfaction were identified in an olfaction habituation/dishabituation assay, indicating that the selective impairments in sociability in Dlx-cKO mice are not the secondary consequence of an inability to discriminate between social and neutral odors (**Figure 4f**).

These data demonstrate that mice lacking CDKL5 from forebrain GABAergic neurons have deficits in social communication and interaction, which is the first of two main criteria of ASD, as defined by the 2013 DSM-5 revision. The other core ASD domain is restrictive and repetitive behaviors, which can be modeled in mice through repetitive behavioral assays and measurements of cognitive flexibility. Therefore, we measured homecage self-grooming and digging behavior, which is believed to be an indicator of repetitive and stereotyped behaviors (Peñagarikano et al., 2011; Silverman et al., 2010). Consistent with decreased sociability, we found that Dlx-cKO mice, but not Nex-cKO mice, spend significantly more time engaging in repetitive homecage grooming and digging behavior relative to WT mice (**Figure 4g**).

To assess cognitive flexibility, or perseverative behavior in mice, we performed a Barnes maze forward and reversal learning test. In this assay, mice are trained in 8 trials over 4 days (2 trials/day) to locate a hidden escape hole from among 20 evenly spaced holes along the perimeter of a circular platform. The platform is placed in a brightly lit room with spatial cues placed along the walls, and mice must learn where the escape hole is relative to the spatial cues. All three genotypes demonstrated similar latency to enter the target box during training, indicating a comparable ability to learn the task (**Figure 5a**). On the 5th day, a probe trial is performed, in which the escape hole is closed and mice must rely solely on the spatial cues along the wall to locate the escape box. In the probe trial, both Nex- and Dlx-cKO show a comparable number of visits to the target hole (**Figure 5b**), a similar pattern of number of visits to each hole (**Figure 5c**) and a

comparable amount of time spent at each hole relative to that of WT (**Figure 5d**). Together, these data indicate that all three genotypes are able to locate the target hole using the spatial cues and do not have impairments in spatial learning.

In the Barnes maze reversal learning assay, the hidden escape hole is moved 180 degrees to the opposite end of the circular platform, while the spatial cues in the room remain the same. Therefore, mice must learn that the escape box has moved to a new location, and poor performance in this task is indicative of poor cognitive flexibility. Similar to that of forward learning, all three genotypes have comparable learning curves during the 8 trials across 4 days of reversal training, showing similar latency to enter the escape boxes (**Figure 5e**). In the reversal probe trial on the 5th day, all three genotypes visit the new target location comparably (**Figure 5f**), indicating the similar use of spatial cues to learn the new location of the target box. The pattern of visits to each hole and the amount of time spent at each hole, however, differs in both Dlx- and Nex-cKO mice, relative to WT (**Figures 5g,h**). Whereas WT mice demonstrate no preference for the old hole in time spent or number of visits, both Dlx- and Nex-cKO mice demonstrate cognitive inflexibility, visiting the old hole significantly more times than WT animals (**Figures 5g,i**) and spending significantly more time at the old hole than WT animals (**Figures 5h,j**). This kind of perseverative behavior has been identified in several ASD mouse models (Crawley, 2007; Nakatani et al., 2009) and is believed to model restrictive interests in ASDs. Surprisingly, the Nex-cKO mice also demonstrate ASD-like cognitive inflexibility, but this phenotype may be related to a context-dependent hyperactivity phenotype (**Figures 8e,f**), discussed below. Overall, these data indicate that the loss of CDKL5 from forebrain GABAergic neurons, but not glutamatergic neurons, mediates the selective development of autistic-like behaviors in mice.

The striking restriction of ASD-like phenotypes to mice lacking CDKL5 from GABAergic neurons prompted us to verify this separation of phenotypes in a different and more broad CDKL5 GABAergic conditional knockout mouse line. Therefore, we generated mice lacking CDKL5 from all GABAergic and glycinergic neurons in the brain, including the hindbrain, by crossing female mice homozygous for the *Cdkl5* floxed allele to male mice heterozygous for the Viaat-Cre allele (Chao et al., 2010), and compared male hemizygous *Cdkl5*$^{2lox/y}$ mice carrying the Viaat-Cre allele (Viaat-cKO) to male

hemizygous *Cdkl5*$^{2lox/y}$ littermates (WT) (**Figure 6a**). Western blots of brain tissue isolated from the striatum, cortex, and cerebellum of Viaat-cKO and WT mice showed, similar to that of Dlx-cKO mice, a selective loss of CDKL5 in the striatum but not the cortex of Viaat-cKO mice. Importantly, the endogenously low levels of CDKL5 in the cerebellum were further reduced in Viaat-cKO mice, thus confirming the specificity and efficiency of our CDKL5 conditional deletion (**Figure 6b**). In behavioral assays, these mice demonstrated autistic-like phenotypes identical to those of Dlx-cKO mice, including reduced preference for a social cylinder relative to a non-social cylinder, reduced time directly interacting with a stimulus mouse, impaired nesting ability, and increased homecage repetitive behavior relative to that of WT mice (**Figures 6c-g**).

Loss of CDKL5 from forebrain glutamatergic neurons leads to development of spontaneous seizures

In contrast to Dlx- and Viaat-cKO mice, Nex-cKO mice do not demonstrate autistic-like phenotypes. While performing behavioral assays, however, we observed spontaneous seizures in several Nex-cKO mice. These seizures ranged in severity and duration, from brief rearing and falling followed by normal behavior, to generalized tonic-clonic seizures following by extended rearing and eventually death (**Figure 7**). The spontaneous seizure phenotype appears to be exclusive to Nex-cKO mice, as we have not observed seizures in WT, Dlx- and Viaat-cKO mice. Future video-EEG monitoring of WT, Dlx- and Nex-cKO mice across different developmental time points will help to identify seizure type, onset, and frequency in mice, and whether the spontaneous seizure phenotype is indeed exclusively related to loss of CDKL5 from glutamatergic neurons. In addition, seizure induction through acute injections of pentylenetetrazol (PTZ) or chemical kindling through chronic PTZ injections will determine whether seizure threshold is altered upon conditional loss of CDKL5 (Dhir, 2012). This finding indicates that *Cdkl5* loss-of-function specifically in forebrain glutamatergic neurons is central to seizure development.

Hindlimb clasping, impaired working memory, and context-dependent hyperactivity upon loss of CDKL5 from forebrain glutamatergic neurons

Other prominent phenotypes in CDKL5 patients include motor impairment and intellectual disability. The CDKL5 constitutive KO mouse recapitulates these phenotypes, demonstrating hindlimb clasping, impairments on the rotarod, and deficits in fear memory and working memory (Amendola et al., 2014; Fuchs et al., 2014; Wang et al., 2012). We therefore characterized these phenotypes in Dlx- and Nex-cKO mice to determine whether these phenotypes segregate upon conditional CDKL5 ablation. We observed hindlimb clasping in Nex-cKO animals, but not in Dcre-cKO or WT animals (**Figure 8a**). On an accelerating rotarod assay, however, all animals showed similar latency to fall across trials and days, indicating that circuit mechanisms underlying motor behavior are complex and may not segregate completely upon conditional CDKL5 ablation (**Figure 8b**). In a Y-maze assay of working memory, we found that Nex-cKO, but not Dlx-cKO, mice show reduced spontaneous alternation. In contrast to WT and Dlx-cKO mice, which show the expected ~67% preference for a previously unexplored arm, Nex-cKO mice do not show any preference and enter previously explored and unexplored arms equally (~50%) (**Figure 8c**).

We noticed that in particular settings, Nex-cKO mice showed increased exploratory and locomotor activity. On the Y-maze, Nex-cKO mice entered significantly more arms than WT animals and Dlx-cKO mice (**Figure 8d**), and in both forward and reversal Barnes maze, Nex-cKO mice were hyperactive, traveling a greater total distance and investigating significantly more holes (**Figures 8e,f**) than both WT and Dlx-cKO mice. Interestingly, however, Nex-cKO mice do not show any difference in locomotor activity relative to that of WT and Dlx-cKO mice in a homecage-like environment, nor do they demonstrate a difference in time spent in the open arm of a zeromaze (**Figures 8g,h**), indicating that Nex-cKO mice are not innately hyperactive or anxious, and that the hyperlocomotor phenotype is related to external stimuli. This hypothesis is supported by the differences in the experimental design of these assays. The locomotor assay is conducted in a homecage-like environment and the zeromaze assay is conducted in extremely low light levels (~4 lux). In contrast, both Barnes maze and Y-maze assays are conducted under bright light, which may be an external stimulus with higher emotional valence. Consistent with this hypothesis, Nex-cKO mice show similar

locomotor activity in Phase 1 of the social approach assay, when cylinders are empty, but upon introduction of a novel object or mouse in Phase 2 of the social approach assay, Nex-cKO mice show significantly greater locomotor activity (**Figure 8i**). Interestingly, hyperactivity and seizures have been linked in some animal models (Gantois et al., 2007; Peters et al., 2005) but determining how context-dependent hyperactivity phenotype in Nex-cKO mice is related to seizure development will require more investigation.

Circuit-level mechanisms underlying separation of phenotypes upon conditional CDKL5 ablation

The separation of autistic and epileptic aspects of CDKL5 disorder-related phenotypes in the complementary Dlx- and Nex-cKO mouse lines suggests that conditional loss of CDKL5 disrupts neural circuits underlying these phenotypes. To assess circuit function in Dlx- and Nex-cKO mice, we measured auditory-evoked event related potentials (ERPs), which are believed to be readouts of sensory information processing (Roberts et al., 2010; Stauder et al., 2006). As described previously (Goffin et al., 2012; 2014; Wang et al., 2012), we implanted tri-polar hippocampal electrodes and measured ERPs in awake behaving animals following the presentation of 250 85-dB white noise stimuli. Interestingly, we did not observe any differences in event-related power between genotypes, as all animals exhibited the stereotypical decrease in power at low frequencies and increase in power at high frequencies following sound presentation (**Figures 9a-c**) (Goffin et al., 2012; Wang et al., 2012). Additionally, all animals showed the stereotypical robust increase in phase-locking factor (PLF), a measure of trial-to-trial reliability, across all frequencies (**Figures 9d-f**). Previous studies from CDKL5 constitutive KO mice showed impairments in both auditory- and visual-evoked ERPs (Amendola et al., 2014; Wang et al., 2012), suggesting that loss of CDKL5 from forebrain excitatory or inhibitory circuits alone is not sufficient to perturb sensory-evoked event-related potentials.

Although the ERP data indicates that circuits mediating auditory sensory information processing appear to be relatively intact upon conditional loss of CDKL5, we reasoned that distinct alterations in neural circuits are likely to underlie the separation of the

epileptic and autistic phenotypes in Nex- and Dlx-cKO mice, and therefore, might be detected using a different assay of circuit function. Given the relevance of hippocampal circuits in the major CDKL5 phenotypes of epilepsy and autism (Ang et al., 2006; Pathak et al., 2007; Tyler et al., 2012), we performed voltage sensitive dye imaging to measure the dentate gyrus (DG) hippocampal microcircuit. In WT animals, low frequency stimulation of entorrhinal cortical afferents, also known as the perforant path, activates the DG, but strong synaptic inhibition mediated by feed-forward inhibitory neurons along with the ratio of synaptic inhibitory/excitatory innervation prevents this activation from reaching CA3 (Figures 10a-c) (Acsády et al., 1998). In Dlx-cKO mice, however, perforant path stimulation results in activation of both DG and downstream hippocampal structures, particularly area CA3 and more distal hilar regions (**Figures 10a-c**), suggesting a disruption in DG filtering of afferent inputs. Nex-cKO mice also show a trend toward disruption in DG filtering, but downstream activation of CA3 in Nex-cKO animals is not significant (**Figure 10c**). Together, these data indicate that conditional loss of CDKL5 may differentially affect neural circuits underlying behaviors, where a disruption in DG filtering properties in Dlx-cKO may be related to the development of autistic-like behavioral phenotypes. Future VSD experiments activating CA3 via mossy fiber afferents of the dentate granule cells or activating CA1 via Schaffer collaterals of CA3 neurons will further isolate the primary loci of hippocampal disruptions mediating the autistic or epileptic phenotypes observed in our CDKL5 conditional knockout animals. The connectivity within these hippocampal microcircuits and their relevance to behaviors has been well characterized (Ang et al., 2005; Leutgeb et al., 2007; Redondo et al., 2014; Wozny et al., 2005). Therefore, understanding how conditional loss of CDKL5 from glutamatergic or GABAergic neurons affects the functionality and E/I balance within these microcircuits will pinpoint key circuit mechanisms and disease-related loci underlying CDKL5 disorder.

Reduced neuronal outgrowth upon conditional loss of CDKL5

The separation of epilepsy and autistic behaviors in Dlx- and Nex-cKO mice suggest that the epileptic and autistic phenotypes of CDKL5 disorder may be mediated by distinct neural circuits or that common neural circuits are differentially affected by loss of CDKL5 from either glutamatergic or GABAergic neurons. The two possibilities, however, are not

mutually exclusive, and due to the complexity of the brain, the *in vivo* mechanism is likely to be a combination of the two. As circuit formation and function can be affected by mislocalization or impaired development of neurons, neuronal outgrowth may serve as a morphological correlate of circuit function. Given that shRNA-mediated *Cdkl5* knockdown has been shown to delay neuronal migration, reduce neuronal outgrowth, and impair dendritic spine formation (Chen et al., 2010; Ricciardi et al., 2012; Zhu et al., 2013), we hypothesized that loss of CDKL5 may alter neural circuit formation by affecting neuronal development. Similar effects on neuronal development in complementary Dlx- and Nex-cKO animals would suggest that the autistic and epileptic phenotypes of CDKL5 disorder are indeed mediated by distinct neural circuits, whereas differential effects on neuronal development would provide evidence for common circuits differentially affected upon conditional loss of CDKL5.

To this end, we have measured soma size and dendritic morphology in CA1 hippocampal pyramidal neurons of Nex-cKO animals. Experimental mice were crossed to a *Thy1-GFP/M* reporter line (Feng et al., 2000), thereby generating WT and Dlx- or Nex-cKO mice in which a sparse population of neurons intrinsically expresses GFP throughout the cell body and dendritic tree, allowing for direct visualization of individual neurons, particularly in the hippocampal CA1 pyramidal layer (**Figure 11a**), as described previously (Wang et al., 2013). To quantify dendritic complexity, we used the Sholl analysis, which measures dendritic crossings through a series of concentric circles with increasing radii centered around the cell soma (SHOLL, 1953). Given the anatomic and functional distinctions between basal and apical dendritic arbors (Spruston, 2008), we imaged and quantified basal and apical dendritic complexity separately and found reduced dendritic complexity in both basal and apical dendritic arbors of CA1 pyramidal neurons of Nex-cKO mice relative to that WT mice (**Figures 11b,c**). Total dendritic length in Nex-cKO animals was reduced as well, but this reduction was not significant (**Figure 11d**). In contrast, soma size did not differ between Nex-cKO and WT mice (**Figure 11e**), indicating that deficits in neuronal connectivity, but not basic intrinsic membrane properties of CA1 neurons, are related to the neural circuits that underlie the development of spontaneous seizures in Nex-cKO mice. As these data were obtained from 3 WT and 3 Nex-cKO mice, these trends should be confirmed with a larger sample size to obtain greater statistical power. Future studies will also measure dendritic

outgrowth and soma size in Dlx-cKO mice, and comparison of morphological phenotypes in the complementary conditional knockouts should address whether CDKL5 regulates neuronal development in a cell autonomous manner and identify how conditional loss of CDKL5 from glutamatergic or GABAergic neurons affects circuit assembly.

Circuit communication is ultimately dictated by synapse function, and disruption of synaptic signaling has been identified in multiple ASD mouse models (Chao et al., 2007; Peça et al., 2011; Tsai et al., 2012). Indeed, knockdown of CDKL5 from cultured hippocampal neurons results in decreased amplitude and frequency of mEPSCs (Ricciardi et al., 2012; Zhu et al., 2013), indicative of impaired synapse function upon loss of CDKL5. We hypothesize that loss of CDKL5 will disrupt synaptic properties and that distinct synaptic phenotypes in Nex- and Dlx-cKO mice may mediate the distinct behavioral and circuit phenotypes. Therefore, measurement of spine density, size, and type should also be performed in both conditional knockout mice in future studies, firstly to resolve the conflicting data supporting how loss of CDKL5 affects spine development (Ricciardi et al., 2012; Zhu et al., 2013), and secondly to establish a morphological correlate for synapse function (**Figure 11f**). In future synaptic electrophysiology experiments, current clamp recordings in CA1 pyramidal neurons will measure basic intrinsic neuronal properties and excitability, and voltage clamp recordings will measure evoked and spontaneous excitatory and inhibitory synaptic activity in both Dlx- and Nex-cKO mice. Together, these experiments should isolate the cell types and synapses that require CDKL5 for proper circuit formation and reveal how changes in synaptic connectivity affect neuronal E/I balance, leading to distinct behavioral phenotypes in Dlx- and Nex-cKO mice.

Isolating the role of CDKL5 in PTEN downstream signaling pathways

The mechanism by which CDKL5 localizes to excitatory synapses is supported by conflicting data, with one study describing a kinase-dependent mechanism (Ricciardi et al., 2012) and the other, a kinase-independent mechanism (Zhu et al., 2013). Akt signaling has been implicated in CDKL5 disease pathogenesis by three independent studies from CDKL5 KO mice, and we previously identified a number of signaling

pathways disrupted upon *Cdkl5* loss-of-function (Wang et al., 2012). Interestingly, the Akt-mTOR, Akt-S6, Akt-GSK3b, and AMPK, MAPK/ERK pathways converge into PTEN downstream signaling pathways (Amendola et al., 2014; Fuchs et al., 2014; Wang et al., 2012). As disruptions in PTEN signaling have been described in both autism and epilepsy (Clipperton-Allen and Page, 2014; Costa-Mattioli and Monteggia, 2013; Gkogkas et al., 2012; Santini et al., 2013; Zhou and Parada, 2012), these data suggest that CDKL5 may play a prominent role in coordinating or regulating PTEN signaling pathways. Future studies pharmacologically and genetically altering PTEN signaling in mice lacking CDKL5 from either glutamatergic or GABAergic neurons should pinpoint the relationship between CDKL5 and PTEN signaling and isolate cell type-specific signaling pathways that are relevant to disease.

Conclusion and future directions

In this study, we developed conditional CDKL5 knockout mouse models and demonstrated that loss of CDKL5 from the brain is sufficient to recapitulate several features of the constitutive CDKL5 KO mouse model, indicating that the role of CDKL5 is primarily in the brain.

We also found that mice lacking CDKL5 exclusively from forebrain GABAergic neurons develop autistic-like phenotypes, whereas mice lacking CDKL5 exclusively from forebrain glutamatergic neurons develop spontaneous seizures. The separation of these CDKL5-related phenotypes in the complementary conditional knockout animals suggests that distinct neural circuits mediate the two behaviors, or that loss of CDKL5 from glutamatergic or GABAergic neurons differentially affects common circuits. VSDI imaging of hippocampal microcircuits indicates that dentate gyrus filtering properties are preferentially disrupted in mice lacking CDKL5 from forebrain GABAergic neurons, implicating this microcircuit in autism-like behavior.

Future studies investigating the properties of CA3 and CA1 hippocampal microcircuits, neuronal development and outgrowth, excitatory and inhibitory synapse function, and PTEN downstream signaling pathways in the complementary CDKL5 conditional knockout animals aim to reveal the cell type-specific function of CDKL5 and isolate pathogenic mechanisms leading to autistic behaviors and epilepsy. Eventually, a clear understanding of CDKL5 biological function should give rise to targeted therapeutics for CDKL5 disorder.

Figure 1

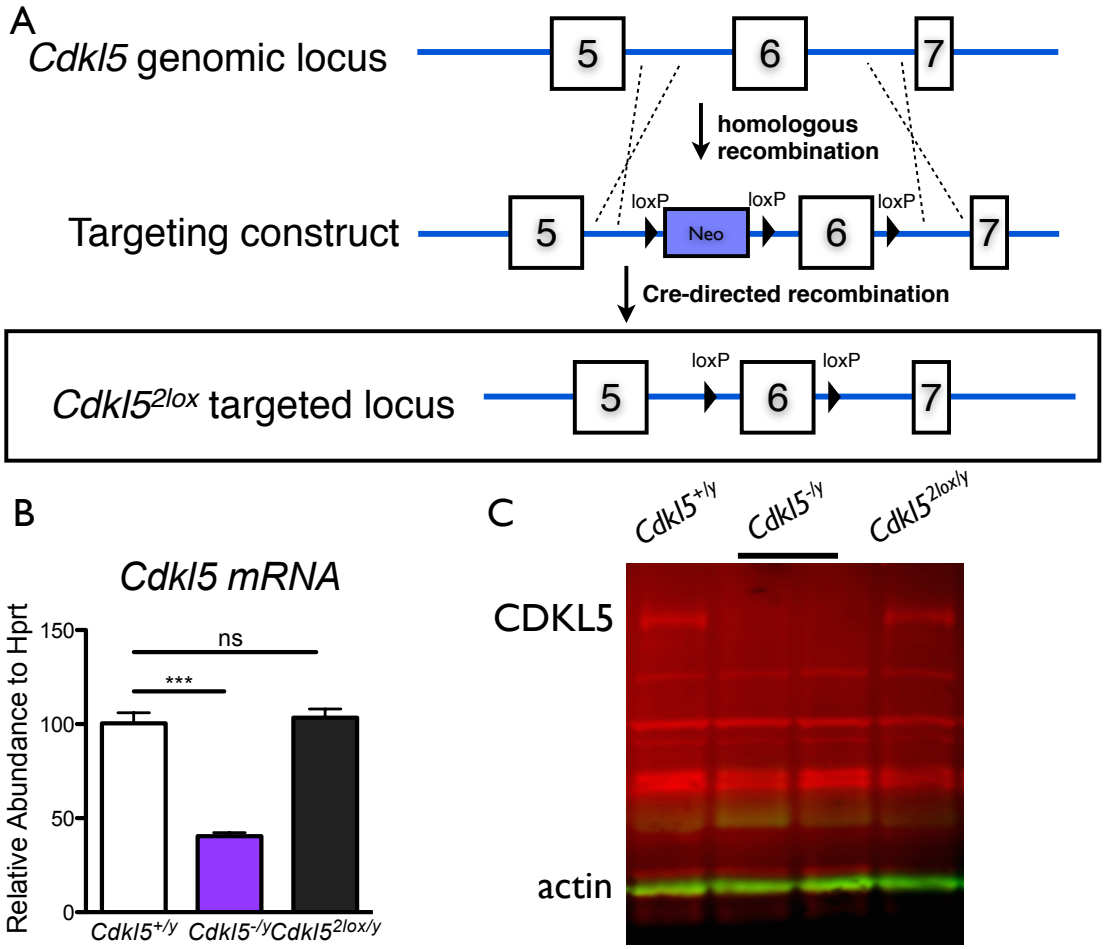

Figure 1. Generation of CDKL5 floxed mice

A. Targeting strategy. Three loxP sites and a neomycin positive selection cassette (Neo) were inserted surrounding the genomic locus of *Cdkl5* exon 6 via homologous recombination. Upon Cre-directed recombination, the Neo cassette is excised, leaving exon 6 flanked by loxP sites.

B. Quantitative PCR of mRNA obtained from brains of *Cdkl5*$^{+/y}$ (WT), *Cdkl5*$^{-/y}$ (KO), *Cdkl5*$^{2lox/y}$ (cKO). *Cdkl5* expression levels are normalized to *Hprt*.

C. Western blot of whole brain lysate obtained from *Cdkl5*$^{+/y}$ (WT), *Cdkl5*$^{-/y}$ (KO), *Cdkl5*$^{2lox/y}$ (cKO) probed with an antibody directed against CDKL5 (red) and actin (green).

Figure 2

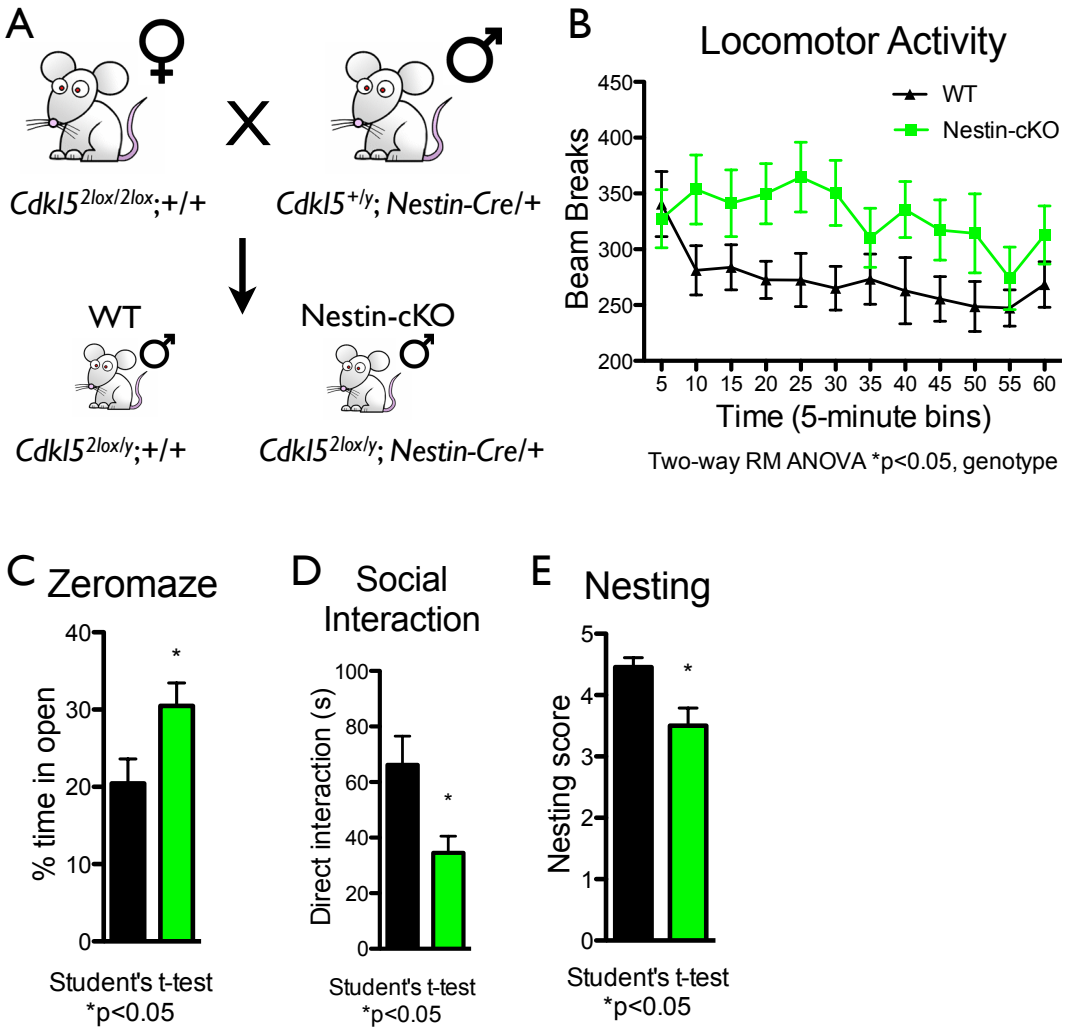

Figure 2. Nestin-cKO behavioral phenotypes

A. Breeding strategy. Female mice homozygous for the *Cdkl5*^{2lox} allele were crossed to male mice carrying the Nestin-Cre transgene. Male progeny were used for behavioral experiments. n = 10-15 per genotype.

B. Sixty-minute locomotor assay, measured by infrared beam breaks in a home cage-like environment. Black (WT), green (Nestin-cKO). p<0.05, Two-way RM-ANOVA (genotype).

C. Zeromaze assay, measured by time spent in open arm relative to total time on maze. *p<0.05, Student's t-test.

D. Three-chambered social approach assay, measured by time spent directly interacting with freely moving stimulus mouse. *p<0.05, Student's t-test.

E. Nest building, scored on 1-5 scale. *p<0.05, Student's t-test.

Figure 3

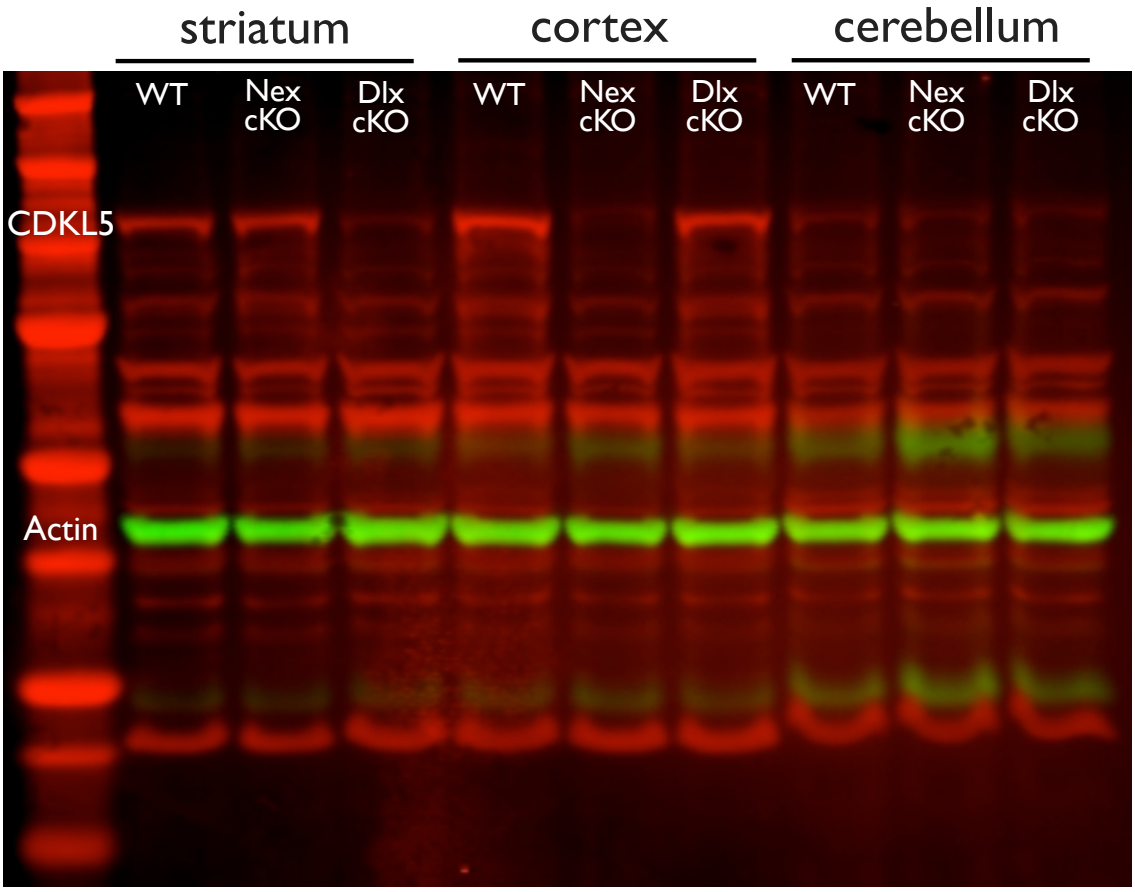

Figure 3. CDKL5 expression in Nex-cKO and Dlx-cKO mice
Whole cell lysates from dissected striatum, cortex, and cerebellum of WT, Nex-cKO, and Dlx-cKO mice were probed with antibodies raised up against CDKL5 and Actin. n = 3-4 animals per genotype.

Figure 4

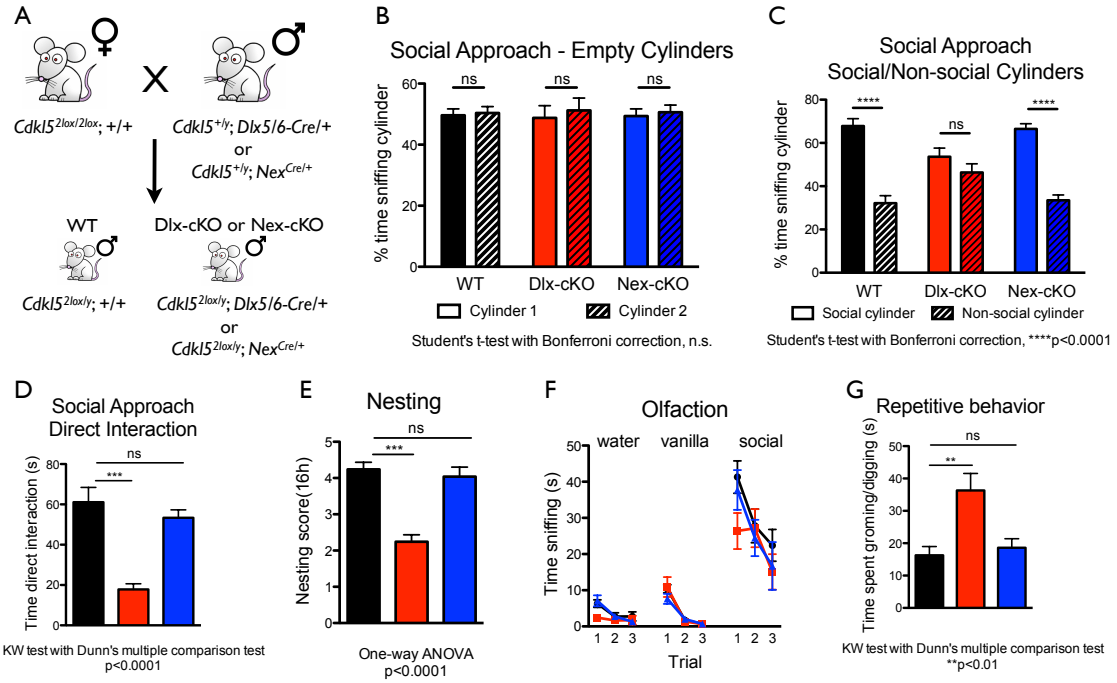

Figure 4. Autistic-like behaviors in mice lacking CDKL5 from forebrain GABAergic neurons

A. Breeding strategy. Female mice homozygous for the *Cdkl5*^{2lox} allele were crossed to male mice carrying the Dlx5/6-Cre transgene or the Nex^{Cre} allele. Male progeny were used for behavioral experiments. n = 15-20 per genotype.

B. Three-chambered social approach assay, time spent investigating empty cylinders. n.s., not significant, Student's t-test with Bonferroni correction. Black (WT), red (Dlx-cKO), blue (Nex-cKO).

C. Three-chambered social approach assay, time spent investigating a cylinder that contains a stimulus mouse (social cylinder) or a cylinder that contains a novel object (non-social cylinder). ****p<0.0001, n.s., not significant, Student's t-test with Bonferroni correction.

D. Three-chambered social approach assay, time spent directly interacting with freely moving stimulus mouse. p<0.0001, Kruskal-Wallis one-way ANOVA with Dunn's multiple comparison post-hoc test.

E. Nest building, scored on 1-5 scale. p<0.0001, One-way ANOVA with Dunnett's multiple-comparison test.

F. Olfactory habituation/dishabituation assay, time spent investigating repeated presentations of odorants water, vanilla extract, and social (swab from soiled bedding of different cage).

G. Repetitive behavior, time spent digging and self-grooming in 10-minute period. **p<0.01, Kruskal-Wallis one-way ANOVA with Dunn's multiple comparison post-hoc test.

Figure 5

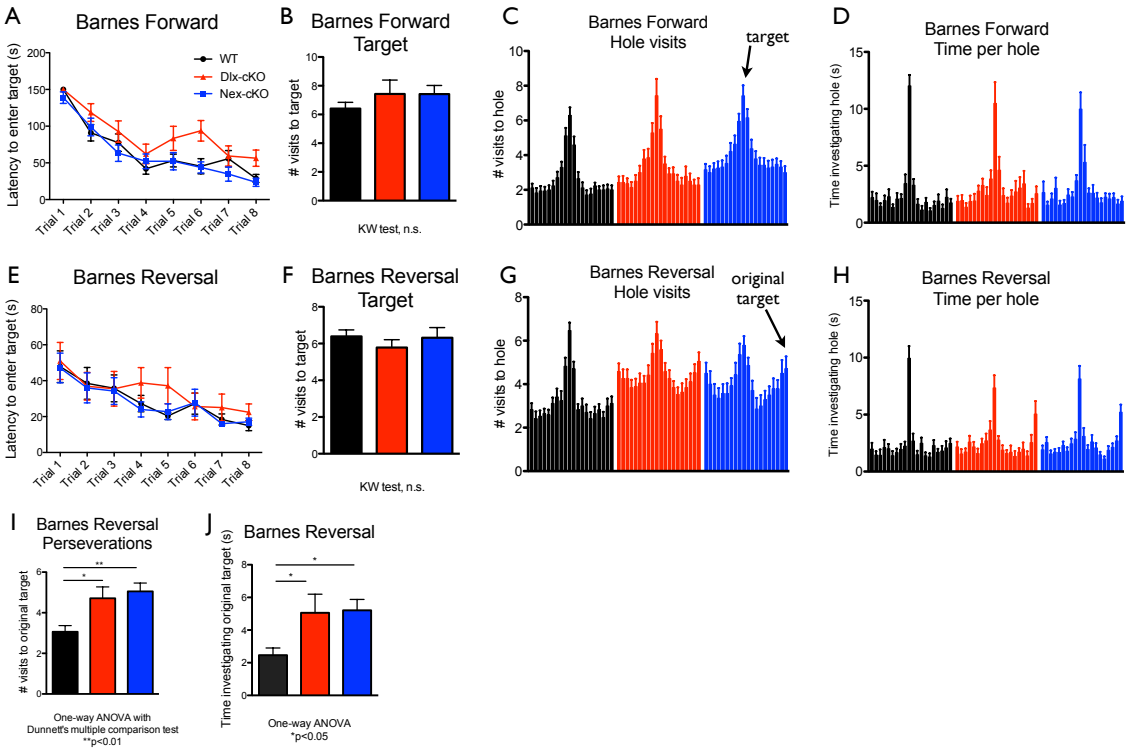

Figure 5. Barnes maze forward and reversal learning

A. Forward learning training, latency to enter target hole at each trial. Two trials were performed per day.

B. Forward learning probe trial (Day 5), number of visits to target hole. n.s. not significant, Kruskal-Wallis one-way ANOVA.

C. Forward learning probe trial (Day 5), number of visits to each hole during 150 second trial. Central peak is target hole, peak to the right of central peak corresponds to clockwise adjacent hole, peak to the left of central peak corresponds to counter-clockwise.

D. Forward learning probe trial (Day 5), time spent investigating each hole during 150-second trial. Central peak is target hole, as described in C.

E. Reversal learning training, latency to enter target hole at each trial. Two trials were performed per day.

F. Reversal learning probe trial (Day 5), number of visits to new target hole. n.s. not significant, Kruskal-Wallis one-way ANOVA.

G. Reversal learning probe trial (Day 5), number of visits to each hole during 150-second trial. Central peak is new target hole, peak to the right of central peak corresponds to clockwise adjacent hole, peak to the left of central peak corresponds to counter-clockwise, peak to the far right corresponds to original target hole.

H. Reversal learning probe trial (Day 5), time spent investigating each hole during 150-second trial. Central peak is new target hole, as described in G.

I. Reversal learning probe trial (Day 5), number of visits to original target hole. **p<0.01, one-way ANOVA with Dunnett's multiple comparison test.

J. Reversal learning probe trial (Day 5), time spent investigating original target hole. *p<0.05, one-way ANOVA with Dunnett's multiple comparison test. n = 10-15 animals per genotype.

Figure 6

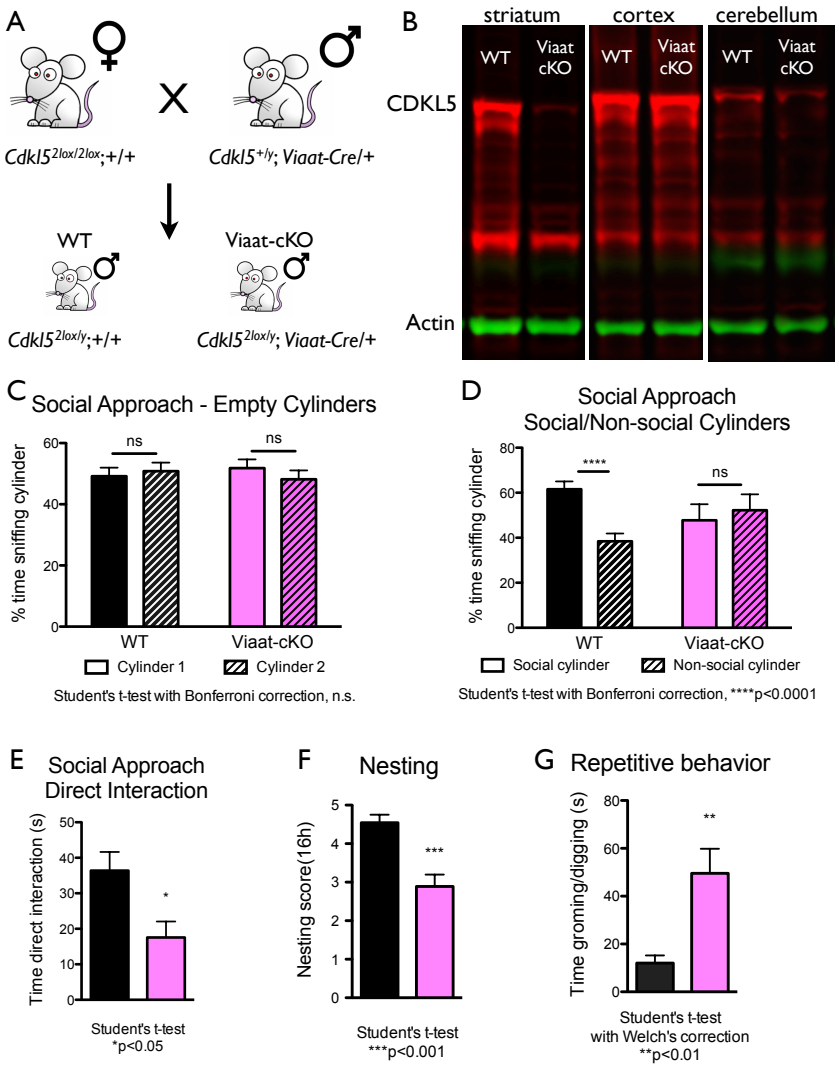

Figure 6. Viaat-cKO behavioral phenotypes

A. Breeding strategy. Female mice homozygous for the *Cdkl5*^{2lox} allele were crossed to male mice carrying the Viaat-Cre transgene. Male progeny were used for behavioral experiments. n = 10-15 per genotype. Black (WT), purple (Viaat-cKO).

B. Western blot. Whole cell lysates from dissected striatum, cortex, and cerebellum of WT and Viaat-cKO and probed with antibodies raised up against CDKL5 and Actin. n = 3-4 animals per genotype.

C. Three-chambered social approach assay, time spent investigating empty cylinders. n.s., not significant, Student's t-test with Bonferroni correction.

D. Three-chambered social approach assay, time spent investigating a cylinder that contains a stimulus mouse (social cylinder) or a cylinder that contains a novel object (non-social cylinder). Student's t-test with Bonferroni correction.

E. Three-chambered social approach assay, time spent directly interacting with freely moving stimulus mouse. *p<0.05, Student's t-test.

F. Nest building, scored on 1-5 scale. ***p<0.001, Student's t-test.

G. Repetitive behavior, time spent digging and self-grooming in 10-minute period. **p<0.01, Student's t-test with Welch's correction.

Figure 7

Figure 7. Representative still images of rearing and falling during spontaneous tonic-clonic seizure observed in Nex-cKO animal.

Figure 8

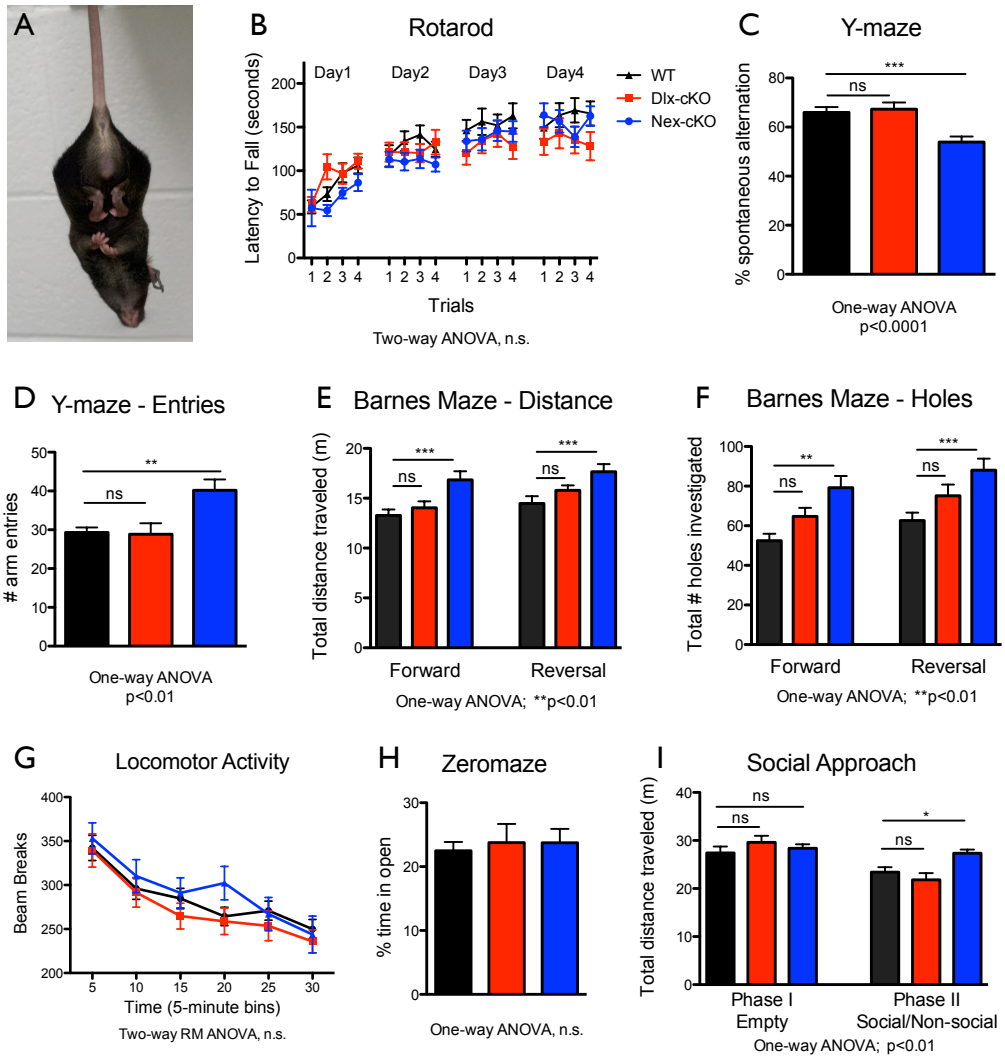

Figure 8. Nex-cKO behavioral phenotypes

A. Hindlimb clasing in Nex-cKO animals.

B. Rotarod assay, measured by latency to fall from cylindrical rod rotating and accelerating. Four trials performed for four days. n.s. not significant, Two-way ANOVA. n = 15-20 per genotype

C. Y-maze assay, measured by percentage of entries into new arm of maze rather than returning to arm previously investigated. p<0.0001, one-way ANOVA with Dunnett's multiple comparison test.

D. Y-maze assay, total number of entries in Y-maze arms. p<0.01, one-way ANOVA with Dunnett's test.

E. Barnes maze forward and reversal probe trials, total distance traveled during 150-second test. **p<0.01, one-way ANOVA with Dunnett's multiple comparison test.

F. Barnes maze forward and reversal probe trials, total number of holes investigated during 150-second test. **p<0.01, one-way ANOVA with Dunnett's multiple comparison test.

G. Sixty-minute locomotor assay, measured by infrared beam breaks in a home cage-like environment. n.s. not significant, two-way RM-ANOVA.

H. Zeromaze assay, time spent in open arm relative to total time on maze. n.s. not significant, one-way ANOVA.

I. Three-chambered social approach assay. Total distance traveled in Phase 1 (when cylinders are empty) and Phase 2 (when cylinders contain stimulus mouse or novel object). **p<0.01, one-way ANOVA with Dunnett's multiple comparison test.

Figure 9

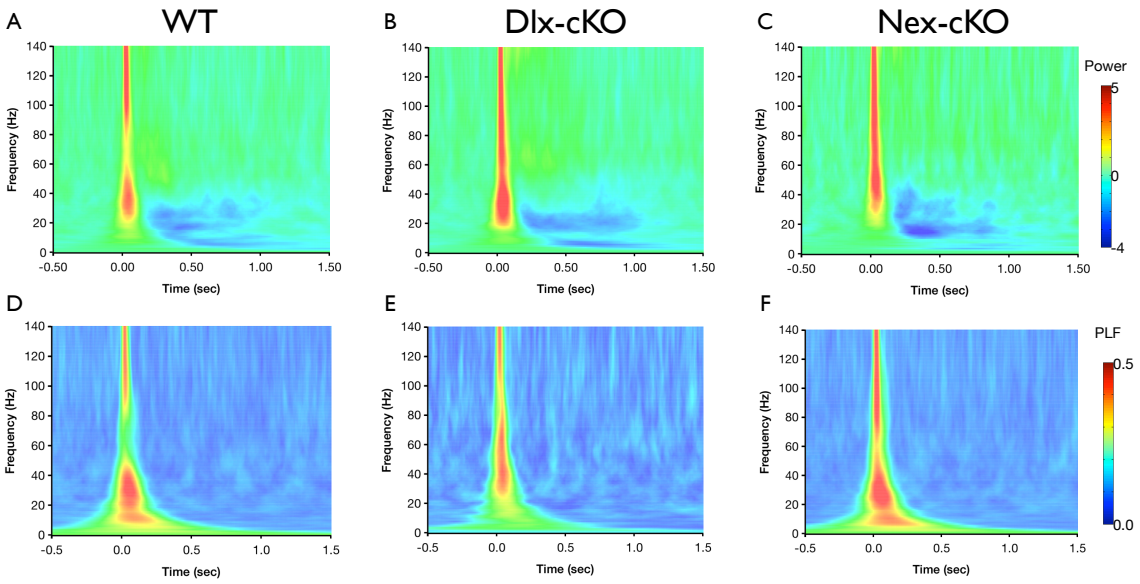

Figure 9. Time-frequency plots of auditory-evoked event-related potentials (ERPs).

A-C. Time-frequency plot showing changes in event-related power following an 85-dB auditory stimulus. Color represents mean power, where warmed colors correspond to increased power and cooler colors correspond to decreased power relative to prestimulus baseline.

D-F. Time-frequency plot showing changes in event-related phase-locking factor (PLF) following an 85-dB auditory stimulus. Color represents PLF, where warmer colors correspond to a higher PLF or lower circular variance in EEG phase across trials. n = 10 animals per genotype.

Figure 10

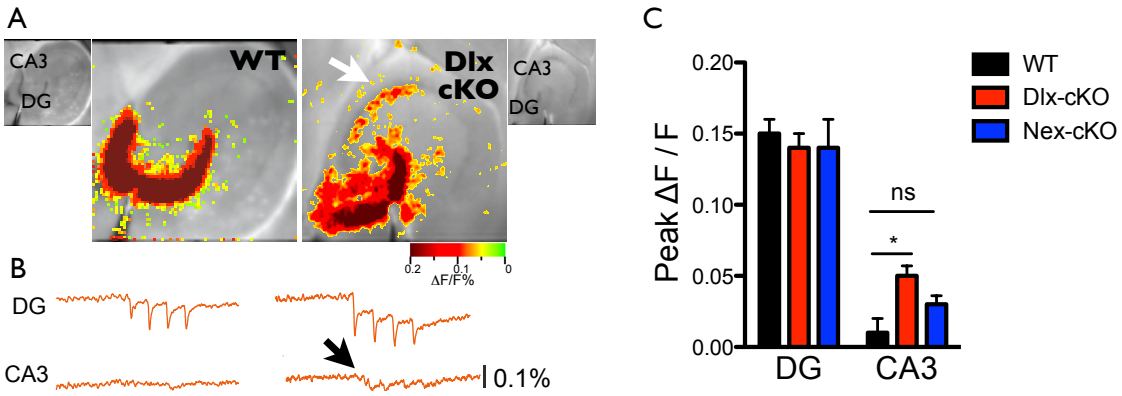

Figure 10. Voltage-sensitive dye imaging of dentate gyrus hippocampal microcircuit

A. Snapshots of peak fluorescence change during a DG EPSP elicited by perforant path stimulation. White arrow: increased activation of CA3 of Dlx-cKO mouse. Insets are grey scale images of slice depicting cell areas.

B. Integrated voltage traces of the responses in A. Black arrow: increased EPSP in CA3 of Dlx-cKO mouse.

C. Quantification of DG and CA3 activation *p<0.05, one-way ANOVA.

Figure 11

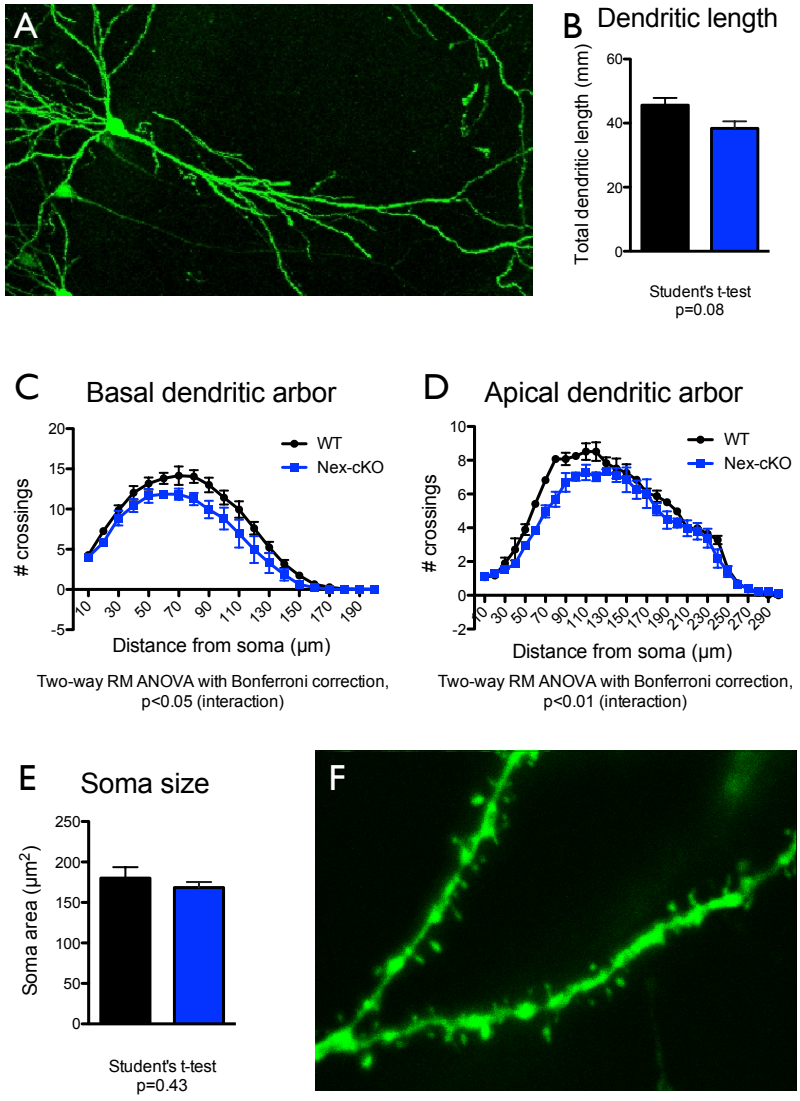

Figure 11. Neuronal morphology of hippocampal CA1 pyramidal neurons

A. *Thy1-GFP/M* reporter imaging strategy. CA1 neurons are labeled with GFP throughout the cell body and dendritic tree.

B. Total dendritic length of CA1 neurons in WT and Nex-cKO mice. n = 3 animals per genotype (12 neurons per animal)

C. Sholl analysis of CA1 basal dendritic arbor. 0 um marks soma position. *p<0.05, two-way ANOVA with Bonferroni correction (interaction).

D. Sholl analysis of CA1 apical dendritic arbor. 0 um marks soma position. **p<0.01, two-way ANOVA with Bonferroni correction (interaction).

E. Soma size of CA1 neurons. n = 3 animals per genotype (at least 50 neurons per animal).

F. *Thy1-GFP/M* reporter imaging strategy. Dendritic spines of CA1 neurons are labeled with GFP.

Chapter 4:

RETT SYNDROME MUTATION MECP2 T158A DISRUPTS METHYL-DNA BINDING, PROTEIN STABILITY AND ERP RESPONSES

Darren Goffin[1], Megan Allen[1,5], Le Zhang[1,5], Maria Amorim[1,5], **I-Ting Judy Wang[1,5]**, Arith-Ruth S. Reyes[1], Amy Mercado-Berton[2], Caroline Ong[4], Sonia Cohen[4], Linda Hu[4], Julie A. Blendy[2], Gregory C. Carlson[3], Steve J. Siegel[3], Michael E. Greenberg[4] and Zhaolan (Joe) Zhou[1,*]

[1]Department of Genetics, [2]Department of Pharmacology, [3]Department of Psychiatry, University of Pennsylvania School of Medicine, Philadelphia, PA 19104; [4]Department of Neurobiology, Harvard Medical School, Boston, MA 02115.

[5]These authors contributed equally to this work.

Received 25 July; accepted 28 October; published online 27 November 2011; doi:10.1038/nn.2997

Published online at http://www.nature.com/natureneuroscience/.
Reprints and permissions information is available online at http://www.nature.com/reprints/index.html.

This chapter represents a collaboration within the lab resulting a *Nature Neuroscience* paper published in 2012 that examines Rett Syndrome (RTT), a severe neurological disorder characterized by the loss of acquired motor skills and cognitive ability and the development of distinctive hand stereotypies. In this paper, we develop and characterized a mouse model of a patient T158 missense mutation and find that MeCP2 T158A mice recapitulate a number of RTT-like behavioral phenotypes, which may be mediated by reduced MeCP2 DNA binding and protein stability. We also find evidence for the requirement of MeCP2 in the developmental of functional circuits. Overall, this paper suggests that stabilizing MeCP2 and enhancing MeCP2 affinity for DNA binding may be relevant for RTT therapeutics, and that developmental assessment of ERPs may serve as a biomarker for RTT disease progression and therapeutic efficacy.

As a co-second author in this *Nature Neuroscience* paper, my contribution to this paper was in both experiments and editing. I measured soma size in mice using a GFP reporter (Fig 1f), and performed all behavioral assays in Figure 2, and edited the paper throughout its various versions.

Abstract

Mutations in the *MECP2* gene cause the autism spectrum disorder Rett Syndrome (RTT). One of the most common mutations associated with RTT occurs at MeCP2 Threonine 158 converting it to Methionine (T158M) or Alanine (T158A). To understand the role of T158 mutation in the pathogenesis of RTT, we generated knockin mice recapitulating MeCP2 T158A mutation. Here we show a causal role for T158A mutation in the development of RTT-like phenotypes including developmental regression, motor dysfunction, and learning and memory deficits. These phenotypes resemble those in *Mecp2*-null mice and manifest through a reduction in MeCP2 binding to methylated DNA and a decrease in MeCP2 protein stability. Importantly, the age-dependent development of event-related neuronal responses are disrupted by MeCP2 mutation, suggesting that impaired neuronal circuitry underlies the pathogenesis of RTT and that assessment of event-related potentials may serve as a biomarker for RTT and treatment evaluation.

Introduction

RTT is an autism spectrum disorder caused by mutations in the X-linked gene encoding methyl-CpG binding protein 2 (MeCP2) (Amir et al., 1999). RTT is associated with different types of mutations within *MECP2*, including missense, nonsense, deletions and insertions (Bienvenu and Chelly, 2006). Classical RTT patients, irrespective of the type of mutation, develop normally for the first 6-18 months of age, after which they enter a period of regression characterized by deceleration of head growth and a loss of acquired motor and language skills. Frequently, patients develop stereotypic hand wringing, abnormal breathing, seizures and autistic behaviors (Chahrour and Zoghbi, 2007). The molecular mechanisms through which different types of *MECP2* mutations lead to disruptions in proper brain function are not fully understood.

Mice engineered with different *Mecp2* alterations present phenotypes that are both similar and distinct from those observed in *Mecp2*-null mice (Chen et al., 2001; Collins et al., 2004; Guy et al., 2001; Jentarra et al., 2010; Kerr et al., 2008; Pelka et al., 2006; Samaco et al., 2008; Shahbazian et al., 2002b). These similarities and differences in mouse models suggest that different *MECP2* mutations are likely to have both shared and distinct biochemical and physiological correlates. Intriguingly, reintroduction of MeCP2 into behaviorally affected *Mecp2*-null mice is sufficient to rescue RTT-like phenotypes (Guy et al., 2007) and restoration of MeCP2 function in astrocytes alone significantly improve the developmental outcome of *Mecp2*-null mice (Lioy et al., 2011), suggesting that RTT is reversible upon restoration of MeCP2 function. Thus, understanding the mechanisms by which different MeCP2 mutations lead to RTT may reveal effective strategies tailored to the particular mutation to restore MeCP2 function.

Mutation of the Threonine 158 (T158) residue, located at the C-terminus of the methyl-CpG binding domain (MBD) of MeCP2, represents one of the most common mutations observed in RTT. Approximately 10% of all RTT cases carry a single nucleotide mutation converting T158 to Methionine (T158M) or in rare cases to Alanine (T158A) (Bienvenu and Chelly, 2006). The T158 residue has been suggested to play an important structural role in the stabilization of the MBD and the binding of MeCP2 to methylated DNA (Ho et

al., 2008). Whether mutation of T158 leads to MeCP2 gain-of-function or loss-of-function, however, is not clear.

The onset of RTT symptoms occurs during the establishment and refinement of neural networks in early postnatal development. Studies in *Mecp2*-null mice have suggested that reductions in connectivity between excitatory pyramidal neurons are associated with RTT-like phenotypes (Dani and Nelson, 2009; Dani et al., 2005; Wood et al., 2009). How reductions in neuronal connectivity lead to the manifestation of the age-dependent cognitive and behavioral deficits in RTT is currently unknown. Cognitive dysfunctions are frequently assessed by measuring the neurophysiological responses that occur during passive processes or during the performance of cognitive, sensory or motor tasks. Brain activations that occur during these tasks manifest as event-related potentials (ERPs). Disruptions in ERPs and the oscillations that underlie them are associated with a number of cognitive disorders such as schizophrenia (Gandal et al., 2012; Uhlhaas and Singer, 2010) and autism (Gandal et al., 2010; Roberts et al., 2010). EEG recordings in *Mecp2*-null mice (Chao et al., 2010; D'Cruz et al., 2010) and ERP recordings in RTT patients (Bader et al., 1989; Stauder et al., 2006) also suggest that alterations in brain activity are associated with behavioral and cognitive deficits. How ERPs are affected by MeCP2 dysfunction and how changes in EEG and ERPs correlate with the age-dependent progression of RTT-like symptoms, however, remains to be determined.

Given the high frequency of T158 mutations in RTT and its role in methyl-DNA binding, we sought to model this mutation *in vivo* and developed knockin mice containing MeCP2 T158A mutation. We found that these mice recapitulate a number of RTT-like symptoms observed in *Mecp2*-null mice including late onset of hypoactivity, poor motor control, irregular breathing, altered anxiety, impaired learning and memory, and shortened lifespan. We demonstrated that T158A mutation decreases the binding of MeCP2 to methylated DNA *in vitro* and *in vivo,* and reduces MeCP2 protein stability. Moreover, the amplitude and latency of ERPs in both MeCP2 T158A and *Mecp2*-null mice are significantly altered. Time-frequency analysis of these ERPs revealed that MeCP2 T158A mice failed to show a developmental increase in event-related power and phase locking in contrast to wild-type (WT) mice, demonstrating that MeCP2 is required for the development of functional neuronal circuits. Our studies suggest that stabilization of

MeCP2 protein and enhancement of its affinity for methylated DNA may provide a potential therapeutic approach to treat patients with MeCP2 T158 mutation. Furthermore, assessment of ERPs may serve as a biomarker for RTT and the evaluation of therapeutic efficacy in RTT treatment.

Results

Generation of MeCP2 T158A and loxP knockin mice

Although mutation of MeCP2 T158A occurs at a lower frequency than T158M in RTT patients, the mechanism through which both mutations impair MeCP2 function is believed to be the same: the lack of hydroxyl group in alanine and methionine destabilizes the tandem Asx-ST motif in the MBD and thus reduces MeCP2 affinity for methylated DNA (Ho et al., 2008). Indeed, patients carrying MeCP2 T158A or T158M mutation are phenotypically similar in the identity and severity of presented symptoms (Schanen et al., 2004; Vacca et al., 2001). To examine the importance of the T158 residue in the functioning of MeCP2, we developed a knockin mouse with T158A mutation to circumvent the potential steric interference brought about by the larger Methionine residue. To facilitate screening of properly targeted ES cells, we incorporated a silent mutation at codon 160 to create a new BstEII restriction site and a floxed Neomycin expression cassette in intron III of the *Mecp2* gene (**Supplementary Fig. 1**). Given that our goal was to test a rather subtle mutation on MeCP2 – a single amino acid change of T158A – we also engineered loxP knockin mice that contain the BstEII restriction site and loxP insertion but that lack T158A mutation, to rule out the possibility that manipulation of the *Mecp2* locus may affect MeCP2 expression (**Supplementary Fig. 1**). Sequencing of MeCP2 mRNA extracted from brain tissues of WT, $Mecp2^{T158A/y}$, and $Mecp2^{loxP/y}$ mice verified that both $Mecp2^{T158A/y}$ and $Mecp2^{loxP/y}$ knockin mice contained the T to C mutation at codon 160 for the generation of the BstEII restriction site, whereas only $Mecp2^{T158A/y}$ mice contain the A to G mutation at codon 158 (**Fig. 1a**). Furthermore, an MeCP2 T158 site-specific antibody, recognized MeCP2 protein from WT and $Mecp2^{loxP/y}$ mice, but not $Mecp2^{T158A/y}$ mice confirming the successful generation of MeCP2 T158A knockin mice (**Fig. 1b**).

MeCP2 T158A mice recapitulate RTT-like phenotypes

RTT is characterized by relatively normal development during the first 6-18 months of life, followed by a period of developmental stagnation leading to motor impairments, breathing abnormalities, and intellectual disability. We evaluated the presence, development and progression of RTT-like phenotypes in MeCP2 T158A mice following a

previously reported scoring system (Guy et al., 2007). We found that male *Mecp2*$^{T158A/y}$ mice present no overt symptoms during the first 4 weeks of life, but become progressively symptomatic after 5 weeks of age as indicated by significantly increasing phenotypic score (**Fig. 1c**). The hindlimb clasping apparent in *Mecp2*-null mice is also observed in *Mecp2*$^{T158A/y}$ mice (**Supplementary Fig. 2a**). *Mecp2*$^{T158A/y}$ mice weighed significantly less than their WT littermates starting from 4 weeks of age but then gradually gained weight to WT levels after 8 weeks (**Supplementary Fig. 2b**). In contrast, the body weights of *Mecp2*$^{loxP/y}$ mice are indistinguishable from their WT littermates (data not shown). Occasionally, we also observed seizure behaviors in *Mecp2*$^{T158A/y}$ mice after 5 weeks of age.

Given that *MECP2* is an X-linked gene and that the majority of RTT patients are girls with mosaic MeCP2 expression due to random X-chromosome inactivation, female *Mecp2*$^{T158A/+}$ mice represent a close genetic match to RTT patients. Phenotypic scoring revealed no apparent symptoms in these mice until 17 weeks of age, after which they become progressively and increasingly symptomatic (**Fig. 1d**). A significant increase in body weight also occurred in female *Mecp2*$^{T158A/+}$ mice at the time of symptom presentation (**Supplementary Fig. 2c**) similar to that observed in heterozygous *Mecp2*$^{-/+}$ female mice (Guy et al., 2007).

An early diagnostic criterion for RTT is a deceleration in head growth often leading to microcephaly by the first two years of life (Armstrong, 2005; Chahrour and Zoghbi, 2007). We observed a significant reduction in the sizes and weights of brains of presymptomatic (P30) and postsymptomatic (P90) *Mecp2*$^{T158A/y}$ mice relative to their WT littermates (**Fig. 1e**), similar to that observed in *Mecp2*-null mice (Chen et al., 2001; Guy et al., 2001). The gross brain anatomy of *Mecp2*$^{T158A/y}$ mice, however, was indistinguishable from their WT littermates (**Supplementary Fig. 2d**). The decreased brain size and weight in *Mecp2*-null mice are purported to occur, at least in part, through a reduction in neuronal soma size (Armstrong, 2005; Chen et al., 2001). To assess whether soma size is affected in *Mecp2*$^{T158A/y}$ mice, we bred MeCP2 T158A mice to those expressing GFP under the control of the *Thy1* promoter (Feng et al., 2000). Focusing on the hippocampal CA1 region, confocal imaging of GFP-positive pyramidal

neurons revealed a significant reduction in soma size in *Mecp2*$^{T158A/y}$ mice compared to WT littermates at both P30 and P90 (**Fig. 1f**).

MeCP2 mutation in boys often leads to infantile lethality (Chahrour and Zoghbi, 2007) and male *Mecp2*-null mice show shortened life span(Chen et al., 2001; Guy et al., 2001; Pelka et al., 2006). We find that male *Mecp2*$^{T158A/y}$ mice die prematurely, with 50% dying by 16 weeks of age (**Fig. 1g**), which is approximately 3-4 weeks longer that germline *Mecp2*-null mice (Chen et al., 2001; Guy et al., 2001). No apparent changes in the survival profiles of female *Mecp2*$^{T158A/+}$ mice were observed before 6 months of age (data not shown). Importantly, we have not observed any significant difference in longevity, body weights or brain weights of *Mecp2*$^{loxP/y}$ knockin mice, supporting the conclusion that these changes are the result of T158A mutation (data not shown). Together, these data demonstrate that mice carrying MeCP2 T158A mutation manifest RTT-like phenotypes.

MeCP2 T158A mice present similar phenotypes to *Mecp2*-null mice

Given the clinical relevance of MeCP2 T158A mutation, we sought to carry out a side-by-side comparison of behavioral phenotypes with a well-studied *Mecp2*-null mouse (Guy et al., 2001). In light of the locomotor deficits, aberrant gait and hindlimb clasping observed in these mice (**Supplementary Video 1**), we assessed locomotor activity in a home cage environment with a cohort of age-matched WT, *Mecp2*$^{T158A/y}$ and *Mecp2*$^{-/y}$ littermates on the same C57BL/6 background at approximately 9 weeks of age. We found a significant reduction in the locomotor activity of both *Mecp2*$^{T158A/y}$ and *Mecp2*$^{-/y}$ mice compared to WT littermates (**Fig. 2a**). However, the reduction in locomotor activity was significant higher in *Mecp2*$^{-/y}$ mice compared to *Mecp2*$^{T158A/y}$ mice (**Fig. 2a**). We also found a significant reduction in distance traveled by *Mecp2*$^{T158A/y}$ mice at 11 but not 3 weeks compared to WT littermates using the open field assay (**Supplementary Fig. 3a**). Similarly, locomotor activity is also significantly reduced in female *Mecp2*$^{T158A/+}$ mice at 20 weeks, but not 12 weeks of age (**Supplementary Fig. 3b**), consistent with the age-dependent hypoactivity observed with phenotypic scoring (**Fig. 1c,d**).

To examine motor coordination and motor learning in these two mouse models, we performed the accelerating rotarod test. WT mice show an increase in the latency to fall

over the course of 4 trials per day and over 4 consecutive days, indicating improvements in motor coordination and learning over time (**Fig. 2b**). However, both *Mecp2*$^{T158A/y}$ and *Mecp2*$^{-/y}$ mice spent significantly less time on the rotarod compared to WT littermates and failed to improve significantly over the course of 4 days suggestive of deficits in motor coordination and motor learning (**Fig. 2b**). The latency to fall from the rotarod was moderately but significantly decreased in *Mecp2*$^{-/y}$ mice compared *Mecp2*$^{T158A/y}$ mice (**Fig. 2b**). We conclude that MeCP2 T158A mutation impairs motor function similar to that seen in RTT patients and to a lesser degree than *Mecp2*-null mice.

RTT patients experience anxiety episodes, particularly in response to distressing events (Chahrour and Zoghbi, 2007). The role of MeCP2 in anxiety in mice, however, is less clear: *Mecp2*-null mice and mice with a 50% reduction in MeCP2 protein expression both show a decreased anxiety phenotype (Pelka et al., 2006), whereas those containing an early-truncating mutation show increased anxiety (Shahbazian et al., 2002b). Using the elevated zero maze paradigm, we found that *Mecp2*$^{T158A/y}$ and *Mecp2*$^{-/y}$ mice spend significantly less time in the closed arm and significantly more time in the open arm compared to their WT littermates (**Fig. 2c**). This suggests that T158A mice show reduced anxiety similar to those observations in *Mecp2*-null mice and mice with decreased MeCP2 protein expression.

Because RTT is the primary cause of intellectual disability in females, we examined whether MeCP2 mutant mice have learning and memory deficits using contextual and cued fear conditioning paradigms. Mice were trained to associate a context (testing box) and a cue (auditory tone) with a co-terminating foot shock. Animals typically freeze in response to the shock. We found no differences in freezing behaviors in WT and *Mecp2*$^{T158A/y}$ littermates prior to or immediately following shocks, suggesting no differences in pain sensitivity. However, *Mecp2*$^{-/y}$ mice exhibit significantly increased freezing even prior to the shock (**Supplementary Fig. 3c**). This is likely due to their decreased locomotor activity and akinesia, thus confounding interpretation of the fear-conditioning test. These mice were therefore excluded from this study. 24 hours after training, *Mecp2*$^{T158A/y}$ mice demonstrate significantly less context- and cue-dependent freezing compared to their WT littermates, suggesting deficits in learning and memory (**Fig. 2d**).

Together, these data demonstrate that MeCP2 T158A knockin mice present phenotypes similar to those observed in *Mecp2*-null mice but to a lesser extent overall. We therefore infer that T158A is a partial loss-of-function mutation.

Decreased MeCP2 protein stability in MeCP2 T158A mice

Alterations in MeCP2 protein levels, such as a 50% reduction or a two-fold increase, leads to the progressive development of neurological deficits in mice, albeit at much later time points than those observed in *Mecp2*-null mice (Collins et al., 2004; Kerr et al., 2008; Samaco et al., 2008). We therefore examined whether T158A mutation alters the expression of MeCP2 protein during development. Quantitative Western blotting on whole-cell lysates from the brains of male *Mecp2*$^{T158A/y}$ mice revealed that MeCP2 protein expression is significantly decreased at P2, P30 and P90 compared to their WT littermates (**Fig. 3a**). The down-regulation of MeCP2 expression is significantly higher at P90, when *Mecp2*$^{T158A/y}$ mice present overt RTT-like phenotypes, than at either P2 or P30, when symptoms are not present (**Fig. 1c**). Importantly, MeCP2 protein levels were not affected in *Mecp2*$^{loxP/y}$ mice indicating that the down-regulation of MeCP2 is due to the presence of the T158A mutation rather than genomic modification (**Fig. 1b**). These changes in MeCP2 expression are likely to be independent of gene transcription since quantitative RT-PCR found no significant differences in the level of MeCP2 mRNA expression between *Mecp2*$^{T158A/y}$ and WT mice at P0, P30 or P90 (**Supplementary Fig. 4**). Despite RTT being primarily a neurological disorder (Chahrour and Zoghbi, 2007), MeCP2 is ubiquitously expressed in all mammalian tissues (Shahbazian et al., 2002a). Indeed, we found that MeCP2 protein levels are decreased to a similar extent in kidney, liver, lung and heart in *Mecp2*$^{T158A/y}$ mice (**Fig. 3b**).

MeCP2 protein levels are also significantly decreased in the brains of female *Mecp2*$^{T158A/+}$ mice compared to their WT littermates (**Fig. 3c**). The magnitude of MeCP2 down-regulation in females is less than that observed in male *Mecp2*$^{T158A/y}$ mice and is likely due to the mosaic expression of MeCP2 T158A in heterozygous *Mecp2*$^{T158A/+}$ mice. To investigate whether mutation at T158 disrupts MeCP2 protein expression in human RTT patients, we obtained fibroblast cultures derived from a female RTT patient with T158M mutation and an age-matched female control. We found that MeCP2 expression

is also significantly down-regulated by about 40% in cells with MeCP2 T158M mutation compared to control cells (**Fig. 3c**). These data demonstrate that T158 mutation, to either A or M, triggers the down-regulation of MeCP2 protein expression in both humans and mice, indicating that the reduction in MeCP2 protein expression may be a contributing factor to RTT.

To investigate whether the reductions in MeCP2 protein levels are the consequence of decreased protein stability, we cultured embryonic day 16 cortical neurons isolated from WT and *Mecp2*$^{T158A/y}$ mice and inhibited new protein translation using Cycloheximide (CHX). The stability of existing MeCP2 protein was assessed at 0, 3, 6 and 9 hours following CHX treatment. We found that MeCP2 protein levels in WT neurons remain relatively constant over the course of the 9-hour CHX treatment compared to vehicle-treated cultures (**Fig. 3d**). In contrast, MeCP2 T158A protein levels are significantly reduced following 6- and 9-hour CHX treatments (**Fig. 3d**), suggesting that T158A mutation decreases MeCP2 protein levels by increasing its rate of degradation. We did not observe destabilization of other proteins such as NeuN in T158A mice (**Fig. 3d**). Therefore, the development of MeCP2 T158A knockin mice has uncovered a novel function of T158 in the stabilization of MeCP2 protein *in vivo*. The reduction in MeCP2 protein stability mediated by T158A mutation may contribute, at least in part, to the etiology of RTT.

T158A mutation disrupts MeCP2 binding to methylated DNA

Located at the 3'-end of the MBD, T158 is believed to play an important role in stabilizing the tertiary structure of MBD and is critical for the binding of MeCP2 to methylated DNA (Ho et al., 2008). We recapitulated these *in vitro* observations using a Southwestern assay **(Fig. 4a**). To examine the role of T158 in the regulation of MeCP2 binding to methylated DNA *in vivo*, we isolated nuclei from brains of WT and *Mecp2*$^{T158A/y}$ mice and performed chromatin immunoprecipitation (ChIP) assays against several known MeCP2 binding loci. MeCP2 has been previously shown to bind across a 39 kb promoter region of the *Bdnf* locus tracking methyl-CpG sites (Skene et al., 2010). Consistent with this, we found a similar MeCP2 binding pattern in brains from P60 WT mice (**Fig. 4b**). MeCP2 ChIP over the same region in *Mecp2*$^{T158A/y}$ brains, however, revealed a 70-75%

reduction in MeCP2 binding across the entire locus (**Fig. 4b**), suggesting that T158A mutation decreases MeCP2 binding at methylated DNA. To validate this finding, we also analyzed the binding of MeCP2 to the *Xist*, *Snrpn* and *Crh* loci, known MeCP2 binding targets (Chahrour et al., 2008; Skene et al., 2010) and found that the binding of MeCP2 at these loci is significantly reduced by approximately 70% in *Mecp2*$^{T158A/y}$ brains (**Fig. 4c**). Thus, the reduction in MeCP2 binding at the *Bdnf*, *Xist*, *Snrpn*, and *Crh* loci likely reflects a decreased binding of MeCP2 T158A to methylated DNA together with reduced MeCP2 protein expression.

We reasoned that if MeCP2 T158A has a reduced affinity to methylated DNA *in vivo*, WT or MeCP2 T158A protein would be extracted differently from nuclei under the same salt conditions. To biochemically assay the reduced affinity of MeCP2 T158A to methylated DNA, we isolated neuronal nuclei from either WT or *Mecp2*$^{T158A/y}$ mouse brains and treated them with increasing concentrations of NaCl to extract proteins into the supernatant. Quantitative Western blot analysis revealed that MeCP2 T158A protein is extracted more readily than WT protein under low salt conditions of 250mM and 300mM NaCl (**Fig. 4d**). When the salt is raised to above 350 mM, both WT and T158A protein are extracted to a similar degree. Thus, mutation of T158A appears to decrease the affinity of MeCP2 for DNA.

MeCP2 predominantly associates with heterochromatic foci in mouse cell nuclei in an MBD- and DNA methylation-dependent manner, resulting in a characteristic punctate pattern of nuclear staining (Nan et al., 1997). Indeed, we demonstrated that MeCP2 immunoreactivity is observed throughout the nucleus with particularly high enrichment at heterochromatin-dense foci in nuclei from P90 WT neurons (**Fig. 4e**). In contrast, in nuclei from P90 *Mecp2*$^{T158A/y}$ neurons, MeCP2 is markedly diffuse with a clear absence of co-localization with DNA, indicating that the binding of MeCP2 to methylated DNA is disrupted (**Fig. 4e**). This difference is unlikely due to changes in heterochromatin formation as no overt differences are seen in DNA staining in T158A mice. We observed similar immunoreactivity patterns in P30 *Mecp2*$^{T158A/y}$ mice prior to symptom presentation (data not shown). Furthermore, MeCP2 immunoreactivity in female *Mecp2*$^{T158A/+}$ mice shows a mosaic expression of MeCP2 with approximately 50% of nuclei showing MeCP2 immunoreactivity at heterochromatin-dense foci with the remaining exhibiting

diffuse immunoreactivity (**Fig. 4f**), as is expected due to random X-chromosome inactivation. Notably, the intensity of MeCP2 immunoreactivity is decreased in T158A neurons compared to WT neurons, consistent with a reduction of MeCP2 T158A protein expression. Together, these data demonstrate that T158A mutation impairs the binding of MeCP2 to methylated DNA *in vivo* and contributes, at least in part, to the etiology of RTT.

Disruption of MeCP2 binding to methylated DNA

Transcriptional profiling of RNA isolated from the hypothalamus or cerebellum of *Mecp2*-null mice revealed changes in the expression of thousands of genes, with many of these changes in a tissue-specific manner (Chahrour et al., 2008). We analyzed the expression of a few representative targets such as *Bdnf*, *Crh* and *Sgk* using quantitative RT-PCR and found that both *Bdnf* and *Crh* transcription are significantly reduced in the hypothalamus but not striatum of T158A mice (**Fig. 5a,b**), whereas, *Sgk*, a gene that is upregulated in *Mecp2*-null mice (Nuber et al., 2005), is elevated in the striatum but not in the hypothalamus of T158A mice (**Fig. 5a,b**). These data support that gene transcription is similarly disrupted in MeCP2 T158A and *Mecp2*-null mice in a tissue- and/or cell-type specific manner.

MeCP2 has been shown to regulate gene transcription through its interaction with histone deacetylases (HDACs) 1 and 2 and the co-repressor Sin3a (Jones et al., 1998; Nan et al., 1997). It is conceivable that T158A mutation may disrupt the ability of MeCP2 to associate with these proteins through alterations in the conformation of MeCP2 and thus disrupt downstream gene regulation. We therefore performed co-immunoprecipitation experiments using an antibody against MeCP2 in nuclear extracts prepared from WT and *Mecp2*$^{T158A/y}$ brains. Consistent with previous studies, WT MeCP2 interacts with HDAC1 and Sin3a (**Fig. 5c**). We also detected the association of MeCP2 T158A with HDAC1 and Sin3A, albeit at a reduced level consistent with the reduced MeCP2 T158A protein expression (**Fig. 5c**). Thus, these data support that MeCP2 T158A protein retains the ability to interact with the co-repressor proteins. Together, we conclude that MeCP2 T158A leads to a deregulation of gene expression through reduced DNA binding and MeCP2 protein stability.

Age-dependent alterations in EEG and ERP recordings

The manifestation of symptoms in RTT patients and *Mecp2*-null mice are thought to occur in part due to alterations in neural network activity. Since RTT symptoms appear at certain developmental time points, we sought to investigate the neural mechanisms underlying age-dependent exhibition of phenotypes in MeCP2 T158A mice. Thus, we performed EEG recordings in WT and *Mecp2*$^{T158A/y}$ mice at two developmental time periods, P30 and P90; that is, prior to and subsequent to the establishment of RTT-like symptoms. EEG recordings in awake, freely mobile mice demonstrated a significant increase in the power of high-gamma frequency (γ_{high}; 70-140 Hz) oscillations in *Mecp2*$^{T158A/y}$ mice at P90 compared to WT littermates (**Fig. 6a,b**). A similar increase in γ_{high} power was also observed in symptomatic *Mecp2*$^{-/y}$ mice (**Supplementary Fig. 5a,b**). γ_{high} activity is known to be associated with epilepsy in the EEG before and during the seizure (Uhlhaas et al., 2011) and may thus reflect an overall hyperexcitability in the brains of *Mecp2*$^{T158A/y}$ and *Mecp2*$^{-/y}$ mice (Chao et al., 2010). However, we did not observe a significant increase in γ_{high} power in pre-symptomatic *Mecp2*$^{T158A/y}$ mice at P30 (**Supplementary Fig. 6a,b**), suggesting that MeCP2 dysfunction induces hyperexcitability in the brain in an age-dependent manner.

In addition to measuring electrical activity during passive processes, it is also possible to measure those that occur during the performance of a cognitive, sensory or motor task. The manifestation of these brain activities is recorded as a series of amplitude deflections in the EEG as a function of time and is referred to as an event-related potential (ERP). ERPs are small compared to the background EEG but can be resolved by averaging single trial epochs. They are characterized as voltage deflections defined by latency and polarity where the amplitude and latency of the polarity peaks are believed to reflect the strength and timing of the cognitive processes related to the event. Notably, RTT patients, as well as patients with schizophrenia and autism, are reported to show alterations in both the amplitudes and latencies of ERP (Bader et al., 1989; Gandal et al., 2010; 2012; Roberts et al., 2010; Stauder et al., 2006).

To examine ERP responses in *Mecp2*$^{T158A/y}$ mice, we performed EEG recordings following the presentation of a series of white noise clicks. We chose to perform auditory-evoked ERP assessments since they can be performed on freely mobile mice

and are not confounded by the motor or attentional deficits associated with MeCP2 dysfunction. The ERP was extracted by averaging the EEG traces over single trial epochs. ERPs in WT and *Mecp2*$^{T158A/y}$ mice show a stereotypical initial positive peak (P1), followed by a negative peak (N1) and a subsequent second positive peak (P2) (**Fig. 6c**). Interestingly, we found significant increases in the latency and significant reductions in the amplitudes of the N1 and P2 peaks in symptomatic P90 *Mecp2*$^{T158A/y}$ mice compared to WT littermates (**Fig. 6c-e**). Similar alterations in ERP amplitudes and latencies were observed in *Mecp2*$^{-/y}$ mice (**Supplementary Fig 5c-e**). However, we observed no significant effect on ERPs in *Mecp2*$^{T158A/y}$ mice at P30, prior to the establishment of RTT-like symptoms (**Supplementary Fig 6c-e**). Importantly, we found no differences in hearing sensitivities between *Mecp2*$^{T158A/y}$ mice or *Mecp2*$^{-/y}$ mice and their WT littermates as measured by auditory brain stem responses, suggesting that these disruptions in ERP are due to alterations in cortical processing of sensory input (**Supplementary Fig. 7**). These data suggest that neural networks underlying information processing are disrupted by MeCP2 dysfunction in an age-dependent manner, corresponding to the behavioral onset of symptoms.

Progressive alterations in event-related power and PLF

One limitation of time-amplitude analysis of ERPs is that oscillatory information not time-locked to the stimulus is lost through signal averaging. Using time-frequency analysis it is possible to analyze changes in oscillatory activity as a function of time and thus gain additional insight into the underlying brain activity and circuitry. Oscillatory responses during the performance of tasks are characterized by the average power and phase locking across trials (Tallon-Baudry and Bertrand, 1999). The degree of event-related power and phase locking at different frequencies may reflect the strength and connectivity of local (at high frequencies) and long-range (at low frequencies) neuronal circuits (Buzsáki and Draguhn, 2004).

Thus, we next performed time-frequency analysis on EEG recordings used to determine auditory-evoked ERPs. We found that the presentation of an auditory stimulus modulated the mean event-related power in a frequency-specific manner. WT mice at P90 showed a significant depression in the mean power of oscillations in the low-

frequency delta (δ; 2-4 Hz), theta (θ; 4-8 Hz) and alpha (α; 8-12 Hz) ranges upon auditory stimulation (**Fig. 7a,b**). The mean event-related power of high-frequency beta (β; 12-30 Hz), low gamma (γ_{low}; 30-50 Hz) and high gamma (γ_{high}; 70-140 Hz) increased following the auditory stimulus and was followed by a sustained depression in power (**Fig. 7a,b**). Notably, these changes are sustained for a number of oscillation cycles at all frequencies and outlast the transient ERP response reflecting an effect in both evoked and ongoing oscillatory processes (**Fig. 7a,b**). Overlaying the ERP with band-pass EEG traces at each frequency range reveals the oscillatory information within the transient ERP response (**Supplementary Fig. 8**). *Mecp2*$^{T158A/y}$ mice, however, exhibited significantly attenuated event-related power in both low- and high-frequency oscillations at P90 when RTT-like symptoms are overt (**Fig. 7a,b and Supplementary Fig. 9a**). Similarly, highly symptomatic *Mecp2*$^{-/y}$ mice show significantly reduced event-related power following auditory stimulation at all frequencies (**Supplementary Fig. 9b, 10a,b**). Notably, we also found a significant reduction in event-related power in low-frequency δ, θ and α in P30 *Mecp2*$^{T158A/y}$ mice prior to symptom onset compared to WT littermates (**Supplementary Fig. 9c, 11a,b**). These data suggests that the underlying deficits in neural activity occur prior to the establishment of behavioral symptoms consistent with *in vitro* electrophysiological studies showing reduced cortical excitability in *Mecp2*$^{-/y}$ mice even at 2-3 weeks of age (Dani et al., 2005).

Time-frequency analysis also allows for the calculation of oscillation phase locking across trials. The phase locking factor (PLF) quantifies the trial-to-trial reliability of oscillation phase with a high PLF corresponding to a low circular variance in oscillation phase as a function of time between trials. High PLF is thought to reflect the reliability and sensitivity of communications between circuits in the brain (Winterer et al., 2000). We find that WT mice at P90 show significant increases in PLF at all frequencies in response to the presentation of auditory stimuli (**Fig. 7c,d**). The increase in PLF in *Mecp2*$^{T158A/y}$ mice at P90, however, is significantly reduced compared to WT mice (**Fig. 7c,d and Supplementary Fig. 9d**). A significant reduction in event-related PLF in *Mecp2*$^{-/y}$ mice was also observed, consistent with the expression of RTT-like phenotypes in both groups of mice (**Supplementary Fig. 9e, 10c,d**). We also detected significant attenuation in PLF in pre-symptomatic P30 *Mecp2*$^{T158A/y}$ mice, although only at δ-and high-gamma frequencies (**Supplementary Fig. 9f, 11c,d**). Importantly, the fact

that we do not observe changes in ERP amplitudes at P30 in *Mecp2*$^{T158A/y}$ mice (**Supplementary Fig. 6, 12**) suggests that time-frequency analysis of event-related power and PLF represents a sensitive approach to probe neural function *in vivo*.

Interestingly, when comparing the event-related neuronal responses in WT mice at two developmental stages, we find that event-related power at all frequencies and PLF at high frequencies are significantly higher in P90 mice than those at P30 (**Fig. 8a,b**). This likely reflects the development and maturation of the underlying neuronal circuitry. In contrast, *Mecp2*$^{T158A/y}$ mice do not show a developmental increase in either event-related power (**Fig. 8c**) or phase locking (**Fig. 8d**) from P30 to P90, suggesting an impairment in age-dependent neural network maturation. These age-dependent differences are only observed using time-frequency but not time-amplitude analysis (**Fig. 8 and Supplementary Fig. 12**). Together, these data reveal that MeCP2 plays an important role in the regulation of event-related neuronal responses and is required for the maturation and restructuring of neural networks. The disruptions in event-related power and PLF may therefore contribute to the deficits in behavioral and cognitive functions observed in RTT. We propose that ERP studies may serve as a sensitive biomarker for the evaluation of treatments in RTT patients.

Discussion

Mutation of MeCP2 T158 to M or in rare cases to A represents one of the most common mutations observed in RTT patients (Bienvenu and Chelly, 2006). Previous *in vitro* experiments established a critical role for this residue in the binding of MeCP2 to methylated DNA. To address the causal role of T158A mutation in the pathogenesis of RTT and the role of methyl-DNA binding in the proper functions of MeCP2, we developed and characterized MeCP2 T158A knockin mice. We found that MeCP2 T158A mice develop normally for the first 4-5 weeks of life after which they present RTT-like symptoms including decreased motor performance, altered anxiety, aberrant gait, hindlimb clasping, breathing abnormalities, and impaired learning and memory. The similarity in the identity and severity of symptoms with those observed in *Mecp2*-null mice indicates that MeCP2 T158A mutation is a partial loss-of-function mutation.

The development of this mouse line allowed us to investigate the biochemical consequences of MeCP2 T158A mutation *in vivo*. In agreement with previous *in vitro* studies, we find that MeCP2 T158A mutation leads to a reduction in the affinity of MeCP2 for methylated DNA *in vivo*. Surprisingly, we also observed that T158A mutation concomitantly decreases MeCP2 protein expression *in vivo*. Consistent with these data, we find that fibroblasts obtained from a female RTT patient carrying MeCP2 T158M mutation express decreased levels of MeCP2 protein. These findings reveal two consequences of T158 mutation*:* impaired MeCP2 binding to DNA and decreased MeCP2 protein stability of MeCP2.

Previous studies have demonstrated that MeCP2 protein levels must be tightly regulated to ensure its proper function. A 50% reduction in MeCP2 protein levels leads to progressive neurological symptoms (Kerr et al., 2008; Samaco et al., 2008), although symptoms appeared later and do not fully recapitulate RTT-like symptoms as in *Mecp2*-null mice. Therefore, the destabilization of MeCP2 protein alone, as observed in our T158A mice, may not be sufficient to cause the RTT-like symptoms. We propose that the combined reduction in MeCP2 protein levels and the decreased binding to methylated DNA contribute to the loss-of-function phenotype in T158A knockin mice. The development of knockin mice carrying other mutations that disrupt DNA binding will

provide further insights into this hypothesis. Given that the reintroduction of MeCP2 protein into *Mecp2*-null mice is sufficient to rescue RTT-like phenotypes (Guy et al., 2007) we suggest a dual approach to restore MeCP2 function in patients carrying MeCP2 T158 mutations: increasing MeCP2 affinity for methylated DNA and enhancing MeCP2 protein stability. Indeed, the feasibility of increasing affinity for DNA has been shown for other DNA-binding proteins such as p53 (Foster et al., 1999). It is conceivable that increasing MeCP2 affinity to methylated DNA may help stabilize MeCP2 protein expression. Targeting one or both of these possibilities may lead to the amelioration of RTT-like phenotypes. Our study also suggests that different therapeutic strategies should be considered for treating patients with different MeCP2 mutations.

Given their neurological origin, many of the symptoms associated with RTT have been hypothesized to result from imbalanced neural networks (Chahrour and Zoghbi, 2007). Evidence to support this arises from observed alterations in synaptic connectivity and plasticity (Dani and Nelson, 2009; Dani et al., 2005; Guy et al., 2007; Kishi and Macklis, 2004; Wood et al., 2009) and hyperexcitability in the EEG (Chao et al., 2010; D'Cruz et al., 2010) of *Mecp2*-null mice. Furthermore, ERP analysis in RTT females suggests alterations in sensory processing of information (Bader et al., 1989; Stauder et al., 2006). Given the delayed onset of symptoms in RTT patients, MeCP2 T158A mice and *Mecp2*-null mice, we sought to examine whether neurophysiological responses as measured by EEG were altered during development in MeCP2 T158A mice. Indeed, we found that the power of high-gamma EEG signals is significantly increased in MeCP2 T158A mice when these mice exhibit RTT-like symptoms, suggesting hyperexcitability in the brain. Furthermore, assessment of auditory-evoked ERPs revealed a significant and marked reduction in the amplitude and increased latency of ERPs in MeCP2 T158A and *Mecp2*-null mice suggesting deficits in information processing in the brain similar to that observed in RTT females (Bader et al., 1989; Stauder et al., 2006), autism (Gandal et al., 2010; Roberts et al., 2010) and other disorders including schizophrenia (Uhlhaas and Singer, 2010). Further studies are needed to address the neuronal mechanisms that underlie these deficits in ERP response.

Our data show that disturbances in event-related power and phase locking also occur in MeCP2 mouse models and may play a role in the etiology of RTT. In humans and

animal models, changes in the power and phase locking of neuronal responses coordinate neuronal activity across different brain regions. These changes are involved in the development and efficacy of motor, perceptual and memory tasks and deficits in neuronal oscillations are consistently observed in neurological disorders in which these functions are impaired (Uhlhaas and Singer, 2006; 2010). Our findings that both low- and high-frequency event-related oscillations are disrupted lead us to hypothesize that deficits in local and long-distance neuronal circuitry occur following MeCP2 dysfunction. The neurophysiological mechanisms that lead to disturbances in these oscillations are not known, but may involve the reduced neuronal connectivity that leads to a redistribution of neuronal activity away from excitation and towards inhibition as observed in *Mecp2*-null mice (Dani and Nelson, 2009; Dani et al., 2005; Wood et al., 2009). Furthermore, given the important role that event-related neuronal responses play in the development of the nervous system (Ben-Ari, 2001), their disruption prior to symptom presentation may augment the deficits in neuronal activity caused by MeCP2 dysfunction. Indeed, MeCP2 T158A mice do not exhibit developmental increases in event-related power or phase locking suggestive of stagnation in the developmental of neuronal circuits. Moreover, our findings that event-related changes in power and phase locking occur in MeCP2 T158A mice with no behavioural symptoms suggest that disruptions in neuronal networks may precede the behavioral RTT-like phenotypes. The identification of the mechanisms that lead to these disturbances will provide valuable insights into the pathogenesis of RTT and the neuronal networks underlying manifestation of behavioral phenotypes in RTT.

In summary, the development of MeCP2 T158A mice has uncovered a novel role for T158 in the pathogenesis of RTT and revealed an alternative strategy to restore MeCP2 function. These mice provide an *in vivo* animal model for assessing therapeutic efficacy in pre-clinical trials. Moreover, given that ERP studies can be readily performed in humans, assessment of ERP and the changes in oscillation and phase locking may serve as a valuable biomarker for evaluating RTT phenotypes.

Figure 1

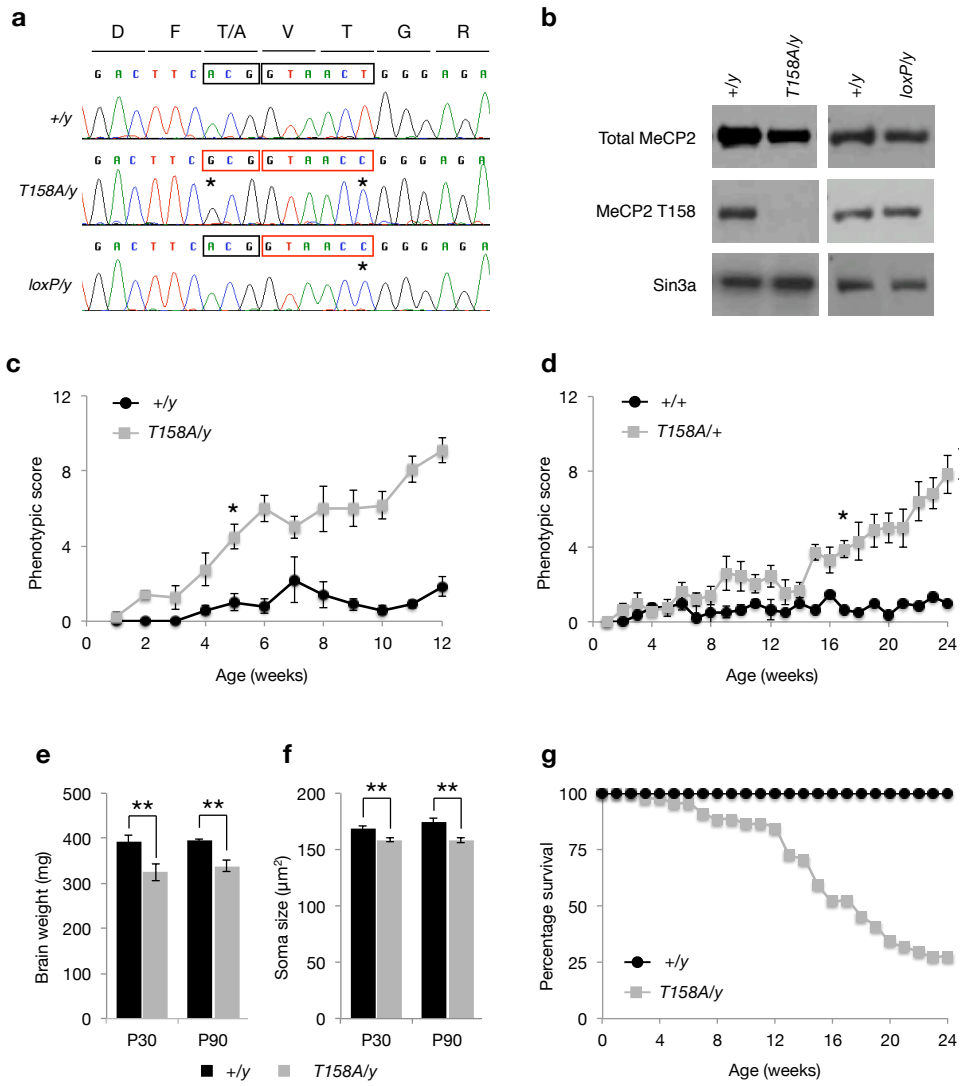

Figure 1. Generation and phenotypic characterization of MeCP2 T158A knockin mice

(a) Sequencing chromatogram of RT-PCR products from MeCP2 mRNA. Mutation of T158 codon ACG to Alanine codon GCG (first box) and creation of BstEII restriction site (second box) with a silent mutation are marked with *.

(b) Western blots probed with a site-specific MeCP2 T158 antibody, a total MeCP2 antibody and Sin3a antibody.

(c) Developmental presentation of RTT-like phenotypes in male *Mecp2*$^{T158A/y}$ mice (n = 6; $F_{1,252}$ = 27.75, *p*-value < 0.0001; two-way ANOVA) relative to WT littermates (n = 5). Symbols represent mean score ± SEM. Phenotypic score is significantly higher in *Mecp2*$^{T158A/y}$ mice compared to WT littermates at 5 weeks and thereafter; * *p*-value < 0.05; two-way ANOVA with Bonferroni correction.

(d) Developmental presentation of RTT-like phenotypes in female *Mecp2*$^{T158A/+}$ mice (n = 7; $F_{1,224}$ = 198.6, *p*-value < 0.0001; two-way ANOVA) relative to *Mecp2*$^{+/+}$ littermates (n = 6). Phenotypic score is significantly higher in *Mecp2*$^{T158A/+}$ mice compared to WT littermates at 17 weeks and thereafter; * *p*-value < 0.05; two-way ANOVA with Bonferroni correction.

(e) Brain weights at P30 (n = 4 for both genotypes) and P90 (n = 6 for both genotypes). Bars represent mean ± SEM. ** *p*-value < 0.01; two-tailed t-test with Bonferroni correction.

(f) Soma size in hippocampal CA1 pyramidal neurons. Bars represent mean ± SEM (n = 100 cells from 5 animals per genotype). ** *p*-value < 0.01; two-tailed t-test with Bonferroni correction.

(g) Survival of male *Mecp2*$^{T158A/y}$ (n = 43) and *Mecp2*$^{+/y}$ littermates (n = 43).

Figure 2

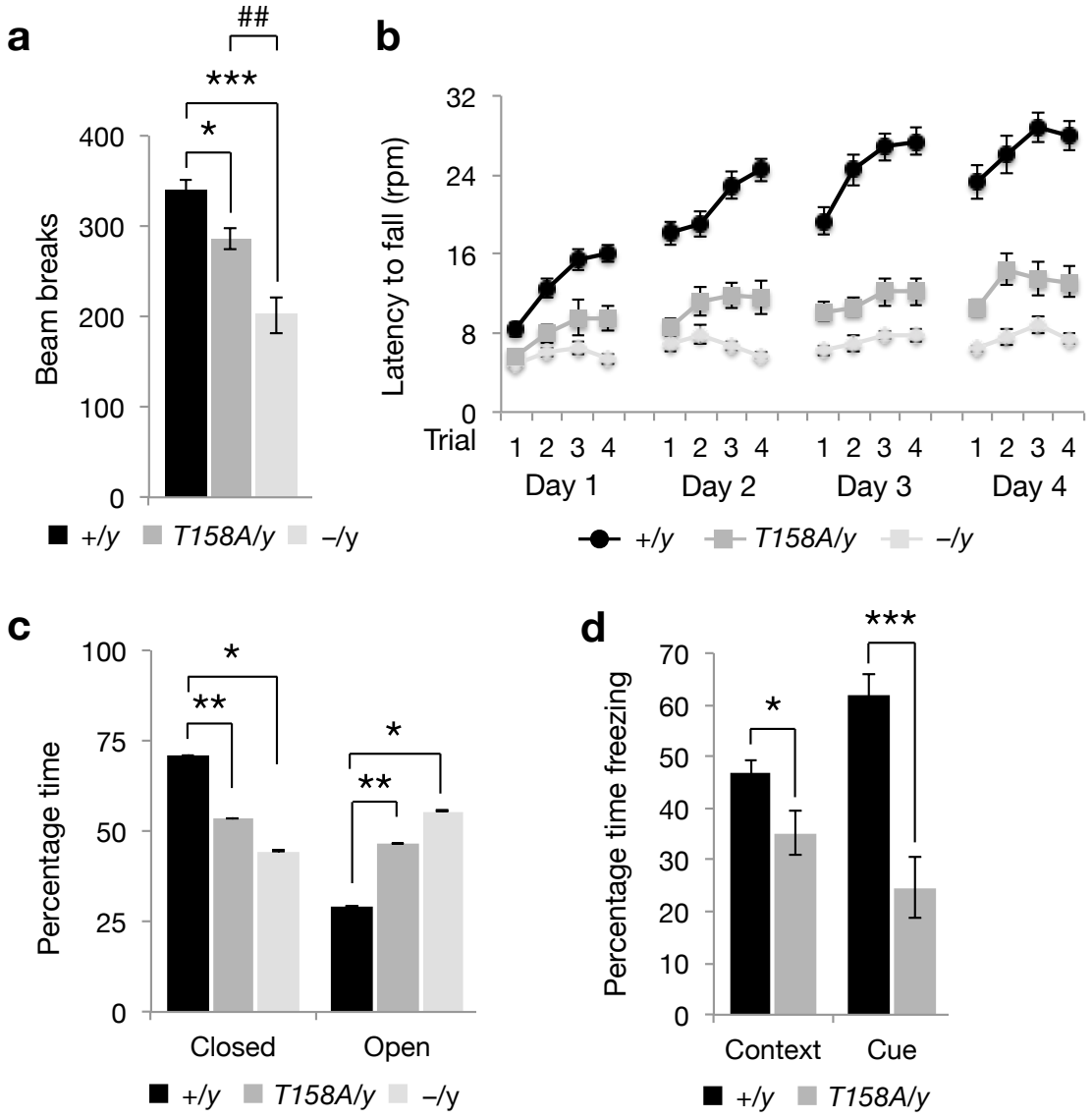

Figure 2. Behavioral characterization of MeCP2 T158A mice

(a) Locomotor activity in *Mecp2*$^{T158A/y}$ mice (n = 15), *Mecp2*$^{-/y}$ mice (n = 14) and *Mecp2*$^{+/y}$ littermates (WT; n = 33) at 9 weeks of age. Bars represent mean ± SEM. * *p*-value < 0.01, *** < 0.001 and ## < 0.01; one-way ANOVA with Tukey's *post hoc* test.

(b) Motor coordination and motor learning assessed using a rotarod assay in *Mecp2*$^{T158A/y}$ mice (n = 16; $F_{1,645}$ = 447.2, *p*-value < 0.0001; two-way ANOVA) and *Mecp2*$^{-/mice}$ (n = 14; $F_{1,602}$ = 841.46, *p*-value < 0.0001; two-way ANOVA) and WT littermates (n = 27) at 9 weeks of age. The deficit in *Mecp2*$^{-/y}$ mice is significantly more than that observed in *Mecp2*$^{T158A/y}$ mice ($F_{1,437}$ = 83.82, *p*-value < 0.0001; two-way ANOVA). Symbols represent mean ± SEM.

(c) Anxiety-like behavior in *Mecp2*$^{T158A/y}$ mice (n = 15) and *Mecp2*$^{-/y}$ mice (n = 11) measured using elevated zero maze compared to WT littermates (n = 32) at 9 weeks of age. Bars represent mean ± SEM. * *p*-value < 0.05 and ** < 0.01; one-way ANOVA with Tukey's *post hoc* test.

(d) Learning and memory assessed using context- and cue-dependent fear conditioning in *Mecp2*$^{T158A/y}$ mice (n = 16) and WT littermates (n = 33) at 10 weeks of age. Bars represent mean ± SEM. * *p*-value < 0.05 and *** < 0.001; two-tailed t-test with Bonferroni correction.

Figure 3

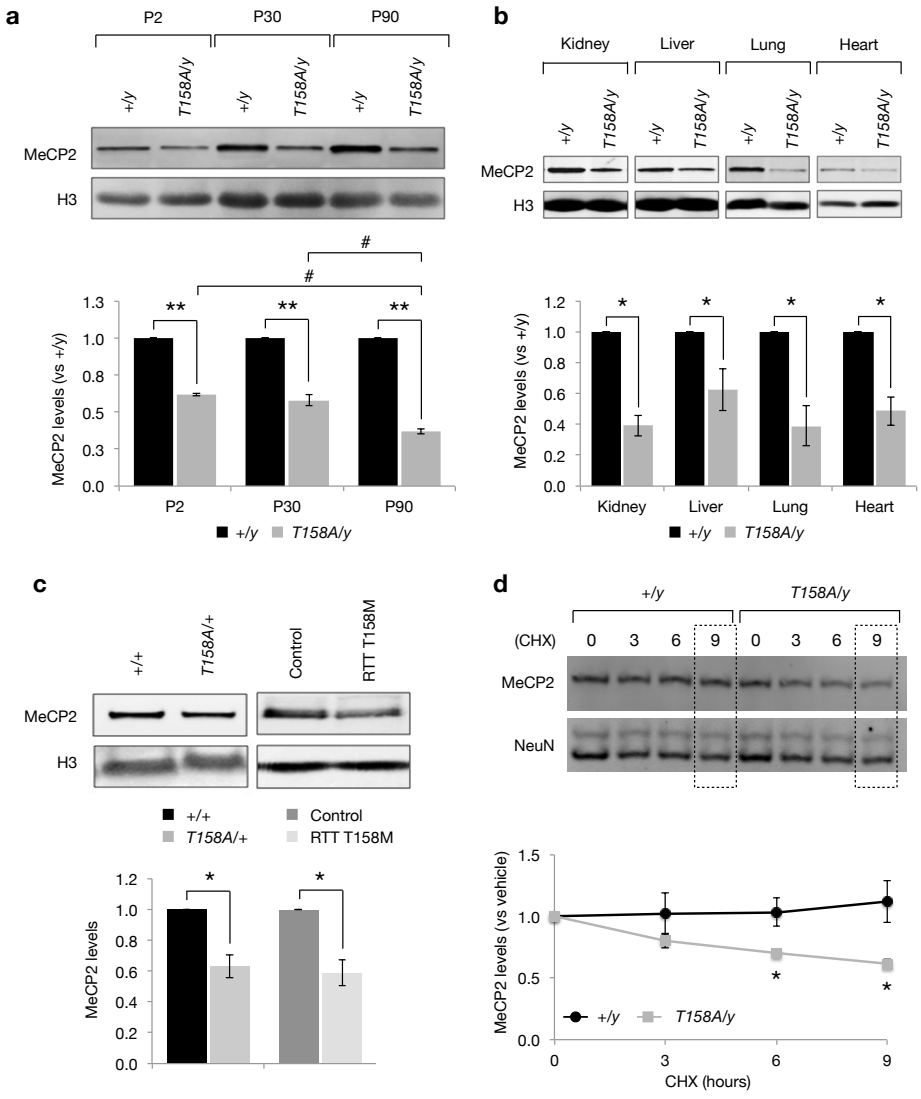

Figure 3. Decreased MeCP2 protein stability in MeCP2 T158A mice

(a) MeCP2 protein levels in forebrains of *Mecp2*$^{T158A/y}$ mice at P2, P30, and P90 compared to *Mecp2*$^{+/y}$ littermates (n = 3 for each genotype). Bars represent mean ± SEM. ** *p*-value < 0.01; one-sample t-test with Bonferroni correction. # < 0.05; one-way ANOVA with Tukey's *post hoc* test.

(b) MeCP2 protein levels are significantly reduced in kidney, liver, lung and heart tissues of *Mecp2*$^{T158A/y}$ (n = 3) compared to *Mecp2*$^{+/y}$ littermates at P90 (n = 3). Bars represent mean ± SEM. * *p*-value < 0.05; one-sample t-test with Bonferroni correction.

(c) MeCP2 protein levels in female *Mecp2*$^{T158A/+}$ mice (n = 3) and *Mecp2*$^{+/y}$ littermates at P90 (n = 3). MeCP2 protein levels in fibroblasts derived from a female RTT patient carrying the MeCP2 T158M mutation compared to fibroblasts derived from an age-matched female control (n = 3 separate passages). Bars represent mean ± SEM. * *p*-value < 0.05; one-sample t-test.

(d) E16 + 7 DIV cortical neurons derived from *Mecp2*$^{T158A/y}$ (n = 3) and *Mecp2*$^{+/y}$ littermates (n = 3) were treated with vehicle (0) or 100 μM Cycloheximide (CHX) for 3, 6 or 9 hours. Bars represent mean MeCP2 levels relative to vehicle ± SEM. * *p*-value < 0.05; two-way ANOVA with Bonferroni correction.

Figure 4

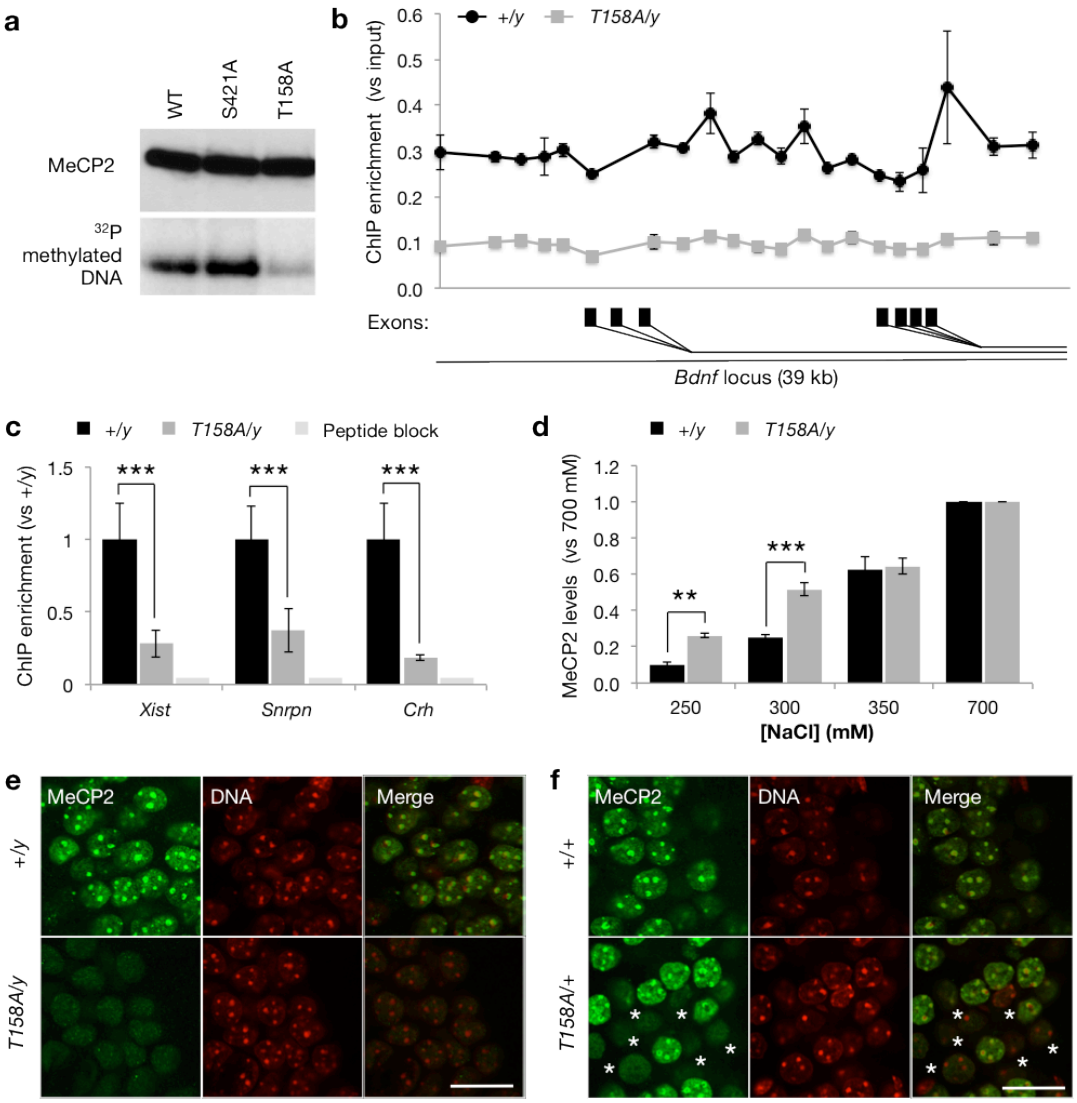

Figure 4. Reduced MeCP2 binding to methylated DNA in T158A mice

(a) MeCP2 binding to methylated DNA (methylated oligonucleotides spanning the -148 CpG site of Bdnf promoter IV) is reduced by T158A mutation relative to WT and MeCP2 S421A mutation in Southwestern assay.

(b) MeCP2 binding across a 39 kb of the promoter region of the *Bdnf* locus in brains obtained from *Mecp2*$^{T158A/y}$ mice mice and *Mecp2*$^{+/y}$ littermates (n = 3; two-way ANOVA, $F_{1,84} = 639.1$, p-value < 0.0001). Symbols represent mean ± SEM. Alternative *Bdnf* exons are indicated with black rectangles.

(c) MeCP2 binding to the *Xist*, *Snrpn*, and *Crh* loci in *Mecp2*$^{T158A/y}$ mice (n = 3) compared to *Mecp2*$^{+/y}$ littermates (n = 3). Bars represent mean ± SEM. *** p-value < 0.001; two-tailed t-test with Bonferroni correction.

(d) Salt extraction of WT MeCP2 and MeCP2 T158A protein with increasing concentrations of NaCl (n = 3). Bars represent mean ± SEM normalized to MeCP2 levels extracted with 700 mM NaCl. ** p-value < 0.01 and *** < 0.001; two-way ANOVA with Bonferroni correction.

(e) MeCP2 co-localization with heterochromatin-dense foci in male WT but not *Mecp2*$^{T158A/y}$ mice at P90. Representative images of neuronal nuclei shown are single confocal planes at 100X magnification. Scale bar corresponds to 20 µm.

(f) MeCP2 staining in nuclei obtained from female *Mecp2*$^{T158A/+}$ mice. Nuclei showing diffuse MeCP2 staining are marked with an *. Scale bar corresponds to 20 µm.

Figure 5

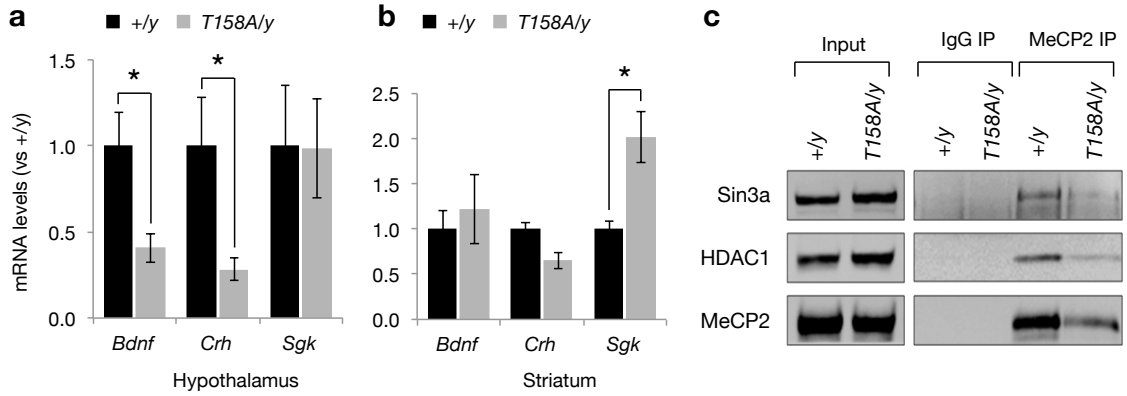

Figure 5. Disruption of MeCP2 methyl-DNA binding leads to deregulation of gene expression

(a) *Bdnf*, *Crh* and Sgk mRNA expression in the hypothalamus of *Mecp2*$^{T158A/y}$ mice compared to *Mecp2*$^{+/y}$ littermates (n = 4). Bars represent mean ± SEM. * *p*-value < 0.05; two-tailed t-test with Bonferroni correction.

(b) *Bdnf*, *Crh* and Sgk mRNA expression in the striatum of *Mecp2*$^{T158A/y}$ mice and *Mecp2*$^{+/y}$ littermates (n = 4). Bars represent mean ± SEM. * *p*-value < 0.05; two-tailed t-test with Bonferroni correction.

(c) MeCP2 T158A mutation does not impair the association of MeCP2 with HDAC1 or Sin3a. MeCP2 immunoprecipitation from brain nuclear extracts prepared from *Mecp2*$^{T158A/y}$ and *Mecp2*$^{+/y}$ littermates are probed with indicated antibodies.

Figure 6

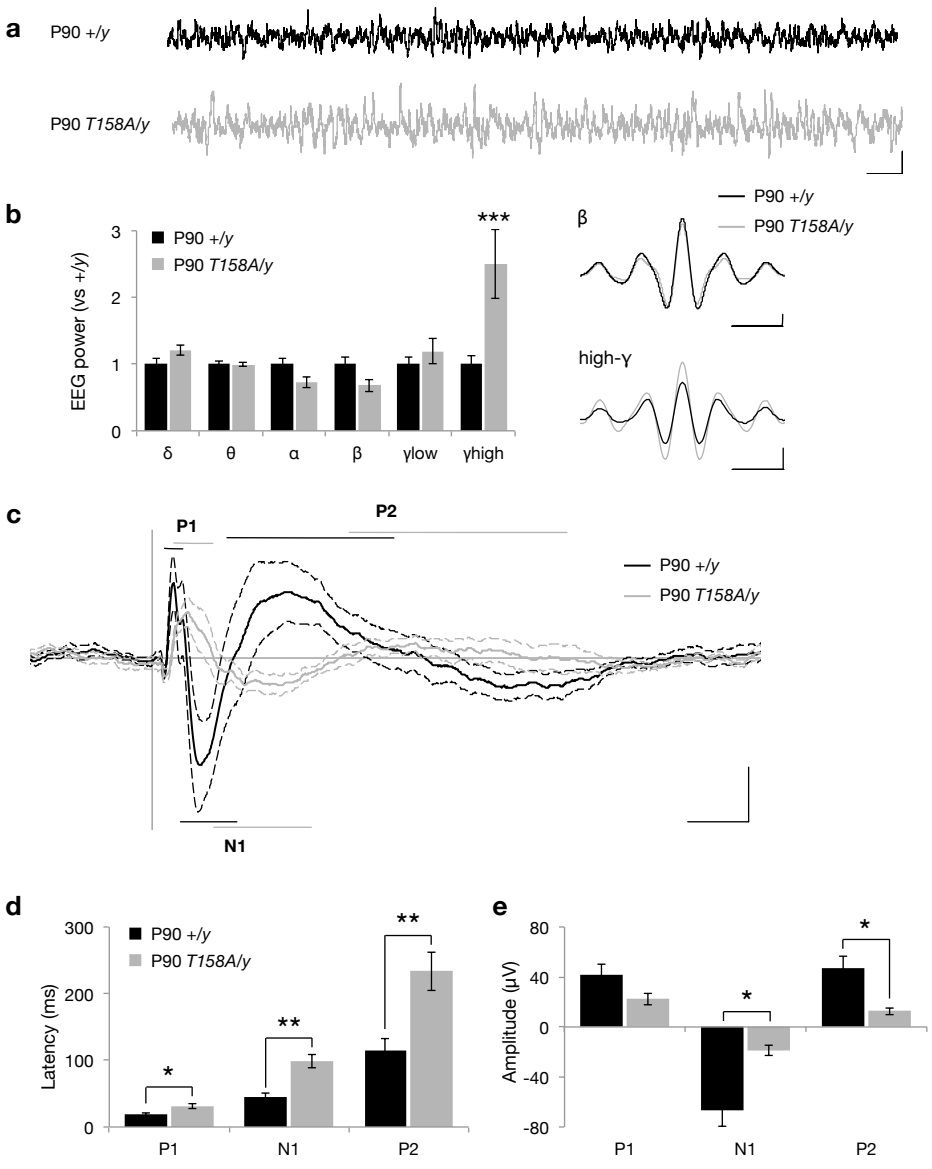

Figure 6. EEG and ERP recordings in MeCP2 T158A mice

(a) Representative EEG traces from awake, freely mobile mice. Scale bar corresponds to 1 second (horizontal) and 200 μA (vertical).

(b) Basal EEG power measurements in P90 *Mecp2*$^{T158A/y}$ mice (n = 7) compared to *Mecp2*$^{+/y}$ littermates (n = 8). Frequency bands are represented as follows: δ (2-4 Hz), θ (4-8 Hz), α (8-12 Hz), β (12 – 30 Hz), low-γ (30-50 Hz), and high-γ (70-140 Hz). Insets show β and high-γ mean amplitudes across EEG recordings. Scale bars represent one oscillation cycle (horizontal) and 20 μA (vertical). Bars represent mean ± SEM. *** *p*-value <0.001; two-tailed t-test with Bonferroni correction.

(c) Grand average event-related potential (ERP) traces following presentation of 85-dB white-noise clicks with 4-second interstimulus intervals. Traces represent mean amplitude (solid line) ± SEM (dashed lines). The characteristic polarity peaks P1, N1 and P2 are highlighted with straight lines with the length indicating latency range. Scale bar corresponds to 50 ms (horizontal) and 20 μA (on vertical).

(d) Latencies and (e) amplitudes of ERP peaks. Bars represent mean ± SEM. * *p*-value < 0.05 and ** < 0.01; two-tailed t-test with Bonferroni correction

Figure 7

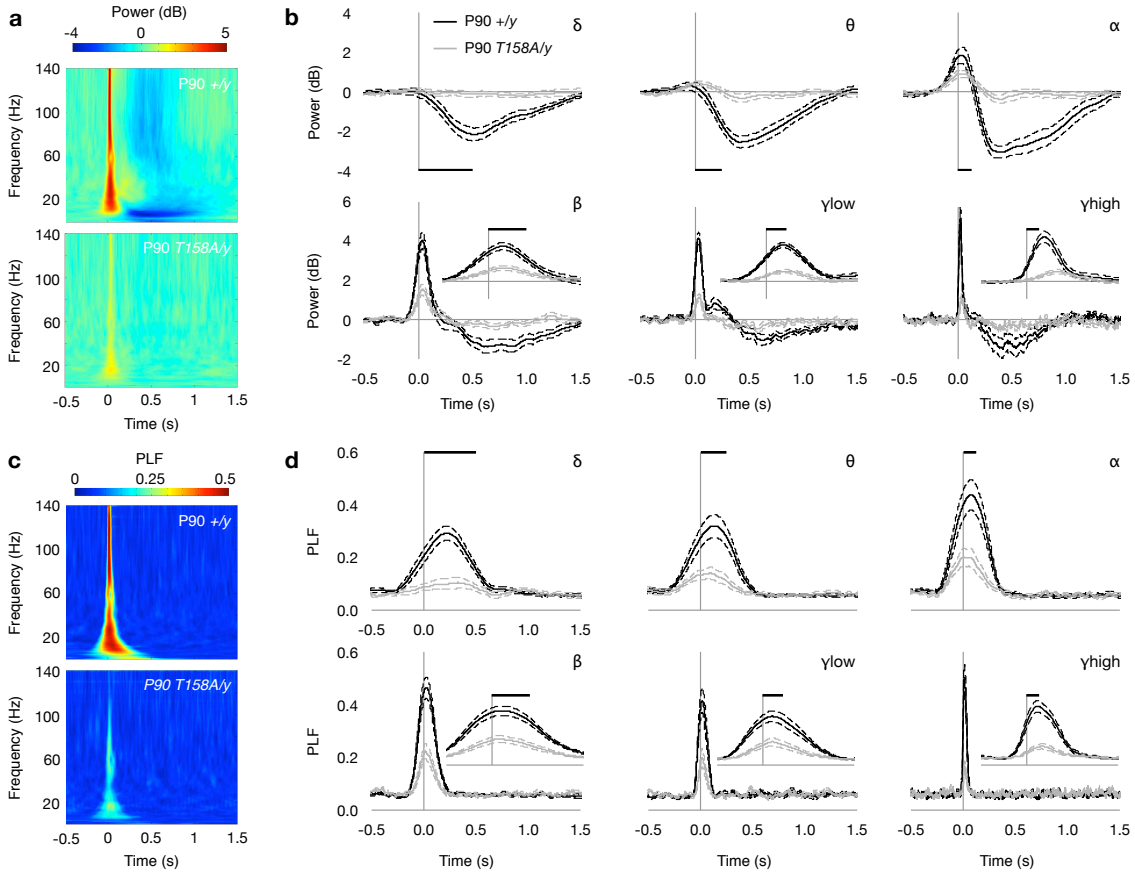

Figure 7. Decreased event-related power and PLF in *Mecp2*$^{T158A/y}$ mice

(a) Time-frequency plots showing changes in event-related power in response to 85-dB auditory stimulation in P90 *Mecp2*$^{T158A/y}$ mice and *Mecp2*$^{+/y}$ littermates. Time is plotted on the abscissa (where *t = 0* at sound presentation) and frequency on the ordinate. Color represents mean power with warmer colors corresponding to an increased power and cooler colors representing decreased power compared to pre-stimulus baseline.

(b) Changes in event-related mean power averaged across δ (2-4 Hz), θ (4-8 Hz), α (8-12 Hz), β (12 – 30 Hz), low-γ (30-50 Hz), and high-γ (70-140 Hz) frequencies. Scale bars represent the length of a single oscillation cycle of the lowest frequency in the range. Insets showed power traces on expanded time-scale denoted by length of single oscillation cycle. Traces represent mean power ± SEM.

(c) Time-frequency plots showing changes in event-related phase locking factor (PLF) in response to 85-dB auditory stimulation. Color represents PLF with warmer colors corresponding to a higher PLF or lower circular variance in EEG phase across trials.

(d) Changes in event-related PLF averaged across frequencies as above. Scale bars represent the length of a single oscillation cycle and insets show traces on expanded time-scale. Traces represent mean PLF ± SEM.

Figure 8

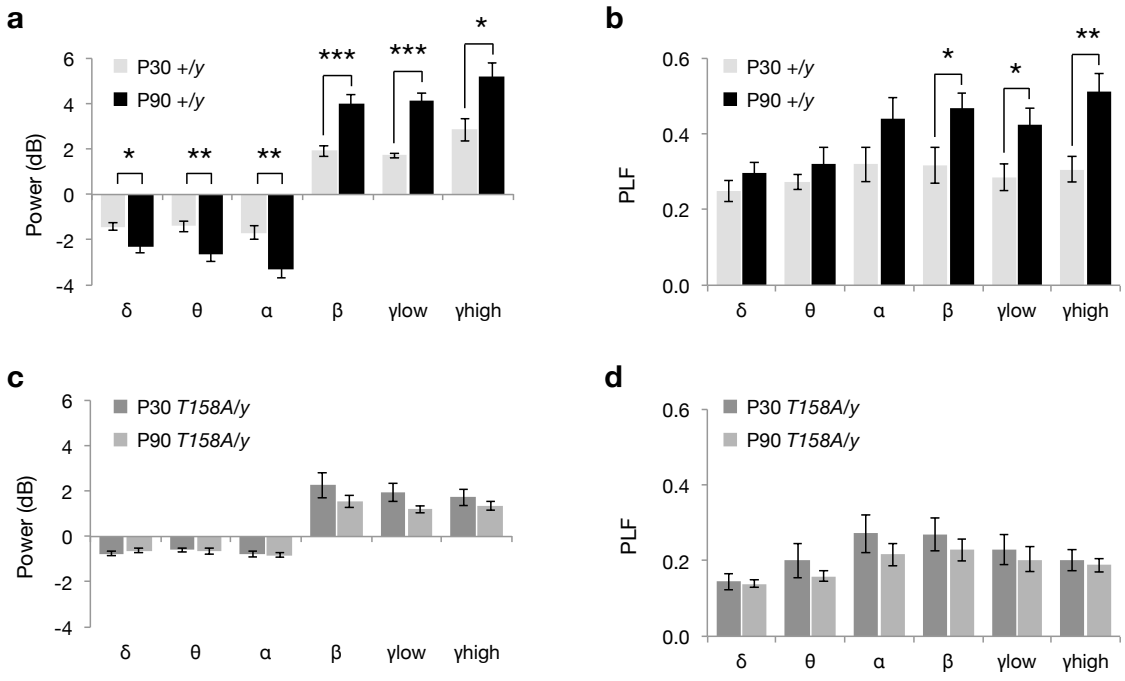

Figure 8. Age-dependent increase in event-related power and PLF is absent in *Mecp2*$^{T158A/y}$ mice
(a) Event-related power changes in *Mecp2*$^{+/y}$ (WT) mice at P30 and P90.
(b) Event-related phase-locking factor (PLF) changes in WT mice at P30 and P90.
(c) Event-related power changes in *Mecp2*$^{T158A/y}$ mice at P30 and P90.
(d) Event-related PLF changes in *Mecp2*$^{T158A/y}$ mice at P30 and P90. Bars represent mean ± SEM. * *p*-value < 0.05, ** < 0.01 and *** < 0.001; two-tailed t-test with Bonferroni correction.

Figure S1

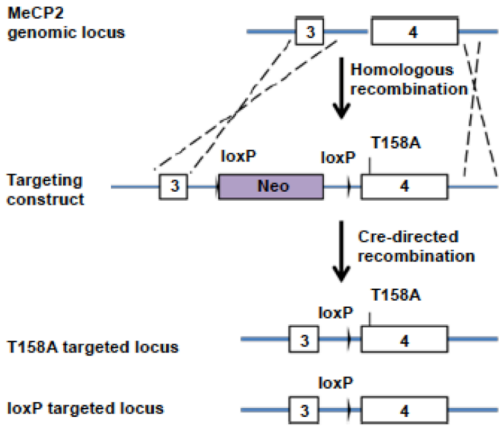

Supplementary Figure 1: Generation of MeCP2 T158A and loxP knockin mice

Targeting strategy to generate MeCP2 T158A and loxP knockin mice. The genomic region surrounding *Mecp2* exons III and IV was targeted for homologous recombination using a construct in which the floxed neomycin positive selection cassette (Neo) was inserted in a non-conserved region of intron III. The location of the mutation in exon IV to create T158A is indicated. Since we were testing for the effects of a single nucleotide mutation, two lines of mice were generated: those with and those without the T158A mutation. Both lines contained floxed loxP sites. Following production of chimera, the Neo cassette was removed using *EIIa-cre* mice. The targeted alleles after cre-mediated removal of the Neo cassette are illustrated.

Figure S2

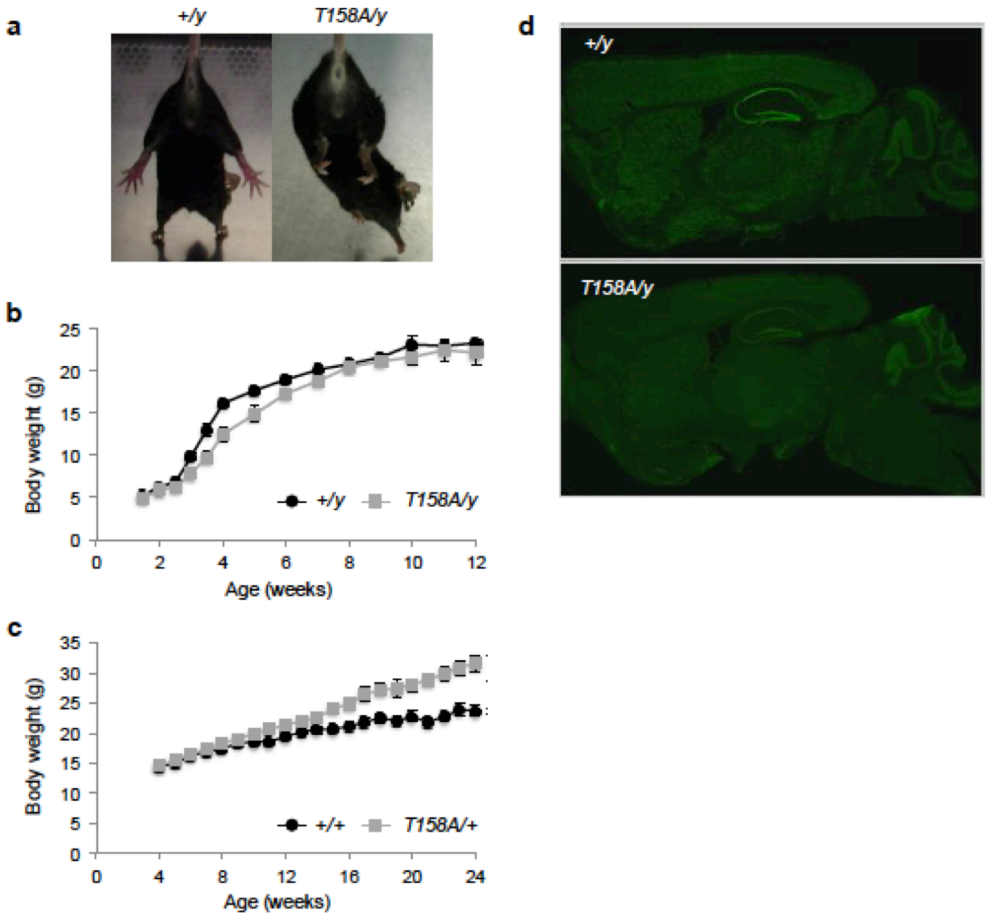

Supplementary Figure 2: Characterization of MeCP2 T158A mice

a. Stereotypical hindlimb clasping upon tail suspension in an *Mecp2*$^{T158A/y}$ mouse at 13 weeks of age versus an age-matched *Mecp2*$^{+/y}$ littermate. **b.** Body weights in male *Mecp2*$^{T158A/y}$ mice (n = 11; $F_{1,252} = 27.75$, $p<0.0001$, two-way ANOVA) compared to WT littermates (n = 9). Points represent mean ± SEM. **c.** Body weights in female *Mecp2*$^{T158A/+}$ mice (n = 7; $F_{1,242} = 176.77$, $p<0.0001$, two-way ANOVA) compared to *Mecp2*$^{+/+}$ littermates (n = 7). Points represent mean ± SEM. **d.** Normal gross brain anatomy in *Mecp2*$^{T158A/y}$ mice compared to *Mecp2*$^{+/y}$ mice. Sagittal sections were stained with an antibody against MeCP2.

Figure S3

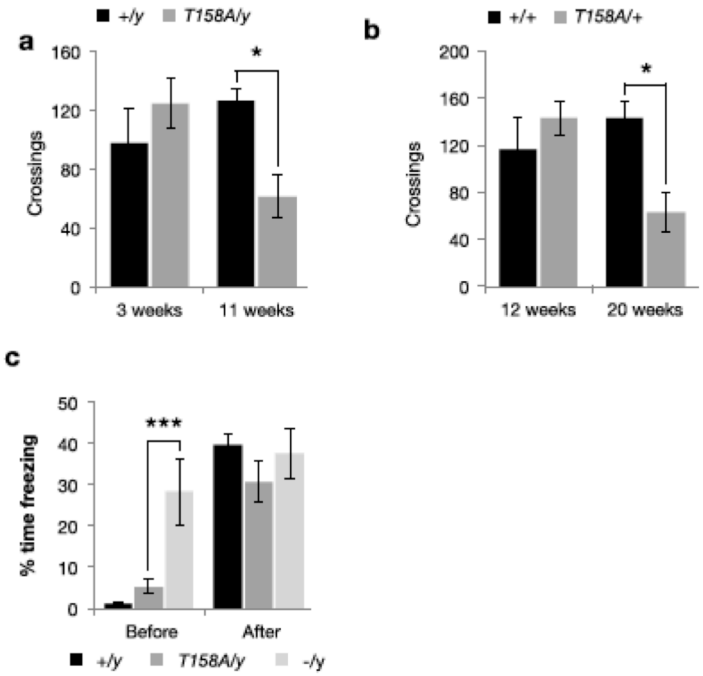

Supplementary Figure 3: Behavioral phenotypes of *Mecp2*$^{T158A/y}$ mice

a. Locomotor activity measured in male mice using an open field assay at 11 and 3 weeks of age. Bars represent mean ± SEM (n = 6 for *Mecp2*$^{+/y}$ and n = 8 for *Mecp2*$^{T158A/y}$). * p-value < 0.05; two-tailed t-test with Bonferroni correction. **b.** Locomotor activity measured in female mice using an open field assay at 20 and 12 weeks of age. Bars represent mean ± SEM (n = 5 for *Mecp2*$^{+/+}$ and n = 5 for *Mecp2*$^{T158A/+}$). * p-value < 0.05; two-tailed t-test with Bonferroni correction. **c.** Percentage time spent freezing in *Mecp2*$^{+/y}$ (n = 33), *Mecp2*$^{T158A/y}$ (n = 16) and *Mecp2*$^{-/y}$ mice (n = 12) prior to, and subsequent to tone and shock on training day of fear conditioning procedure. *Mecp2*$^{-/y}$ mice freeze significantly more than WT or *Mecp2*$^{T158A/y}$ mice prior to experimentation obviating them from further analysis. Bars represent mean ± SEM. *** p-value < 0.001; two-tailed t-test with Bonferroni correction.

Figure S4.

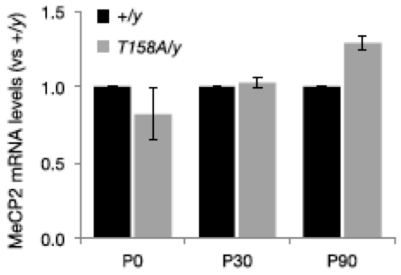

Supplementary Figure 4: MeCP2 mRNA expression is not affected by T158A mutation

MeCP2 mRNA levels in *Mecp2*$^{T158A/y}$ mice (n = 3) at P0, P30 or P90 compared to *Mecp2*$^{+/y}$ littermates (n = 3). Bars represent mean ± SEM. Statistics performed using one-sample t-tests.

Figure S5

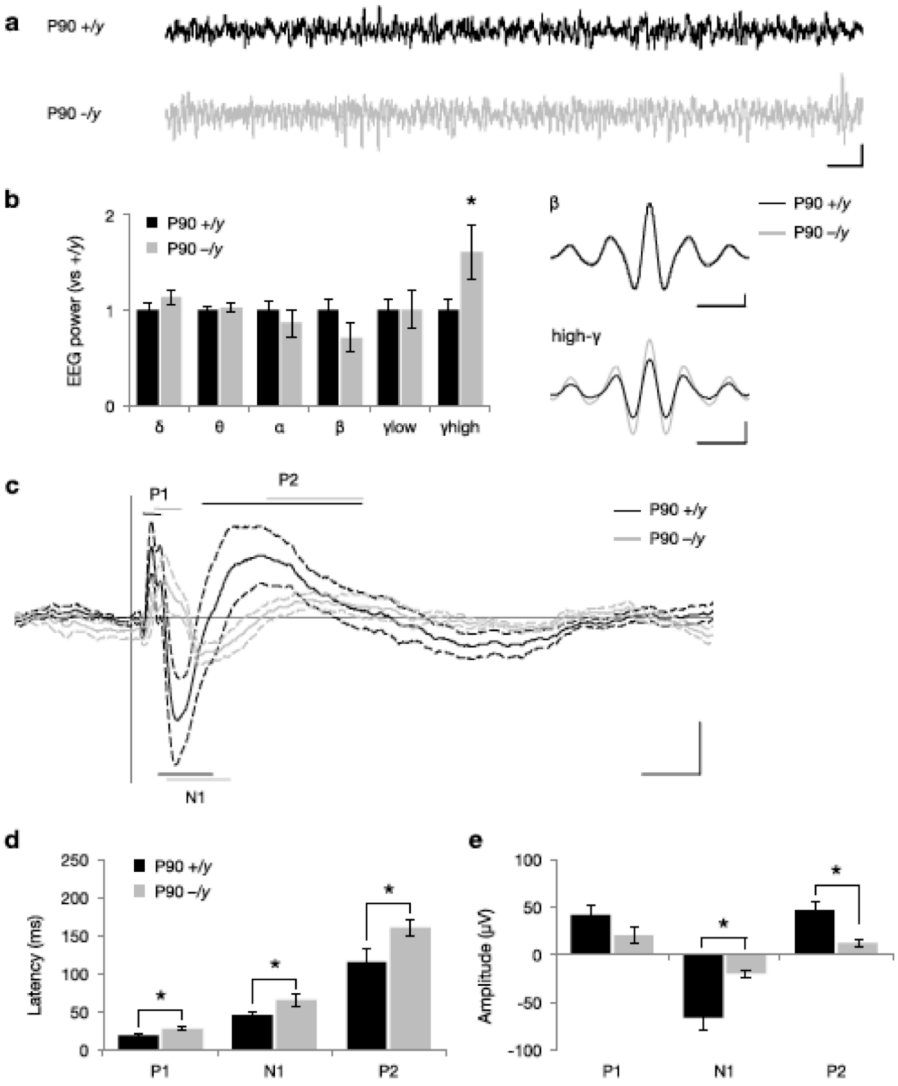

Supplementary Figure 5: ***Mecp2*-null mice exhibit alterations in auditory-evoked ERPs**

a. Representative EEG traces of awake, freely mobile mice. Scale bar corresponds to 1 second (horizontal) and 200 μA (vertical). **b.** Basal EEG power measurements in *Mecp2*$^{-/y}$ mice (n = 8) and *Mecp2*$^{+/y}$ littermates (n = 8). Bars represent mean ± SEM. * p-value < 0.05; two-tailed t-test with Bonferroni correction. Insets show β and high-γ mean amplitudes across EEG recordings. Scale bars represent one oscillation cycle (horizontal) and 20 μA (vertical). **c.** Grand average ERPs following 85-dB sound presentation. Traces represent mean amplitude (solid line) ± SEM (dashed lines). The characteristic polarity peaks P1, N1 and P2 are highlighted with straight lines with the length indicating latency range. Scale bar corresponds to 50 ms (horizontal) and 20 μA (on vertical). **d.** Latencies and **e.** amplitudes of ERP peaks. Bars represent mean ± SEM. * p-value < 0.05; two-tailed t-test with Bonferroni correction.

Figure S6

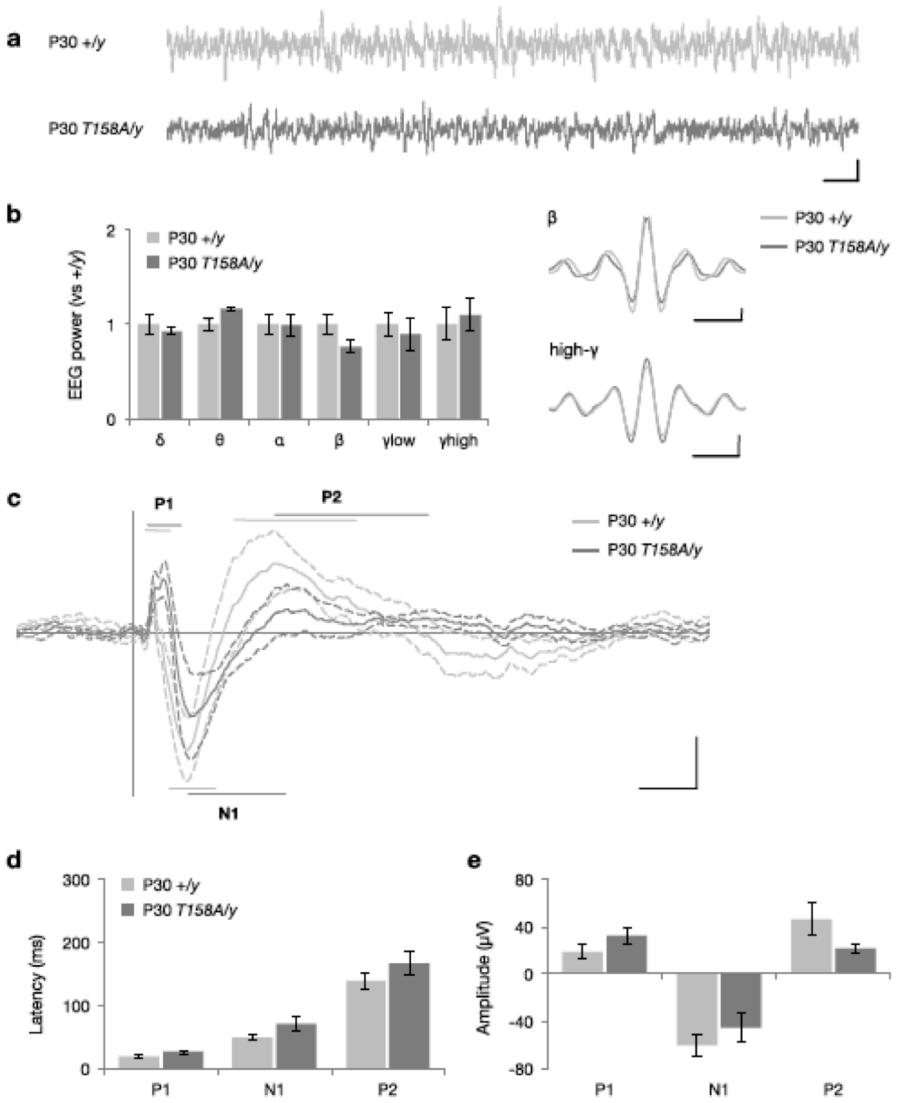

Supplementary Figure 6: Auditory-evoked ERPs are not affected in *Mecp2*$^{T158A/y}$ mice at P30

a. Representative EEG traces of awake, freely mobile mice. Scale bar corresponds to 1 second (horizontal) and 200 μA (vertical). **b.** Basal EEG power measurements in P30 *Mecp2*$^{T158A/y}$ mice (n = 7) and *Mecp2*$^{+/y}$ littermates (n = 8). Bars represent mean ± SEM. * p-value < 0.05; two-tailed t-test with Bonferroni correction. Insets show β and high-γ mean amplitudes across EEG recordings. Scale bars represent one oscillation cycle (horizontal) and 20 μA (vertical). **c.** Grand average ERPs following 85-dB sound presentation. Traces represent mean amplitude (solid line) ± SEM (dashed lines). The characteristic polarity peaks P1, N1 and P2 are highlighted with straight lines with the length indicating latency range. Scale bar corresponds to 50 ms (horizontal) and 20 μA (on vertical). **d.** Latencies and **e.** amplitudes of ERP peaks. Bars represent mean ± SEM. Statistics performed using two-tailed t-tests with Bonferroni correction.

Figure S7

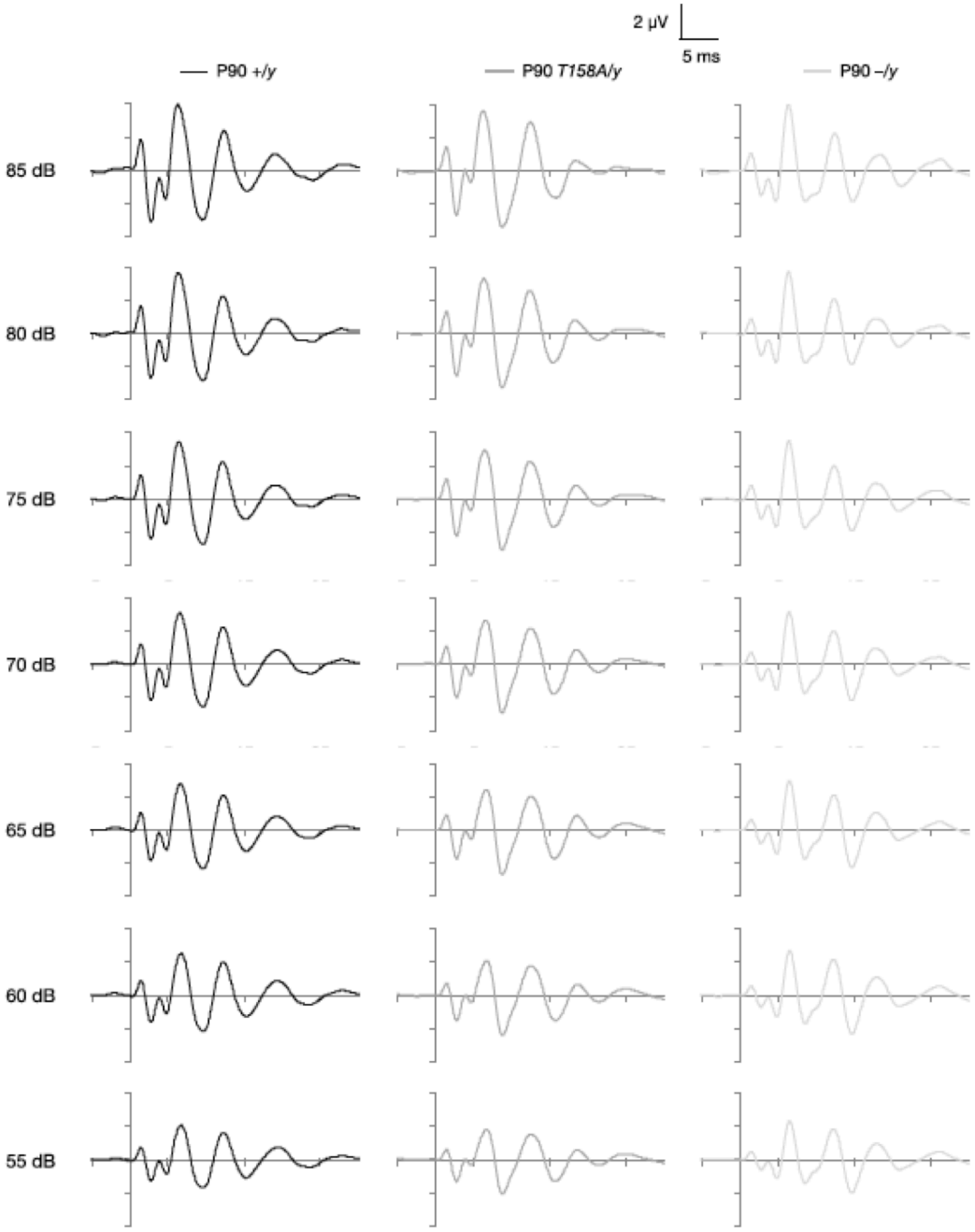

Supplementary Figure 7: Auditory brainstem responses

Auditory brain stem responses from P90 *Mecp2*$^{+/y}$, *Mecp2*$^{T158A/y}$ and *Mecp2*$^{-/y}$ mice. Mice were presented with 4,000 white-noise clicks (3 ms duration, 125 ms inter-stimulus interval) ranging from 85-dB to 55 dB sound pressures. ABR responses decreased to a similar extent in all three genotypes with decreasing sound pressure.

Figure S8

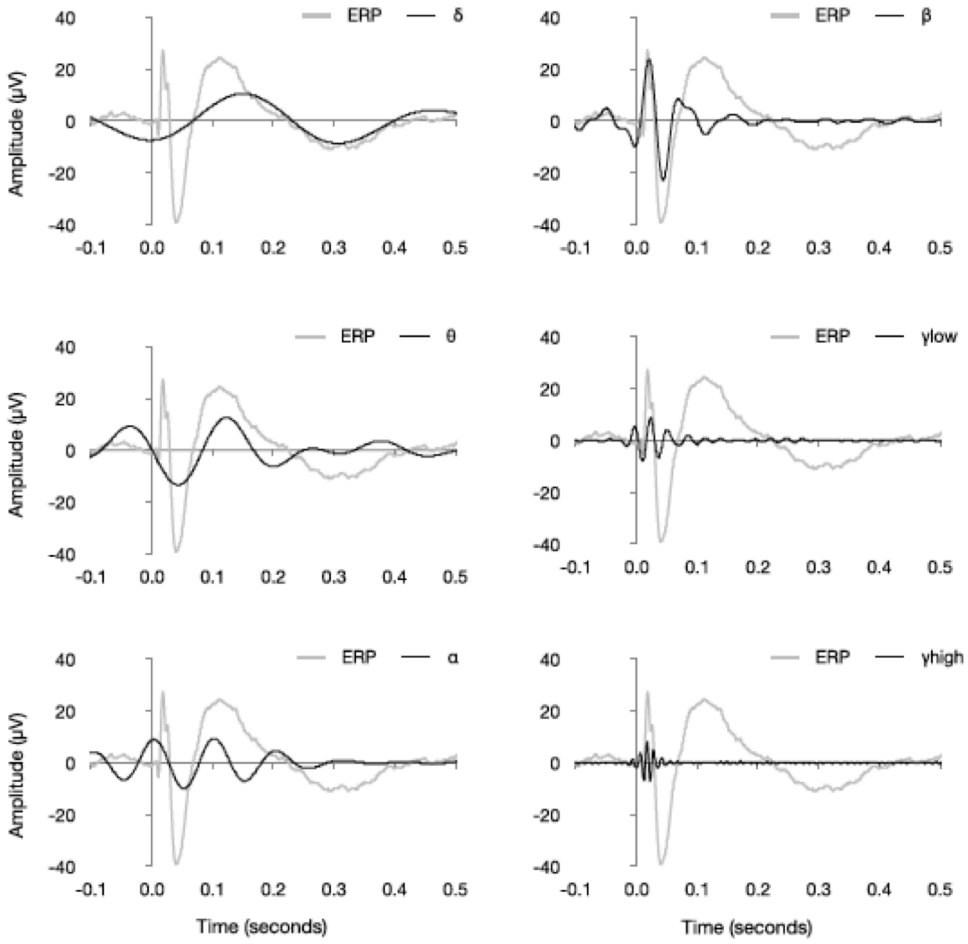

Supplementary Figure 8: Oscillation changes occur for multiple cycles during ERPs

EEG traces were band pass filtered in frequency ranges defined as δ (2-4 Hz), θ (4-8 Hz), α (8-12 Hz), β (12-30 Hz), γlow (30-50 Hz) and γhigh (70-140 Hz). The P1 peak consists primarily of oscillations in the β, low- and high-γ ranges. The N1 peak is composed primarily of α and β frequencies. The P2 peak is primarily composed of δ and θ frequencies.

Figure S9

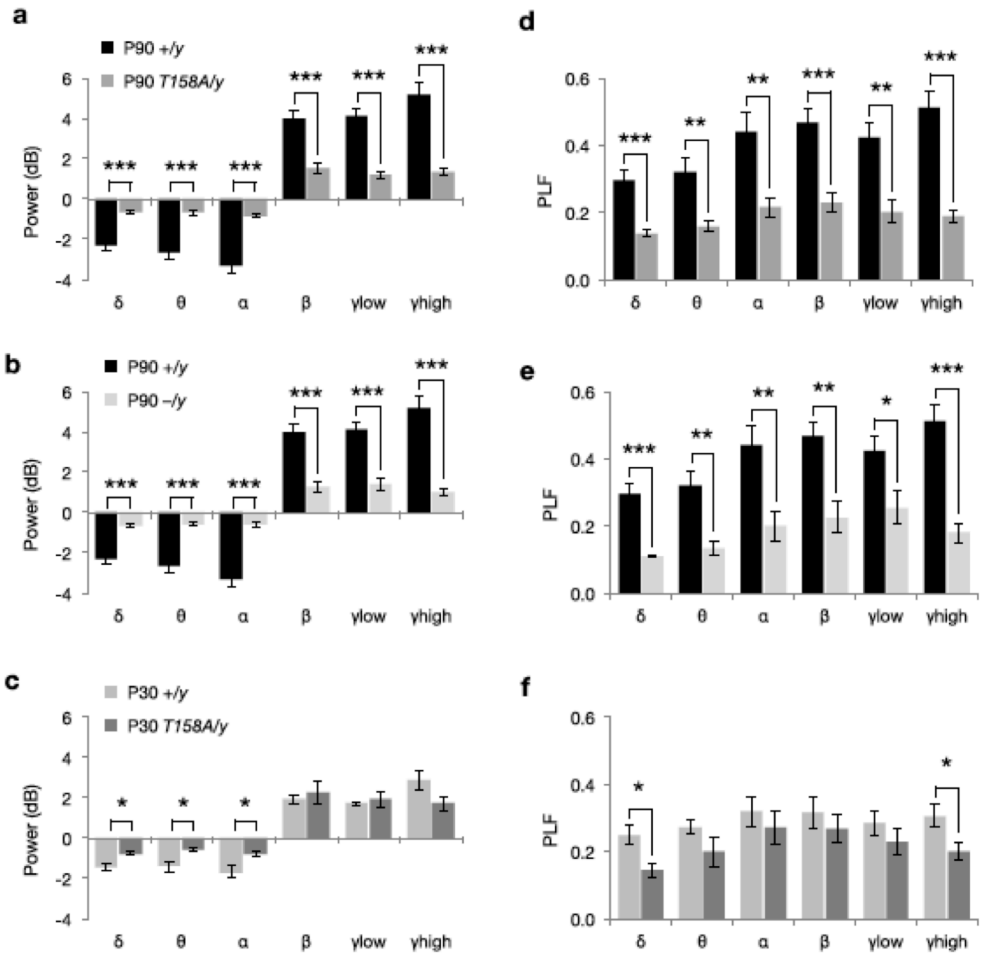

Supplementary Figure 9: Quantification of event-related power and PLF changes

a. Event-related power changes in *Mecp2*$^{T158A/y}$ mice and *Mecp2*$^{+/y}$ littermates at P90. **b.** Event-related power changes in *Mecp2*$^{-/y}$ mice and *Mecp2*$^{+/y}$ littermates at P90. **c.** Event-related power changes in *Mecp2*$^{T158A/y}$ mice and *Mecp2*$^{+/y}$ littermates at P30. **d.** Event-related PLF in *Mecp2*$^{T158A/y}$ mice and *Mecp2*$^{+/y}$ littermates at P90. **e.** Event-related PLF in *Mecp2*$^{-/y}$ mice and *Mecp2*$^{+/y}$ littermates at P90. **f.** Event-related PLF in *Mecp2*$^{T158A/y}$ mice and *Mecp2*$^{+/y}$ littermates at P30. Bars represent mean ± SEM. * p-value < 0.05, ** < 0.01 and *** < 0.001; two-tailed t-test with Bonferroni correction.

Figure S10

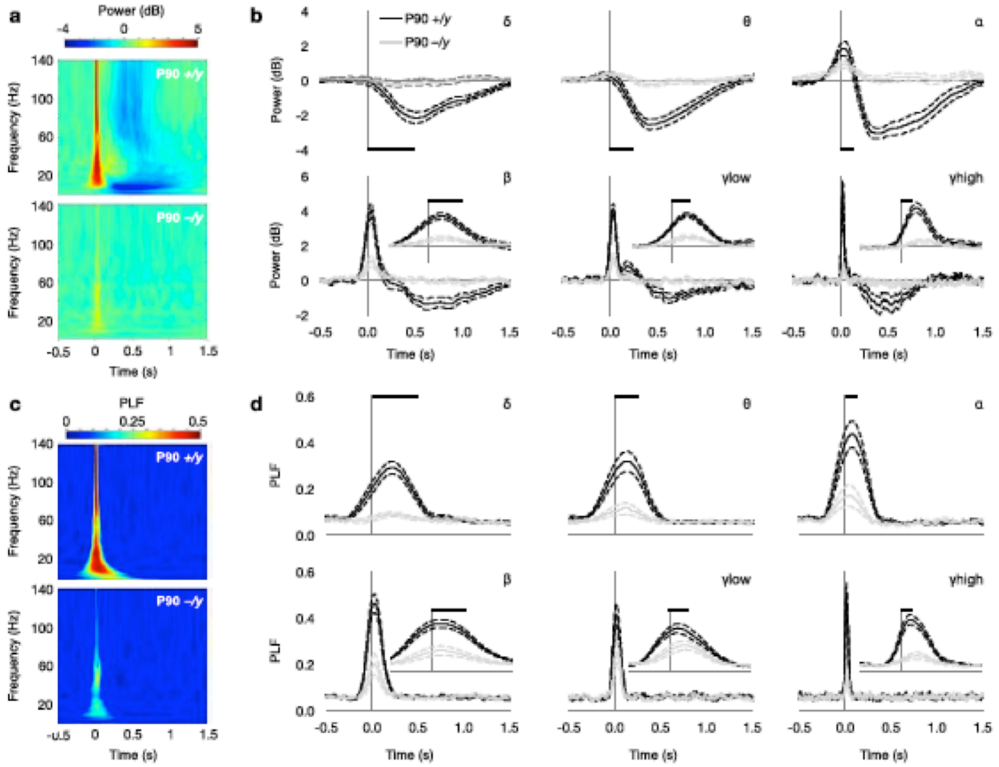

Supplementary Figure 10: Time-frequency analysis in *Mecp2*$^{-/y}$ mice

a. Time-frequency plots showing event-related power in response to 85-dB white-noise clicks. Time is plotted on the abscissa (where $t = 0$ at sound presentation) and frequency on the ordinate. Color represents mean power with warmer colors corresponding to an increased power and cooler colors representing decreased power compared to pre-stimulus baseline. **b.** Event-related power changes were separated into δ-, θ-, α-, β-, low γ- and high γ-frequency bands. Scale bars represent one oscillation cycle for the lowest frequency (longest duration cycle) in each band. Insets show traces on expanded time scale. Data are presented as mean power ± SEM. **c.** Time-frequency plots showing changes in phase locking factor (PLF) as a function of time and frequency. Color represents PLF with warmer colors corresponding to a higher PLF or lower circular variance in EEG phase across trials. **d.** PLF was separated into frequency bands. Data are presented as mean PLF ± SEM.

Figure S11

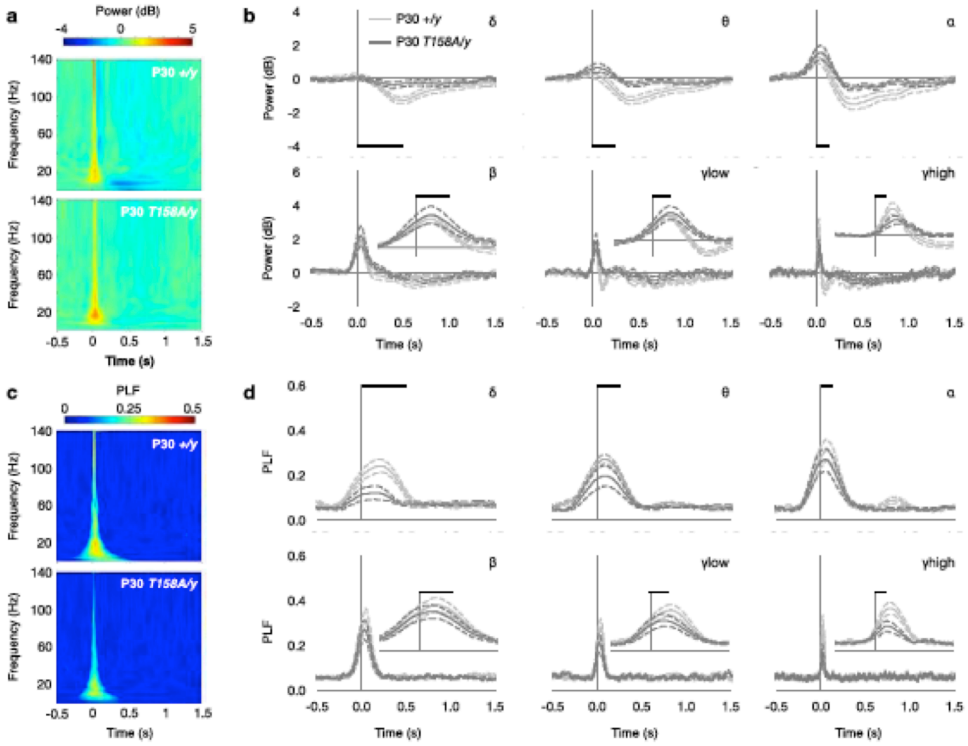

Supplementary Figure 11: Time-frequency analysis in P30 *Mecp2*$^{T158A/y}$ mice

a. Time-frequency plots showing event-related power in response to an 85-dB white noise clicks. Time is plotted on the abscissa (where $t = 0$ at sound presentation) and frequency on the ordinate. Color represents mean power with warmer colors corresponding to an increased power and cooler colors representing decreased power compared to pre-stimulus baseline. **b.** Event-related power changes were separated into δ-, θ-, α-, β-, low γ- and high γ-frequency bands. Scale bars represent one oscillation cycle for the lowest frequency (longest duration cycle) in each band. Insets show traces on expanded time scale. Data are presented as mean power ± SEM. **c.** Changes in phase locking factor (PLF) as a function on time and frequency. Color represents PLF with warmer colors corresponding to a higher PLF or lower circular variance in EEG phase across trials. **d.** PLF was separated into frequency bands. Data are presented as mean PLF ± SEM.

Figure S12

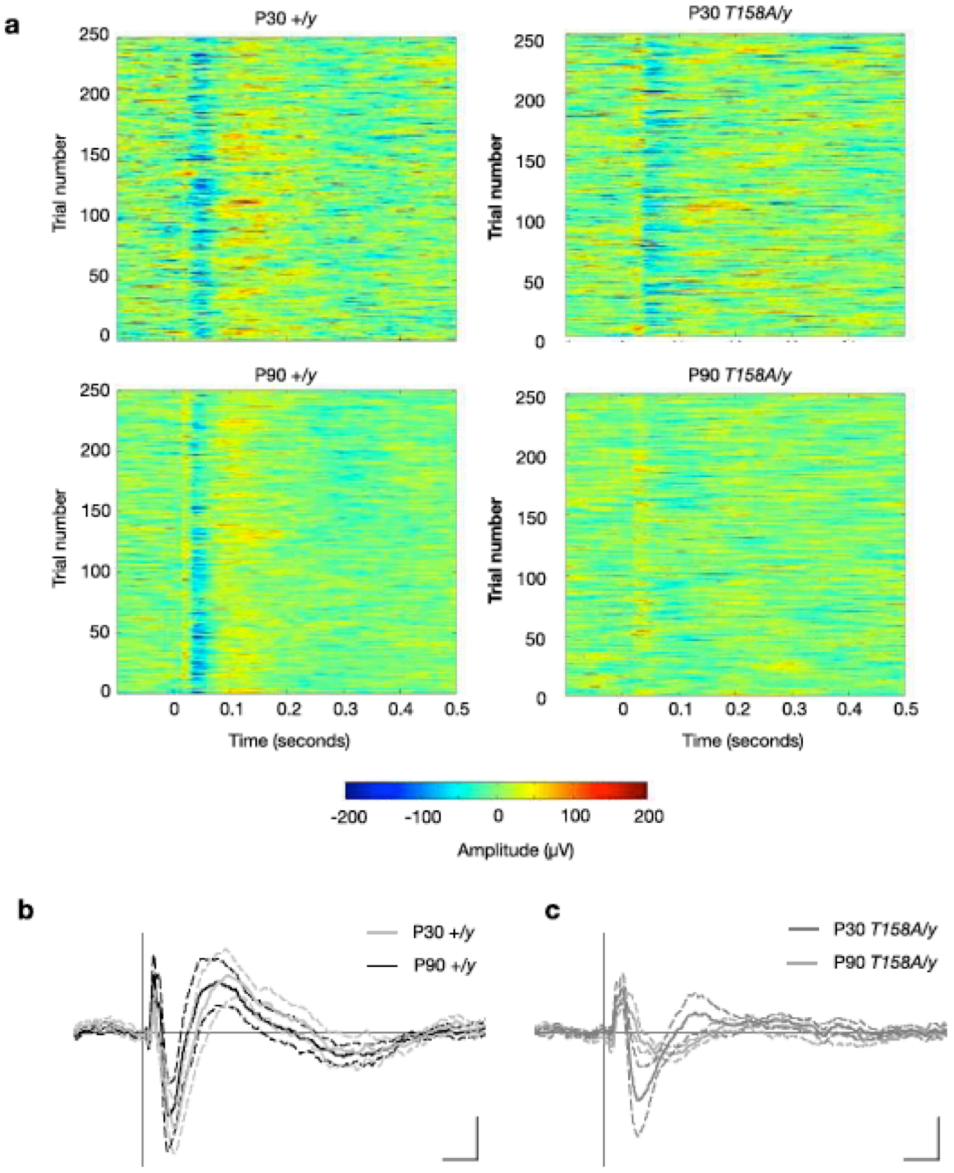

Supplementary Figure 12: Auditory-evoked ERPs in *Mecp2*$^{+/y}$ and *Mecp2*$^{T158A/y}$ mice

a. Heat maps showing ERPs recorded following presentation of 250 white-noise clicks (10 ms duration, 85-dB sound pressure, 4 second interstimulus intervals). Time is shown on the abscissa and trial number on the ordinate with the color representing EEG amplitude (μV). **b.** Grand average ERPs for *Mecp2*$^{+/y}$ mice at P30 and P90. Traces represent mean amplitude ± SEM. Scale bar corresponds to 50 ms (horizontal) and 20 μA (on vertical). **c.** Grand average ERPs for *Mecp2*$^{T158A/y}$ mice at P30 and P90. Traces represent mean amplitude ± SEM. Scale bar corresponds to 50 ms (horizontal) and 20 μA (on vertical).

Figure S13

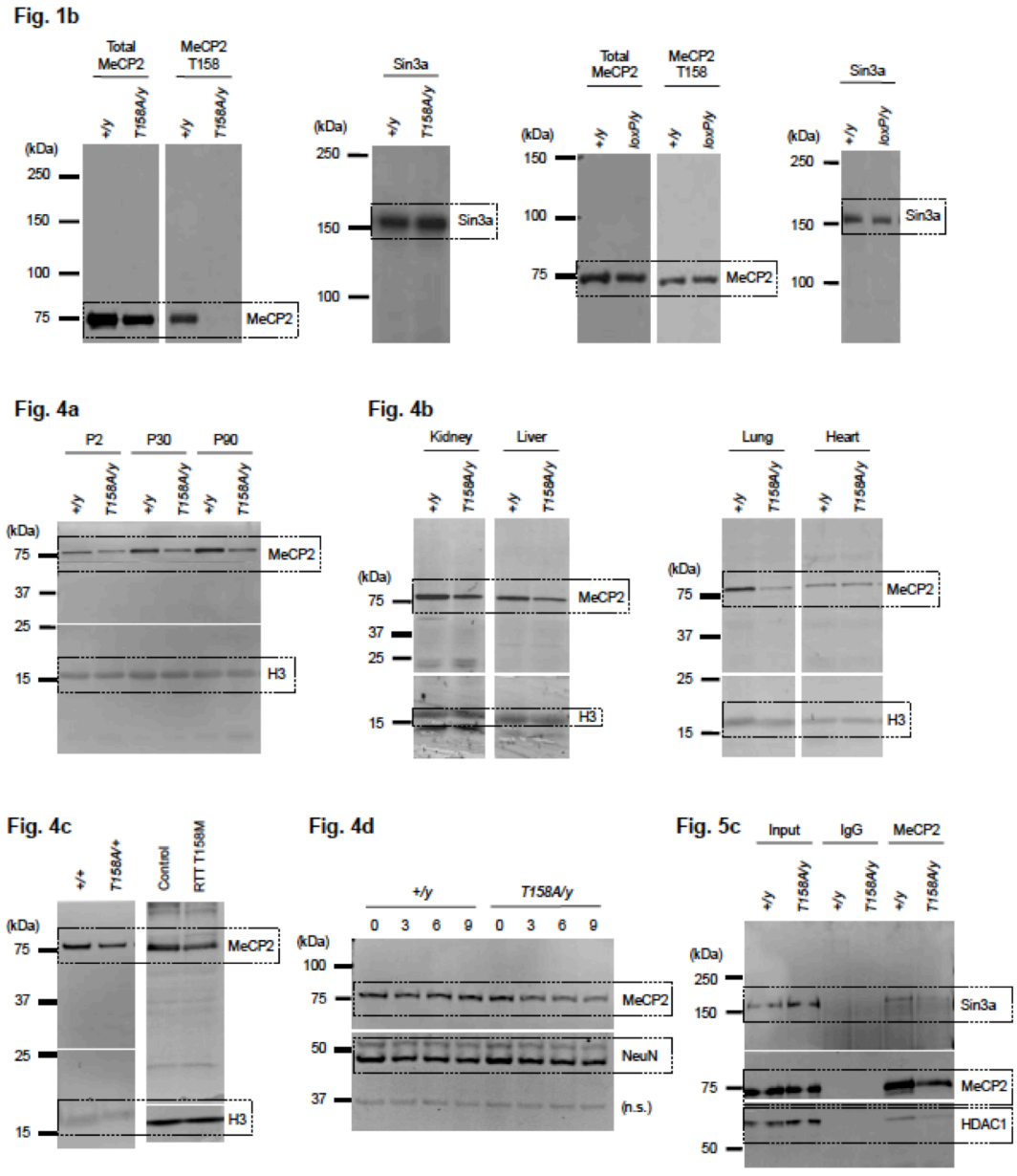

Supplementary Figure 13: Full-length pictures of the blots presented in the main figures. To examine proteins of interest on the same sample, blots in figures 4 and 5 were cut first and then probed with indicated antibodies.

Figure S14

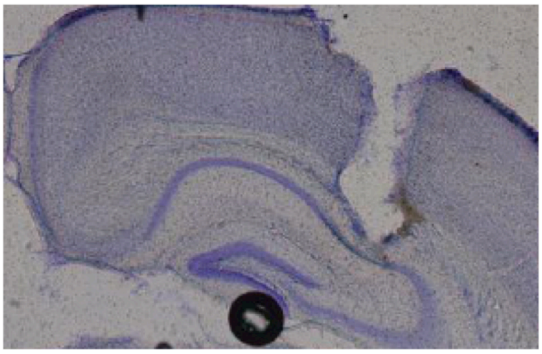

Supplementary Figure 14: EEG electrode placement in hippocampus

Representative 100 μm brain section with Nissl staining showing electrode placement in hippocampus.

Figure S15

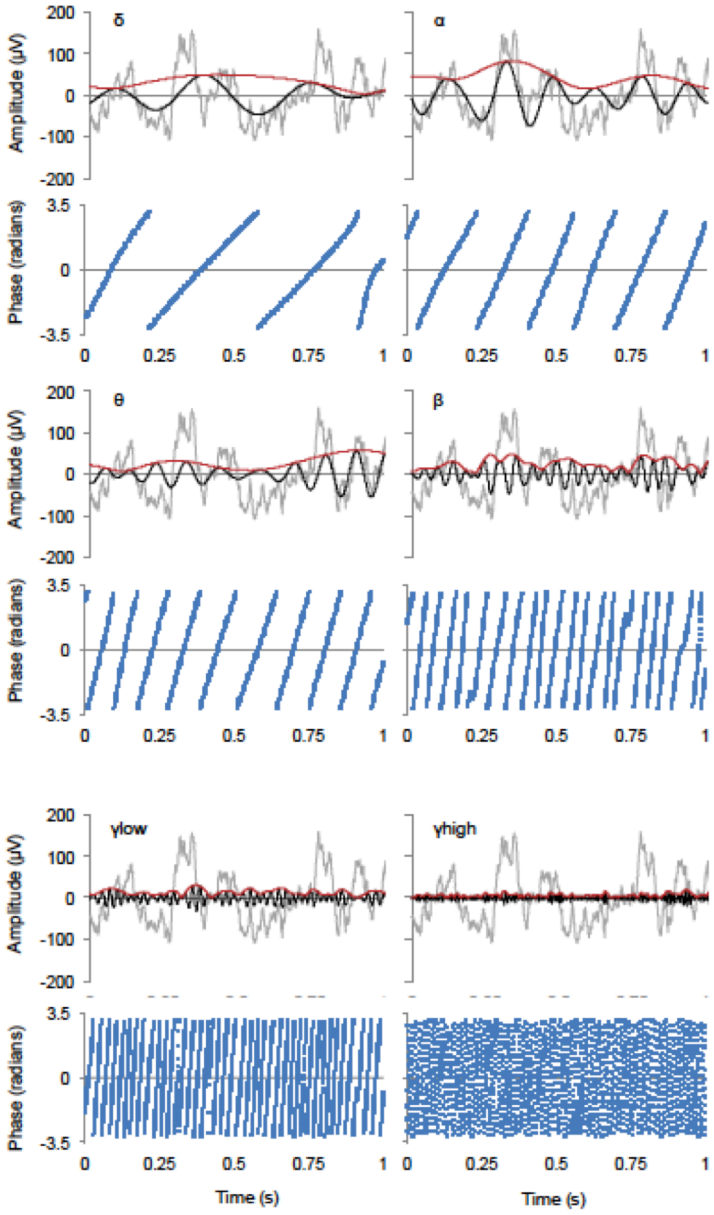

Supplementary Figure 15: EEG analysis using Hilbert transform

Time-frequency analysis was calculated using Hilbert transform to generate instantaneous amplitude and phase measurement. Traces show 1 second raw EEG trace in gray from P90 *Mecp2*$^{+/y}$ (WT) mice with the trace filtered at δ (2-4 Hz), θ (4-8 Hz), α (8-12 Hz), β (12-30 Hz), γlow (30-50 Hz) and γhigh (70-140 Hz) frequencies and shown in black. Amplitude envelope calculated from Hilbert transform is shown in red. Phase calculation is shown underneath with values expressed in radians.

Chapter 5:

NEURONAL MORPHOLOGY IN MECP2 MOUSE MODELS IS INTRINSICALLY VARIABLE AND DEPENDS ON AGE, CELL TYPE, AND MECP2 MUTATION

I-Ting J Wang[1*], Arith-Ruth S Reyes[1*], Zhaolan Zhou[1]

[1]Department of Genetics, University of Pennsylvania Perelman School of Medicine, Philadelphia, Pennsylvania, 19104, USA

[*]**These authors contributed equally to this work.**

Article history:
Received 2 March 2013 Revised 16 April 2013 Accepted 23 April 2013 Available online 6 May 2013

http://dx.doi.org/10.1016/j.nbd.2013.04.020

Keywords: Rett Syndrome, MECP2, neuronal morphology, dendritic branching, soma size, mouse model

This chapter consists of my 2013 first-author *Neurobiology of Disease* publication describing neuronal morphology and soma size across development in three independent *Mecp2* mouse models that represent *Mecp2* loss-of-function, partial loss-of-function, and gain-of-function mutations. Arith Reyes, an undergraduate student-turned-lab manager, co-first authored the manuscript with me and performed much of the imaging and analysis. Overall, we found that *Mecp2* loss-of-function reduces dendritic complexity in a brain region-specific manner that correlates with the onset of behavioral phenotype. The degree of these changes, however, is mild, domain-specific, and dependent on *Mecp2* mutation. In contrast, a robust decrease in soma size persists throughout development in both *Mecp2* loss-of-function mouse models. *Mecp2* gain-of-function does not affect dendritic outgrowth or soma size, even after onset of behavioral phenotypes. Together, these data suggest that changes soma size are more consistent than changes in dendritic complexity upon *Mecp2* loss-of-function mutation, and may therefore be a more reliable marker in assessing MeCP2 function and therapeutic efficacy in RTT studies.

Abstract

Rett Syndrome (RTT), a progressive neurological disorder characterized by developmental regression and loss of motor and language skills, is caused by mutations in the X-linked gene encoding methyl-CpG binding protein 2 (*MECP2*). Neurostructural phenotypes including decreased neuronal size, dendritic complexity, and spine density have been reported in post-mortem RTT brain tissue and in *Mecp2* animal models. How these changes in neuronal morphology are related to RTT-like phenotype and MeCP2 function, and the extent to which restoration of neuronal morphology can be used as a cellular readout in therapeutic studies, however, remain unclear. Here, we systematically examined neuronal morphology *in vivo* across three *Mecp2* mouse models representing *Mecp2* loss-of-function, partial loss-of-function, and gain-of-function mutations, at developmental time points corresponding to early- and late-symptomatic RTT-like behavioral phenotypes. We found that in *Mecp2* loss-of-function mouse models, dendritic complexity is reduced in a mild, age-dependent, and brain region-specific manner, whereas soma size is reduced consistently throughout development. Neither phenotype, however, is altered in *Mecp2* gain-of-function mice. Our results suggest that, in the cell types we examined, the use of dendritic morphology as a cellular readout of RTT phenotype and therapeutic efficacy should be cautioned, as it is intrinsically variable. In contrast, soma size may be a robust and reliable marker for evaluation of MeCP2 function in *Mecp2* loss-of-function studies.

Introduction

Rett Syndrome (RTT) is a neurological disorder that is caused by mutations in the X-linked gene encoding methyl-CpG binding protein 2 (*MECP2*) (Amir et al., 1999). It primarily affects young girls, with a prevalence of 1 in 10-15,000 live births. One striking feature of RTT is the time course at which clinical symptoms appear. After 6-18 months of apparently normal development, affected individuals enter a period of developmental stagnation, characterized by microcephaly, growth arrest and hypotonia. This stage is followed by a period of developmental regression, where patients display stereotypic hand wringing and social withdrawal, lose acquired motor and speech skills, and develop respiratory abnormalities (Chahrour and Zoghbi, 2007).

Phenotypic variability is present within the classic RTT profile, where affected girls differ by clinical severity (Chahrour and Zoghbi, 2007). This variability may be attributed to random X-chromosome inactivation and the variety of *MECP2* mutations, including missense, nonsense, deletion, and insertion mutations, that have been identified in RTT patients (Bienvenu and Chelly, 2006). *In vitro* biochemical studies have demonstrated that the majority of these mutations lead to *Mecp2* loss-of-function (Kriaucionis and Bird, 2003). Notably, genetic studies have also identified patients carrying duplication or triplication of *MECP2* (Bienvenu and Chelly, 2006). These patients are classified under *MECP2* duplication syndrome and bear a similar but distinct clinical profile to that of classical RTT (Chahrour and Zoghbi, 2007). Mice carrying two-fold levels of *Mecp2* expression also show behavioral abnormalities (Collins et al., 2004; Luikenhuis et al., 2004), highlighting the importance of MeCP2 dosage and the detrimental effect of *Mecp2* gain-of-function.

Histological analysis of postmortem RTT brain tissue has revealed morphological phenotypes including decreased cellular size with increased cell-packing density (Bauman et al., 1995), decreased dendritic complexity (Armstrong, 2005; Belichenko et al., 1994), and decreased spine density (Belichenko et al., 1994; Chapleau et al., 2009). Interestingly, these changes are selective, as decreased dendritic complexity has been observed in the motor, frontal, and inferior temporal cortices, but not in the visual cortex or hippocampus (Armstrong, 2005). Moreover, these changes appear to be cortical

layer-specific, even within the same cortical area (Armstrong, 2005). No evidence of neuronal degeneration or atrophy has been identified (Armstrong, 2005; Jellinger et al., 1988), indicating that these morphological changes are a consequence of impaired neuronal development or structural maintenance, rather than neurodegeneration. What remains unclear, however, is how mutations in *MECP2* lead to these changes in neuronal morphology and whether they contribute to RTT disease pathology or are secondary consequences of long-term illness.

To investigate the pathogenic mechanisms underlying RTT, several mouse models harboring different *Mecp2* loss-of-function mutations have been developed and characterized (Brendel et al., 2011; Chen et al., 2001; Goffin et al., 2012; Guy et al., 2001; Jentarra et al., 2010; Pelka et al., 2006; Shahbazian et al., 2002a). Although the mouse models recapitulate several RTT clinical features, each *Mecp2* mutation confers a discrete behavioral profile, supporting the link between heterogeneity in *MECP2* mutations and phenotypic variability in RTT. Similarly, underlying cellular structure in *Mecp2* mutant mice differs across *Mecp2* mutation (Belichenko et al., 2008; 2009b). While reduced dendritic complexity, soma size, and spine density are commonly identified in *Mecp2* mutant mice (Belichenko et al., 2009a; 2009b; Fukuda et al., 2005; Kishi and Macklis, 2004; Robinson et al., 2012; Stuss et al., 2012; Tropea et al., 2009), these structural phenotypes also differ by cellular subtype and developmental time point (Chapleau et al., 2012; Fukuda et al., 2005). The extent to which these factors influence cellular structure, however, is not well understood, as the use of different techniques and *Mecp2* mouse models have made direct comparisons across studies difficult (Belichenko et al., 2008; 2009a; Chapleau et al., 2009; Cohen et al., 2011; Fukuda et al., 2005; Jentarra et al., 2010; Kishi and Macklis, 2004; Metcalf et al., 2006; Moretti et al., 2006; Robinson et al., 2012; Stuss et al., 2012; Zhou et al., 2006). For example, reduced spine density has been reported in motor cortex layer II/III and V pyramidal neurons in 3-week-old *Mecp2*-null mice (Belichenko et al., 2009a; 2009b), and in layer V at 8 weeks (Tropea et al., 2009), while no change in spine density has been reported in the somatosensory cortex layer II/III pyramidal neurons in 8-week-old *Mecp2*-null mice (Kishi and Macklis, 2004). Whether these dissimilar findings are consequences of brain region-specific or age-dependent regulation of neuronal morphology is difficult to evaluate, as studies have used different imaging techniques, including Golgi staining, neuron dye

labeling, and fluorescent reporters, and different *Mecp2* mutant mice (Chen et al., 2001; Guy et al., 2001). Indeed, Golgi staining has revealed reduced spine density in hippocampus CA1 of 12-week-old *Mecp2*-null mice (Robinson et al., 2012), but DiI labeling shows decreased spine density in the same cells at 1 week, and not at 2 or 7 weeks (Chapleau et al., 2012). A comprehensive and systematic analysis using a single experimental method, therefore, is needed to clarify how age, brain region, and *Mecp2* mutation influence RTT-related neuronal morphology.

Importantly, recent studies have shown that RTT-like symptoms can be ameliorated through the reintroduction of MeCP2 in mice (Giacometti et al., 2007; Guy et al., 2007; Lioy et al., 2011; Robinson et al., 2012). The reversibility of RTT phenotypes has stimulated wide interest in developing cellular assays to measure MeCP2 function. Morphological phenotypes such as spine density, dendritic outgrowth, and soma size have been used as readouts of therapeutic efficacy upon restoration of MeCP2 (Giacometti et al., 2007; Robinson et al., 2012) or IGF-1 treatment in mice and induced pluripotent stem cells (iPSCs) (Marchetto et al., 2010; Tropea et al., 2009). Thus, understanding the relationship between MeCP2 function, neuronal structure, and RTT-like phenotype, as well as identifying robust and reproducible morphological phenotypes as readouts of MeCP2 function, are imperative.

In this study, we systematically analyzed neuronal morphology in three *Mecp2* mouse models, $Mecp2^{-/y}$, $Mecp2^{T158A/y}$, and $Mecp2^{Tg1}$, that represent the spectrum of *MECP2* mutations contributing to the phenotypic heterogeneity of RTT and *MECP2* duplication syndrome. The $Mecp2^{-/y}$ mice lack MeCP2 and demonstrate the most severe behavioral phenotype, representing *Mecp2* loss-of-function (Guy et al., 2001). The $Mecp2^{T158A/y}$ mice, mimicking a common RTT patient missense mutation at the Threonine 158 residue, demonstrate a moderately severe behavioral phenotype, representing *Mecp2* partial loss-of-function (Goffin et al., 2012). Lastly, the $Mecp2^{Tg1}$ mice express two-fold levels of MeCP2 and are believed to model *MECP2* duplication syndrome, representing *Mecp2* gain-of-function (Collins et al., 2004). Importantly, although neuronal morphology in *Mecp2* loss-of-function models has been individually studied (Belichenko et al., 2008; 2009a; Chapleau et al., 2009; Fukuda et al., 2005; Kishi and Macklis, 2004; Moretti et al., 2006; Robinson et al., 2012; Stuss et al., 2012), a direct comparison of

morphological phenotypes in *Mecp2* mouse models across the RTT phenotypic spectrum, including the less severe partial loss-of-function *Mecp2* mutations and *Mecp2* duplication, has yet to be conducted.

Given the progressive nature of RTT-like phenotypic onset, we focused on early and late developmental time points representative of none-to-mild behavioral phenotype ("early" time point) and overt behavioral phenotype ("late" time point) in each mouse model. By using the same experimental method to analyze neuronal morphology *in vivo* across these mouse models and developmental time points, we aimed to address the following questions in this study: 1) The effect of *Mecp2* loss- or gain-of-function on the development of neuronal morphology, 2) The relationship between RTT-like behavioral symptomatic severity and underlying neuronal morphology, and 3) The brain region or cell type-specific effects of *Mecp2* mutation on neuronal morphology.

We found that *Mecp2* loss-of-function reduces dendritic complexity in a brain region-specific manner that correlates with the onset of behavioral phenotype. The degree of changes in dendritic complexity, however, was mild, domain-specific, and dependent on *Mecp2* mutation. In contrast, a significant decrease in soma size upon *Mecp2* loss-of-function persisted throughout development and across both *Mecp2* loss-of-function mutations. *Mecp2* gain-of-function, however, did not affect dendritic outgrowth or soma size, even after onset of gain-of-function behavioral phenotypes, suggesting that changes in cellular structure may not be effective readouts of therapeutics targeted toward *MECP2* duplication syndrome. The subtlety of changes in dendritic outgrowth and the dependence on *Mecp2* mutation, developmental time point, and brain region raise caution in using dendritic complexity as a cellular readout of RTT-like phenotype. Changes in soma size, however, are reproducible and robust, suggesting that soma size may be a more reliable marker in assessing MeCP2 function and therapeutic efficacy in RTT studies.

Results

Neuron imaging strategy

To minimize experimental manipulation and variation in our analysis of neuronal morphology in *Mecp2* mutant mice, we took advantage of a genetic labeling approach that has been successfully utilized in other RTT morphological studies, a *Thy1-GFP/M* reporter line (Belichenko et al., 2009a; Cohen et al., 2011). In this line, a sparse population of neurons intrinsically expresses GFP throughout the cell body and dendritic tree in various brain regions (**Figure 1a, 1b**), allowing for direct visualization of individual neurons (Feng et al., 2000). To visualize neurons in *Mecp2* mutant mice, we crossed male *Thy1-GFP/M* reporter mice to female *Mecp2* heterozygotes ($Mecp2^{-/+}$, $Mecp2^{T158A/+}$, or $Mecp2^{Tg1}$). Given the confounding effects of mosaic MeCP2 expression in females from random X-chromosome inactivation, all experiments were performed using male littermates with the following genotypes: $Mecp2^{-/y}$;*Thy1-GFP/M* and $Mecp2^{+/y}$;*Thy1-GFP/M*; $Mecp2^{T158A/y}$;*Thy1-GFP/M* and $Mecp2^{+/y}$;*Thy1-GFP/*; or $Mecp2^{Tg1}$;*Thy1-GFP/M* and $Mecp2^{+/y}$;*Thy1-GFP*. For simplicity, we will refer to $Mecp2^{+/y}$;*Thy1-GFP/M* as WT and *Mecp2* mutant mice expressing the *Thy1-GFP/M* transgene as $Mecp2^{-/y}$, $Mecp2^{T158A/y}$, or $Mecp2^{Tg1}$.

Previous studies have shown that disruption of MeCP2 results in deficits in neuronal organization, dendritic complexity and synaptic connectivity in the somatosensory cortex in both postmortem RTT tissue and mice (Cohen et al., 2011; Dani and Nelson, 2009; Kaufmann and Moser, 2000). We therefore analyzed neuronal morphology in layer V pyramidal neurons of the somatosensory cortex. These neurons are distinct in their cellular architecture, characterized by apical and basal dendritic trees and a pyramid-shaped soma (Spruston, 2008), and thus can be consistently identified. We measured dendritic complexity and soma size in layer V pyramidal neurons extending their apical dendrites to the pial surface and their basal dendrites into deep layer VI (**Fig 1c**). Given the anatomic and functional distinctions between basal and apical dendritic arbors (Spruston, 2008), we imaged and quantified basal and apical dendritic complexity separately, using Sholl analysis (**Fig 1d-e**), which measures dendritic crossings through a series of concentric circles with increasing radii centered around the cell soma (SHOLL, 1953).

Dendritic complexity in *Mecp2* loss-of-function mice

The majority of mutations in *MECP2* leading to RTT are loss-of-function mutations (Chahrour and Zoghbi, 2007). Therefore, we first assessed neuronal morphology in *Mecp2*-null mice (*Mecp2*$^{-/y}$) that lack both *Mecp2* transcript and MeCP2 protein, and represent one of the most phenotypically severe *Mecp2* mutant mice (Guy et al., 2001). Like RTT patients, *Mecp2*$^{-/y}$ mice show no initial RTT-like phenotype, but begin to develop aberrant gait and reduced mobility around 3 postnatal weeks. By 8 postnatal weeks, *Mecp2*$^{-/y}$ mice display overt RTT-like phenotypes including hindlimb clasping, tremor, and irregular breathing. We therefore chose to investigate neuronal morphology upon *Mecp2* loss-of-function at P30 and P60, time points representative of early-symptomatic and late-symptomatic RTT-like phenotype, respectively. At the early-symptomatic P30 time point, Sholl analysis of somatosensory cortex layer V pyramidal neurons revealed a statistically significant decrease in dendritic complexity in *Mecp2*$^{-/y}$ mice relative to WT littermates (WT: n=24 neurons, *Mecp2*$^{-/y}$: n=19 neurons; $p<0.0001$) (**Fig. 2a**). *Post hoc* tests revealed that this decrease was most pronounced in *Mecp2*$^{-/y}$ mice in both basal and proximal apical dendrites 140–160 μm from soma and in the distal apical tuft 700 μm from soma. As RTT-like behavioral phenotypes in P30 *Mecp2*$^{-/y}$ mice are mild but present, these data suggest that decreased dendritic complexity accompanies RTT-like behavioral phenotype.

At the late-symptomatic P60 time point, *Mecp2*$^{-/y}$ mice also showed reduced dendritic complexity (WT: n=36 neurons; *Mecp2*$^{-/y}$: n=31 neurons; $p<0.0001$) (**Fig. 2b**). Although mild, these decreases were more widespread than that of P30 and most pronounced in the basal arbor 100–140 μm from soma and in the distal apical arbor 680–700 μm from soma, where the significant reduction in the apical tuft is likely a reflection of reduced cortical thickness and brain size in these mice (Kishi and Macklis, 2004). Given the overt RTT-like behavioral phenotypes in P60 *Mecp2*$^{-/y}$ mice, the mild reduction in dendritic complexity is surprising but consistent with reports of normal cortical lamination and organization in 7–10 week-old *Mecp2*$^{-/y}$ mice (Belichenko et al., 2008; Guy et al., 2001; Metcalf et al., 2006) and unaffected dendritic length and complexity from *in vitro* studies using the same mice (Chao et al., 2007). Therefore, as excitatory input onto proximal dendrites comes primarily from local or adjacent collaterals, while input onto distal dendrites comes from more distant cortical or thalamic projections (Spruston, 2008), our

data indicate that the mild but widespread reduction in dendritic complexity across domains results in altered total excitatory input onto *Mecp2*$^{-/y}$ neurons, both in early-symptomatic and late-symptomatic *Mecp2*$^{-/y}$ mice.

Dendritic complexity in MeCP2 T158A partial loss-of-function mice

One of the most common *MECP2* missense mutations occurs at Threonine 158, converting it to methionine (T158M) or alanine (T158A). We recently developed and characterized an *Mecp2* T158A knockin mouse and found that *Mecp2*$^{T158A/y}$ mice show a similar but delayed progression of RTT-like behavioral phenotypes relative to that of *Mecp2*$^{-/y}$ mice, where phenotypes begin to develop at 4–5 weeks and are overt by 13 weeks (Goffin et al., 2012). At P60, *Mecp2*$^{T158A/y}$ mice express milder locomotor, anxiety, and motor coordination phenotypes compared to age-matched *Mecp2*$^{-/y}$ mice, indicating that *Mecp2* T158A is a partial loss-of-function mutation. In addition, the MeCP2 T158A protein is expressed but is less stable and shows reduced binding to methylated DNA (Goffin et al., 2012). To investigate neuronal morphology upon *Mecp2* partial loss-of-function, we measured dendritic complexity at P30, prior to onset of RTT-like phenotypes, and P90, when RTT-like phenotypes are overt. Sholl analysis of layer V pyramidal neurons in the somatosensory cortex of P30 animals revealed a similar pattern of dendritic complexity in *Mecp2*$^{T158A/y}$ and WT littermates (WT: n=40 neurons; *Mecp2*$^{T158A/y}$: n=34 neurons; $p>0.05$; **Fig. 3a**). Although both *Mecp2*$^{T158A/y}$ and *Mecp2*$^{-/y}$ mice represent *Mecp2* loss-of-function mutations, their RTT-behavioral profiles at P30 are distinct, where RTT-like phenotypes are mild in *Mecp2*$^{-/y}$ mice but absent in *Mecp2*$^{T158A/y}$ mice. These data, therefore, support the hypothesis that decreased dendritic complexity accompanies RTT-like phenotype.

At the late-symptomatic P90 time point, *Mecp2*$^{T158A/y}$ mice showed decreased dendritic complexity relative to WT littermates (WT: n=36 neurons; *Mecp2*$^{T158A/y}$: n=39; $p<0.0001$; **Fig. 3B**). Strikingly, the decrease was specific to the basal arbor 60–140 μm from soma and was not present in the apical arbor. Given that pyramidal neuron dendritic domains are believed to receive unique synaptic inputs and contain synapses with distinct properties (Spruston, 2008), the domain-specific decrease in dendritic complexity in *Mecp2*$^{T158A/y}$ mice suggests a cellular mechanism underlying a distinct behavioral profile.

Although both P60 *Mecp2*$^{-/y}$ mice and P90 *Mecp2*$^{T158A/y}$ mice show similar RTT-like phenotypic severity, the selective decrease in basal dendritic complexity in *Mecp2*$^{T158A/y}$ mice in contrast to the widespread morphological phenotype seen in *Mecp2*$^{-/y}$ mice supports an *Mecp2* mutation-specific effect on neuronal architecture that may underlie RTT-like phenotypic heterogeneity.

Brain region-specific dendritic complexity in *Mecp2* partial loss-of-function

Given the brain region-specific changes in neuronal architecture in RTT post-mortem tissue (Armstrong, 2005) and compartment-specific changes in *Mecp2* mouse models (Stuss et al., 2012), we next addressed whether the age-dependent and domain-specific decrease in dendritic complexity identified in the somatosensory cortex of *Mecp2*$^{T158A/y}$ mice would be replicated in a different brain region from the same mice. Therefore, we examined neuronal morphology in hippocampal CA1 pyramidal neurons in *Mecp2*$^{T158A/y}$ mice at the pre- and post-symptomatic ages P30 and P90. Similar to what we observed in the cortex, *Mecp2* partial loss-of-function did not affect dendritic complexity in hippocampal CA1 pyramidal neurons at the early-symptomatic P30 time point (WT: n=27 neurons; *Mecp2*$^{T158A/y}$: n=33 neurons; $p>0.05$; **Fig. 4a**). At the late-symptomatic P90 time point, however, we observed a small but significant change in dendritic complexity in *Mecp2*$^{T158A/y}$ mice (WT: n=32 neurons; *Mecp2*$^{T158A/y}$: n=40 neurons; $p<0.05$; **Fig. 4b**). *Post hoc* tests revealed that this difference was specific to the basal dendritic arbor, and does not reflect a decrease in dendritic complexity, but rather, is a result of a shift towards the soma, as peak branching in *Mecp2*$^{T158A/y}$ mice is similar to that of controls (**Fig 4c**). This shift toward the soma may reflect reduced hippocampal volume, which has been reported in *Mecp2* loss-of-function mice (Belichenko et al., 2008). The age-dependent and domain-specific decrease in dendritic complexity in *Mecp2*$^{T158A/y}$ mice, therefore, is specific to layer V somatosensory cortex and absent in CA1 hippocampus, consistent with RTT post-mortem studies (Armstrong et al., 1995). Together, these data support age-dependent and brain region-specific regulation of dendritic outgrowth upon *Mecp2* loss-of-function.

Soma size is regulated throughout development by MeCP2

As both reduced dendritic outgrowth and soma size are believed to contribute to RTT patient microcephaly and reduced soma size has been reported in RTT post-mortem tissue (Bauman et al., 1995), we also measured soma size in our *Mecp2* mutation mice at both early- and late-symptomatic time points. In striking contrast to the age-dependence and brain region-specificity of changes in dendritic complexity, we found that changes in soma size persisted throughout development and were consistent between *Mecp2* loss-of-function mutations. Soma size in somatosensory cortex layer V pyramidal neurons was reduced in both P30 early-symptomatic $Mecp2^{-/y}$ mice (WT: 282.9 ± 4.0 μm^2, n=124 neurons; $Mecp2^{-/y}$: 237.6 ± 4.7μm^2, n=103 neurons; $p<0.01$) and in P60 late-symptomatic $Mecp2^{-/y}$ mice (WT: 287.9 ± 4.4 μm^2, n=126 neurons; $Mecp2^{-/y}$: 237.2 ± 4.4 μm^2, n=104 neurons; $p<0.01$; **Fig. 5a**), relative to WT littermates, indicating that *Mecp2* loss-of-function leads to reduced soma size in both early and late development of RTT-like phenotypes. Similarly, soma size was reduced in both P30 pre-symptomatic $Mecp2^{T158A/y}$ mice (WT: 290.6 ± 3.9 μm^2, n=115 neurons; $Mecp2^{T158A/y}$: 251.3 ± 4.6 μm^2, n=121 neurons; $p < 0.01$) and in P90 late-symptomatic $Mecp2^{T158A/y}$ mice (WT: 311.1 ± 5.0 μm^2, n=81 neurons; $Mecp2^{T158A/y}$: 262.6 ± 3.3 μm^2, n=106 neurons; $p<0.01$) relative to WT littermates (**Fig 5b**), indicating that reduced soma size may even precede onset of RTT behavioral phenotypes and is a consequence of *Mecp2* loss-of-function. Moreover, we previously reported that hippocampal CA1 pyramidal neuron soma size is decreased in both pre- and post-symptomatic $Mecp2^{T158A/y}$ mice (Goffin et al., 2012). The persistent reduction in soma size in *Mecp2* loss-of-function mouse models throughout development contrasted with the age-dependent and brain region-specific changes in dendritic complexity suggests that MeCP2 regulates dendritic outgrowth and soma size through distinct mechanisms and that soma size may be a more reproducible and reliable cellular marker for MeCP2 function than dendritic complexity.

Dendritic complexity in *Mecp2* gain-of-function mice

As the importance of MeCP2 dosage has been highlighted though the link between gain-of-function *MECP2* mutations and neurodevelopmental disorder (Chahrour and Zoghbi, 2007), we next examined a transgenic mouse line expressing two-fold levels of MeCP2

(*Mecp2*^{Tg1}) to determine how *Mecp2* gain-of-function affects neuronal morphology (Collins et al., 2004). Importantly, neuronal morphology has yet to be described in *Mecp2* gain-of-function mice. While these mice, similar to that of *Mecp2* loss-of-function models, develop normally, they show enhanced LTP and learning behavior by 20 postnatal weeks and after 30 postnatal weeks, exhibit seizures, ataxia, and premature death (Collins et al., 2004). We therefore examined dendritic complexity and soma size in *Mecp2*^{Tg1} mice at P30 and P140, time points representative of pre- and post-development of gain-of-function phenotype, respectively. Strikingly, we found similar patterns of dendritic complexity in *Mecp2*^{Tg1} mice and WT littermates in layer V somatosensory cortex by Sholl analysis at P30 (WT: n=16 neurons; *Mecp2*^{Tg1}: n=19 neurons; $p>0.05$) (**Fig. 6a**) and P140 (WT: n=23 neurons; *Mecp2*^{Tg1}: n=23 neurons; $p>0.05$) (**Fig 6b**). These data are in contrast to the reduced dendritic complexity observed in late-symptomatic *Mecp2* loss-of-function animals (Fig 2b, 3b), and suggest a separate mechanism of dendritic outgrowth regulation in *Mecp2* gain-of-function that is not coupled to behavioral phenotype.

Similarly, we found no changes in soma size in *Mecp2*^{Tg1} mice relative to WT littermates, both prior to (P30; WT: 266.3 ± 4.3 μm^2, n=101 neurons; *Mecp2*^{Tg1}: 272.8 ± 3.0 μm^2, n=110 neurons) and after the development of behavioral phenotypes (P140; WT: 268.9 ± 4.2 μm^2, n=110 neurons; *Mecp2*^{Tg1}: 265.0 ± 4.2 μm^2, n=113 neurons; $p>0.05$) (**Fig. 6c**). This finding is consistent with *in vitro* studies showing no effect of MeCP2 overexpression on soma size (Jugloff et al., 2005). Together, these data suggest that neuronal morphology may be affected by *Mecp2* loss-of-function, but is not sensitive to two-fold MeCP2 dosage. This is not surprising, as *MECP2* duplication syndrome is considered to be a separate neurodevelopmental disorder from typical RTT (Ramocki et al., 2009) and likely has a distinct pathogenic mechanism. Neuronal morphology, therefore, may be an appropriate therapeutic readout specifically for RTT patients with *MECP2* loss-of-function mutations.

Discussion

RTT phenotypes are believed to originate from disruptions in neuronal circuits caused by MeCP2 dysfunction in the brain (Goffin and Zhou, 2012; Katz et al., 2012), and changes in neuronal morphology provide a cellular basis for alterations in circuit function. Given the rise in the use of morphological phenotypes as readouts of therapeutic efficacy (Marchetto et al., 2010; Tropea et al., 2009) or restoration of MeCP2 function (Giacometti et al., 2007; Robinson et al., 2012), understanding how *MECP2* mutations impact the maintenance of proper neuronal structure and the relationship between RTT-like phenotype and underlying cellular morphology has become vital. Robust and reproducible RTT-related morphological phenotypes have been difficult to identify, as the use of different techniques, animal models, cell types, and developmental time points across different labs have made direct comparisons between studies difficult. Therefore, we sought to eliminate the confounds of methodological bias by using the same experimental method to analyze neuronal morphology *in vivo* across the development of *Mecp2* loss-of-function, partial loss-of-function, and gain-of-function mouse models. Given the successful utilization of *Thy1-GFP/M* reporter mice in other cortical and hippocampal morphological studies (Belichenko et al., 2009a; Cohen et al., 2011) and the absence of added experimental manipulations for cellular visualization, we chose to cross our *Mecp2* mutant mice to a *Thy1-GFP/M* reporter line in which neurons are intrinsically labeled with GFP in a mosaic manner in several brain regions, including the somatosensory cortex and hippocampus CA1 (Feng et al., 2000). In our study, we aimed to address the following three questions: 1) How does *Mecp2* loss- or gain-of-function affect the development of neuronal morphology? 2) What is the relationship between RTT-like behavioral phenotypic severity and underlying neuronal morphology? 3) Are these changes in neuronal morphology brain region or cell type-specific?

To address the first question, we measured dendritic complexity and soma size in $Mecp2^{-/y}$ and $Mecp2^{T158A/y}$ mice, representing *Mecp2* loss-of-function and *Mecp2* partial loss-of-function, respectively, and $Mecp2^{Tg1}$ mice, representing *Mecp2* gain-of-function. We found decreased dendritic complexity and soma size in *Mecp2* loss-of-function mice ($Mecp2^{-/y}$, $Mecp2^{T158A/y}$) and no change in either phenotype in *Mecp2* gain-of-function mice ($Mecp2^{Tg1}$) relative to WT littermates. These data suggest that MeCP2 expression

levels may play a role in the regulation of neuronal outgrowth, but increased MeCP2 expression has no structural effect. Our data also indicate that a greater reduction in MeCP2 may cause more severe morphological defects, as we observed a more widespread reduction in dendritic branching in *Mecp2*$^{-/y}$ mice, which lack MeCP2 protein (Guy et al., 2001), relative to *Mecp2*$^{T158A/y}$ mice, which have reduced MeCP2 protein expression (Goffin et al., 2012).

To our knowledge, neuronal morphology has not been studied in *Mecp2* gain-of-function mouse models, and the effect of MeCP2 overexpression *in vitro* on neuronal morphology remains unclear due to reports of increased (Jugloff et al., 2005; Larimore et al., 2009), decreased {Zhou:2006dp}, and unchanged dendritic complexity {Chapleau:2009bf} in cultured neurons and organotypic slices, and decreased dendritic outgrowth in *Drosophila* and *Xenopus* models {Marshak:2012gl, Vonhoff:2012bs}. Our findings suggest that both dendritic outgrowth and soma size are reduced upon *Mecp2* loss-of-function, whereas neither phenotype is affected by *Mecp2* gain-of-function with two-fold MeCP2 expression. Notably, *Mecp2*^{Tg1} mice were maintained on a mixed FVB/C57BL/6 background, and both *Mecp2* loss-of-function models were maintained on a pure C57BL/6 background. Therefore, the different genetic backgrounds may contribute to the differences seen between loss-of-function and gain-of-function models. It is possible that, although two-fold expression of MeCP2 is sufficient to impair synaptic function leading to circuit defects {Chao:2007jg, Na:2012fu}, it is not sufficient to disrupt cellular morphology *in vivo*. Future study of neuronal morphology in mice expressing three-fold levels of MeCP2 may address this hypothesis, as *MECP2* triplication produces more severe phenotypes both clinically and in mice (Samaco et al., 2012; Van Esch et al., 2007).

To address the second question, the relationship between RTT-like phenotypic severity and underlying neuronal morphology, we measured dendritic complexity and soma size in *Mecp2*$^{-/y}$ and *Mecp2*$^{T158A/y}$ mice prior to or at the onset of RTT-like phenotypes (P30) and after development of RTT-like phenotypes. Because RTT-like behavioral progression differs across these mouse models, the ages corresponding to late-symptomatic RTT similarly differed (P60, P90, respectively). Overall, we observed a

subtle age-dependent effect of *Mecp2* mutation on dendritic complexity in *Mecp2* loss-of function, where progression of RTT-like behavioral phenotype correlates with underlying cellular changes. At the early-symptomatic P30 time point, only the mildly-symptomatic *Mecp2*$^{-/y}$ mice showed decreased dendritic complexity, while the pre-symptomatic *Mecp2*$^{T158A/y}$ mice did not, indicating that early in the development of RTT-like phenotypes, changes in neuronal structure vary across different *Mecp2* mutations and may reflect development of RTT-like behavioral phenotypes. This hypothesis is consistent with findings from a comparative study of brain morphology in two 3-week-old *Mecp2* loss-of-function mouse models, in which *Mecp2*$^{-/y}$ mice with a more severe RTT-like phenotype exhibited more widespread and marked changes in brain structure than *Mecp2*$^{-/y}$ mice with a milder RTT-like phenotype (Belichenko et al., 2008).

Similarly, we found greater changes in dendritic complexity in late-symptomatic P60 *Mecp2*$^{-/y}$ and P90 *Mecp2*$^{T158A/y}$ mice relative to that of P30. The reduction in dendritic complexity in P60 *Mecp2*$^{-/y}$ mice was slightly more widespread than that of P30 *Mecp2*$^{-/y}$ mice, and P90 *Mecp2*$^{T158A/y}$ showed changes in dendritic complexity that were absent at the pre-symptomatic time point. These data indicate that changes in dendritic outgrowth accompany the development of RTT-like phenotypes upon *Mecp2* loss-of-function and are consistent with RTT post-mortem histological data showing a correlation between the degree of morphological abnormality and RTT symptom severity at time of death (Bauman et al., 1995).

The developmental changes in dendritic complexity we identified, however, were relatively mild, compared to reports from other *Mecp2* loss-of-function studies (Kishi and Macklis, 2004; Robinson et al., 2012; Stuss et al., 2012), and limited to specific dendritic domains. This is surprising, as the overt behavioral phenotypes present at both late-symptomatic time points would predict underlying cellular architecture to be severely disrupted. One factor in this subtle dendritic outgrowth phenotype may be experimental bias from the *Thy1-GFP/M* reporter line. While an interaction between MeCP2 and a different reporter transgene *Thy1-YFP/H* has been reported (Stuss et al., 2012), we did not identify GFP-labeling biases in our mice. Our selection of layer V cortical neurons extending their apical tufts to the pial surface, however, could have introduced a bias for analysis of neurons with a less severe morphological phenotype within the *Mecp2*

mutant neuronal network. As changes in dendritic morphology have been shown to widely differ between individual neurons within a population (Belichenko et al., 2009b), we cannot exclude the possibility that our experimental method was selective for neurons with intact dendritic structures, resulting in a mild dendritic complexity phenotype.

Data from other *Mecp2* mouse models, however, indicate that changes in dendritic arborization may not reflect the severity of behavioral phenotype. While MeCP2 A140V knockin mice with no obvious RTT-like behavioral phenotypes show decreased dendritic complexity (Jentarra et al., 2010), *Mecp2*$^{308/y}$ mice with motor, social, and learning deficits that model an MeCP2 early truncation show no changes in dendritic complexity or post-synaptic density in cortical and hippocampal CA1 neurons, both before and after onset of RTT-like phenotypes (Moretti et al., 2006). In addition, a developmental time window may exist in which neuronal morphology is more sensitive to MeCP2 function, as previous work has shown that newborn neurons in the hippocampus are severely affected by *Mecp2* loss-of-function (Smrt et al., 2007). Together, these data suggest that while decreases in dendritic arborization may accompany the development of RTT-like behavioral phenotypes in *Mecp2* loss-of-function, the degree of these changes does not necessarily match the behavioral phenotypic severity and therefore, dendritic arborization may not be a robust and consistent cellular readout of RTT-like phenotype.

In contrast to the intrinsic variability of dendritic outgrowth in *Mecp2* mice, we found that MeCP2 soma size regulation is persistent throughout development and dependent on MeCP2 function. Both *Mecp2* loss-of-function mouse models, *Mecp2*$^{-/y}$ and *Mecp2*$^{T158A/y}$, showed decreased soma size at early- and late-symptomatic time points relative to WT, suggesting that soma size decreases upon *Mecp2* loss-of-function but does not change with increasing RTT-like symptomatic severity. These data are consistent with findings from ESC-differentiated neurons, where neurons originating from several lines of *Mecp2* loss-of-function mice show decreased soma size relative to controls throughout the course of neuronal maturation (Yazdani et al., 2012), and can be rescued upon restoration of MeCP2. Together, these data indicate that soma size is regulated by MeCP2 function throughout development and can be an indicator of MeCP2 function.

To address the third question, whether changes in neuronal morphology are brain region or cell type-specific, we assessed neuronal morphology in a separate brain region by measuring dendritic complexity in hippocampal CA1 pyramidal neurons in pre-and post-symptomatic *Mecp2*$^{T158A/y}$ mice. In contrast to the age-dependent decrease in basal dendritic complexity we observed in somatosensory cortex layer V pyramidal neurons of *Mecp2*$^{T158A/y}$ mice, we found no age-dependent reduction in dendritic complexity of hippocampal CA1 pyramidal neurons. These data are consistent with region-specific morphological phenotypes identified in RTT post-mortem brain tissue, where pyramidal neurons of the motor, frontal, and inferior temporal cortices show decreased dendritic complexity, but pyramidal neurons in the visual cortex and hippocampus exhibit no change with respect to age-matched controls (Armstrong et al., 1995; Belichenko et al., 1994). Specificity may even extend to cortical layer, as decreased dendritic arborization has been identified in both basal and apical dendrites of layer V motor cortex cells but only in basal dendrites of layer III motor cortex cells (Armstrong et al., 1995). A comparison of data from different studies also supports a cortical layer-specific regulation of neuronal morphology in mice, where neocortical layer II/III pyramidal neurons show decreased dendritic complexity in both proximal basal and apical dendrites and no change in spine density (Kishi and Macklis, 2004) but layer V pyramidal neurons show decreased dendritic complexity in only proximal basal and distal apical dendrites and decreased spine density (Stuss et al., 2012).

In contrast to the cell type-specific changes in dendritic outgrowth, multiple lines of evidence indicate that soma size is consistent across cell types. We previously reported decreased soma size in hippocampal CA1 pyramidal neurons in both pre- and post-symptomatic *Mecp2*$^{T158A/y}$ mice (Goffin et al., 2012), similar to what we observed in the somatosensory cortex in this study. In addition, decreased soma size has been reported in RTT post-mortem brain tissue (Armstrong, 2005) and in the locus ceruleus (Taneja et al., 2009), hippocampus CA2 (Chen et al., 2001), layer II/III somatosensory cortex (Kishi and Macklis, 2004), layer II/III motor cortex (Robinson et al., 2012), and layer V motor cortex (Stuss et al., 2012) of different *Mecp2*-null mouse strains. Moreover, various lines of *Mecp2*-deficient ESC-derived neurons (Yazdani et al., 2012) and RTT patient-derived induced pluripotent stem cells (Marchetto et al., 2010) also show reduced soma sizes, indicating that, in contrast to dendritic arborization, a reduction in soma size upon *Mecp2*

loss-of-function is a phenotype that is consistent across cell types and experimental systems. Similarly, our finding that soma size is not affected upon *Mecp2* gain-of-function has also been observed *in vitro* (Jugloff et al., 2005), indicating that the absence of a change in soma size upon *Mecp2* gain-of-function is also conserved across cell types.

This consistent and robust reduction in soma size across studies, *Mecp2* mutations, experimental systems, cell types, and developmental time points, is in sharp contrast to changes in dendritic complexity, which varies across these parameters and can be subtle and context-dependent (Stuss et al., 2012). Therefore, in accordance with a recent study evaluating spine density throughout development in *Mecp2* loss-of-function mice (Chapleau et al., 2012), we caution the use of dendritic complexity as a phenotypic endpoint for therapeutic evaluation, and suggest that soma size may be a more robust and reproducible readout of MeCP2 function. Evidence supporting soma size as a reliable morphologic phenotype comes from existing rescue experiments, where activation of a quiescent *Mecp2* gene in adults results in partial restoration of dendritic complexity and length but a full restoration of soma size (Robinson et al., 2012). In addition, postnatal neuron-specific reactivation of MeCP2 sufficient to rescue hippocampal and cortical soma size in *Mecp2*-deficient mice (Giacometti et al., 2007) and neuronal size is restored by the re-expression of MeCP2 in several strains of MeCP2-deficient ESC-derived neurons (Yazdani et al., 2012). Future studies are needed to understand how soma size and dendritic outgrowth are differentially regulated by MeCP2. It is conceivable that dendritic arborization is more sensitive to the cellular environment, growth factors, and homeostatic regulation, whereas soma size is more directly affected by the function of nuclear proteins such as MeCP2.

Overall, our data indicates that within a population of excitatory neurons in RTT mouse models, *in vivo* changes in dendritic complexity upon *Mecp2* loss-of-function are brain region-specific, correlated with behavioral phenotype, and mild. In contrast, soma size is regulated throughout development and may be a reliable marker for evaluating MeCP2 function and therapeutic efficacy. These phenotypes are specific to *Mecp2* loss-of-function, as *in vivo* morphological changes upon *Mecp2* gain-of-function are absent. The use of neuronal morphology as a cellular readout of RTT phenotype and restoration of

neuronal circuitry, therefore, should be cautioned, as morphological phenotypes are intrinsically variable.

Figure 1

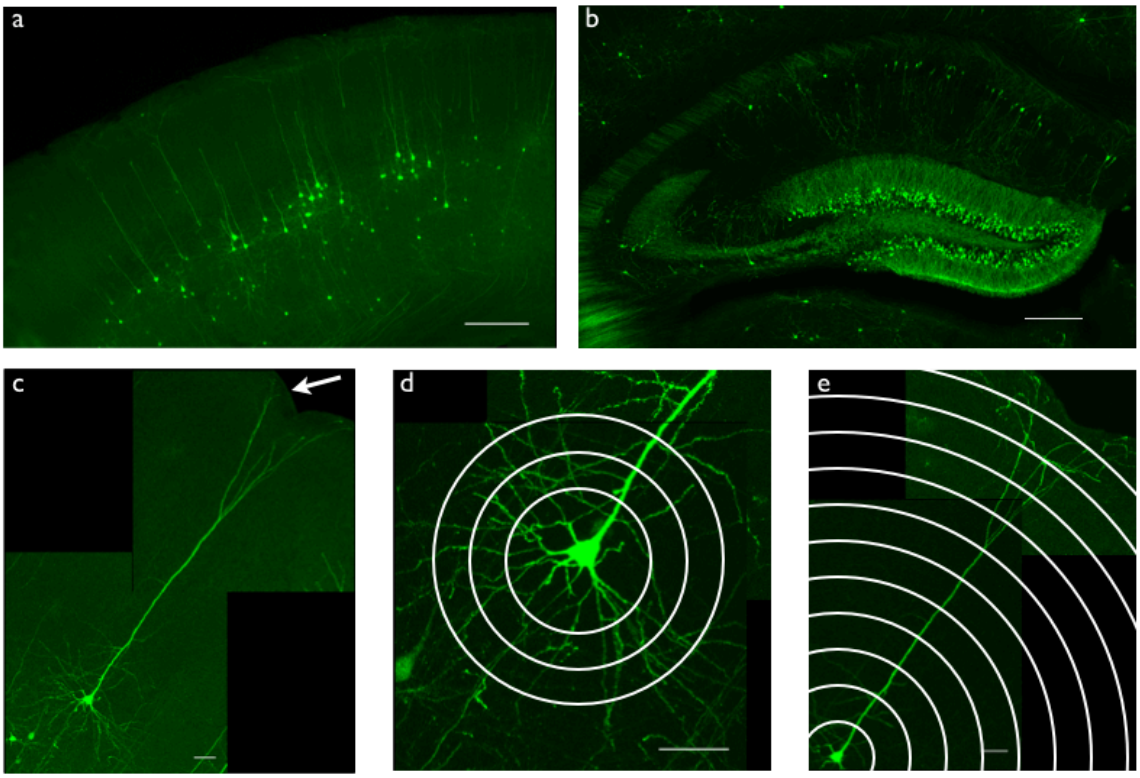

Figure 1. *Thy1-GFP/M* reporter imaging strategy.

(a) Somatosensory cortex layer V pyramidal neurons are labeled with GFP throughout the cell body and dendritic tree in *Thy1-GFP/M* reporter mice. Scale bar = 250 µm.

(b) Hippocampus CA1 pyramidal neurons are labeled with GFP throughout the cell body and dendritic tree in *Thy1-GFP/M* reporter mice. Scale bar = 250 µm.

(c) Somatosensory cortex layer V pyramidal neurons extend their apical dendrites to the pial surface (arrow) and their basal dendrites deep into layer VI. Scale bar = 50 µm.

(d) Basal dendrites of somatosensory cortex layer V pyramidal neurons, quantified by Sholl analysis, measuring number of intersections between concentric circles drawn around the cell soma (Sholl radii) and dendritic branches. Scale bar = 50 µm.

(e) Apical dendrites of somatosensory cortex layer V pyramidal neurons, quantified by Sholl analysis. Scale bar = 50 µm.

Figure 2

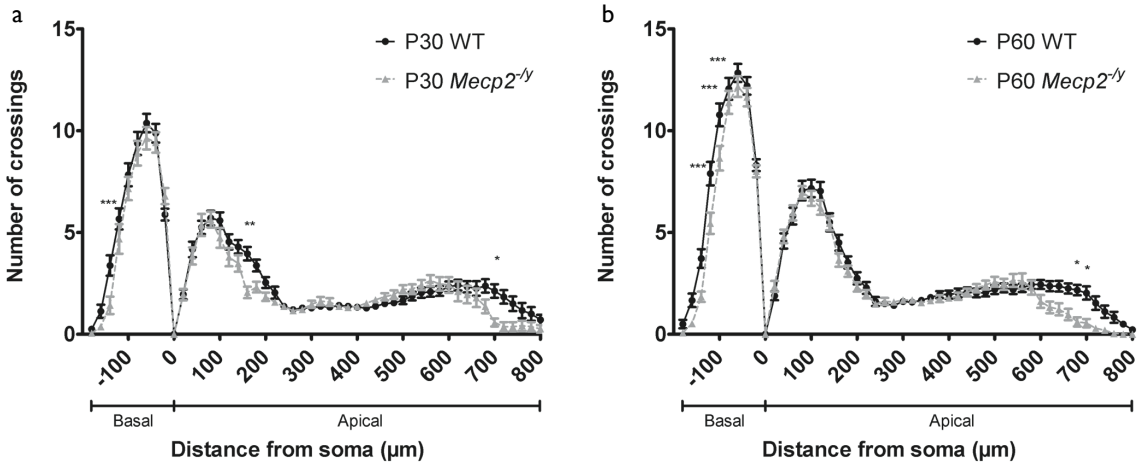

Figure 2. Dendritic complexity in somatosensory cortex of *Mecp2*$^{-/y}$ mice.

(a) Sholl analysis of somatosensory cortex layer V pyramidal neurons in P30 WT (n=24 neurons from 4 mice) and *Mecp2*$^{-/y}$ mice (n=19 neurons from 4 mice) shows reduced dendritic complexity in *Mecp2*$^{-/y}$ mice relative to WT. Basal dendritic arbor is denoted by negative distance from soma, 0 µm marks soma position within cortex, and apical dendritic arbor is denoted by positive distance from soma. Two-way ANOVA with Bonferroni correction, $p<0.0001$ (interaction); *$p<0.05$, **$p<0.01$, ***$p<0.001$. Bars represent mean ± sem.

(b) Sholl analysis of somatosensory cortex layer V pyramidal neurons in P60 WT (n=36 neurons from 4 mice) and *Mecp2*$^{-/y}$ mice (n=31 neurons from 4 mice) show more widespread reduction in dendritic complexity in *Mecp2*$^{-/y}$ mice relative to WT than seen in P30 animals. Two-way ANOVA with Bonferroni correction, $p<0.0001$ (interaction); *$p<0.05$, ***$p<0.001$.

Figure 3

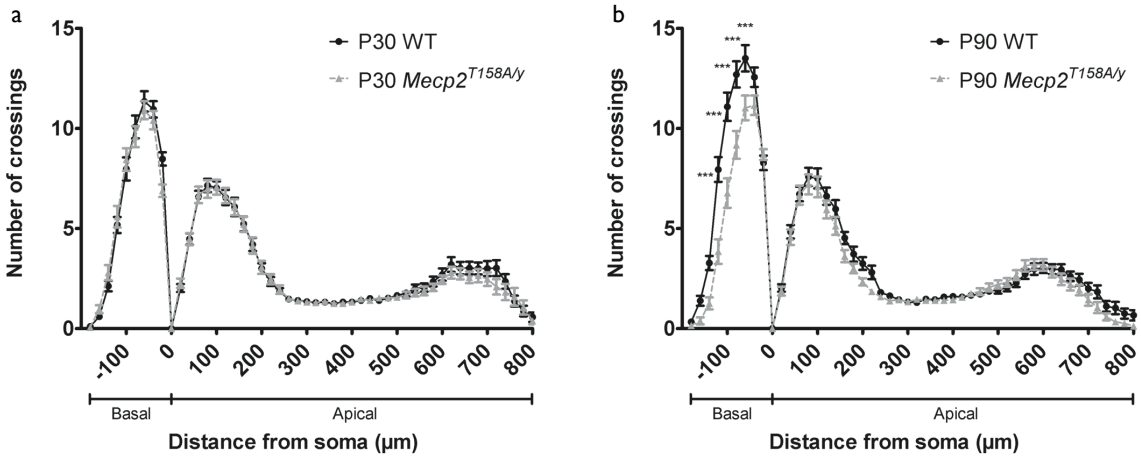

Figure 3. Dendritic complexity in somatosensory cortex of *Mecp2*$^{T158A/y}$ mice.

(a) Sholl analysis of somatosensory cortex layer V pyramidal neurons in P30 WT (n=40 neurons from 4 animals) and *Mecp2*$^{T158A/y}$ mice (n=34 neurons from 4 animals) show no change dendritic complexity in *Mecp2*$^{T158A/y}$ mice relative to WT. Two-way ANOVA, $p>0.05$. Bars represent mean ± sem.

(b) Sholl analysis of somatosensory cortex layer V pyramidal neurons in P90 WT (n=36 neurons from 4 mice) and *Mecp2*$^{T158A/y}$ mice (n=39 neurons from 4 mice) show reduced dendritic complexity in *Mecp2*$^{T158A/y}$ mice relative to WT specifically in the basal dendritic arbor. Two-way ANOVA with Bonferroni correction, $p<0.0001$ (interaction); $^{**}p<0.01$.

Figure 4

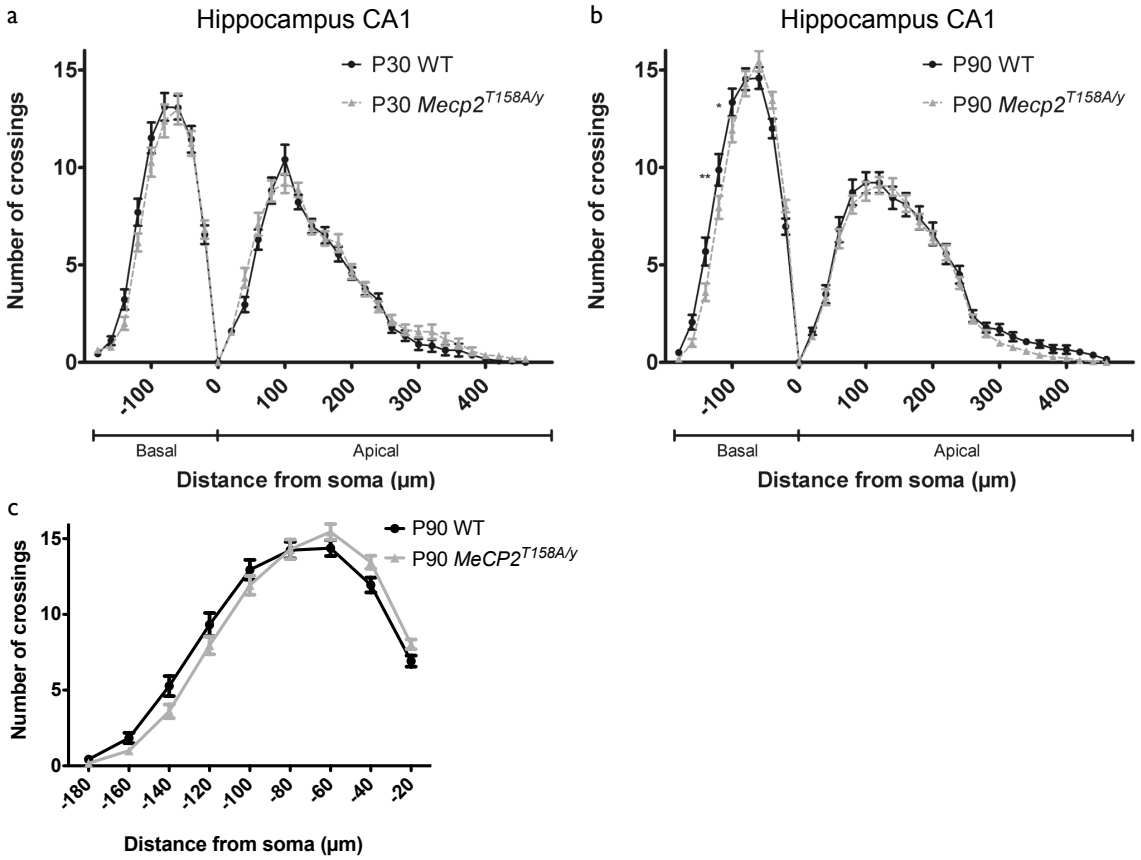

Figure 4. Dendritic complexity in hippocampus CA1 of *Mecp2*$^{T158A/y}$ mice.

(a) Sholl analysis of hippocampal CA1 pyramidal neurons in P30 WT (27 neurons from 5 mice) and *Mecp2*$^{T158A/y}$ mice (n=33 neurons from 5 mice) show no change dendritic complexity in *Mecp2*$^{T158A/y}$ mice relative to WT. Two-way ANOVA, p>0.05. Bars represent mean ± sem.

(b) Sholl analysis of hippocampal CA1 pyramidal neurons in P90 WT (n=32 neurons from 5 mice) and *Mecp2*$^{T158A/y}$ mice (n=40 neurons from 5 mice) show altered dendritic complexity in *Mecp2*$^{T158A/y}$ mice relative to WT specifically in the basal dendritic arbor. Two-way ANOVA with Bonferroni correction, p<0.0001 (interaction); *p<0.05, **p<0.01.

(c) Sholl analysis of basal dendritic complexity of hippocampal CA1 pyramidal neurons in P90 WT and *Mecp2*$^{T158A/y}$ mice show no difference in peak number of crossings in *Mecp2*$^{T158A/y}$ mice relative to WT.

Figure 5

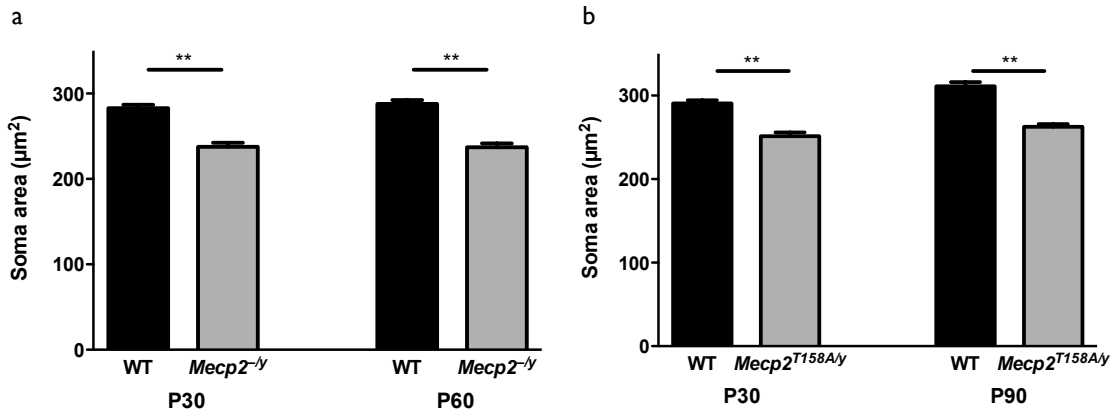

Figure 5. Soma size is regulated throughout development by MeCP2 function.

(a) Somatosensory cortex layer V pyramidal neuron soma size is reduced in *Mecp2*$^{-/y}$ mice relative to WT at both P30 (WT: n=124 neurons from 4 mice; *Mecp2*$^{-/y}$: n=103 neurons from 4 mice) and P60 (WT: n=126 neurons from 4 mice; *Mecp2*$^{-/y}$: n=104 neurons from 4 mice). **p<0.01, unpaired two-tailed Student t-test with Bonferroni correction. Bars represent mean ± SEM.

(b) Somatosensory cortex layer V pyramidal neuron soma size is reduced in *Mecp2*$^{T158A/y}$ mice relative to WT at both P30 (WT: n=115 neurons from 4 mice; *Mecp2*$^{T158A/y}$: n=121 neurons from 4 mice) and P90 (WT: n=81 neurons from 4 mice; *Mecp2*$^{T158A/y}$: n=106 neurons from 4 mice). **p<0.01, unpaired two-tailed Student t-test with Bonferroni correction.

Figure 6

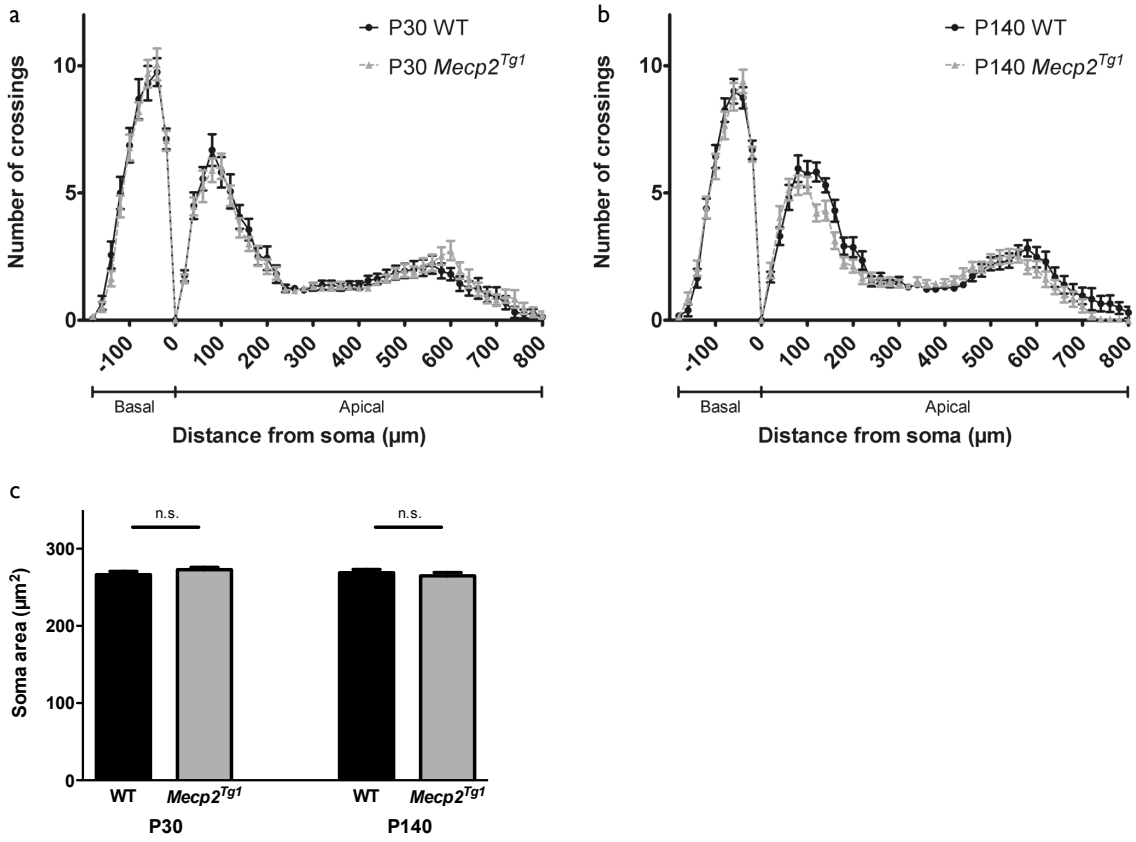

Figure 6. Dendritic complexity in *Mecp2*^{Tg1} mice.

(a) Sholl analysis of somatosensory cortex layer V pyramidal neurons in P30 WT (n=16 neurons from 2 mice) and *Mecp2*^{Tg1} mice (n=19 neurons from 2 mice) show no change dendritic complexity in *Mecp2*^{Tg1} mice relative to WT. Two-way ANOVA, $p>0.05$. Bars represent mean ± sem.

(b) Sholl analysis of somatosensory cortex layer V pyramidal neurons in P140 WT (n=23 neurons from 2 mice) and *Mecp2*^{Tg1} mice (n=23 neurons from 2 mice) show no change dendritic complexity in *Mecp2*^{Tg1} mice relative to WT. Two-way ANOVA, $p>0.05$.

(c) Somatosensory cortex layer V pyramidal neuron soma size is not affected in *Mecp2*^{Tg1} mice relative to WT at both P30 (WT: n=101 neurons from 2 mice; *Mecp2*^{Tg1}: n=110 neurons from 2 mice) and P140 (P140; n=110 neurons from 2 mice; *Mecp2*^{Tg1}: n=113 neurons from 2 mice). $p>0.05$, unpaired two-tailed Student t-test.

Chapter 6:
DISCUSSION

The bulk of this thesis aims to understand the pathogenic mechanisms underlying the early-onset epileptic encephalopathy CDKL5 disorder. In the first body of work (Chapter 2), I developed and characterized the first CDKL5 animal model, and found that mice lacking CDKL5 recapitulate a number of clinically relevant behavioral phenotypes, including autistic-like deficits in social interaction, motor impairment, and reduced fear memory. In addition, these mice show alterations in neuronal circuit communication and disruption of multiple signal transduction pathways that converge into PTEN downstream signaling. Prior to this study, studies of CDKL5 function were limited to *in vitro* and knockdown studies, which often yielded inconsistent results with unconfirmed *in vivo* relevance. Therefore, the generation of a mouse model that mimicked a *CDKL5* patient mutation was necessary in order to establish a framework and platform for future mechanistic studies. In addition, this study was the first to establish a causal role of mutations in *Cdkl5* and disease pathogenesis.

In the second body of work (Chapter 3), I sought to address the mechanisms by which mutations in *CDKL5* lead to disease using a CDKL5 conditional knockout mouse line. To investigate the brain-specific role of CDKL5 in disease pathogenesis, I generated mice lacking CDKL5 from the nervous system and found that these mice recapitulate a number of behavioral phenotypes identified in the CDKL5 null mutant, including hyperactivity, decreased anxiety, and reduced sociability. Next, I sought to dissect the neuronal subpopulations in which *Cdkl5* loss-of-function leads to disease. Therefore, I generated mice lacking CDKL5 from either glutamatergic or GABAergic neurons, which are the two major neuronal subtypes in the brain. Behavioral phenotyping of these mice showed that CDKL5-related phenotypes separate upon conditional ablation of CDKL5, such that mice lacking CDKL5 from forebrain GABAergic neurons demonstrate autistic-like phenotypes, whereas mice lacking CDKL5 from forebrain glutamatergic neurons demonstrate impairments in working memory and develop spontaneous seizures. Importantly, these data suggest that disease mechanisms underlying CDKL5 disorder and Rett Syndrome are distinct, as conditional ablation of MeCP2 in these two neuronal

populations results in phenotypes that are distinct from those of CDKL5 conditional knockouts (Goffin et al., 2014). Moreover, these data support a mechanism that is consistent with emerging data on CDKL5 function (Chen et al., 2010; Ricciardi et al., 2012; Zhu et al., 2013).

The dissection of these two major phenotypes of CDKL5 disorder, seizures and autistic-like behaviors, in the two complementary conditional knockout mice have raised several hypotheses for CDKL5 biological function. First, it is possible that CDKL5 plays a role in the synapses of glutamatergic neurons that is distinct from its role in the synapses of GABAergic neurons. Immunostaining experiments have demonstrated that CDKL5 is localized to excitatory, but not inhibitory, synapses onto pyramidal neurons (Ricciardi et al., 2012). Electrophysiological recordings from primary cultures after shRNA-mediated CDKL5 knockdown show reduced amplitude and frequency of mEPSCs, indicating that loss of CDKL5 impairs synaptic maturation. These data, combined with the role of CDKL5 in regulation of neuronal migration, outgrowth, and spine development (Chen et al., 2010; Ricciardi et al., 2012; Zhu et al., 2013), suggest a disease mechanism by which loss of CDKL5 from glutamatergic neurons impairs neuronal development and connectivity and weakens excitatory synapses. Mice lacking CDKL5 from glutamatergic neurons, however, develop spontaneous seizures, suggesting an imbalance in neuronal excitation and inhibition that is expected in epilepsy, where excitation is favored over inhibition. Therefore, future synapse electrophysiological measurement of excitatory and inhibitory neurotransmission in Nex-cKO mice, along with morphological measurements performed in parallel, will illuminate how *Cdkl5* loss-of-function affects excitatory synapses *in vivo*, and whether a shift in E/I balance contributes to the development of spontaneous seizures and behavioral phenotypes.

Although CDKL5 is not localized to inhibitory synapses onto excitatory neurons, the prominent autistic-like behavioral phenotypes in mice lacking CDKL5 from GABAergic neurons suggests that CDKL5 plays a role in GABAergic cells. It is currently unknown whether CDKL5 is localized to excitatory or inhibitory synapses onto inhibitory neurons, so it is possible that it may play a role at these synapses. Therefore, future experiments examining the localization of CDKL5 at these two synapses, as well as neurotransmission at these synapses will determine whether E/I imbalance is relevant to

autistic-like phenotypes. Indeed, an increased ratio of excitation/inhibition has been proposed to underlie autism (Rubenstein and Merzenich, 2003) and optogenetic elevation of E/I balance has been shown to produce autistic-like phenotypes (Yizhar et al., 2011).

Another explanation for the separation of phenotypes in CDKL5 conditional knockout animals is the possibility that CDKL5 may be involved in distinct signaling pathways in glutamatergic and GABAergic neurons. Studies from CDKL5 KO mice suggest that CDKL5 may be involved in PTEN downstream signaling (Amendola et al., 2014; Fuchs et al., 2014; Wang et al., 2012). Its involvement in this pathway, however, may be limited to a particular cell type, or it may be differentially involved in glutamatergic cells and GABAergic cells. To investigate this possibility, future experiments will aim to determine firstly whether PTEN downstream signaling, including Akt/mTOR, Akt/S6K, and Akt/GSK-3b, are differentially affected in Nex- or Dlx-cKO mice, particularly in glutamatergic or GABAergic neurons from these mice. Then, the relationship between CDKL5 and PTEN signaling can be assessed by pharmacologic or genetic manipulation of PTEN in Nex- or Dlx-cKO mice. As PTEN is the master regulator of this pathway, loss of PTEN should restore pAkt levels, and behavioral and electrophysiogical experiments can measure whether restoration of this signaling pathway in Nex- or Dlx-cKO animals is sufficient to rescue the neural circuit or behavioral phenotypes identified in Chapter 3. Ultimately, this work aims to identify signaling pathways that are regulated by CDKL5 and can therefore be targeted for therapeutic intervention.

At the circuit level, it is possible that loss of CDKL5 from glutamatergic or GABAergic neurons differentially disrupts neural circuits, or that the neural circuits mediating autistic behavior and epilepsy are inherently distinct and that CDKL5 plays a role in both circuits. To examine these possibilities, future experiments should continue to assess neural circuit function using hippocampal microcircuits as a model. VSD imaging of the dentate gyrus microcircuit showed a preferential breakdown of the dentate filter in Dlx-cKO mice, indicating that loss of CDKL5 from GABAergic neurons preferentially disrupts the dentate gyrus. Identification of disease-related microcircuits may not only serve as readouts for therapeutic efficacy, but may also aid in pinpointing key circuit mechanisms underlying disease.

Finally, future experiments should address the therapeutic relevance of these studies. Gene mutations occur in germ cells and persist throughout the organism's lifetime, but therapeutic intervention in the clinic is likely constrained to postnatal time points, either during development or in adulthood. Therefore, the reversibility of CDKL5 disorder must be established. In Rett Syndrome mouse models, restoration of MeCP2 in post-symptomatic adult mice is sufficient to rescue many, but not all, disease-related phenotypes (Guy et al., 2007), suggesting that Rett Syndrome is reversible and therefore, treatable. This finding also indicates that MeCP2 may play a maintenance role and that many circuits and pathways regulated by MeCP2 are plastic. Performing similar experiments on CDKL5 mouse models will be an important step in translating animal research into clinically relevant therapeutic strategies.

In the second half of this thesis, I collaborated with other members of the lab to investigate Rett Syndrome. In the third body of work (Chapter 4), I helped to characterize a novel *Mecp2* mouse model containing a knockin mutation at the MeCP2 Threonine 158 residue. This residue is located within the methyl-binding domain of MeCP2 and is the most common site for *MECP2* missense mutations. We found that MeCP2 158A mutant mice recapitulate a number of RTT-like behavioral phenotypes and demonstrate developmental impairments in auditory-evoked event-related processing. Biochemical assays identified that MeCP2 T158A mutation causes a reduction in MeCP2 protein stability and DNA binding, suggesting that stabilization of MeCP2 and enhancement of affinity for DNA may be possibilities for RTT therapeutic development, and that measurement of ERPs during development may serve as a biomarker for Rett Syndrome progression.

In the final body of work (Chapter 5), I engaged in a collaboration to perform a comprehensive and systematic analysis of how age, brain region, and *Mecp2* mutation influences RTT-related neuronal morphology. We found that *Mecp2* loss-of-function mutations mildly reduce dendritic complexity in a brain region- and *Mecp2* mutation-specific manner that correlates with the onset of behavioral phenotype. Soma size, in contrast, is robustly reduced upon *Mecp2* loss-of-function across development, whereas *Mecp2* gain-of-function does not influence dendritic complexity or soma size. These

data suggest that soma size, rather than dendritic complexity, may be a more reliable and robust marker for MeCP2 function.

Together, this body of work represents significant advancement in the understanding of how mutations in *CDKL5* lead to disease and in the mechanisms underlying Rett Syndrome pathogenesis. The generation and characterization of multiple mouse models of CDKL5 disorder and Rett Syndrome with face validity that mimic patient mutations have provided valuable tools and reagents for the research community and have identified novel protein functions and signaling pathways that may serve as potential targets for therapeutic intervention.

BIBLIOGRAPHY

Abrahams, B.S., and Geschwind, D.H. (2008). Advances in autism genetics: on the threshold of a new neurobiology. Nat. Rev. Genet. *9*, 341–355.

Acsády, L., Kamondi, A., Sík, A., Freund, T., and Buzsáki, G. (1998). GABAergic cells are the major postsynaptic targets of mossy fibers in the rat hippocampus. J. Neurosci. *18*, 3386–3403.

Amendola, E., Zhan, Y., Mattucci, C., Castroflorio, E., Calcagno, E., Fuchs, C., Lonetti, G., Silingardi, D., Vyssotski, A.L., Farley, D., et al. (2014). Mapping Pathological Phenotypes in a Mouse Model of CDKL5 Disorder. PLoS ONE *9*, e91613.

Amir, R.E., Van den Veyver, I.B., Wan, M., Tran, C.Q., Francke, U., and Zoghbi, H.Y. (1999). Rett syndrome is caused by mutations in X-linked MECP2, encoding methyl-CpG-binding protein 2. Nat. Genet. *23*, 185–188.

Ang, C.W., Carlson, G.C., and Coulter, D.A. (2005). Hippocampal CA1 circuitry dynamically gates direct cortical inputs preferentially at theta frequencies. Journal of Neuroscience *25*, 9567–9580.

Ang, C.W., Carlson, G.C., and Coulter, D.A. (2006). Massive and specific dysregulation of direct cortical input to the hippocampus in temporal lobe epilepsy. Journal of Neuroscience *26*, 11850–11856.

Archer, H.L., Evans, J., Edwards, S., Colley, J., Newbury-Ecob, R., O'Callaghan, F., Huyton, M., O'Regan, M., Tolmie, J., Sampson, J., et al. (2006). CDKL5 mutations cause infantile spasms, early onset seizures, and severe mental retardation in female patients. Journal of Medical Genetics *43*, 729–734.

Armstrong, D., Dunn, J.K., Antalffy, B., and Trivedi, R. (1995). Selective dendritic alterations in the cortex of Rett syndrome. J. Neuropathol. Exp. Neurol. *54*, 195–201.

Armstrong, D.D. (2005). Neuropathology of Rett syndrome. Journal of Child Neurology *20*, 747–753.

Arts, W.F.M. (2011). CDKL5 gene-related epileptic encephalopathy: electroclinical findings in the first year of life. Dev Med Child Neurol *53*, 296–297.

Artuso, R., Mencarelli, M.A., Polli, R., Sartori, S., Ariani, F., Pollazzon, M., Marozza, A., Cilio, M.R., Specchio, N., and Vigevano, F. (2010). Early-onset seizure variant of Rett syndrome: Definition of the clinical diagnostic criteria. Brain and Development *32*, 17–24.

Bader, G.G., Witt-Engerström, I., and Hagberg, B. (1989). Neurophysiological findings in the Rett syndrome, II: Visual and auditory brainstem, middle and late evoked responses. Brain and Development *11*, 110–114.

Bahi-Buisson, N., and Bienvenu, T. (2012). CDKL5-Related Disorders: From Clinical Description to Molecular Genetics. Mol Syndromol *2*, 137–152.

Bahi-Buisson, N., Girard, B., Gautier, A., Nectoux, J., Fichou, Y., Saillour, Y., Poirier, K., Chelly, J., and Bienvenu, T. (2010). Epileptic encephalopathy in a girl with an interstitial deletion of Xp22 comprising promoter and exon 1 of the CDKL5 gene. Am. J. Med. Genet. B Neuropsychiatr. Genet. *153B*, 202–207.

Bahi-Buisson, N., Kaminska, A., Boddaert, N., Rio, M., Afenjar, A., Gérard, M., Giuliano, F., Motte, J., Héron, D., Morel, M.A.N., et al. (2008a). The three stages of epilepsy in patients with CDKL5 mutations. Epilepsia *49*, 1027–1037.

Bahi-Buisson, N., Nectoux, J., Rosas-Vargas, H., Milh, M., Boddaert, N., Girard, B., Cances, C., Ville, D., Afenjar, A., Rio, M., et al. (2008b). Key clinical features to identify girls with CDKL5 mutations. Brain *131*, 2647–2661.

Bahi-Buisson, N., Villeneuve, N., Caietta, E., Jacquette, A., Maurey, H., Matthijs, G., Van Esch, H., Delahaye, A., Moncla, A., Milh, M., et al. (2012). Recurrent mutations in the CDKL5 gene: Genotype-phenotype relationships. Am. J. Med. Genet. A.

Barlow, C., Hirotsune, S., Paylor, R., Liyanage, M., Eckhaus, M., Collins, F., Shiloh, Y., Crawley, J.N., Ried, T., Tagle, D., et al. (1996). Atm-deficient mice: a paradigm of ataxia telangiectasia. Cell *86*, 159–171.

Bartnik, M., Derwińska, K., Gos, M., Obersztyn, E., Kołodziejska, K.E., Erez, A., Szpecht-Potocka, A., Fang, P., Terczyńska, I., Mierzewska, H., et al. (2011). Early-onset seizures due to mosaic exonic deletions of CDKL5 in a male and two females. Genet. Med. *13*, 447–452.

Bauman, M.L., Kemper, T.L., and Arin, D.M. (1995). Pervasive neuroanatomic abnormalities of the brain in three cases of Rett's syndrome. Neurology *45*, 1581–1586.

Belichenko, N.P., Belichenko, P.V., and Mobley, W.C. (2009a). Evidence for both neuronal cell autonomous and nonautonomous effects of methyl-CpG-binding protein 2 in the cerebral cortex of female mice with Mecp2 mutation. Neurobiol. Dis. *34*, 71–77.

Belichenko, N.P., Belichenko, P.V., Li, H.H., Mobley, W.C., and Francke, U. (2008). Comparative study of brain morphology in Mecp2 mutant mouse models of Rett syndrome. J. Comp. Neurol. *508*, 184–195.

Belichenko, P.V., Oldfors, A., Hagberg, B., and Dahlström, A. (1994). Rett syndrome: 3-D confocal microscopy of cortical pyramidal dendrites and afferents. Neuroreport *5*, 1509–1513.

Belichenko, P.V., Wright, E.E., Belichenko, N.P., Masliah, E., Li, H.H., Mobley, W.C., and Francke, U. (2009b). Widespread changes in dendritic and axonal morphology in Mecp2-mutant mouse models of Rett syndrome: evidence for disruption of neuronal networks. J. Comp. Neurol. *514*, 240–258.

Ben-Ari, Y. (2001). Developing networks play a similar melody. Trends Neurosci. *24*, 353–360.

Bertani, I., Rusconi, L., Bolognese, F., Forlani, G., Conca, B., De Monte, L., Badaracco, G.,

Landsberger, N., and Kilstrup-Nielsen, C. (2006). Functional consequences of mutations in CDKL5, an X-linked gene involved in infantile spasms and mental retardation. J. Biol. Chem. *281*, 32048–32056.

Bhaskar, P.T., and Hay, N. (2007). The two TORCs and Akt. Developmental Cell *12*, 487–502.

Bienvenu, T., and Chelly, J. (2006). Molecular genetics of Rett syndrome: when DNA methylation goes unrecognized. Nat. Rev. Genet. *7*, 415–426.

Bill, B.R., and Geschwind, D.H. (2009). Genetic advances in autism: heterogeneity and convergence on shared pathways. Curr. Opin. Genet. Dev. *19*, 271–278.

Boutry-Kryza, N., Ville, D., Labalme, A., Calender, A., Dupont, J.-M., Touraine, R., Edery, P., Portes, des, V., Sanlaville, D., and Lesca, G. (2014). Complex mosaic CDKL5 deletion with two distinct mutant alleles in a 4-year-old girl. Am. J. Med. Genet. A *164A*, 2025–2028.

Brendel, C., Belakhov, V., Werner, H., Wegener, E., Gärtner, J., Nudelman, I., Baasov, T., and Huppke, P. (2011). Readthrough of nonsense mutations in Rett syndrome: evaluation of novel aminoglycosides and generation of a new mouse model. J. Mol. Med. *89*, 389–398.

Brooks-Kayal, A. (2010). Epilepsy and autism spectrum disorders: are there common developmental mechanisms? Brain and Development *32*, 731–738.

Buzsáki, G. (2005). Theta rhythm of navigation: link between path integration and landmark navigation, episodic and semantic memory. Hippocampus *15*, 827–840.

Buzsáki, G., and Draguhn, A. (2004). Neuronal oscillations in cortical networks. Science *304*, 1926–1929.

Carouge, D., Host, L., Aunis, D., Zwiller, J., and Anglard, P. (2010). CDKL5 is a brain MeCP2 target gene regulated by DNA methylation. Neurobiol. Dis. *38*, 414–424.

Castrén, M., Gaily, E., Tengström, C., Lähdetie, J., Archer, H., and Ala-Mello, S. (2011). Epilepsy caused by CDKL5 mutations. European Journal of Paediatric Neurology *15*, 65–69.

Chahrour, M., and Zoghbi, H.Y. (2007). The Story of Rett Syndrome: From Clinic to Neurobiology. Neuron *56*, 422–437.

Chahrour, M., Jung, S.Y., Shaw, C., Zhou, X., Wong, S.T.C., Qin, J., and Zoghbi, H.Y. (2008). MeCP2, a key contributor to neurological disease, activates and represses transcription. Science *320*, 1224–1229.

Chao, H.-T., Chen, H., Samaco, R.C., Xue, M., Chahrour, M., Yoo, J., Neul, J.L., Gong, S., Lu, H.-C., Heintz, N., et al. (2010). Dysfunction in GABA signalling mediates autism-like stereotypies and Rett syndrome phenotypes. Nature *468*, 263–269.

Chao, H.-T., Zoghbi, H.Y., and Rosenmund, C. (2007). MeCP2 controls excitatory synaptic

strength by regulating glutamatergic synapse number. Neuron *56*, 58–65.

Chapleau, C.A., Boggio, E.M., Calfa, G., Percy, A.K., Giustetto, M., and Pozzo-Miller, L. (2012). Hippocampal CA1 Pyramidal Neurons of Mecp2 Mutant Mice Show a Dendritic Spine Phenotype Only in the Presymptomatic Stage. Neural Plast. *2012*, 1–9.

Chapleau, C.A., Calfa, G.D., Lane, M.C., Albertson, A.J., Larimore, J.L., Kudo, S., Armstrong, D.L., Percy, A.K., and Pozzo-Miller, L. (2009). Dendritic spine pathologies in hippocampal pyramidal neurons from Rett syndrome brain and after expression of Rett-associated MECP2 mutations. Neurobiol. Dis. *35*, 219–233.

Chen, Q., Zhu, Y.-C., Yu, J., Miao, S., Zheng, J., Xu, L., Zhou, Y., Li, D., Zhang, C., Tao, J., et al. (2010). CDKL5, a protein associated with rett syndrome, regulates neuronal morphogenesis via Rac1 signaling. Journal of Neuroscience *30*, 12777–12786.

Chen, R.Z., Akbarian, S., Tudor, M., and Jaenisch, R. (2001). Deficiency of methyl-CpG binding protein-2 in CNS neurons results in a Rett-like phenotype in mice. Nat. Genet. *27*, 327–331.

Chen, W.G., Chang, Q., Lin, Y., Meissner, A., West, A.E., Griffith, E.C., Jaenisch, R., and Greenberg, M.E. (2003). Derepression of BDNF transcription involves calcium-dependent phosphorylation of MeCP2. Science *302*, 885–889.

Chergui, K., Svenningsson, P., and Greengard, P. (2005). Physiological role for casein kinase 1 in glutamatergic synaptic transmission. Journal of Neuroscience *25*, 6601–6609.

Clipperton-Allen, A.E., and Page, D.T. (2014). Pten haploinsufficient mice show broad brain overgrowth but selective impairments in autism-relevant behavioral tests. Human Molecular Genetics *23*, 3490–3505.

Cohen, S., Gabel, H.W., Hemberg, M., Hutchinson, A.N., Sadacca, L.A., Ebert, D.H., Harmin, D.A., Greenberg, R.S., Verdine, V.K., Zhou, Z., et al. (2011). Genome-Wide Activity-Dependent MeCP2 Phosphorylation Regulates Nervous System Development and Function. Neuron *72*, 72–85.

Collins, A.L., Levenson, J.M., Vilaythong, A.P., Richman, R., Armstrong, D.L., Noebels, J.L., David Sweatt, J., and Zoghbi, H.Y. (2004). Mild overexpression of MeCP2 causes a progressive neurological disorder in mice. Human Molecular Genetics *13*, 2679–2689.

Costa-Mattioli, M., and Monteggia, L.M. (2013). mTOR complexes in neurodevelopmental and neuropsychiatric disorders. Nat Neurosci *16*, 1537–1543.

Córdova-Fletes, C., Rademacher, N., Müller, I., Mundo-Ayala, J.N., Morales-Jeanhs, E.A., García-Ortiz, J.E., León-Gil, A., Rivera, H., Domínguez, M.G., and Kalscheuer, V.M. (2010). CDKL5 truncation due to a t(X;2)(p22.1;p25.3) in a girl with X-linked infantile spasm syndrome. Clinical Genetics *77*, 92–96.

Crawley, J.N. (2007). Mouse behavioral assays relevant to the symptoms of autism. Brain Pathol. *17*, 448–459.

D'Cruz, J.A., D'Cruz, J.A., Wu, C., Wu, C., Zahid, T., Zahid, T., El-Hayek, Y., El-Hayek, Y., Zhang, L., Zhang, L., et al. (2010). Alterations of cortical and hippocampal EEG activity in MeCP2-deficient mice. Neurobiol. Dis. *38*, 8–16.

Dani, V.S., and Nelson, S.B. (2009). Intact long-term potentiation but reduced connectivity between neocortical layer 5 pyramidal neurons in a mouse model of Rett syndrome. Journal of Neuroscience *29*, 11263–11270.

Dani, V.S., Chang, Q., Maffei, A., Turrigiano, G.G., Jaenisch, R., and Nelson, S.B. (2005). Reduced cortical activity due to a shift in the balance between excitation and inhibition in a mouse model of Rett syndrome. Proceedings of the National Academy of Sciences of the United States of America *102*, 12560–12565.

Das, D.K., Mehta, B., Menon, S.R., Raha, S., and Udani, V. (2013). Novel mutations in cyclin-dependent kinase-like 5 (CDKL5) gene in Indian cases of Rett syndrome. Neuromolecular Med. *15*, 218–225.

Dawson, G., Klinger, L.G., Panagiotides, H., Lewy, A., and Castelloe, P. (1995). Subgroups of autistic children based on social behavior display distinct patterns of brain activity. J Abnorm Child Psychol *23*, 569–583.

Deacon, R.M.J. (2006). Assessing nest building in mice. Nat Protoc *1*, 1117–1119.

Del Pino, I., Garcia-Frigola, C., Dehorter, N., Brotons-Mas, J.R., Alvarez-Salvado, E., Martínez de Lagrán, M., Ciceri, G., Gabaldón, M.V., Moratal, D., Dierssen, M., et al. (2013). Erbb4 Deletion from Fast-Spiking Interneurons Causes Schizophrenia-like Phenotypes. Neuron *79*, 1152–1168.

Dhir, A. (2012). Pentylenetetrazol (PTZ) kindling model of epilepsy. Curr Protoc Neurosci *Chapter 9*, Unit9.37.

Diebold, B., Delépine, C., Gataullina, S., Delahaye, A., Nectoux, J., and Bienvenu, T. (2013). Mutations in the C-terminus of CDKL5: proceed with caution. Eur. J. Hum. Genet.

Elia, M., Falco, M., Ferri, R., Spalletta, A., Bottitta, M., Calabrese, G., Carotenuto, M., Musumeci, S.A., Giudice, Lo, M., and Fichera, M. (2008). CDKL5 mutations in boys with severe encephalopathy and early-onset intractable epilepsy. Neurology *71*, 997–999.

Erez, A., Patel, A.J., Wang, X., Xia, Z., Bhatt, S.S., Craigen, W., Cheung, S.W., Lewis, R.A., Fang, P., Davenport, S.L.H., et al. (2009). Alu-specific microhomology-mediated deletions in CDKL5 in females with early-onset seizure disorder. Neurogenetics *10*, 363–369.

Ermel, E.L., Carneiro, L.C., Souza, C.F.M. de, Crippa, A.C. de S., Sanseverino, M.T.V., and Raskin, S. (2013). Epileptic encephalopathy and atypical Rett syndrome with mutations in CDKL5: clinical and molecular characterization of two Brazilian patients. Arq Neuropsiquiatr *71*, 414–415.

Evans, J.C., Archer, H.L., Colley, J.P., Ravn, K., Nielsen, J.B., Kerr, A., Williams, E., Christodoulou, J., Gécz, J., Jardine, P.E., et al. (2005). Early onset seizures and Rett-like features associated with

mutations in CDKL5. Eur. J. Hum. Genet. *13*, 1113–1120.

Fan, G., Beard, C., Chen, R.Z., Csankovszki, G., Sun, Y., Siniaia, M., Biniszkiewicz, D., Bates, B., Lee, P.P., Kuhn, R., et al. (2001). DNA hypomethylation perturbs the function and survival of CNS neurons in postnatal animals. Journal of Neuroscience *21*, 788–797.

Fehr, S., Wilson, M., Downs, J., Williams, S., Murgia, A., Sartori, S., Vecchi, M., Ho, G., Polli, R., Psoni, S., et al. (2012). The CDKL5 disorder is an independent clinical entity associated with early-onset encephalopathy. Eur. J. Hum. Genet.

Feng, G., Mellor, R.H., Bernstein, M., Keller-Peck, C., Nguyen, Q.T., Wallace, M., Nerbonne, J.M., Lichtman, J.W., and Sanes, J.R. (2000). Imaging neuronal subsets in transgenic mice expressing multiple spectral variants of GFP. Neuron *28*, 41–51.

Fichou, Y., Nectoux, J., Bahi-Buisson, N., Chelly, J., and Bienvenu, T. (2011). An isoform of the severe encephalopathy-related CDKL5 gene, including a novel exon with extremely high sequence conservation, is specifically expressed in brain. J. Hum. Genet. *56*, 52–57.

Foster, B.A., Coffey, H.A., Morin, M.J., and Rastinejad, F. (1999). Pharmacological rescue of mutant p53 conformation and function. Science *286*, 2507–2510.

Foxe, J.J., and Snyder, A.C. (2011). The Role of Alpha-Band Brain Oscillations as a Sensory Suppression Mechanism during Selective Attention. Front Psychol *2*, 154.

Froyen, G., Van Esch, H., Bauters, M., Hollanders, K., Frints, S.G.M., Vermeesch, J.R., Devriendt, K., Fryns, J.-P., and Marynen, P. (2007). Detection of genomic copy number changes in patients with idiopathic mental retardation by high-resolution X-array-CGH: important role for increased gene dosage of XLMR genes. Hum. Mutat. *28*, 1034–1042.

Fuchs, C., Trazzi, S., Torricella, R., Viggiano, R., De Franceschi, M., Amendola, E., Gross, C., Calzà, L., Bartesaghi, R., and Ciani, E. (2014). Loss of CDKL5 impairs survival and dendritic growth of newborn neurons by altering AKT/GSK-3β signaling. Neurobiol. Dis. *70C*, 53–68.

Fukuda, T., Itoh, M., Ichikawa, T., Washiyama, K., and Goto, Y.-I. (2005). Delayed maturation of neuronal architecture and synaptogenesis in cerebral cortex of Mecp2-deficient mice. J. Neuropathol. Exp. Neurol. *64*, 537–544.

Gandal, M.J., Edgar, J.C., Ehrlichman, R.S., Mehta, M., Roberts, T.P.L., and Siegel, S.J. (2010). Validating γ Oscillations and Delayed Auditory Responses as Translational Biomarkers of Autism. Biological Psychiatry *68*, 1100–1106.

Gandal, M.J., Edgar, J.C., Klook, K., and Siegel, S.J. (2012). Gamma synchrony: towards a translational biomarker for the treatment-resistant symptoms of schizophrenia. Neuropharmacology *62*, 1504–1518.

Gantois, I., Fang, K., Jiang, L., Babovic, D., Lawrence, A.J., Ferreri, V., Teper, Y., Jupp, B., Ziebell, J., Morganti-Kossmann, C.M., et al. (2007). Ablation of D1 dopamine receptor-expressing cells

generates mice with seizures, dystonia, hyperactivity, and impaired oral behavior. Proceedings of the National Academy of Sciences of the United States of America *104*, 4182–4187.

Geschwind, D.H. (2009). Advances in autism. Annu. Rev. Med. *60*, 367–380.

Geschwind, D.H. (2011). Genetics of autism spectrum disorders. Trends Cogn. Sci. (Regul. Ed.) *15*, 409–416.

Giacometti, E., Luikenhuis, S., Beard, C., and Jaenisch, R. (2007). Partial rescue of MeCP2 deficiency by postnatal activation of MeCP2. Proceedings of the National Academy of Sciences of the United States of America *104*, 1931–1936.

Gkogkas, C.G., Khoutorsky, A., Ran, I., Rampakakis, E., Nevarko, T., Weatherill, D.B., Vasuta, C., Yee, S., Truitt, M., Dallaire, P., et al. (2012). Autism-related deficits via dysregulated eIF4E-dependent translational control. Nature.

Goebbels, S., Bormuth, I., Bode, U., Hermanson, O., Schwab, M.H., and Nave, K.-A. (2006). Genetic targeting of principal neurons in neocortex and hippocampus of NEX-Cre mice. Genesis *44*, 611–621.

Goffin, D., and Zhou, Z. (2012). The neural circuit basis of Rett syndrome. Front. Biol. *7*, 428–435.

Goffin, D., Allen, M., Zhang, L., Amorim, M., Wang, I.-T.J., Reyes, A.-R.S., Mercado-Berton, A., Ong, C., Cohen, S., Hu, L., et al. (2012). Rett syndrome mutation MeCP2 T158A disrupts DNA binding, protein stability and ERP responses. Nat Neurosci *15*, 274–283.

Goffin, D., Brodkin, E.S., Blendy, J.A., Siegel, S.J., and Zhou, Z. (2014). Cellular origins of auditory event-related potential deficits in Rett syndrome. Nat Neurosci *17*, 804–806.

Grosso, S., Brogna, A., Bazzotti, S., Renieri, A., Morgese, G., and Balestri, P. (2007). Seizures and electroencephalographic findings in CDKL5 mutations: case report and review. Brain and Development *29*, 239–242.

Guerrini, R., and Parrini, E. (2012). Epilepsy in Rett syndrome, and CDKL5- and FOXG1-gene-related encephalopathies. Epilepsia.

Guy, J., Hendrich, B., Holmes, M., Martin, J.E., and Bird, A. (2001). A mouse Mecp2-null mutation causes neurological symptoms that mimic Rett syndrome. Nat. Genet. *27*, 322–326.

Guy, J., Gan, J., Selfridge, J., Cobb, S., and Bird, A. (2007). Reversal of neurological defects in a mouse model of Rett syndrome. Science *315*, 1143–1147.

Hadzsiev, K., Polgár, N., Bene, J., Komlosi, K., Karteszi, J., Hollody, K., Kosztolanyi, G., Renieri, A., and Melegh, B. (2011). Analysis of Hungarian patients with Rett syndrome phenotype for MECP2, CDKL5 and FOXG1 gene mutations. J. Hum. Genet. *56*, 183–187.

Hagebeuk, E.E.O., van den Bossche, R.A.S., and de Weerd, A.W. (2013). Respiratory and sleep

disorders in female children with atypical Rett syndrome caused by mutations in the CDKL5 gene. Dev Med Child Neurol *55*, 480–484.

Hanefeld, F. (1985). The clinical pattern of the Rett syndrome. Brain and Development *7*, 320–325.

Ho, K.L., McNae, I.W., Schmiedeberg, L., Klose, R.J., Bird, A.P., and Walkinshaw, M.D. (2008). MeCP2 binding to DNA depends upon hydration at methyl-CpG. Mol. Cell *29*, 525–531.

Hong, W., Kim, D.-W., and Anderson, D.J. (2014). Antagonistic control of social versus repetitive self-grooming behaviors by separable amygdala neuronal subsets. Cell *158*, 1348–1361.

Huppke, P., Ohlenbusch, A., Brendel, C., Laccone, F., and Gärtner, J. (2005). Mutation analysis of the HDAC 1, 2, 8 and CDKL5 genes in Rett syndrome patients without mutations in MECP2. Am. J. Med. Genet. A *137*, 136–138.

Intusoma, U., Hayeeduereh, F., Plong-On, O., Sripo, T., Vasiknanonte, P., Janjindamai, S., Lusawat, A., Thammongkol, S., Visudtibhan, A., and Limprasert, P. (2011). Mutation screening of the CDKL5 gene in cryptogenic infantile intractable epilepsy and review of clinical sensitivity. Eur. J. Paediatr. Neurol. *15*, 432–438.

Jähn, J., Caliebe, A., Spiczak, von, S., Boor, R., Stefanova, I., Stephani, U., Helbig, I., and Muhle, H. (2013). CDKL5 mutations as a cause of severe epilepsy in infancy: clinical and electroencephalographic long-term course in 4 patients. Journal of Child Neurology *28*, 937–941.

Jellinger, K., Armstrong, D., Zoghbi, H.Y., and Percy, A.K. (1988). Neuropathology of Rett syndrome. Acta Neuropathol. *76*, 142–158.

Jentarra, G.M., Olfers, S.L., Rice, S.G., Srivastava, N., Homanics, G.E., Blue, M., Naidu, S., and Narayanan, V. (2010). Abnormalities of cell packing density and dendritic complexity in the MeCP2 A140V mouse model of Rett syndrome/X-linked mental retardation. BMC Neurosci *11*, 19.

Jeste, S.S., Sahin, M., Bolton, P., Ploubidis, G.B., and Humphrey, A. (2008). Characterization of autism in young children with tuberous sclerosis complex. Journal of Child Neurology *23*, 520–525.

Jones, P.L., Veenstra, G.J., Wade, P.A., Vermaak, D., Kass, S.U., Landsberger, N., Strouboulis, J., and Wolffe, A.P. (1998). Methylated DNA and MeCP2 recruit histone deacetylase to repress transcription. Nat. Genet. *19*, 187–191.

Jugloff, D.G.M., Jung, B.P., Purushotham, D., Logan, R., and Eubanks, J.H. (2005). Increased dendritic complexity and axonal length in cultured mouse cortical neurons overexpressing methyl-CpG-binding protein MeCP2. Neurobiol. Dis. *19*, 18–27.

Ka, M., Condorelli, G., Woodgett, J.R., and Kim, W.-Y. (2014). mTOR regulates brain morphogenesis by mediating GSK3 signaling. Development.

Kalscheuer, V.M., Tao, J., Donnelly, A., Hollway, G., Schwinger, E., Kübart, S., Menzel, C., Hoeltzenbein, M., Tommerup, N., Eyre, H., et al. (2003). Disruption of the serine/threonine kinase 9 gene causes severe X-linked infantile spasms and mental retardation. Am. J. Hum. Genet. *72*, 1401–1411.

Kameshita, I., Sekiguchi, M., Hamasaki, D., Sugiyama, Y., Hatano, N., Suetake, I., Tajima, S., and Sueyoshi, N. (2008). Cyclin-dependent kinase-like 5 binds and phosphorylates DNA methyltransferase 1. Biochem. Biophys. Res. Commun. *377*, 1162–1167.

Kankirawatana, P., Leonard, H., Ellaway, C., Scurlock, J., Mansour, A., Makris, C.M., Dure, L.S., Friez, M., Lane, J., Kiraly-Borri, C., et al. (2006). Early progressive encephalopathy in boys and MECP2 mutations. Neurology *67*, 164–166.

Katz, D.M., Berger-Sweeney, J.E., Eubanks, J.H., Justice, M.J., Neul, J.L., Pozzo-Miller, L., Blue, M.E., Christian, D., Crawley, J.N., Giustetto, M., et al. (2012). Preclinical research in Rett syndrome: setting the foundation for translational success. Dis Model Mech *5*, 733–745.

Kaufmann, W.E., and Moser, H.W. (2000). Dendritic anomalies in disorders associated with mental retardation. Cereb. Cortex *10*, 981–991.

Kerr, B., Alvarez-Saavedra, M., Sáez, M.A., Saona, A., and Young, J.I. (2008). Defective body-weight regulation, motor control and abnormal social interactions in Mecp2 hypomorphic mice. Human Molecular Genetics *17*, 1707–1717.

Kilstrup-Nielsen, C., Rusconi, L., La Montanara, P., Ciceri, D., Bergo, A., Bedogni, F., and Landsberger, N. (2012). What We Know and Would Like to Know about CDKL5 and Its Involvement in Epileptic Encephalopathy. Neural Plast. *2012*, 728267.

Kishi, N., and Macklis, J.D. (2004). MECP2 is progressively expressed in post-migratory neurons and is involved in neuronal maturation rather than cell fate decisions. Mol. Cell. Neurosci. *27*, 306–321.

Klein, K.M., Yendle, S.C., Harvey, A.S., Antony, J.H., Wallace, G., Bienvenu, T., and Scheffer, I.E. (2011). A distinctive seizure type in patients with CDKL5 mutations: Hypermotor-tonic-spasms sequence. Neurology *76*, 1436–1438.

Kriaucionis, S., and Bird, A. (2003). DNA methylation and Rett syndrome. Human Molecular Genetics *12 Spec No 2*, R221–R227.

Larimore, J.L., Chapleau, C.A., Kudo, S., Theibert, A., Percy, A.K., and Pozzo-Miller, L. (2009). Bdnf overexpression in hippocampal neurons prevents dendritic atrophy caused by Rett-associated MECP2 mutations. Neurobiol. Dis. *34*, 199–211.

Leutgeb, J.K., Leutgeb, S., Moser, M.-B., and Moser, E.I. (2007). Pattern separation in the dentate gyrus and CA3 of the hippocampus. Science *315*, 961–966.

Li, M.-R., Pan, H., Bao, X.-H., Zhang, Y.-Z., and Wu, X.-R. (2007). MECP2 and CDKL5 gene

mutation analysis in Chinese patients with Rett syndrome. J. Hum. Genet. *52*, 38–47.

Li, M.-R., Pan, H., Bao, X.-H., Zhu, X.-W., Cao, G.-N., Zhang, Y.-Z., and Wu, X.-R. (2009). [Methyl-CpG-binding protein 2 gene and CDKL5 gene mutation in patients with Rett syndrome: analysis of 177 Chinese pediatric patients]. Zhonghua Yi Xue Za Zhi *89*, 224–229.

Liang, J.-S., Shimojima, K., Takayama, R., Natsume, J., Shichiji, M., Hirasawa, K., Imai, K., Okanishi, T., Mizuno, S., Okumura, A., et al. (2011). CDKL5 alterations lead to early epileptic encephalopathy in both genders. Epilepsia *52*, 1835–1842.

Liao, W., Gandal, M.J., Ehrlichman, R.S., Siegel, S.J., and Carlson, G.C. (2012). MeCP2+/- mouse model of RTT reproduces auditory phenotypes associated with Rett syndrome and replicate select EEG endophenotypes of autism spectrum disorder. Neurobiol. Dis. *46*, 88–92.

Lin, C., Franco, B., and Rosner, M.R. (2005). CDKL5/Stk9 kinase inactivation is associated with neuronal developmental disorders. Human Molecular Genetics *14*, 3775–3786.

Lioy, D.T., Garg, S.K., Monaghan, C.E., Raber, J., Foust, K.D., Kaspar, B.K., Hirrlinger, P.G., Kirchhoff, F., Bissonnette, J.M., Ballas, N., et al. (2011). A role for glia in the progression of Rett's syndrome. Nature *475*, 497–500.

Livide, G., Patriarchi, T., Amenduni, M., Amabile, S., Yasui, D., Calcagno, E., Rizzo, Lo, C., De Falco, G., Ulivieri, C., Ariani, F., et al. (2014). GluD1 is a common altered player in neuronal differentiation from both MECP2-mutated and CDKL5-mutated iPS cells. Eur. J. Hum. Genet.

Luikenhuis, S., Giacometti, E., Beard, C.F., and Jaenisch, R. (2004). Expression of MeCP2 in postmitotic neurons rescues Rett syndrome in mice. Proceedings of the National Academy of Sciences of the United States of America *101*, 6033–6038.

Maortua, H., Martínez-Bouzas, C., Calvo, M.-T., Domingo, M.-R., Ramos, F., García-Ribes, A., Martínez, M.-J., López-Aríztegui, M.-A., Puente, N., Rubio, I., et al. (2012). CDKL5 gene status in female patients with epilepsy and Rett-like features: two new mutations in the catalytic domain. BMC Med. Genet. *13*, 68.

Marchetto, M.C.N., Carromeu, C., Acab, A., Yu, D., Yeo, G.W., Mu, Y., Chen, G., Gage, F.H., and Muotri, A.R. (2010). A model for neural development and treatment of Rett syndrome using human induced pluripotent stem cells. Cell *143*, 527–539.

Mari, F., Azimonti, S., Bertani, I., Bolognese, F., Colombo, E., Caselli, R., Scala, E., Longo, I., Grosso, S., Pescucci, C., et al. (2005). CDKL5 belongs to the same molecular pathway of MeCP2 and it is responsible for the early-onset seizure variant of Rett syndrome. Human Molecular Genetics *14*, 1935–1946.

Marshak, S., Meynard, M.M., De Vries, Y.A., Kidane, A.H., and Cohen-Cory, S. (2012). Cell-Autonomous Alterations in Dendritic Arbor Morphology and Connectivity Induced by Overexpression of MeCP2 in Xenopus Central Neurons In Vivo. PLoS ONE *7*, e33153.

Masliah-Plachon, J., Auvin, S., Nectoux, J., Fichou, Y., Chelly, J., and Bienvenu, T. (2010). Somatic mosaicism for a CDKL5 mutation as an epileptic encephalopathy in males. Am. J. Med. Genet. A *152A*, 2110–2111.

Mastrangelo, M., and Leuzzi, V. (2012). Genes of early-onset epileptic encephalopathies: from genotype to phenotype. Pediatr. Neurol. *46*, 24–31.

McLin, J.P., and Steward, O. (2006). Comparison of seizure phenotype and neurodegeneration induced by systemic kainic acid in inbred, outbred, and hybrid mouse strains. Eur. J. Neurosci. *24*, 2191–2202.

Mei, D., Darra, F., Barba, C., Marini, C., Fontana, E., Chiti, L., Parrini, E., Dalla Bernardina, B., and Guerrini, R. (2014). Optimizing the molecular diagnosis of CDKL5 gene-related epileptic encephalopathy in boys. Epilepsia.

Mei, D., Marini, C., Novara, F., Bernardina, B.D., Granata, T., Fontana, E., Parrini, E., Ferrari, A.R., Murgia, A., Zuffardi, O., et al. (2010). Xp22.3 genomic deletions involving the CDKL5 gene in girls with early onset epileptic encephalopathy. Epilepsia *51*, 647–654.

Melani, F., Mei, D., Pisano, T., Savasta, S., Franzoni, E., Ferrari, A.R., Marini, C., and Guerrini, R. (2011). CDKL5 gene-related epileptic encephalopathy: electroclinical findings in the first year of life. Dev Med Child Neurol *53*, 354–360.

Metcalf, B.M., Mullaney, B.C., Johnston, M.V., and Blue, M.E. (2006). Temporal shift in methyl-CpG binding protein 2 expression in a mouse model of Rett syndrome. Neuroscience *139*, 1449–1460.

Mirzaa, G.M., Paciorkowski, A.R., Marsh, E.D., Berry-Kravis, E.M., Medne, L., Grix, A., Wirrell, E.C., Powell, B.R., Nickels, K.C., Burton, B., et al. (2013). CDKL5 and ARX mutations in males with early-onset epilepsy. Pediatr. Neurol. *48*, 367–377.

Monory, K., Massa, F., Egertová, M., Eder, M., Blaudzun, H., Westenbroek, R., Kelsch, W., Jacob, W., Marsch, R., Ekker, M., et al. (2006). The endocannabinoid system controls key epileptogenic circuits in the hippocampus. Neuron *51*, 455–466.

Montini, E., Andolfi, G., Caruso, A., Buchner, G., Walpole, S.M., Mariani, M., Consalez, G., Trump, D., Ballabio, A., and Franco, B. (1998). Identification and characterization of a novel serine-threonine kinase gene from the Xp22 region. Genomics *51*, 427–433.

Moretti, P., Levenson, J.M., Battaglia, F., Atkinson, R., Teague, R., Antalffy, B., Armstrong, D., Arancio, O., Sweatt, J.D., and Zoghbi, H.Y. (2006). Learning and memory and synaptic plasticity are impaired in a mouse model of Rett syndrome. Journal of Neuroscience *26*, 319–327.

Moritz, A., Li, Y., Guo, A., Villén, J., Wang, Y., Macneill, J., Kornhauser, J., Sprott, K., Zhou, J., Possemato, A., et al. (2010). Akt-RSK-S6 kinase signaling networks activated by oncogenic receptor tyrosine kinases. Sci Signal *3*, ra64.

Moseley, B.D., Dhamija, R., Wirrell, E.C., and Nickels, K.C. (2012). Historic, Clinical, and Prognostic Features of Epileptic Encephalopathies Caused by CDKL5 Mutations. Pediatr. Neurol. *46*, 101–105.

Na, E.S., Nelson, E.D., Adachi, M., Autry, A.E., Mahgoub, M.A., Kavalali, E.T., and Monteggia, L.M. (2012). A Mouse Model for MeCP2 Duplication Syndrome: MeCP2 Overexpression Impairs Learning and Memory and Synaptic Transmission. Journal of Neuroscience *32*, 3109–3117.

Nabbout, R., and Dulac, O. (2011). Epilepsy. Genetics of early-onset epilepsy with encephalopathy. Nat Rev Neurol *8*, 129–130.

Nakatani, J., Tamada, K., Hatanaka, F., Ise, S., Ohta, H., Inoue, K., Tomonaga, S., Watanabe, Y., Chung, Y.J., Banerjee, R., et al. (2009). Abnormal behavior in a chromosome-engineered mouse model for human 15q11-13 duplication seen in autism. Cell *137*, 1235–1246.

Nan, X., Campoy, F.J., and Bird, A. (1997). MeCP2 is a transcriptional repressor with abundant binding sites in genomic chromatin. Cell *88*, 471–481.

Nectoux, J., Héron, D., Tallot, M., Chelly, J., and Bienvenu, T. (2006). Maternal origin of a novel C-terminal truncation mutation in CDKL5 causing a severe atypical form of Rett syndrome. Clinical Genetics *70*, 29–33.

Nectoux, J., Fichou, Y., Cagnard, N., Bahi-Buisson, N., Nusbaum, P., Letourneur, F., Chelly, J., and Bienvenu, T. (2011). Cell cloning-based transcriptome analysis in cyclin-dependent kinase-like 5 mutation patients with severe epileptic encephalopathy. J. Mol. Med. *89*, 193–202.

Nemos, C., Lambert, L., Giuliano, F., Doray, B., Roubertie, A., Goldenberg, A., Delobel, B., Layet, V., N'guyen, M., Saunier, A., et al. (2009). Mutational spectrum of CDKL5in early-onset encephalopathies: a study of a large collection of French patients and review of the literature. Clinical Genetics *76*, 357–371.

Neul, J.L., Kaufmann, W.E., Glaze, D.G., Christodoulou, J., Clarke, A.J., Bahi-Buisson, N., Leonard, H., Bailey, M.E.S., Schanen, N.C., Zappella, M., et al. (2010). Rett syndrome: revised diagnostic criteria and nomenclature. Ann. Neurol. *68*, 944–950.

Nuber, U.A., Kriaucionis, S., Roloff, T.C., Guy, J., Selfridge, J., Steinhoff, C., Schulz, R., Lipkowitz, B., Ropers, H.H., Holmes, M.C., et al. (2005). Up-regulation of glucocorticoid-regulated genes in a mouse model of Rett syndrome. Human Molecular Genetics *14*, 2247–2256.

Ozkan, E.D., Creson, T.K., Kramár, E.A., Rojas, C., Seese, R.R., Babyan, A.H., Shi, Y., Lucero, R., Xu, X., Noebels, J.L., et al. (2014). Reduced Cognition in Syngap1 Mutants Is Caused by Isolated Damage within Developing Forebrain Excitatory Neurons. Neuron *82*, 1317–1333.

Paine, S.M.L., Munot, P., Carmichael, J., Das, K., Weber, M.A., Prabhakar, P., and Jacques, T.S. (2012). The neuropathological consequences of CDKL5 mutation. Neuropathol Appl Neurobiol *38*, 744–747.

Palva, S., and Palva, J.M. (2007). New vistas for alpha-frequency band oscillations. Trends Neurosci. *30*, 150–158.

Pathak, H.R., Weissinger, F., Terunuma, M., Carlson, G.C., Hsu, F.-C., Moss, S.J., and Coulter, D.A. (2007). Disrupted dentate granule cell chloride regulation enhances synaptic excitability during development of temporal lobe epilepsy. Journal of Neuroscience *27*, 14012–14022.

Peça, J., Feliciano, C., Ting, J.T., Wang, W., Wells, M.F., Venkatraman, T.N., Lascola, C.D., Fu, Z., and Feng, G. (2011). Shank3 mutant mice display autistic-like behaviours and striatal dysfunction. Nature *472*, 437–442.

Pelka, G.J., Watson, C.M., Radziewic, T., Hayward, M., Lahooti, H., Christodoulou, J., and Tam, P.P.L. (2006). Mecp2 deficiency is associated with learning and cognitive deficits and altered gene activity in the hippocampal region of mice. Brain *129*, 887–898.

Peñagarikano, O., Peñagarikano, O., Abrahams, B.S., Abrahams, B.S., Herman, E.I., Herman, E.I., Winden, K.D., Winden, K.D., Gdalyahu, A., Gdalyahu, A., et al. (2011). Absence of CNTNAP2 Leads to Epilepsy, Neuronal Migration Abnormalities, and Core Autism-Related Deficits. Cell *147*, 235–246.

Peters, H.C., Hu, H., Pongs, O., Storm, J.F., and Isbrandt, D. (2005). Conditional transgenic suppression of M channels in mouse brain reveals functions in neuronal excitability, resonance and behavior. Nat Neurosci *8*, 51–60.

Pini, G., Bigoni, S., Engerström, I.W., Calabrese, O., Felloni, B., Scusa, M.F., Di Marco, P., Borelli, P., Bonuccelli, U., Julu, P.O.O., et al. (2013). Variant of Rett Syndrome and CDKL5 Gene: Clinical and Autonomic Description of 10 Cases. *43*, 37–43.

Pintaudi, M., Baglietto, M.G., Gaggero, R., Parodi, E., Pessagno, A., Marchi, M., Russo, S., and Veneselli, E. (2008). Clinical and electroencephalographic features in patients with CDKL5 mutations: two new Italian cases and review of the literature. Epilepsy Behav *12*, 326–331.

Prince, E., and Ring, H. (2011). Causes of learning disability and epilepsy: a review. Curr. Opin. Neurol. *24*, 154–158.

Psoni, S., Willems, P.J., Kanavakis, E., Mavrou, A., Frissyra, H., Traeger-Synodinos, J., Sofokleous, C., Makrythanassis, P., and Kitsiou-Tzeli, S. (2010). A novel p.Arg970X mutation in the last exon of the CDKL5 gene resulting in late-onset seizure disorder. Eur. J. Paediatr. Neurol. *14*, 188–191.

Rademacher, N., Hambrock, M., Fischer, U., Moser, B., Ceulemans, B., Lieb, W., Boor, R., Stefanova, I., Gillessen-Kaesbach, G., Runge, C., et al. (2011). Identification of a novel CDKL5 exon and pathogenic mutations in patients with severe mental retardation, early-onset seizures and Rett-like features. Neurogenetics *12*, 165–167.

Rajaei, S., Rajaei, S., Erlandson, A., Erlandson, A., Kyllerman, M., Kyllerman, M., Albage, M., Albage, M., Lundstrom, I., Lundstrom, I., et al. (2011). Early Infantile Onset ''Congenital“” Rett Syndrome Variants: Swedish Experience Through Four Decades and Mutation Analysis. Journal

of Child Neurology *26*, 65–71.

Ramocki, M.B., Peters, S.U., Tavyev, Y.J., Zhang, F., Carvalho, C.M.B., Schaaf, C.P., Richman, R., Fang, P., Glaze, D.G., Lupski, J.R., et al. (2009). Autism and other neuropsychiatric symptoms are prevalent in individuals with MeCP2 duplication syndrome. Ann. Neurol. *66*, 771–782.

Raymond, L., Diebold, B., Leroux, C., Maurey, H., Drouin-Garraud, V., Delahaye, A., Dulac, O., Metreau, J., Melikishvili, G., Toutain, A., et al. (2013). Validation of high-resolution DNA melting analysis for mutation scanning of the CDKL5 gene: identification of novel mutations. Gene *512*, 70–75.

Redondo, R.L., Kim, J., Arons, A.L., Ramirez, S., Liu, X., and Tonegawa, S. (2014). Bidirectional switch of the valence associated with a hippocampal contextual memory engram. Nature *513*, 426–430.

Ricciardi, S., Boggio, E.M., Grosso, S., Lonetti, G., Forlani, G., Stefanelli, G., Calcagno, E., Morello, N., Landsberger, N., Biffo, S., et al. (2011). Reduced AKT/mTOR signaling and protein synthesis dysregulation in a Rett syndrome animal model. Human Molecular Genetics *20*, 1182–1196.

Ricciardi, S., Kilstrup-Nielsen, C., Bienvenu, T., Jacquette, A., Landsberger, N., and Broccoli, V. (2009). CDKL5 influences RNA splicing activity by its association to the nuclear speckle molecular machinery. Human Molecular Genetics *18*, 4590–4602.

Ricciardi, S., Ungaro, F., Hambrock, M., Rademacher, N., Stefanelli, G., Brambilla, D., Sessa, A., Magagnotti, C., Bachi, A., Giarda, E., et al. (2012). CDKL5 ensures excitatory synapse stability by reinforcing NGL-1-PSD95 interaction in the postsynaptic compartment and is impaired in patient iPSC-derived neurons. Nat. Cell Biol. *14*, 911–923.

Roberts, T.P.L., Khan, S.Y., Rey, M., Monroe, J.F., Cannon, K., Blaskey, L., Woldoff, S., Qasmieh, S., Gandal, M., Schmidt, G.L., et al. (2010). MEG detection of delayed auditory evoked responses in autism spectrum disorders: towards an imaging biomarker for autism. Autism Res *3*, 8–18.

Robinson, L., Guy, J., McKay, L., Brockett, E., Spike, R.C., Selfridge, J., De Sousa, D., Merusi, C., Riedel, G., Bird, A., et al. (2012). Morphological and functional reversal of phenotypes in a mouse model of Rett syndrome. Brain *135*, 2699–2710.

Rosas-Vargas, H., Bahi-Buisson, N., Philippe, C., Nectoux, J., Girard, B., N'Guyen Morel, M.A., Gitiaux, C., Lazaro, L., Odent, S., Jonveaux, P., et al. (2008). Impairment of CDKL5 nuclear localisation as a cause for severe infantile encephalopathy. Journal of Medical Genetics *45*, 172–178.

Rosner, M., Siegel, N., Valli, A., Fuchs, C., and Hengstschläger, M. (2010). mTOR phosphorylated at S2448 binds to raptor and rictor. Amino Acids *38*, 223–228.

Rubenstein, J.L.R., and Merzenich, M.M. (2003). Model of autism: increased ratio of excitation/inhibition in key neural systems. Genes Brain Behav. *2*, 255–267.

Rusconi, L., Kilstrup-Nielsen, C., and Landsberger, N. (2011). Extrasynaptic NMDA receptor stimulation induces CDKL5 cytoplasmic translocation and proteasomal degradation. J. Biol. Chem.

Rusconi, L., Salvatoni, L., Giudici, L., Bertani, I., Kilstrup-Nielsen, C., Broccoli, V., and Landsberger, N. (2008). CDKL5 expression is modulated during neuronal development and its subcellular distribution is tightly regulated by the C-terminal tail. J. Biol. Chem. *283*, 30101–30111.

Russo, S., Marchi, M., Cogliati, F., Bonati, M.T., Pintaudi, M., Veneselli, E., Saletti, V., Balestrini, M., Ben-Zeev, B., and Larizza, L. (2009). Novel mutations in the CDKL5 gene, predicted effects and associated phenotypes. Neurogenetics *10*, 241–250.

Saitsu, H., Osaka, H., Nishiyama, K., Tsurusaki, Y., Doi, H., Miyake, N., and Matsumoto, N. (2012). A girl with early-onset epileptic encephalopathy associated with microdeletion involving CDKL5. Brain and Development *34*, 364–367.

Sakai, Y., Shaw, C.A., Dawson, B.C., Dugas, D.V., Al-Mohtaseb, Z., Hill, D.E., and Zoghbi, H.Y. (2011). Protein interactome reveals converging molecular pathways among autism disorders. Sci Transl Med *3*, 86ra49.

Samaco, R.C., Fryer, J.D., Ren, J., Fyffe, S., Chao, H.-T., Sun, Y., Greer, J.J., Zoghbi, H.Y., and Neul, J.L. (2008). A partial loss of function allele of methyl-CpG-binding protein 2 predicts a human neurodevelopmental syndrome. Human Molecular Genetics *17*, 1718–1727.

Samaco, R.C., McGraw, C.M., Ward, C.S., Sun, Y., Neul, J.L., and Zoghbi, H.Y. (2012). Female Mecp2+/- mice display robust behavioral deficits on two different genetic backgrounds providing a framework for pre-clinical studies. Human Molecular Genetics.

Sankoorikal, G.M.V., Kaercher, K.A., Boon, C.J., Lee, J.K., and Brodkin, E.S. (2006). A mouse model system for genetic analysis of sociability: C57BL/6J versus BALB/cJ inbred mouse strains. Biological Psychiatry *59*, 415–423.

Santini, E., Huynh, T.N., MacAskill, A.F., Carter, A.G., Pierre, P., Ruggero, D., Kaphzan, H., and Klann, E. (2013). Exaggerated translation causes synaptic and behavioural aberrations associated with autism. Nature *493*, 411–415.

Sartori, S., Di Rosa, G., Polli, R., Bettella, E., Tricomi, G., Tortorella, G., and Murgia, A. (2009). A novel CDKL5 mutation in a 47,XXY boy with the early-onset seizure variant of Rett syndrome. Am. J. Med. Genet. A *149A*, 232–236.

Scala, E., Ariani, F., Mari, F., Caselli, R., Pescucci, C., Longo, I., Meloni, I., Giachino, D., Bruttini, M., Hayek, G., et al. (2005). CDKL5/STK9 is mutated in Rett syndrome variant with infantile spasms. Journal of Medical Genetics *42*, 103–107.

Schanen, C., Houwink, E.J.F., Dorrani, N., Lane, J., Everett, R., Feng, A., Cantor, R.M., and Percy, A. (2004). Phenotypic manifestations of MECP2 mutations in classical and atypical Rett syndrome. Am. J. Med. Genet. A *126A*, 129–140.

Schmeisser, M.J., Ey, E., Wegener, S., Bockmann, J., Stempel, A.V., Kuebler, A., Janssen, A.-L., Udvardi, P.T., Shiban, E., Spilker, C., et al. (2012). Autistic-like behaviours and hyperactivity in mice lacking ProSAP1/Shank2. Nature *486*, 256–260.

Sekiguchi, M., Katayama, S., Hatano, N., Shigeri, Y., Sueyoshi, N., and Kameshita, I. (2013). Identification of amphiphysin 1 as an endogenous substrate for CDKL5, a protein kinase associated with X-linked neurodevelopmental disorder. Arch. Biochem. Biophys. *535*, 257–267.

Shahbazian, M.D., Antalffy, B., Armstrong, D.L., and Zoghbi, H.Y. (2002a). Insight into Rett syndrome: MeCP2 levels display tissue- and cell-specific differences and correlate with neuronal maturation. Human Molecular Genetics *11*, 115–124.

Shahbazian, M., Young, J., Yuva-Paylor, L., Spencer, C., Antalffy, B., Noebels, J., Armstrong, D., Paylor, R., and Zoghbi, H. (2002b). Mice with truncated MeCP2 recapitulate many Rett syndrome features and display hyperacetylation of histone H3. Neuron *35*, 243–254.

SHOLL, D.A. (1953). Dendritic organization in the neurons of the visual and motor cortices of the cat. J. Anat. *87*, 387–406.

Silverman, J.L., Yang, M., Lord, C., and Crawley, J.N. (2010). Behavioural phenotyping assays for mouse models of autism. Nat. Rev. Neurosci. *11*, 490–502.

Skene, P.J., Illingworth, R.S., Webb, S., Kerr, A.R.W., James, K.D., Turner, D.J., Andrews, R., and Bird, A.P. (2010). Neuronal MeCP2 is expressed at near histone-octamer levels and globally alters the chromatin state. Mol. Cell *37*, 457–468.

Smrt, R.D., Eaves-Egenes, J., Barkho, B.Z., Santistevan, N.J., Zhao, C., Aimone, J.B., Gage, F.H., and Zhao, X. (2007). Mecp2 deficiency leads to delayed maturation and altered gene expression in hippocampal neurons. Neurobiol. Dis. *27*, 77–89.

Sprovieri, T., Conforti, F.L., Fiumara, A., Mazzei, R., Ungaro, C., Citrigno, L., Muglia, M., Arena, A., and Quattrone, A. (2009). A novel mutation in the X-linked cyclin-dependent kinase-like 5 (CDKL5) gene associated with a severe Rett phenotype. Am. J. Med. Genet. A *149A*, 722–725.

Spruston, N. (2008). Pyramidal neurons: dendritic structure and synaptic integration. Nat. Rev. Neurosci. *9*, 206–221.

Stalpers, X.L., Spruijt, L., Yntema, H.G., and Verrips, A. (2011). Clinical Phenotype of 5 Females With a CDKL5 Mutation. Journal of Child Neurology.

Stauder, J.E.A., Smeets, E.E.J., van Mil, S.G.M., and Curfs, L.G.M. (2006). The development of visual- and auditory processing in Rett syndrome: an ERP study. Brain and Development *28*, 487–494.

Stroganova, T.A., Nygren, G., Tsetlin, M.M., Posikera, I.N., Gillberg, C., Elam, M., and Orekhova, E.V. (2007). Abnormal EEG lateralization in boys with autism. Clin Neurophysiol *118*, 1842–1854.

Stuss, D.P., Boyd, J.D., Levin, D.B., and Delaney, K.R. (2012). MeCP2 Mutation Results in Compartment-Specific Reductions in Dendritic Branching and Spine Density in Layer 5 Motor Cortical Neurons of YFP-H Mice. PLoS ONE *7*, e31896.

Szafranski, P., Golla, S., Jin, W., Fang, P., Hixson, P., Matalon, R., Kinney, D., Bock, H.-G., Craigen, W., Smith, J.L., et al. (2014). Neurodevelopmental and neurobehavioral characteristics in males and females with CDKL5 duplications. Eur. J. Hum. Genet.

Takahashi, K., Tanabe, K., Ohnuki, M., Narita, M., Ichisaka, T., Tomoda, K., and Yamanaka, S. (2007). Induction of pluripotent stem cells from adult human fibroblasts by defined factors. Cell *131*, 861–872.

Talkowski, M.E., Rosenfeld, J.A., Blumenthal, I., Pillalamarri, V., Chiang, C., Heilbut, A., Ernst, C., Hanscom, C., Rossin, E., Lindgren, A.M., et al. (2012). Sequencing chromosomal abnormalities reveals neurodevelopmental loci that confer risk across diagnostic boundaries. Cell *149*, 525–537.

Tallon-Baudry, C., and Bertrand, O. (1999). Oscillatory gamma activity in humans and its role in object representation. Trends Cogn. Sci. (Regul. Ed.) *3*, 151–162.

Taneja, P., Ogier, M., Brooks-Harris, G., Schmid, D.A., Katz, D.M., and Nelson, S.B. (2009). Pathophysiology of locus ceruleus neurons in a mouse model of Rett syndrome. Journal of Neuroscience *29*, 12187–12195.

Tao, J., Van Esch, H., Hagedorn-Greiwe, M., Hoffmann, K., Moser, B., Raynaud, M., Sperner, J., Fryns, J.-P., Schwinger, E., Gécz, J., et al. (2004). Mutations in the X-linked cyclin-dependent kinase-like 5 (CDKL5/STK9) gene are associated with severe neurodevelopmental retardation. Am. J. Hum. Genet. *75*, 1149–1154.

Thompson, C.L., Ng, L., Menon, V., Martinez, S., Lee, C.-K., Glattfelder, K., Sunkin, S.M., Henry, A., Lau, C., Dang, C., et al. (2014). A high-resolution spatiotemporal atlas of gene expression of the developing mouse brain. Neuron *83*, 309–323.

Thorson, L., Bryke, C., Rice, G., Artzer, A., Schilz, C., Israel, J., Huber, S., Laffin, J., and Raca, G. (2010). Clinical and molecular characterization of overlapping interstitial Xp21-p22 duplications in two unrelated individuals. Am. J. Med. Genet. A *152A*, 904–915.

Tronche, F., Kellendonk, C., Kretz, O., Gass, P., Anlag, K., Orban, P.C., Bock, R., Klein, R., and Schutz, G. (1999). Disruption of the glucocorticoid receptor gene in the nervous system results in reduced anxiety. Nat. Genet. *23*, 99–103.

Tropea, D., Giacometti, E., Wilson, N.R., Beard, C., McCurry, C., Fu, D.D., Flannery, R., Jaenisch, R., and Sur, M. (2009). Partial reversal of Rett Syndrome-like symptoms in MeCP2 mutant mice. Proceedings of the National Academy of Sciences of the United States of America *106*, 2029–2034.

Tsai, P.T., Hull, C., Chu, Y., Greene-Colozzi, E., Sadowski, A.R., Leech, J.M., Steinberg, J., Crawley,

J.N., Regehr, W.G., and Sahin, M. (2012). Autistic-like behaviour and cerebellar dysfunction in Purkinje cell Tsc1 mutant mice. Nature *488*, 647–651.

Tyler, A.L., Mahoney, J.M., Richard, G.R., Holmes, G.L., Lenck-Santini, P.-P., and Scott, R.C. (2012). Functional network changes in hippocampal CA1 after status epilepticus predict spatial memory deficits in rats. Journal of Neuroscience *32*, 11365–11376.

Uhlhaas, P., and Singer, W. (2006). Neural Synchrony in Brain Disorders: Relevance for Cognitive Dysfunctions and Pathophysiology. Neuron *52*, 155–168.

Uhlhaas, P.J., and Singer, W. (2010). Abnormal neural oscillations and synchrony in schizophrenia. Nat. Rev. Neurosci. *11*, 100–113.

Uhlhaas, P.J., Pipa, G., Neuenschwander, S., Wibral, M., and Singer, W. (2011). A new look at gamma? High- (>60 Hz) γ-band activity in cortical networks: Function, mechanisms and impairment. Progress in Biophysics and Molecular Biology *105*, 14–28.

Vacca, M., Filippini, F., Budillon, A., Rossi, V., Ragione, Della, F., De Bonis, M.L., Mercadante, G., Manzati, E., Gualandi, F., Bigoni, S., et al. (2001). MECP2 gene mutation analysis in the British and Italian Rett Syndrome patients: hot spot map of the most recurrent mutations and bioinformatic analysis of a new MECP2 conserved region. Brain and Development *23 Suppl 1*, S246–S250.

Valli, E., Trazzi, S., Fuchs, C., Erriquez, D., Bartesaghi, R., Perini, G., and Ciani, E. (2012). CDKL5, a novel MYCN-repressed gene, blocks cell cycle and promotes differentiation of neuronal cells. Biochim. Biophys. Acta *1819*, 1173–1185.

Van Esch, H., Jansen, A., Bauters, M., Froyen, G., and Fryns, J.-P. (2007). Encephalopathy and bilateral cataract in a boy with an interstitial deletion of Xp22 comprising the CDKL5 and NHS genes. Am. J. Med. Genet. A *143*, 364–369.

Veeramah, K.R., Johnstone, L., Karafet, T.M., Wolf, D., Sprissler, R., Salogiannis, J., Barth-Maron, A., Greenberg, M.E., Stuhlmann, T., Weinert, S., et al. (2013). Exome sequencing reveals new causal mutations in children with epileptic encephalopathies. Epilepsia.

Viniegra, J.G., Martínez, N., Modirassari, P., Hernández Losa, J., Parada Cobo, C., Sánchez-Arévalo Lobo, V.J., Aceves Luquero, C.I., Alvarez-Vallina, L., Ramón y Cajal, S., Rojas, J.M., et al. (2005). Full activation of PKB/Akt in response to insulin or ionizing radiation is mediated through ATM. J. Biol. Chem. *280*, 4029–4036.

Voineagu, I., Wang, X., Johnston, P., Lowe, J.K., Tian, Y., Horvath, S., Mill, J., Cantor, R.M., Blencowe, B.J., and Geschwind, D.H. (2011). Transcriptomic analysis of autistic brain reveals convergent molecular pathology. Nature.

Vonhoff, F., Williams, A., Ryglewski, S., and Duch, C. (2012). Drosophila as a model for MECP2 gain of function in neurons. PLoS ONE *7*, e31835.

Wang, I.-T.J., Reyes, A.-R.S., and Zhou, Z. (2013). Neuronal morphology in MeCP2 mouse models is intrinsically variable and depends on age, cell type, and Mecp2 mutation. Neurobiol. Dis. *58C*, 3–12.

Wang, I.-T.J., Allen, M., Goffin, D., Zhu, X., Fairless, A.H., Brodkin, E.S., Siegel, S.J., Marsh, E.D., Blendy, J.A., and Zhou, Z. (2012). Loss of CDKL5 disrupts kinome profile and event-related potentials leading to autistic-like phenotypes in mice. Proceedings of the National Academy of Sciences of the United States of America *109*, 21516–21521.

Ward, L.M. (2003). Synchronous neural oscillations and cognitive processes. Trends Cogn. Sci. (Regul. Ed.) *7*, 553–559.

Weaving, L.S., Christodoulou, J., Williamson, S.L., Friend, K.L., McKenzie, O.L.D., Archer, H., Evans, J., Clarke, A., Pelka, G.J., Tam, P.P.L., et al. (2004). Mutations of CDKL5 cause a severe neurodevelopmental disorder with infantile spasms and mental retardation. Am. J. Hum. Genet. *75*, 1079–1093.

White, R., Ho, G., Schmidt, S., Scheffer, I.E., Fischer, A., Yendle, S.C., Bienvenu, T., Nectoux, J., Ellaway, C.J., Darmanian, A., et al. (2010). Cyclin-dependent kinase-like 5 (CDKL5) mutation screening in Rett syndrome and related disorders. Twin Res Hum Genet *13*, 168–178.

Willemsen, M.H., Rensen, J.H.M., van Schrojenstein-Lantman de Valk, H.M.J., Hamel, B.C.J., and Kleefstra, T. (2012). Adult Phenotypes in Angelman- and Rett-Like Syndromes. Mol Syndromol *2*, 217–234.

Williamson, S.L., Giudici, L., Kilstrup-Nielsen, C., Gold, W., Pelka, G.J., Tam, P.P.L., Grimm, A., Prodi, D., Landsberger, N., and Christodoulou, J. (2011). A novel transcript of cyclin-dependent kinase-like 5 (CDKL5) has an alternative C-terminus and is the predominant transcript in brain. Hum Genet.

Winterer, G., Ziller, M., Dorn, H., Frick, K., Mulert, C., Wuebben, Y., Herrmann, W.M., and Coppola, R. (2000). Schizophrenia: reduced signal-to-noise ratio and impaired phase-locking during information processing. Clin Neurophysiol *111*, 837–849.

Won, H., Lee, H.-R., Gee, H.Y., Mah, W., Kim, J.-I., Lee, J., Ha, S., Chung, C., Jung, E.S., Cho, Y.S., et al. (2012). Autistic-like social behaviour in Shank2-mutant mice improved by restoring NMDA receptor function. Nature *486*, 261–265.

Wong, V.C.-N., and Kwong, A.K.-Y. (2014). CDKL5 variant in a boy with Infantile Epileptic Encephalopathy: Case report. Brain and Development.

Wood, L., Gray, N.W., Zhou, Z., Greenberg, M.E., and Shepherd, G.M.G. (2009). Synaptic circuit abnormalities of motor-frontal layer 2/3 pyramidal neurons in an RNA interference model of methyl-CpG-binding protein 2 deficiency. Journal of Neuroscience *29*, 12440–12448.

Wozny, C., Gabriel, S., Jandova, K., Schulze, K., Heinemann, U., and Behr, J. (2005). Entorhinal cortex entrains epileptiform activity in CA1 in pilocarpine-treated rats. Neurobiol. Dis. *19*, 451–

460.

Yazdani, M., Deogracias, R., Guy, J., Poot, R.A., Bird, A., and Barde, Y.-A. (2012). Disease modeling using embryonic stem cells: MeCP2 regulates nuclear size and RNA synthesis in neurons. Stem Cells *30*, 2128–2139.

Yizhar, O., Fenno, L.E., Prigge, M., Schneider, F., Davidson, T.J., O'Shea, D.J., Sohal, V.S., Goshen, I., Finkelstein, J., Paz, J.T., et al. (2011). Neocortical excitation/inhibition balance in information processing and social dysfunction. Nature *477*, 171–178.

Zhang, H., Zha, X., Tan, Y., Hornbeck, P.V., Mastrangelo, A.J., Alessi, D.R., Polakiewicz, R.D., and Comb, M.J. (2002). Phosphoprotein analysis using antibodies broadly reactive against phosphorylated motifs. J. Biol. Chem. *277*, 39379–39387.

Zhao, Y., Zhang, X., Bao, X., Zhang, Q., Zhang, J., Cao, G., Zhang, J., Li, J., Wei, L., Pan, H., et al. (2014). Clinical features and gene mutational spectrum of CDKL5-related diseases in a cohort of Chinese patients. BMC Med. Genet. *15*, 24.

Zhou, J., and Parada, L.F. (2012). PTEN signaling in autism spectrum disorders. Curr. Opin. Neurobiol. *22*, 873–879.

Zhou, Z., Hong, E.J., Cohen, S., Zhao, W.-N., Ho, H.-Y.H., Schmidt, L., Chen, W.G., Lin, Y., Savner, E., Griffith, E.C., et al. (2006). Brain-specific phosphorylation of MeCP2 regulates activity-dependent Bdnf transcription, dendritic growth, and spine maturation. Neuron *52*, 255–269.

Zhu, Y.-C., Li, D., Wang, L., Lu, B., Zheng, J., Zhao, S.-L., Zeng, R., and Xiong, Z.-Q. (2013). Palmitoylation-dependent CDKL5-PSD-95 interaction regulates synaptic targeting of CDKL5 and dendritic spine development. Proceedings of the National Academy of Sciences of the United States of America *110*, 9118–9123.

Zoncu, R., Efeyan, A., and Sabatini, D.M. (2011). mTOR: from growth signal integration to cancer, diabetes and ageing. Nat. Rev. Mol. Cell Biol. *12*, 21–35.